COMPUTATIONAL DESIGN OF AN EXPERIMENTAL LASER-POWERED THRUSTER

Submitted by

San-Mou Jeng, Ronald Litchford
and
Dennis Keefer

Center for Laser Applications
The University of Tennessee Space Institute
Tullahoma, TN 37388-8897
(615) 455-0631

March 24, 1988

Final Report, Contract Number NAS8-36220

REPORT DOCUMENTATION PAGE		READ INSTRUCTIONS BEFORE COMPLETING FORM
1. REPORT NUMBER	2. GOVT ACCESSION NO.	3. RECIPIENT'S CATALOG NUMBER
4. TITLE (and Subtitle) Computational Design of an Experimental Laser-Powered Thruster		5. TYPE OF REPORT & PERIOD COVERED FINAL REPORT Sept 9, 1986-Mar 8, 1988 6. PERFORMING ORG. REPORT NUMBER
7. AUTHOR(s) S.M. Jeng, Ronald Litchford and Dennis Keefer		8. CONTRACT OR GRANT NUMBER(s) CONTRACT NO.: NAS8-36220
9. PERFORMING ORGANIZATION NAME AND ADDRESS The University of Tennessee Space Institute Tullahoma, TN 37388		10. PROGRAM ELEMENT, PROJECT, TASK AREA & WORK UNIT NUMBERS
11. CONTROLLING OFFICE NAME AND ADDRESS ONRRR, Georgia Institute of Technology 206 O'Keefe Bldg.(AP29-F/Irene Dolin) Atlanta, GA 30332		12. REPORT DATE March 24, 1988 13. NUMBER OF PAGES
14. MONITORING AGENCY NAME & ADDRESS(if different from Controlling Office) George C. Marshall Space Flight Center ATTN: Procurement Office (F. Harris, AP29-C) National Aeronautics & Space Administration Marshall Space Flight Center, AL 35812		15. SECURITY CLASS. (of this report) UNCLASSIFIED 15a. DECLASSIFICATION/DOWNGRADING SCHEDULE

16. DISTRIBUTION STATEMENT (of this Report)

AP29-C*
AP29-F*(ONRRR)*
AS24D (5 cys)
AT01
CC01/Wofford
AP29-H*
EM13A/Oran Hunter
EP53/Richard Eskridge(1 + repro)
NASA Scientific & Tech. Info. Fac. (1 + repro)

*Copy of letter of transmittal only

17. DISTRIBUTION STATEMENT (of the abstract entered in Block 20, if different from Report)

18. SUPPLEMENTARY NOTES

19. KEY WORDS (Continue on reverse side if necessary and identify by block number)

20. ABSTRACT (Continue on reverse side if necessary and identify by block number)

SEE ATTACHED

DD FORM 1 JAN 73 1473 EDITION OF 1 NOV 65 IS OBSOLETE

COMPUTATIONAL DESIGN OF AN EXPERIMENTAL LASER-POWERED THRUSTER

Submitted by

San-Mou Jeng, Ronald Litchford
and
Dennis Keefer

Center for Laser Applications
The University of Tennessee Space Institute
Tullahoma, TN 37388-8897
(615) 455-0631

March 24, 1988

Final Report, Contract Number NAS8-36220

ABSTRACT

An extensive numerical experiment, using the developed computer code, has been conducted to design an optimized laser-sustained hydrogen plasma thruster. The plasma was sustained using a 30 kW CO_2 laser beam operated at 10.6 μm focused inside the thruster. The adopted physical model considers two-dimensional compressible Navier-Stokes equations coupled with the laser power absorption process, geometric ray tracing for the laser beam, and the thermodynamically equilibrium (LTE) assumption for the plasma thermophysical and optical properties.

A pressure based Navier-Stokes solver using body-fitted coordinate was used to calculate the laser-supported rocket flow which consists of both recirculating and transonic flow regions. The computer code was used to study the behavior of laser-sustained plasmas within a pipe over a wide range of forced convection and optical arrangements before it was applied to the thruster design, and these theoretical calculations agree well with existing experimental results.

Several different throat size thrusters operated at 150 and 300 kPa chamber pressure were evaluated in the numerical experiment. It is found that the thruster performance (vacuum specific impulse) is highly dependent on the operating conditions, and that an adequately designed laser-supported thruster can have a specific impulse around 1500 secs. The heat loading on the wall of the calculated thrusters were also estimated, and it is comparable to heat loading on the conventional chemical rocket. It was also found that the specific impulse of the calculated thrusters can be reduced by 200 secs due to the finite chemical reaction rate.

TABLE OF CONTENTS

LIST OF TABLES

LIST OF FIGURES

NOMENCLATURE

A	coefficient in difference equation for variable ϕ
I	local laser ray intensity
J	Jacobian of inverse coordinate transformation
k	conductivity
p	pressure
q_1, q_2, q_3	geometric relations between coordinate systems
$\dot{q}$	optically thin radiation
R, S, T	source term in equations 6, 7, 15, respectively
s	distance along laser ray
U, V	velocity component along $\varsigma-$ and $\eta-$axis, respectively
u, v	velocity component along $x-$ and $r-$axis, respectively
ς, η	axes of curvilinear coordinate system
ϕ	general dependent variable
ρ	density
Γ	effective diffusion coefficient
μ	viscosity
α	absorption coefficient

Subscript

E, W, N, S	four adjacent nodes to P
e, w, n, s	four surfaces of the control volume centered at P
i	for laser ray i
P	nodal point to be solved in difference equation
rad	radiation
ς, η	partial derivative with respect to ς, η
ϕ	for dependent variable ϕ

Superscript

$*$	values based on given pressure field
$'$	corrected values according to corrected pressure field

I. INTRODUCTION

A propulsion system supported by a laser-sustained plasma has been the subject of many studies. A schematic of a c.w. laser supported thruster is shown in Figure 1. The high power laser beam from a remote site is focused into the thruster. The plasma is initiated and continuous sustained near the laser focus. The plasma is used to absorb the power from the laser beam and convert it into the propellant. Since the focusing lens is positioned at the end of the thruster, the propellant flows into chamber radially through annular slots. Two slots are shown in the Figure 1. The propellant flowing through the slot near the lens is relatively cold and serves for lens cooling purposes. The major propellant enters the thruster through the other slot and has relatively high temperature. This temperature is dependent on the regenerative heating from the thruster wall to the propellant originally at the storage temperature. In the thruster, flow convects high enthalpy plasma downstream and mixes with other propellant to uniformize the radial temperature distribution. Then the propellant thermal energy is converted to the kinetic energy and produces the required thrust for the rocket through a converging and diverging nozzle. The major advantage of the laser thruster, compared to the chemical thruster, is higher specific impulse (about 1000-2000 secs) since the lowest molecular weight propellant (hydrogen) and the higher propellant temperature (not limited to the flame temperature of a combustion process) can be used.

The modeling of the laser-sustained plasma (LSP) for propulsion began with the one-dimensional work of Raizer.[1] Jeng and Keefer[2] had extensively reviewed the early analytical work using one-dimensional and semi-two-dimensional models. A full two-dimensional model on the LSP was first numerically solved by Merkle and coworkers[3,4]. The objective of their work is to demonstrate the capability of the developed numerical method, and part of the governing process of LSP model were simplified. For example, the plasma radiation were neglected in their model. They succeeded in the calculation of a low temperature LSP (peak temperature about 4,000 K) in the hydrogen flow seeded with cesium. They adopted the rocket geometry; however, the calculations were limited to the subsonic flow region. It is feasible to extend their approach to a pure hydrogen plasma, but the higher peak temperature (about 16,000 K) and much stronger nonlinear optical properties of the pure hydrogen plasma can result in numerical stability problems.

Jeng and Keefer[2] obtained the numerical solutions for a rigorous two-dimensional model with realistic gas properties for the LSP in pure argon subsonic pipe flow. Their results for the argon flows agree well with experimental data[5,6] in the prediction of plasma position, size, shape and peak temperature. Jeng and Keefer[7,8] also extend the model for the pure LSP in the pure hydrogen subsonic flow, and studied the effect of laser power, flow rate, static pressure and optical geometry on the LSP flows. A study using the different laser beam profile and wavelength of the potential developed high power laser were also investigated recently[9]. Their work indicated that there are no fatal errors in the laser propulsion concept, and the critical parameters, for example plasma size, position, radiation heat loss and energy conversion efficiency, can be controlled using an appropriate

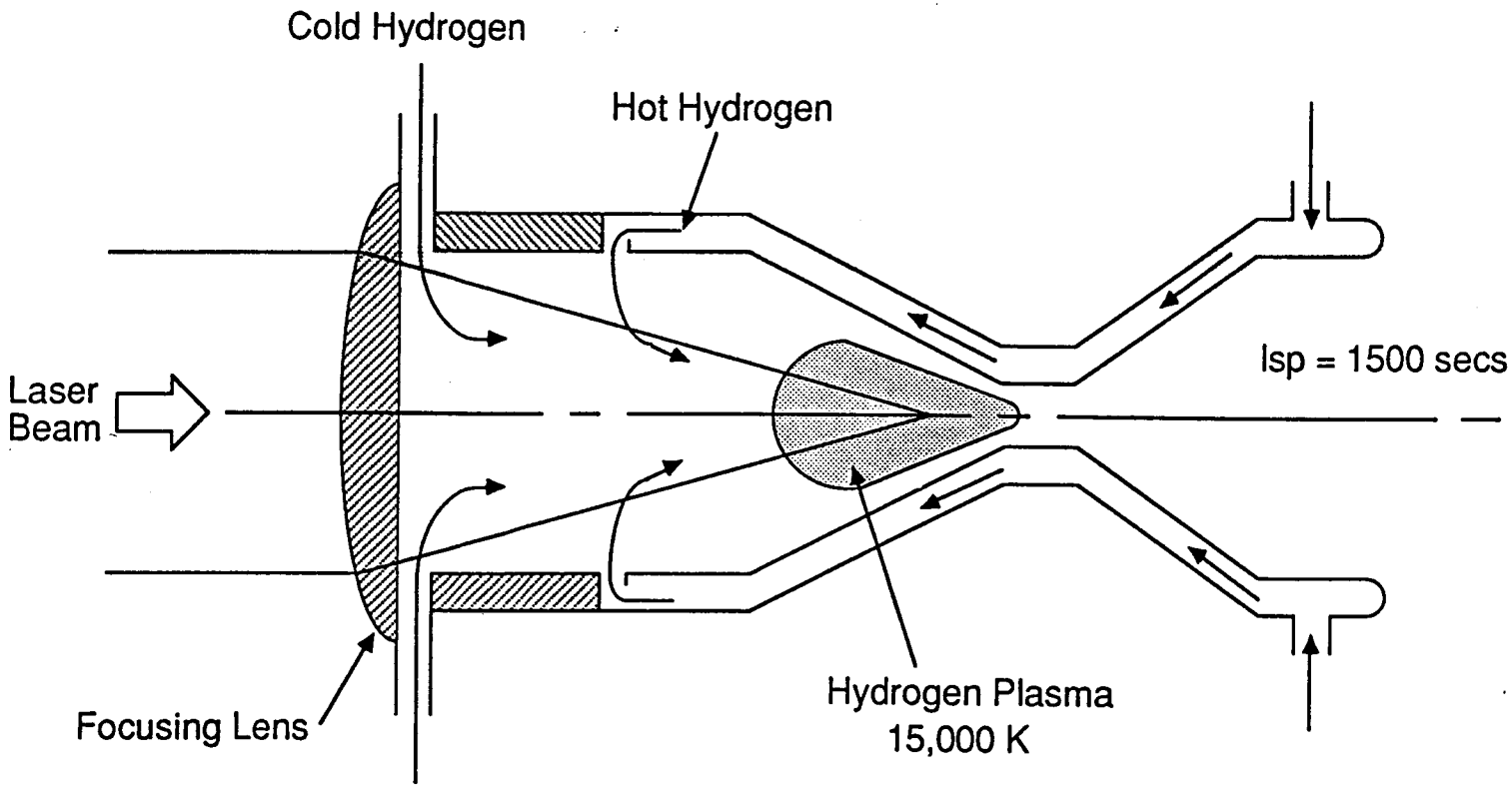

Figure 1. Schematic of laser-sustained plasma thruster

optical arrangement and a suitable flow configuration.

The objectives of the current study are to extend the developed numerical code for calculating the realistic rocket thrusters, and to perform extensive numerical experiment for a optimized rocket design powered by a 30 kW CO_2 laser. In this report, the physical model and numerical algorithm used by the developed code and their verification will be first discussed followed by the thruster design study.

II. THEORETICAL MODEL

2.1 LASER BEAM

The geometric optics was used to describe the laser beam which was assumed to be consisted from a finite number of individual laser rays. Each laser ray path through the optical system to the plasma flow was calculated using real-ray tracing. Diffraction of the laser beam due to the finite aperture of the lens, and effects due to the inhomogeneous refractive index within the plasma were neglected in the calculation. The local intensity of each individual ray i was described by Beer's law written in the the following form.

$$\frac{dI_i}{ds_i} = \alpha I_i \tag{1}$$

where s_i is the distance along the laser propagation direction for ray i, and α is absorption coefficient and depends on local plasma temperature and pressure.

2.2 PLASMA FLOW

The model assumed that the flow is laminar, steady-state, axisymmetric and has variable physical properties. The pressure of the plasma is relatively high so local thermodynamic equilibrium (LTE) for the plasma can be assumed with little error. Therefore, the plasma can be described by a single temperature, and its physical properties are only a function of this temperature and pressure. The model also considered the thermal radiation emitted from the plasma which included the contributions from free to free, free to bound, and bound to bound transitions. These radiation properties are a strong function of wavelength, and the current model adopted the simplified approach, developed by Kemp et al[10] and Caledonia et al.[11] to solve the hydrogen plasma radiation transport equations. Radiation transport was divided into two parts depending on wavelength: wavelength longer than 0.095 μm, optical depth is long and an optically thin approximation, which all radiation escapes from the plasma, was used; and in other wavelength region, optical depth is short and an optically thick approximation, which can be described as a diffusion process, was assumed. Following the above assumptions, the equations of conservation of mass, momentum and energy for the flow can be written as :

$$\frac{\partial(\rho u)}{\partial x}+\frac{1}{r}\frac{\partial(r\rho v)}{\partial r}=0, \tag{2}$$

$$\frac{\partial(\rho uu)}{\partial x}+\frac{1}{r}\frac{\partial(rpuv)}{\partial r}=-\frac{\partial p}{\partial x}+\frac{\partial}{\partial x}\left(\mu\frac{\partial u}{\partial x}\right)$$
$$+\frac{1}{r}\frac{\partial}{\partial r}\left(\mu r\frac{\partial u}{\partial r}\right)+\frac{\partial}{\partial x}\left(\mu\frac{\partial u}{\partial x}\right)+\frac{1}{r}\frac{\partial}{\partial r}\left(\mu r\frac{\partial v}{\partial x}\right)$$
$$-\frac{\partial}{\partial x}\left[\frac{2\mu}{3}\left(\frac{\partial u}{\partial x}+\frac{1}{r}\frac{\partial(rv)}{\partial r}\right)\right], \tag{3}$$

$$\frac{\partial(\rho uv)}{\partial x}+\frac{1}{r}\frac{\partial(r\rho vv)}{\partial r}=-\frac{\partial p}{\partial r}+\frac{\partial}{\partial x}\left(\mu\frac{\partial v}{\partial x}\right)$$
$$+\frac{1}{r}\frac{\partial}{\partial r}\left(\mu r\frac{\partial v}{\partial r}\right)+\frac{\partial}{\partial x}\left(\mu\frac{\partial u}{\partial r}\right)+\frac{1}{r}\frac{\partial}{\partial r}\left(\mu r\frac{\partial v}{\partial r}\right)-\frac{2\mu v}{r^2}$$
$$-\frac{1}{r}\frac{\partial}{\partial r}\left[\frac{2\mu r}{3}\left(\frac{\partial u}{\partial x}+\frac{1}{r}\frac{\partial(rv)}{\partial r}\right)\right]+\frac{2\mu}{3r}\left(\frac{\partial u}{\partial x}+\frac{1}{r}\frac{\partial(rv)}{\partial r}\right), \tag{4}$$

$$\frac{\partial(\rho uh)}{\partial x}+\frac{1}{r}\frac{\partial(r\rho vh)}{\partial r}=\frac{\partial}{\partial x}\left(\frac{k_{eff}}{c_p}\frac{\partial h}{\partial x}\right)$$
$$+\frac{1}{r}\frac{\partial}{\partial r}\left(\frac{rk_{eff}}{c_p}\frac{\partial h}{\partial r}\right)-\frac{\partial\left(\rho u(\frac{1}{2}u^2+\frac{1}{2}v^2)\right)}{\partial x}$$
$$-\frac{\partial\left(r\rho v(\frac{1}{2}u^2+\frac{1}{2}v^2)\right)}{r\partial r}+\frac{4}{3}\mu\left(\left(\frac{\partial u}{\partial x}\right)^2+\left(\frac{\partial v}{\partial r}\right)^2\right)$$
$$+\mu\left(\left(\frac{\partial v}{\partial x}\right)^2+\left(\frac{\partial u}{\partial r}\right)^2\right)+\frac{4}{3}\mu\frac{\partial u}{\partial x}\frac{\partial v}{\partial r}+2\mu\frac{\partial v}{\partial x}\frac{\partial u}{\partial r}$$
$$+\frac{1}{r}\left(\frac{4}{3}\mu\frac{v^2}{r}-\frac{4}{3}\mu v\left(\frac{\partial v}{\partial x}+\frac{\partial v}{\partial r}\right)\right)$$
$$+\sum\alpha I_i-\dot{q}_{rad} \tag{5},$$

where k_{eff} is the sum of molecular thermal conductivity and radiation-induced thermal conductivity in the optically thick limit; $\dot{q}_{rad}$ is radiative heat loss in the optically thin limit; $\alpha\Sigma I_i$ represents local power addition from laser beam to the flow; and as mentioned before, the physical properties involved in equations (2-5) are a function of the local temperatures and pressures, and Ref. 7 has a detailed description of the thermophysical and optical properties sources used in this work.

In the thruster calculations, constant wall temperature was assumed. Total pressure, total temperature and flow streamline were specified at the inlet, and upstream running Riemann invariants extrapolation plus the isentropic relations were used to calculate other properties. At the exit, the properties were linearly extrapolated from the interior flow field.

III. NUMERICAL ALGORITHM

An extensive discussion of the adopted numerical algorithm can be found in Appendix (A). Only a brief description of this algorithm is presented in this section.

3.1 COORDINATE TRANSFORMATION

The set of transport equations (3-5) can be written in the cylindrical system coordinates for the dependent variable, ϕ, in the following generalized form:

$$\frac{\partial}{\partial x}(r\rho u\phi) + \frac{\partial}{\partial r}(r\rho v\phi) = \frac{\partial}{\partial x}(\Gamma^{\phi} r\frac{\partial \phi}{\partial x}) + \frac{\partial}{\partial r}(\Gamma^{\phi} r\frac{\partial \phi}{\partial r}) + R^{\phi}(x,r) \tag{6}$$

where $\Gamma^{\phi}{}_{eff}$ is the effective diffusion coefficient and $R^{\phi}(x,r)$ is source term. The above source term for the momentum equations (3,4) also includes the diffusion terms from the dilation effect. When new independent variables ς and η are introduced, Eq. (6) changes according to the general transformation ς and η. A schematic illustration of the relations between the physical domain and the transformed domain is shown in Figure 2. Equation (6) is rewritten in ς and η coordinates as follows:

$$\frac{1}{J}\frac{\partial}{\partial \xi}(r\rho U\phi) + \frac{1}{J}\frac{\partial}{\partial \eta}(r\rho V\phi) = \frac{1}{J}\frac{\partial}{\partial \xi}\left[\frac{\Gamma^{\phi} r}{J}(q_1\phi_{\xi} - q_2\phi_{\eta})\right] + \frac{1}{J}\frac{\partial}{\partial \eta}\left[\frac{\Gamma^{\phi} r}{J}(-q_2\phi_{\xi} + q_3\phi_{\eta})\right] + S^{\phi}(\xi,\eta) \tag{7}$$

where

$$U = ur_{\eta} - vx_{\eta} \tag{8}$$

$$V = vx_{\xi} - ur_{\xi} \tag{9}$$

$$q_1 = x_{\eta}^2 + r_{\eta}^2 \tag{10}$$

$$q_2 = x_{\xi}x_{\eta} + r_{\xi}r_{\eta} \tag{11}$$

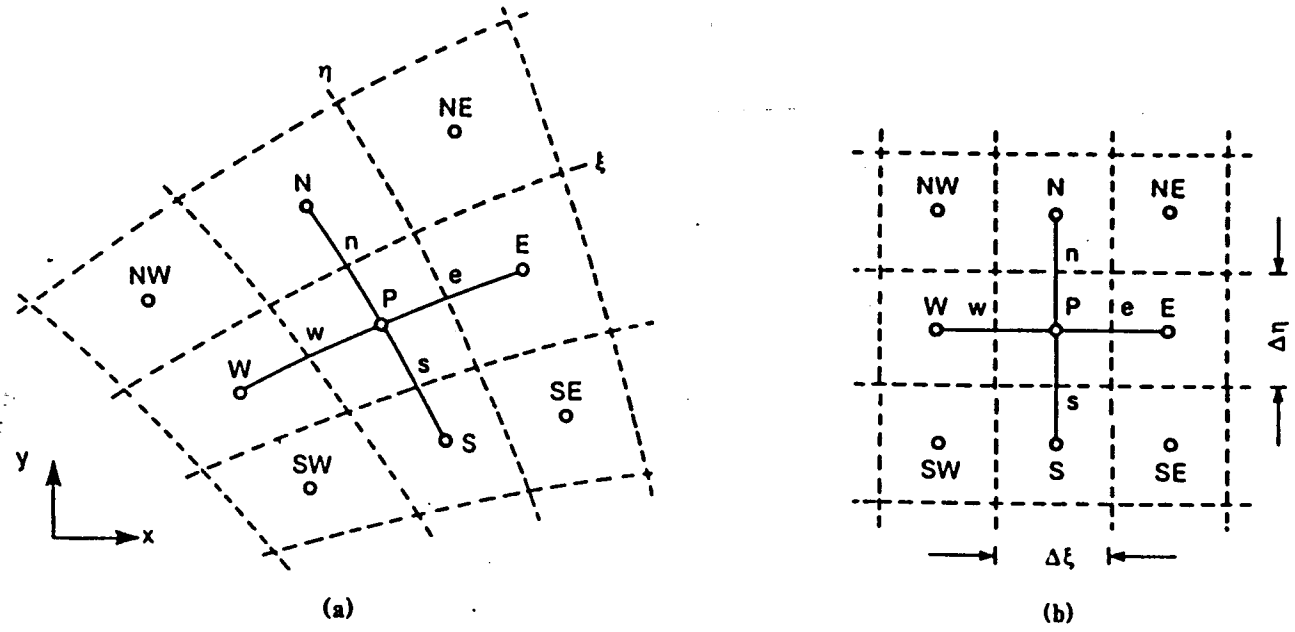

Figure 2. Schematic of coordinate transformation

$$q_3 = x_\xi^2 + y_\xi^2 \tag{12}$$

$$J = x_\xi r_\eta - x_\eta r_\xi \tag{13}$$

and $S^\phi(\varsigma, \eta)$ is the source term in the ς and η coordinates.

3.2 FINITE DIFFERENCE METHOD

A nonstaggered grid system, as shown in Figure 2, is adopted in the calculations. For a typical grid node P, where u, v, p and h five unknown are located, are enclosed in its cell and surrounded by its neighbors N, S, E, and W. The integral of Eq. 7 over its control volume, by arbitrarily taking $\Delta\varsigma = 1$ and $\Delta\eta = 1$, becomes

$$\begin{aligned}
&(r\rho U\phi)_e - (r\rho U\phi)_w + (r\rho V\phi)_n - (r\rho V\phi)_s \\
&= \left[\frac{r\Gamma^\phi}{J}(q_1\phi_\xi - q_2\phi_\eta)\right]_e - \left[\frac{r\Gamma^\phi}{J}(q_1\phi_\xi - q_2\phi_\eta)\right]_w \\
&+ \left[\frac{r\Gamma^\phi}{J}(-q_2\phi_\xi + q_3\phi_\eta)\right]_n - \left[\frac{r\Gamma^\phi}{J}(-q_2\phi_\xi + q_3\phi_\eta)\right]_s \\
&+ r \cdot J \cdot S^\phi(\varsigma, \eta)
\end{aligned} \tag{14}$$

The second-order center differencing is used to discretize the above equation except for the convective terms when cell Reynolds number is greater than 2. In that case, the first order upwind differencing is used. A staggered grid system in the body-fitted coordinates has been widely used in the literature,[12] and it has been known that the oscillatory field will be produced using the nonstaggered grid system. The artificial viscosity term proposed by Rhie and Chow[13] to cure the problem was also implemented in this study. The cross derivatives in the diffusion terms of Eq. (14) are the results of nonorthogonal coordinate system and are usually small. In order to use the solution procedure for the five-point unknowns, these terms are combined with the source term and treated as known quantities and the resulting relation between ϕ_P and the neighboring values can be written as :

$$A_p\phi_p = A_E\phi_E + A_N\phi_N + A_S\phi_S + S^\phi r \cdot T^\phi(\varsigma, \eta)J, \tag{15}$$

where the coefficients A involve the flow properties of convection, diffusion, area, etc, and $T^\phi(\varsigma, \eta)$ includes the source term $S^\phi(\varsigma, \eta)$ and the cross derivatives in the diffusion terms.

3.3 PRESSURE CORRECTION PROCEDURE

While the above general transport equation, Eq. (15), was used to solved momentum and energy equations, the pressure field must be solved using the continuity equation. The procedure used in this work is an adoption of algorithm developed by Rhie,[14] and only a brief discussion is presented in this section. The pressure equation used in the adopted

procedure is similar to that of SIMPLER[15] and PISO,[16,17] except the density term is treated implicitly for the compressible flow. The basic idea is to use the following relations to correct the mass flux obtained from momentum equations.

$$\rho u = \rho^* u^* + \rho' u^* + \rho^* u' \tag{16}$$

$$\rho v = \rho^* v^* + \rho' v^* + \rho^* v' \tag{17}$$

and the discretized pressure equation becomes a transport equation for compressible flow instead of Poission equation. The ratio of diffusion term to convection term is dependent on Mach number, and as Mach number increases, the convection term becomes dominant. The split operator concept similar to PISO were also adopted in the current study to solve the pressure correction equation.

IV. MODEL VERIFICATION

Because of the lack of hydrogen plasma data, the model evaluation procedure is based on the existing argon plasma data. The model has been compared with a wide variety of experimental results given by Welle et al[5,6] in order to learn the capability and limitations of the model. Both calculations and experiments were limited to the LSP within a constant area pipe. Detailed discussion on the calculation procedure can be found in Refs. 2 and 7. Since the spectroscopic measurements were limited to temperatures greater than 10,000 K, the following figures contain only those isotherms within that temperature range, and a limited portion of the calculation domain is plotted in order to gain a clearer comparison. Only a few typical comparisons are presented in this section, and extensive discussion of the model performance can be found in Refs. 2 and 7.

4.1 INLET VELOCITY EFFECT

The performance of the model for two different inlet velocities, using an 8-in. focal length lens, is demonstrated in Figures 3 and 4, respectively. The static pressure and laser power of these two LSP's differ by less than 1 percent, and the inlet velocity of the LSP in Figure 3 is about seven times that in Figure 4. The model calculates the size and position of both plasmas well. As the inlet velocity increases, the radius of the plasma decreases, and the plasma is located further downstream. Two local maximum temperatures within the low-velocity LSP are predicted by the model. One is on the laser path upstream of the focal zone, and another is at the focal zone. Both calculated maximum temperatures are about 1,000 K higher than the measured peak temperature (14,500 K). Only a single maximum temperature was measured, and it is located neither on the laser path nor at the focal zone. The predicted local peak temperature at the focal zone, which was not observed in the experiment, may result from the neglect of diffraction and refraction of the laser beam. Although it has been demonstrated experimentally that this assumption leads to only a small effect on the measured global laser power absorption, the predictive model can suffer more serious effects. If refraction of the laser beam within the LSP is considered, it results in a larger focal spot size and reduced laser intensity. The spot size for the refracted

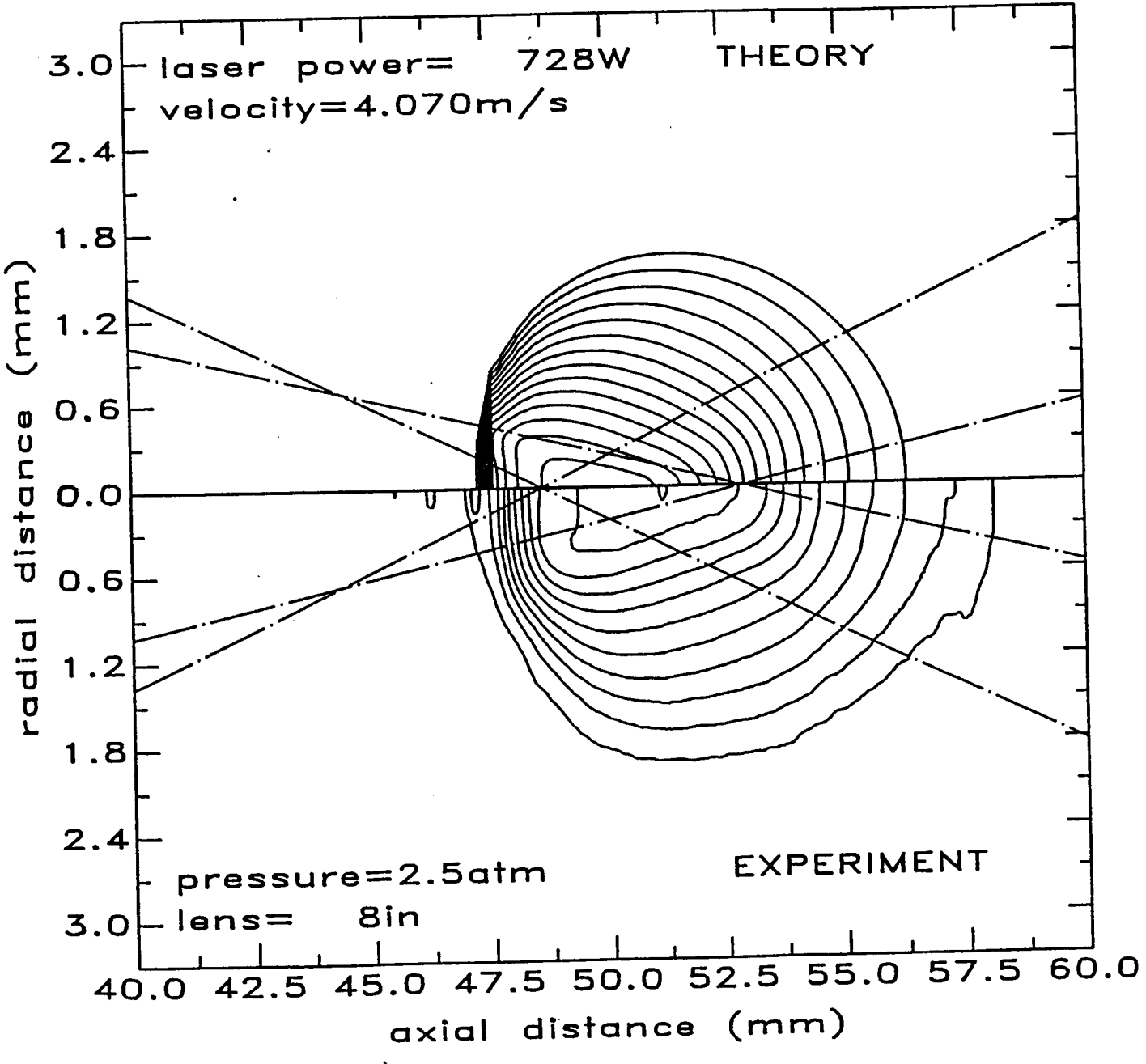

Figure 3. Temperature contour plot of a high-velocity plasma (contour lines starting from 10,500 K with 500 K increments)

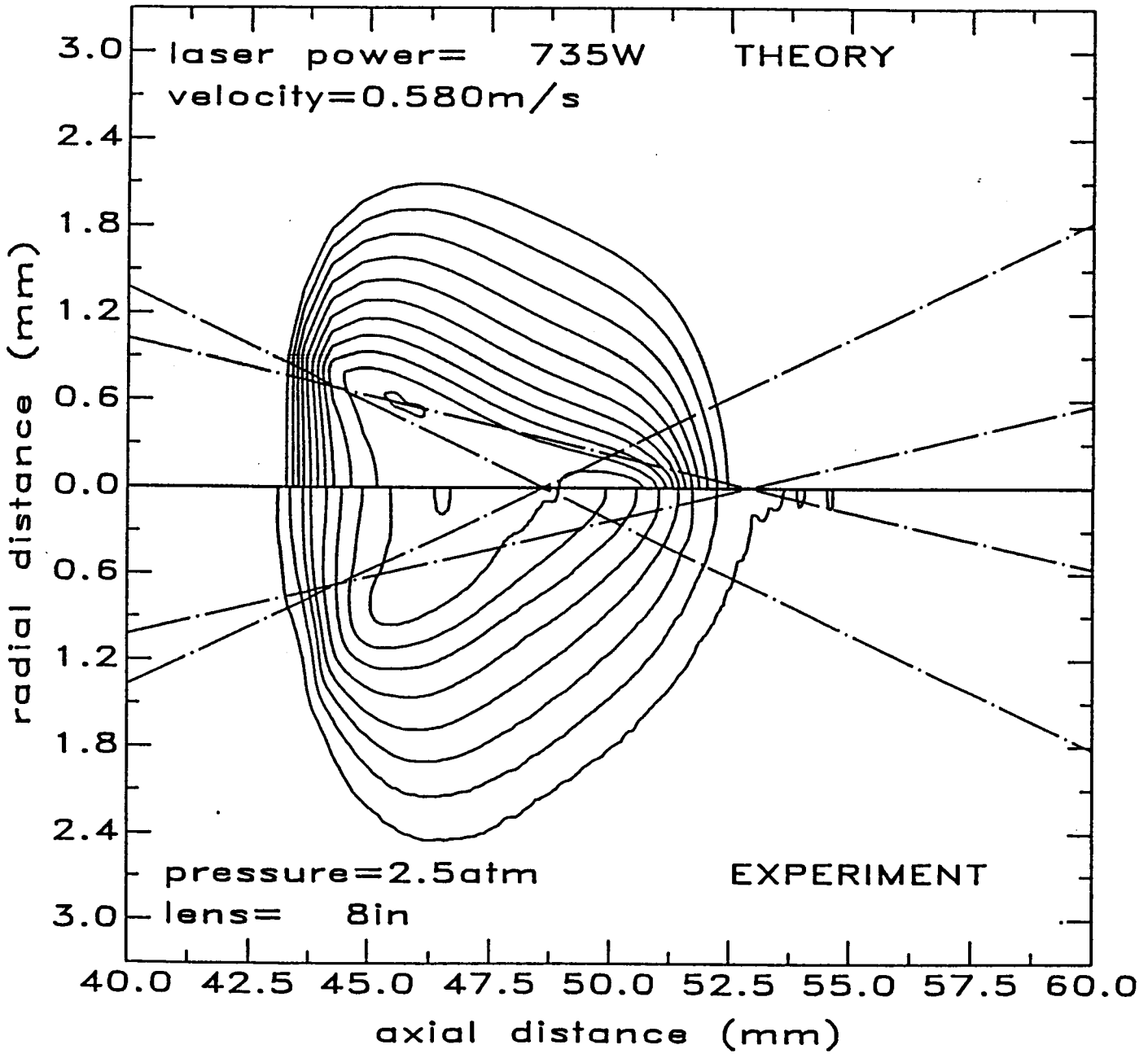

Figure 4. Temperature contour plot of a low-velocity plasma (contour lines starting from 10,500 K with 500 K increments)

beam is highly dependent on the LSP position and size. For a low-velocity LSP, most of the plasma is located upstream of the focal zone, and this makes the focal spot larger. When diffraction is also considered, the diffraction limited focal spot is approximately twice the size of that calculated from a geometric ray trace. The combination of laser beam refraction and diffraction, and the longer absorption pathlength ahead of the focal zone results in an actual laser intensity which is smaller near the laser focal zone than that which is predicted by the model. Thus, the local temperature maximum will not be generated there in the low-velocity LSP. This may explain why the calculations are not consistent with the experiments in this detail.

Since the size and temperature of these LSP were well predicted, it is not surprising that the calculated thermal radiation power loss (316 and 445 W for high and low velocity, respectively) agreed with the experimental results (326 and 392 W for high and low velocity, respectively). The model prediction for the transmitted laser power in the high-velocity LSP also agrees reasonably well (110 W and 159 W for prediction and experiment, respectively). However, the predicted transmitted laser power (91 W) in the low-velocity LSP is much smaller than the measurement (246 W). This is because the predicted second local maximum temperature near the focal zone absorbs an unrealistically large amount of additional laser power.

4.2 LENS EFFECT

Isotherms are shown in Figure 5 for an LSP with operating conditions similar to those of Figure 4 except for use of a 12-in. focal length lens instead of the 8-in. lens. Both calculation and experiment show that the plasma moves further upstream than in Figure 4, and the model predicted the upstream position and the radius of the plasma well. Again, the model predicts a local maximum temperature near the focal zone, which was not measured in the experiment. The effect of laser beam refraction and diffraction, which was discussed in the last section, is probably responsible. Similar to the 8-in. LSP, the thermal radiation from the LSP is well predicted, and the transmitted laser power is underestimated.

4.3 LASER POWER EFFECT

Figures 6 and 7 show the effect of laser power on the structure of the plasma. Both cases use the 12-in. focal length lens with similar flow conditions. The calculations are quite consistent with the experiments. As laser power increases, the plasma becomes larger and moves upstream. For the 10,500 K isotherms, the model underpredicted the length. However, the experimental results exhibit more noise in these isotherms than in the higher temperature isotherms, and if the 11,500 K isotherms are used then the model predicts the length of this isotherm within 10 percent. The calculated positions of both plasmas are about 1 mm downstream of the experiments. After carefully reviewing the experimental data, it was found that the on-axis maximum temperatures are not on the laser beam path (using real ray tracing and neglecting the inhomogeneous refractive index effect). If

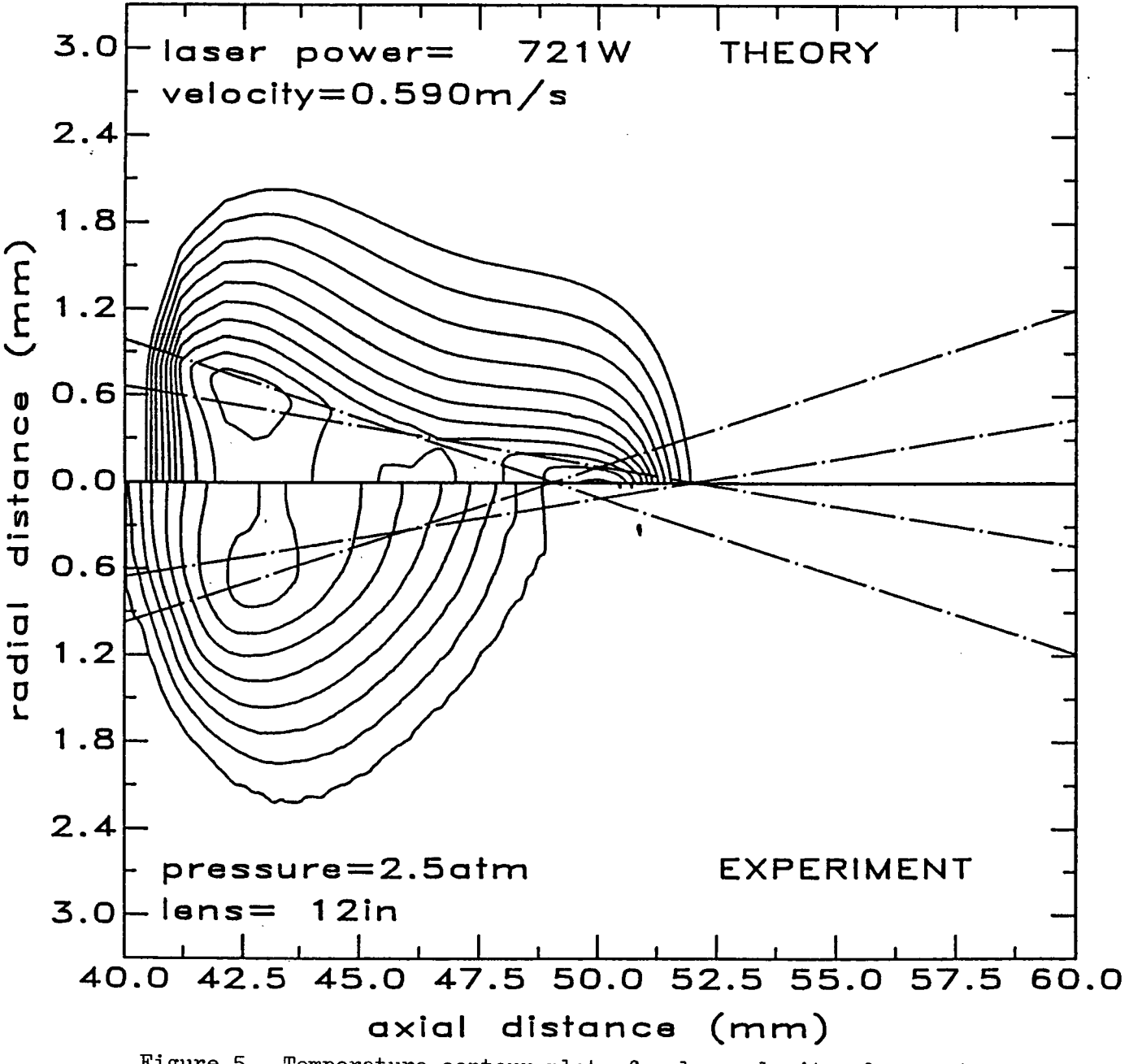

Figure 5. Temperature contour plot of a low-velocity plasma with the 12 inch focal length lens (contour lines starting from 10,500 K with 500 K increments)

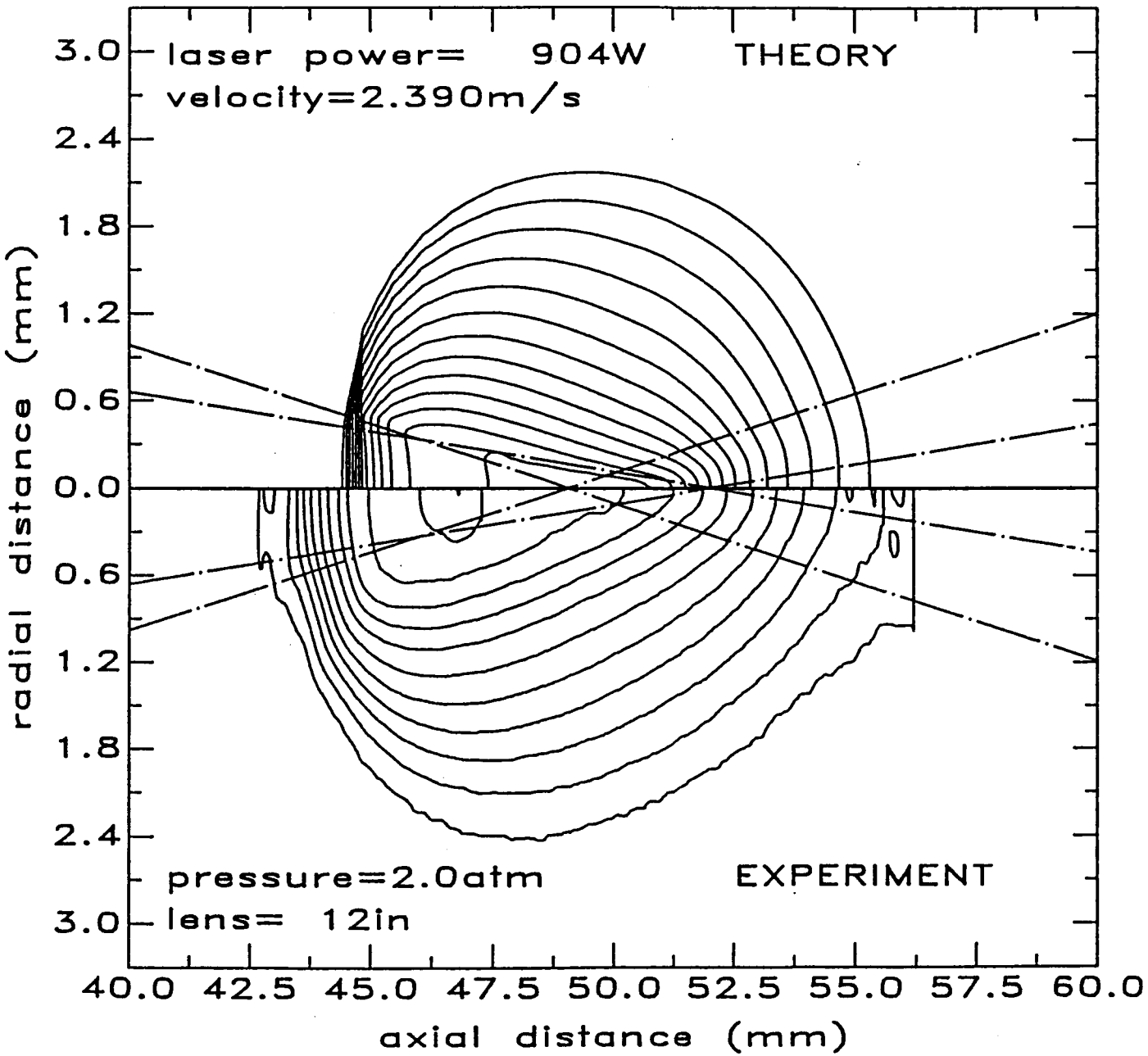

Figure 6. Temperature contour plot of a plasma with high laser power (contour lines starting from 10,500 K with 500 K increments)

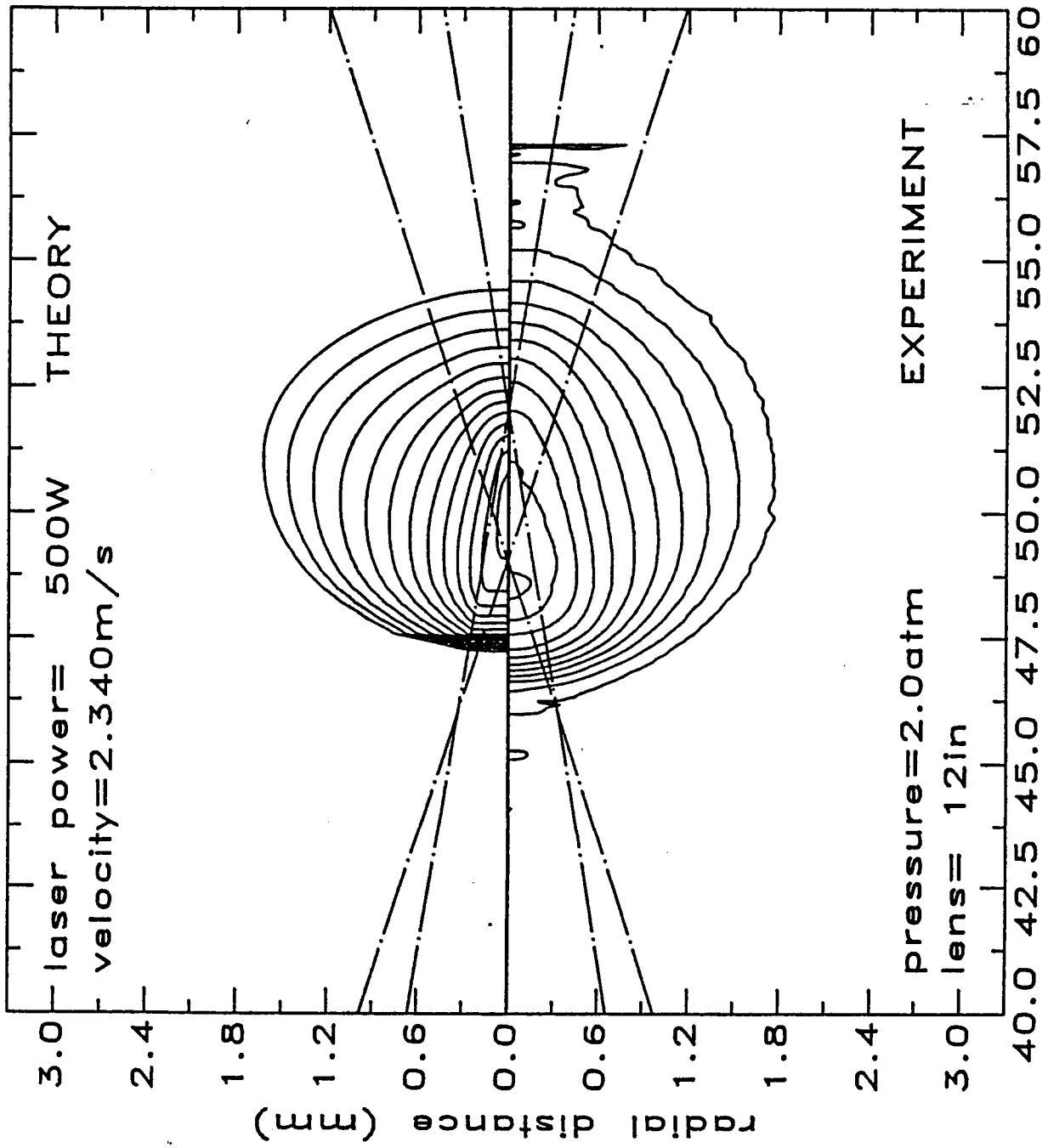

Figure 7. Temperature contour plot of a plasma with low laser power (contour lines starting from 10,500 K with 500 K increments)

the experimental results are shifted downstream by 1 mm, which is within the accuracy claimed by Welle et al, the locations of peak temperatures are on the laser path. In this case, the model predictions agree well with the experimental LSP positions. The predicted global properties are also in reasonable agreement with the experiments: the transmitted laser power is within 10 percent, and the thermal radiation from the LSP is underpredicted within 30 percent.

4.4 STATIC PRESSURE EFFECT

All the LSP's shown in the previous sections have either 2.0 or 2.5 atm static pressure, and the model performed well at these pressures. In this section, the effects of the static pressure are presented. The intrinsic properties of plasmas are highly pressure dependent, especially the optical properties. The absorption coefficient of the plasma at the laser wavelength and the thermal radiation from the plasma are approximately proportional to $p^{1.5}$. Figures 8 and 9 show the plasmas at 3.0 and 1.5 atm, respectively. Both plasmas have similar laser power levels and inlet mass flow rates (but different inlet velocity). In the low-pressure case, the predicted plasma size is much smaller than the experiment. In the 3 atm case, the model provides an excellent prediction.

After reviewing the model assumptions, we concluded that the treatment of the optically thick thermal radiation was the weakest link, and was probably responsible for the failure of the model in the low-pressure case. As mentioned before, the validity of the diffusion approximation for short range radiation is dependent on pressure and the size of the plasma. As the pressure decreases, the required size of the plasma increases. For the present calculation, the size of the 1.5 atm plasma is below the minimum size required for valid use of the diffusion approximation found by Kopainsky18. Although the diffusion approximation for short-range thermal radiation is not valid for the low pressure plasma, a sensitivity study using this approximation was performed to investigate the sensitivity of the solutions to radiative transport. For small, low-pressure plasmas, the radiation induced thermal conductivity should be smaller than that for a large, low-pressure plasma.

A calculated result, where the radiation induced thermal conductivity was reduced to 50 percent of the value used for the calculation in Figure 8, is illustrated in Figure 10. The size of this plasma is much larger than the previous calculation, and agrees well with the experimental results. The role of a change in thermal conductivity on the results can be understood qualitatively. As conductivity decreases, the conduction heat transfer loss from the portion of the plasma along the laser path is reduced, which increases the plasma temperature along the laser path. Due to this increased temperature, the absorption coefficient at the laser wavelength increases and the plasma absorbs more laser power, which in turn generates a larger plasma. The exact solution of radiation heat transport will not be easy to achieve in the near future, and the optically thin and thick approximations for the radiative transport process should be retained for the near term. Although in some pressure and dimension ranges, the optically thick approximation is not quite valid, this concept can still be utilized with some adjustment for the magnitude of the radiation

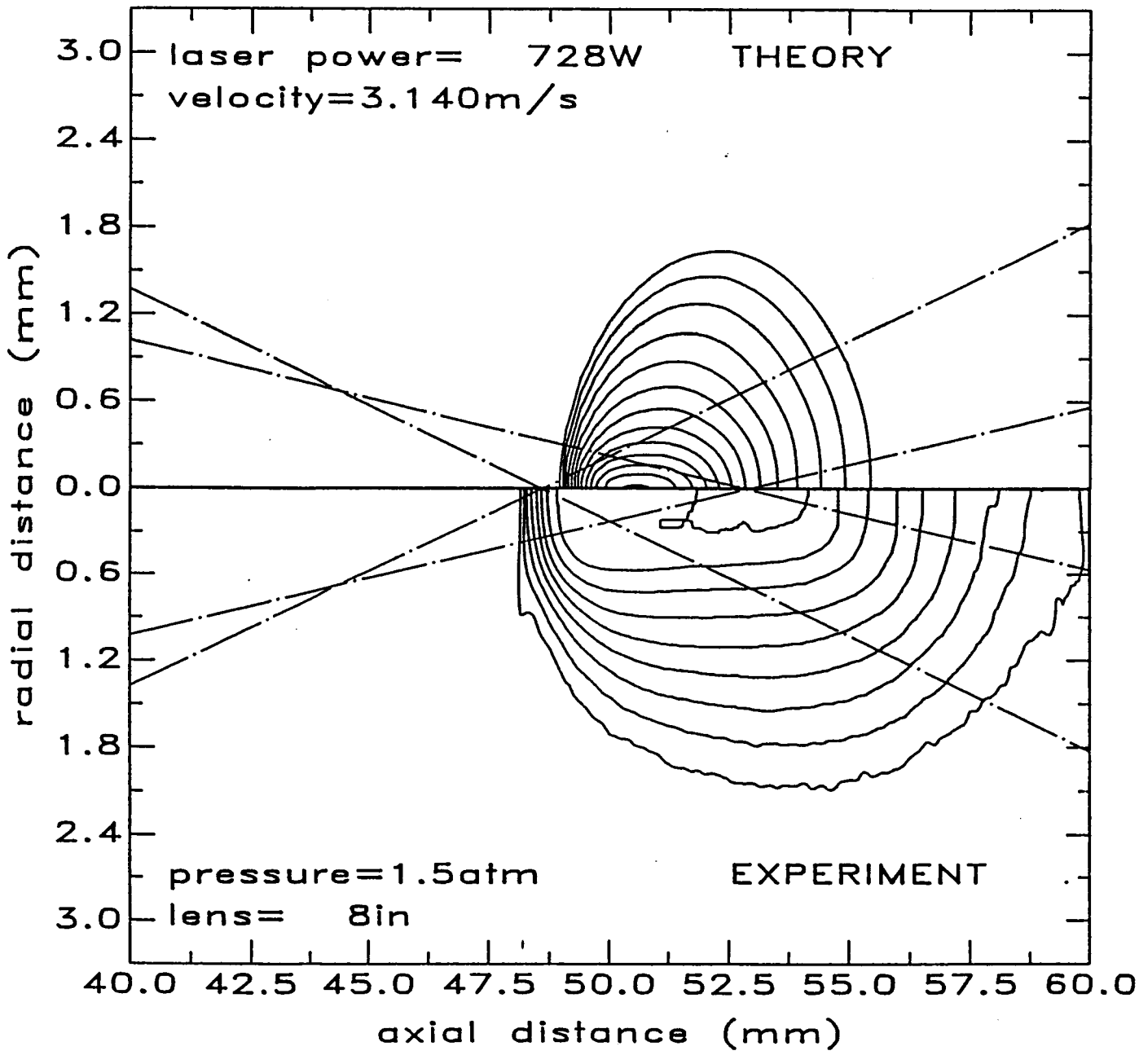

Figure 8. Temperature contour plot of a low-pressure (1.5 atm) plasma (contour lines starting from 10,500 K increments)

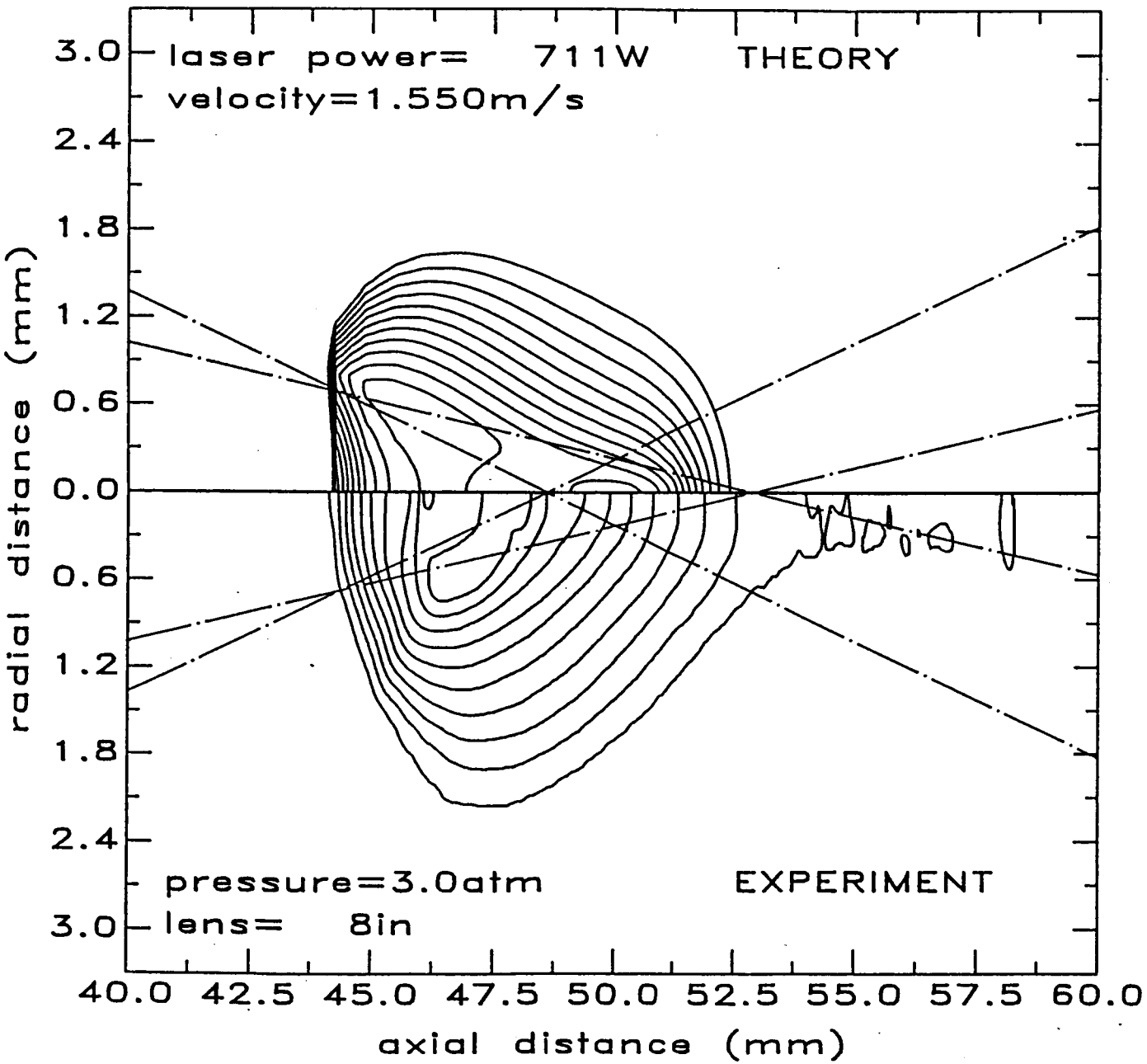

Figure 9. Temperature contour plot of a high-pressure (3.0 atm) plasma (contour lines starting from 10,500 K with 500 K increments)

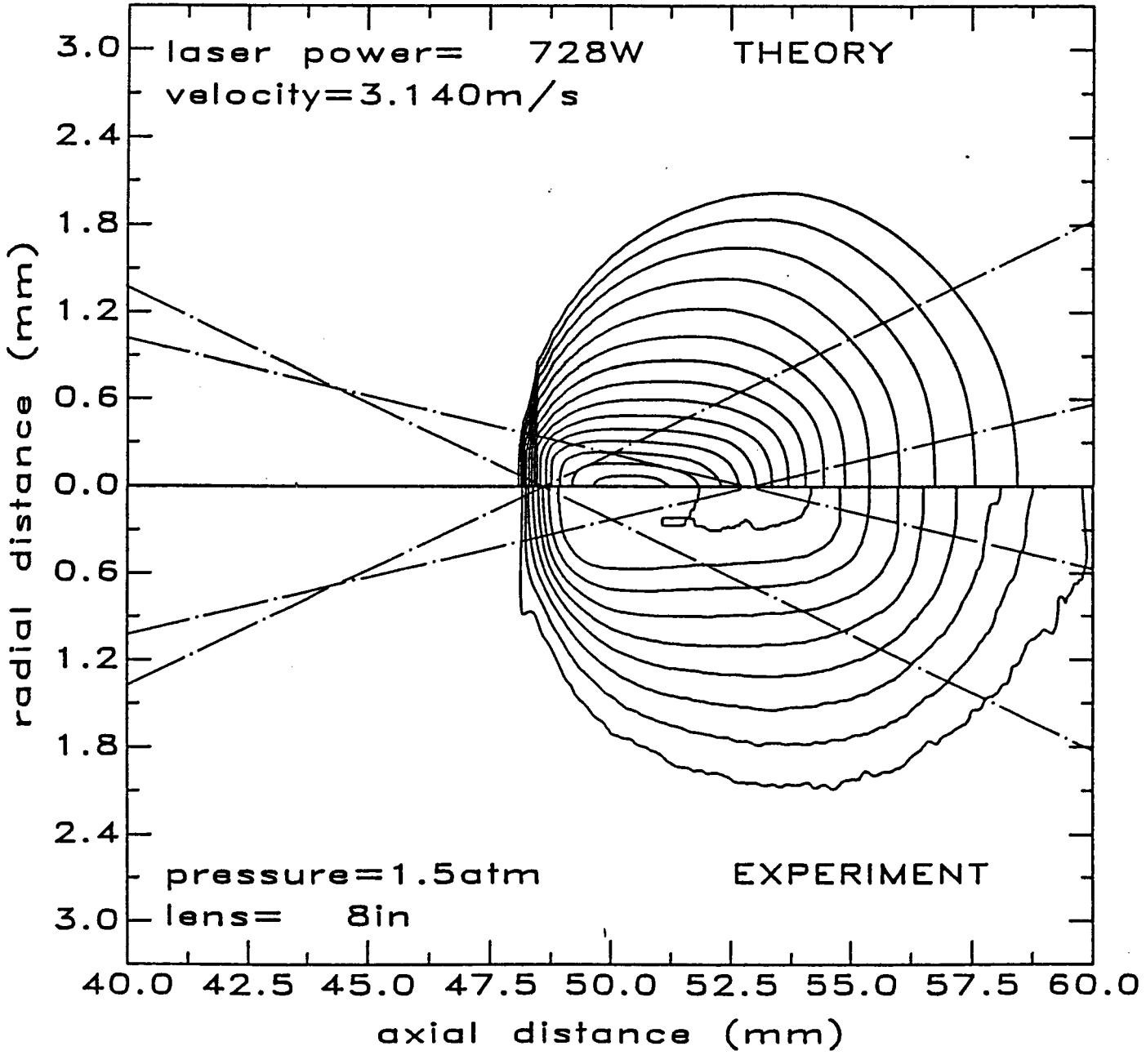

Figure 10. Temperature contour plot of a low-pressure (1.5 atm) plasma using 50% of radiation induced thermal conductivity (contour lines starting from 10,500 K with 500 K increments)

induced thermal conductivity.

V. LASER-SUSTAINED HYDROGEN PLASMA

The behavior of laser-sustained hydrogen plasmas within a constant area pipe were also extensively studied. Parametric study includes the use of different wavelength lasers as well as various forced convections. Due to the lack of experimental data, only theoretical calculations are presented. The detailed structure of LSP using either hydrogen or argon are similar, and detailed discussion on this aspect can be found in Ref. 19. In the following, only the global energy conversion efficiency from laser beam to the flows and the LSP structure using different wavelength lasers are discussed.

5.1 POWER CONVERSION EFFICIENCY

Figures 11, 12 and 13 show power conversion efficiencies under various forced convection conditions. At 1 atm a large amount of laser power is transmitted through the LSP. Transmitted laser power, which decreases as pressure increases, is less than 2 percent in the plasmas with a static pressure greater than 3 atm. The thermal power radiated in the constant inlet velocity cases decreases as pressure increases, but the thermal power radiated first increases with pressure, then decreases for pressures greater than 5 atm in the constant mass flow rate cases. Generally speaking, the energy conversion efficiency has only a weak dependence on pressure in the constant mass flow rate cases. However, in the constant velocity cases, the energy conversion efficiency is greater at higher static pressure. Influence of laser power and force convection on laser power conversion efficiency is shown in Figs. 12 and 13, respectively. If the laser power is larger than 10 kW and the static pressure is higher than 3 atm, the LSP absorbs nearly all of laser power. In these situations, the optically thin radiation heat loss is the critical factor in the energy conversion efficiency.

5.2 WAVELENGTH DEPENDENCE

All of the known experiments with continuous laser sustained plasmas have used the 10.6 micrometer wavelength from the carbon dioxide laser. However, it now appears that lasers capable of providing the megawatt powers required for a practical propulsion system are likely to operate at shorter wavelengths. The high power lasers which are currently under development and are candidates for laser propulsion are either free-electron lasers or chemical lasers. Free-electron lasers can be operated over a wide range of wavelengths and could be tuned to the atmospherical transmission window near 2.2 micrometers for a ground based system. The chemical lasers operate in the wavelength range from 3.3 to 4.3 micrometers, depending on the particular chemical reacting system. We have used our computer model to predict the characteristics of plasmas sustained with three different wavelengths: including 10.6 micrometers as a benchmark case, and 3.9 micrometers and 2.2 micrometers as representative of the free-electron laser and chemical laser, respectively.

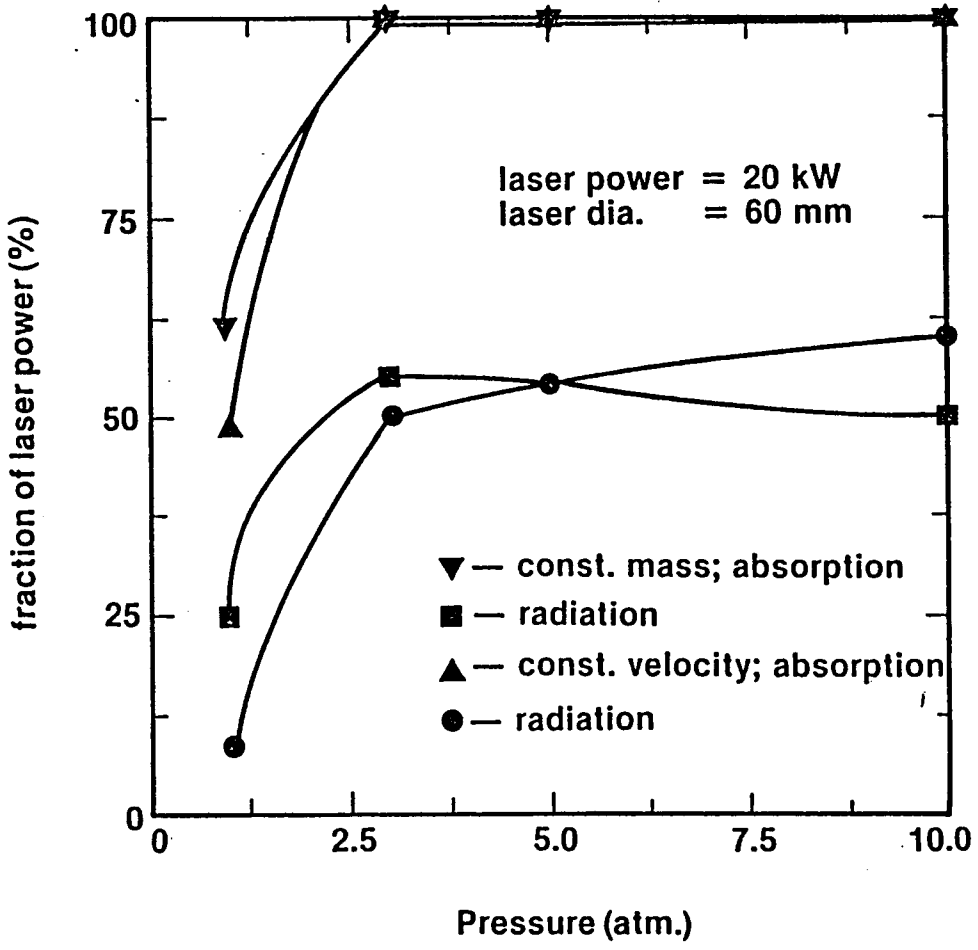

Figure 11. Fractions of the incident laser power that are absorbed and radiated for several static pressures

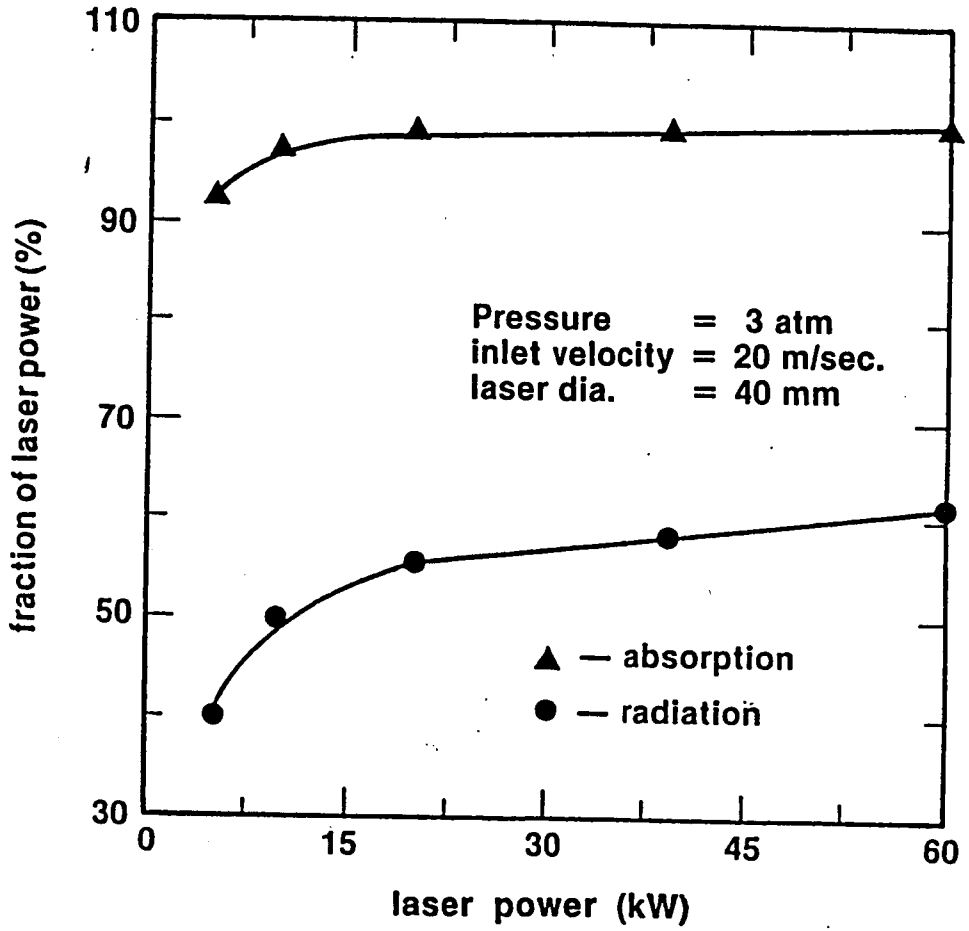

Figure 12. Fractions of the incident laser power that are absorbed and radiated for a range of incident laser powers

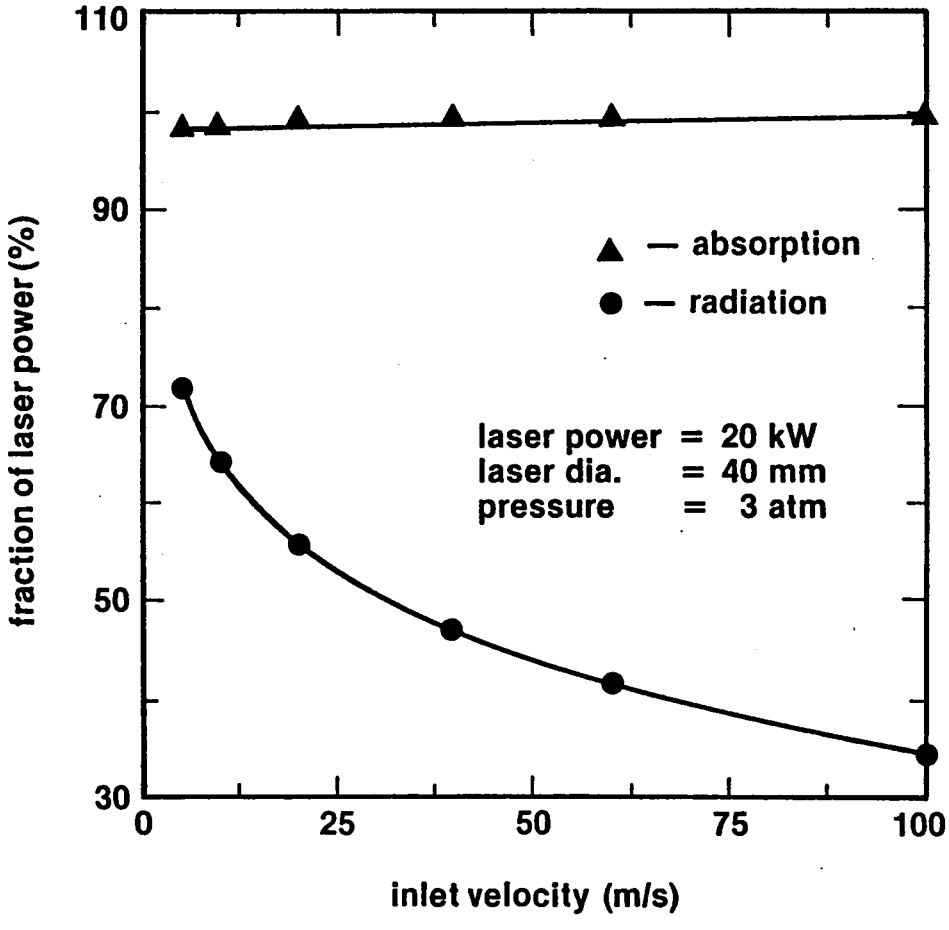

Figure 13. Fractions of the incident laser power that are absorbed and radiated for different inlet velocities

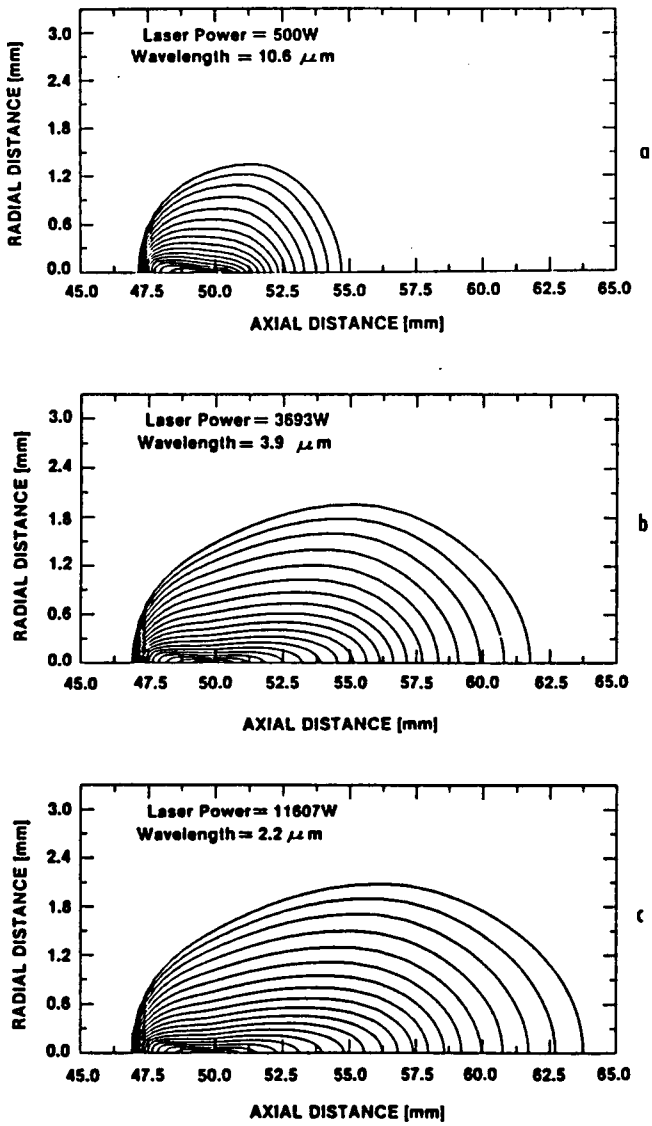

Figure 14. Temperature contour plot of plasma using three wavelength lasers

The major interaction between the laser beam and the plasma is the absorption of laser radiation by the plasma. For the three laser wavelengths considered in this study, plasma absorption occurs through an inverse bremsstrahlung process consisting of electron-ion, electron-atom, and ion-ion absorption. The absorption coefficient of the plasma in the LSP temperature range (less than 20,000 K) is approximately inversely proportional to the square of the wavelength. This relationship and the absorption coefficient at 10.6 micrometers adopted in Reference 8 were used in the current study.

Calculated isotherms for three plasmas are shown in Figure 14(a-c). The incident laser power for the different wavelengths was scaled inversely proportional to the absorption coefficient. The incident laser beam profile and the radius of the lens were the same as those used in the Ref. 8, but the incoming laser beam diameter was chosen to be five times larger to keep the power density at the lens within reasonable values. This results in an f/number of 3.46 which was constant for each of the three cases.

The scaling factor for the incoming laser power that was used for this study (inversely proportional to the square of the wavelength), was chosen so the local laser power absorbed by the plasma (product of local laser intensity and absorption coefficient) was approximately the same for the three wavelengths. The attenuation of the laser beam intensity depends on the product of the absorption coefficient and the physical length. For the same propagation distance through the plasma, a greater fraction of the incident laser power will be absorbed for the longer wavelength laser. This difference in the characteristic absorption length is reflected in the inverse relationship between plasma length and wavelength shown in Figure 12(a-c). The extended tail of the plasma downstream of the focus is sustained by the larger fraction of incoming laser power that passes beyond the focus for the shorter wavelengths. The fraction of the incident laser power that is absorbed by the plasmas was highest for 10.6 micrometers among the three test cases, but the total laser power absorbed by the plasma was the smallest.

VI. ROCKET DESIGN AND PERFORMANCE

The extensive numerical calculations have been performed to have optimized thrusters. The preliminary rocket design effort using the developed code are reported in Ref. 19. In the following section, the discussion will limited to four thruster designs. The test conditions and geometry of theses thrusters are shown in Figure 15 and Table 1. The calculated isotherms and normalized streamlines for rocket No. 1 are shown in Figure 16 and Figure 17, respectively. The plasma is positioned near the throat with a peak temperature of 15,800 K upstream of the laser focus. Most of the propellant within the thruster is not directly heated by the laser beam. However, nearly all of the propellant mixes with the hot plasma and raises the propellant bulk temperature up to approximately 10,000 K before it enters the diverging section of the thruster. Eighty four percent of laser power (25 kW) is absorbed by the propellant, and most of the remaining laser power is transmitted through the throat, except for a very small portion that reaches the thruster wall.

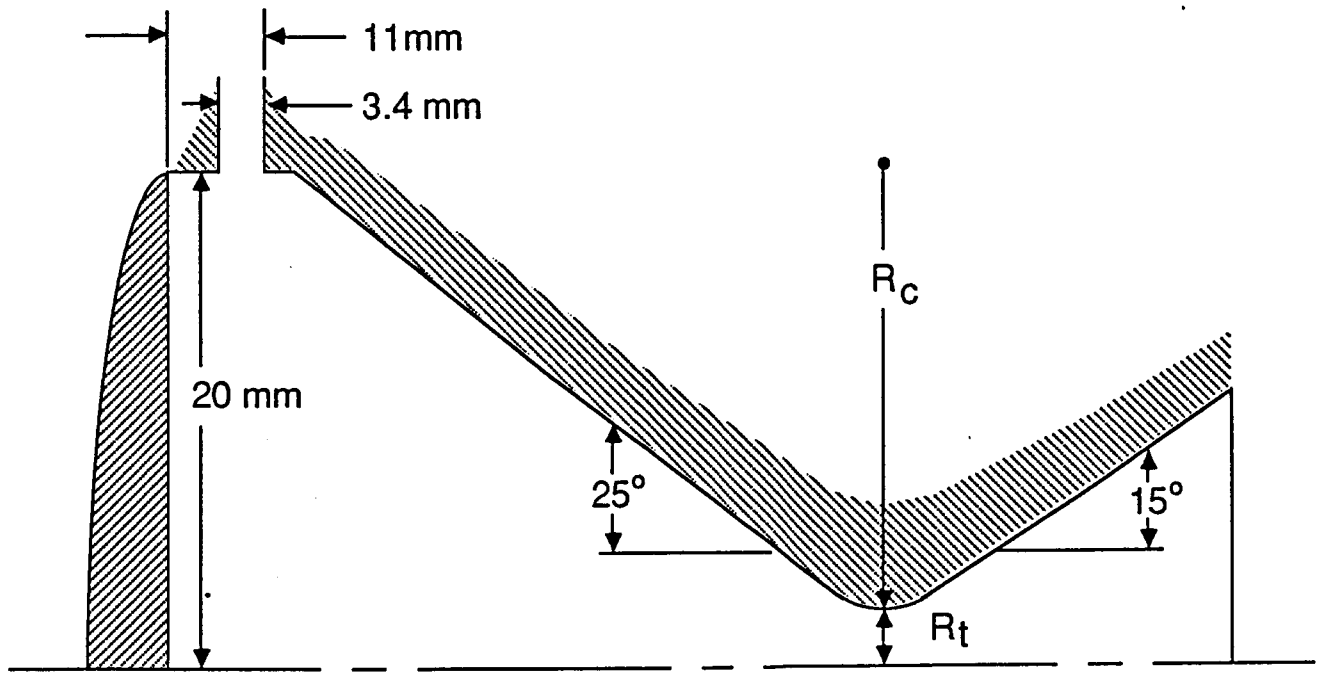

Figure 15. Thruster geometry adopted for the computation

TABLE I.
Test Conditions

ROCKET NO.	1	2	3	4
Throat Radius (mm)	1.2	1.3	1.1	0.8
Inlet Pressure (kPa)	150	150	150	300

CG-0691

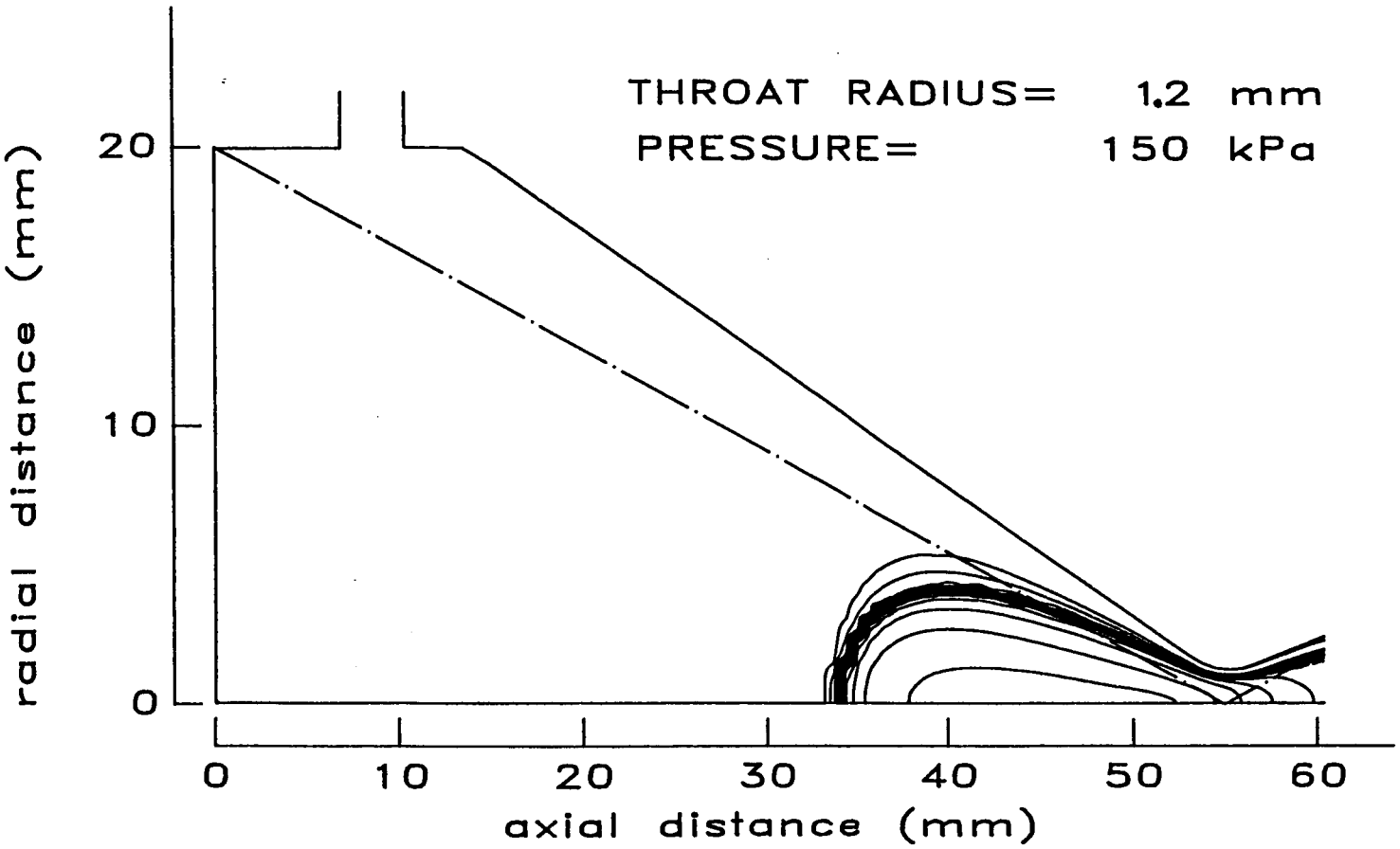

Figure 16. Isotherms for rocket No. 1 (starting from 2,000 K to 15,000 K with 1,000 K increments)

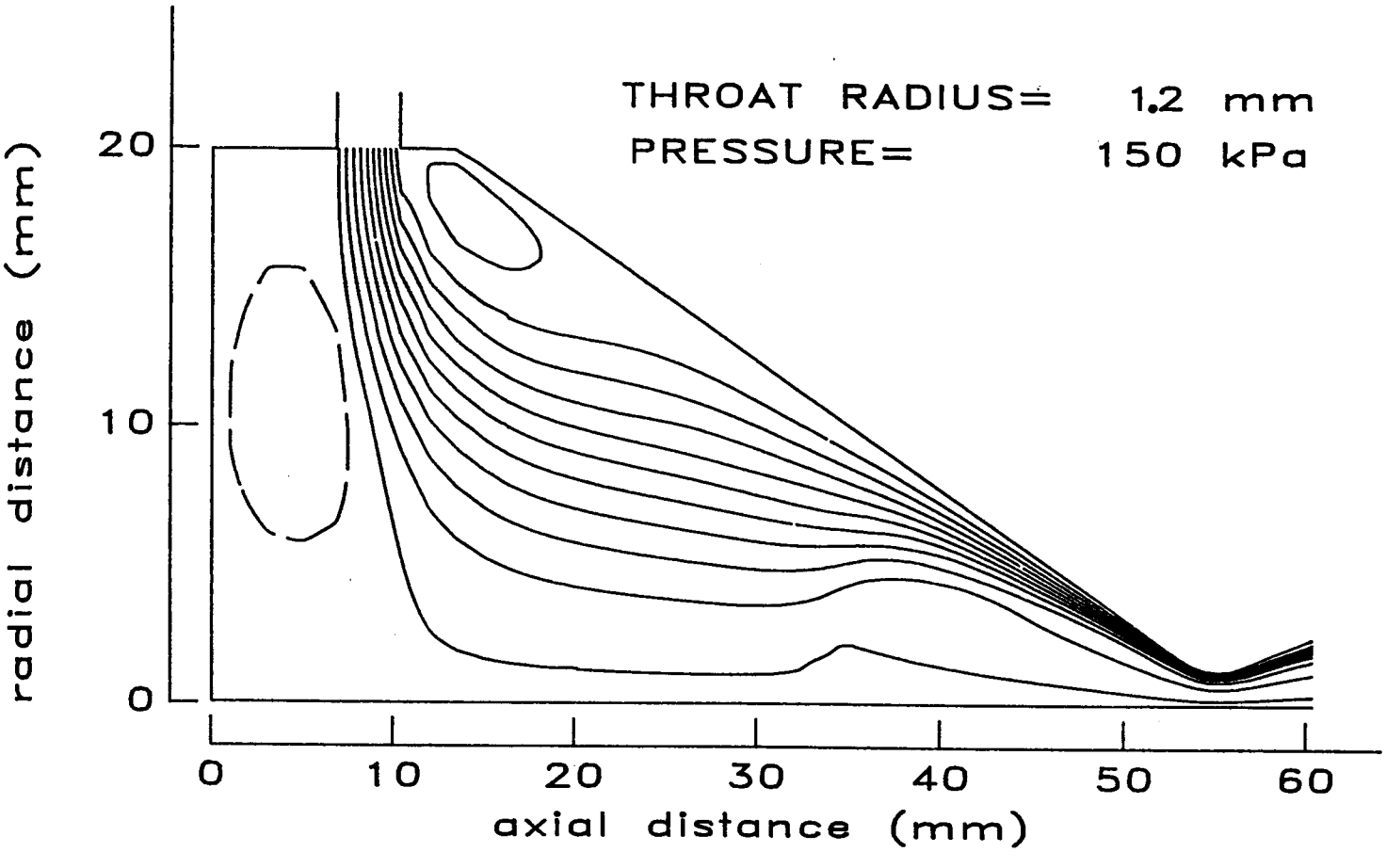

Figure 17. Normalized streamlines for rocket No. 1 (starting from - 0.09 to 1.01 with 0.1 increments)

Since the propellant enters the chamber radially through a slot away from the lens, part of the propellant is expected to recirculate within the thruster. As shown in Figure 17, two recirculation zones occur in this thruster. A large one exists near the focusing lens, and the other one is near the thruster wall downstream of the inlet slot. The streamlines near the centerline upstream of the plasma indicate the flow has an outward direction. This is because the downstream hot plasma propellant (low density) generates a locally unfavorable axial pressure gradient in the flow. This phenomena was also observed in the previous work[2,7,8] for the LSP within a constant area pipe.

An enlarged view of the isotherms and constant axial velocity contours around the throat are shown in Figure 18 and Figure 19, respectively. The leading edge of the LSP is 11 mm upstream of the throat. The axial temperature gradient at the leading edge is very high since the axial heat transfer of convection and conduction is in opposite directions. The detailed discussion of how LSP structures are influenced by forced convection and optical geometry can be found in the previous work.[2,7,8] At the throat the propellant is very hot, approximately 13,500 K on the centerline. The temperature decreases radially from the centerline and reachs a value near 1250 K, which corresponds to the sonic temperature of the adiabatic (without heat addition from the laser beam) propellant. Then the temperature increases due to the wall heat transfer and viscous dissipation effects.

The traditional chemical rockets are preferred to have a uniform temperature distribution at the throat to minimize the two-dimensional loss of thruster performance (Isp). For rockets supported by a laser beam, the spatial distribution of heat addition is highly nonuniform, and a nonuniform temperature distribution is likely to exit at the throat as shown in Figure 18. Actually, it is required to have some kind of nonuniform temperature distribution around the throat for a practical high performance laser supported thruster (around 10,000 K propellant temperature at the throat), or the thruster wall will be damaged. The heat loading on the thruster wall, which will be discussed later in this paper, is primary due to irradiation from the plasma. A stream of cold propellant near the wall as shown in Figure 18, which results in some loss of rocket performance, is required to cool the wall.

Upstream of the leading edge of the plasma a local minimum in the axial velocity occurs on the centerline where the propellant is unheated by the laser beam. The radial distribution of the axial velocity within the center plasma core region is relatively uniform with the peak axial velocity on the centerline. Large radial variations of the axial velocity is found near the thruster wall where the large radial temperature gradient is also located. The exit temperature and axial velocity on the centerline are 10,700 K and 25,300 m/s, respectively. The predicted vacuum specific impulse for this rocket, with exit area expansion ratio of 4, is 960 secs. With further expansion of this rocket, the estimated specific impulse of this rocket can be approximately 1500 secs.

The isotherms for two other throat radius thrusters operated at 150 kPa pressure, rockets Nos. 2 and 3, are shown in Figure 20. The leading edge and size of these plasmas

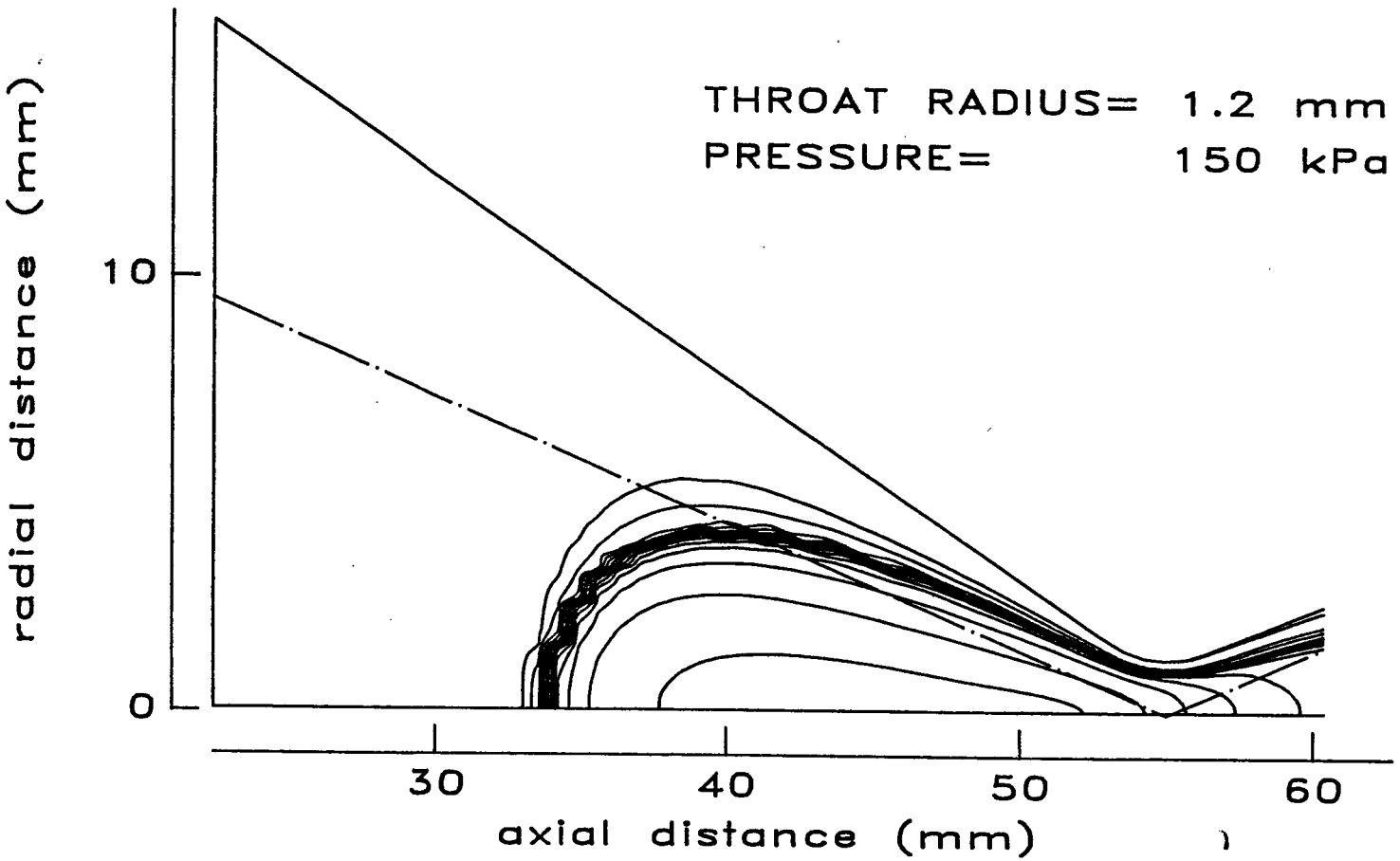

Figure 18. Enlarged view of isotherms for rocket No. 1 (starting from 2,000 K to 15,000 K with 1,000 K increments)

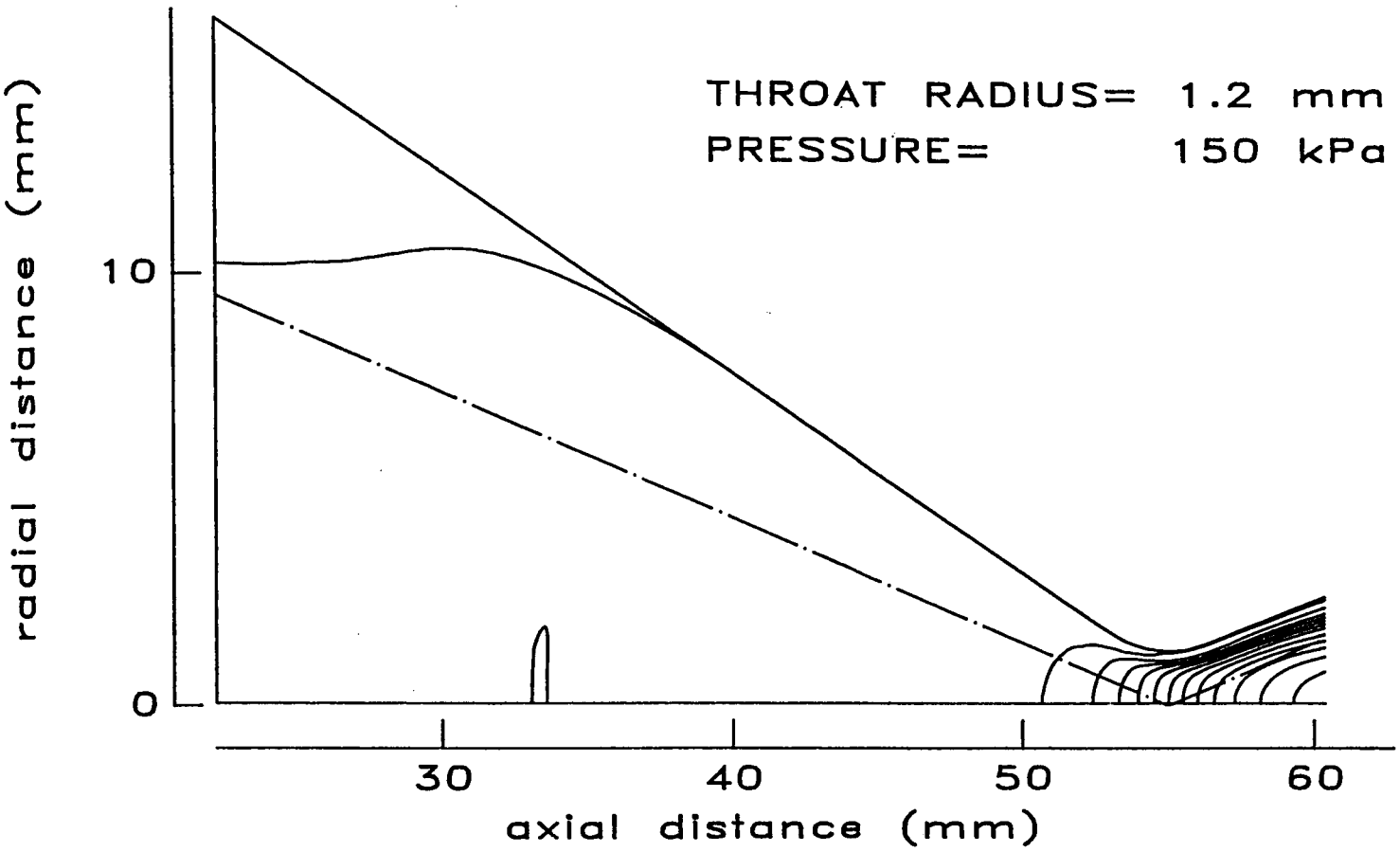

Figure 19. Axial velocity contours for rocket No. 1 (starting from 50 m/s to 24,050 m/s with 2,000 m/s increments)

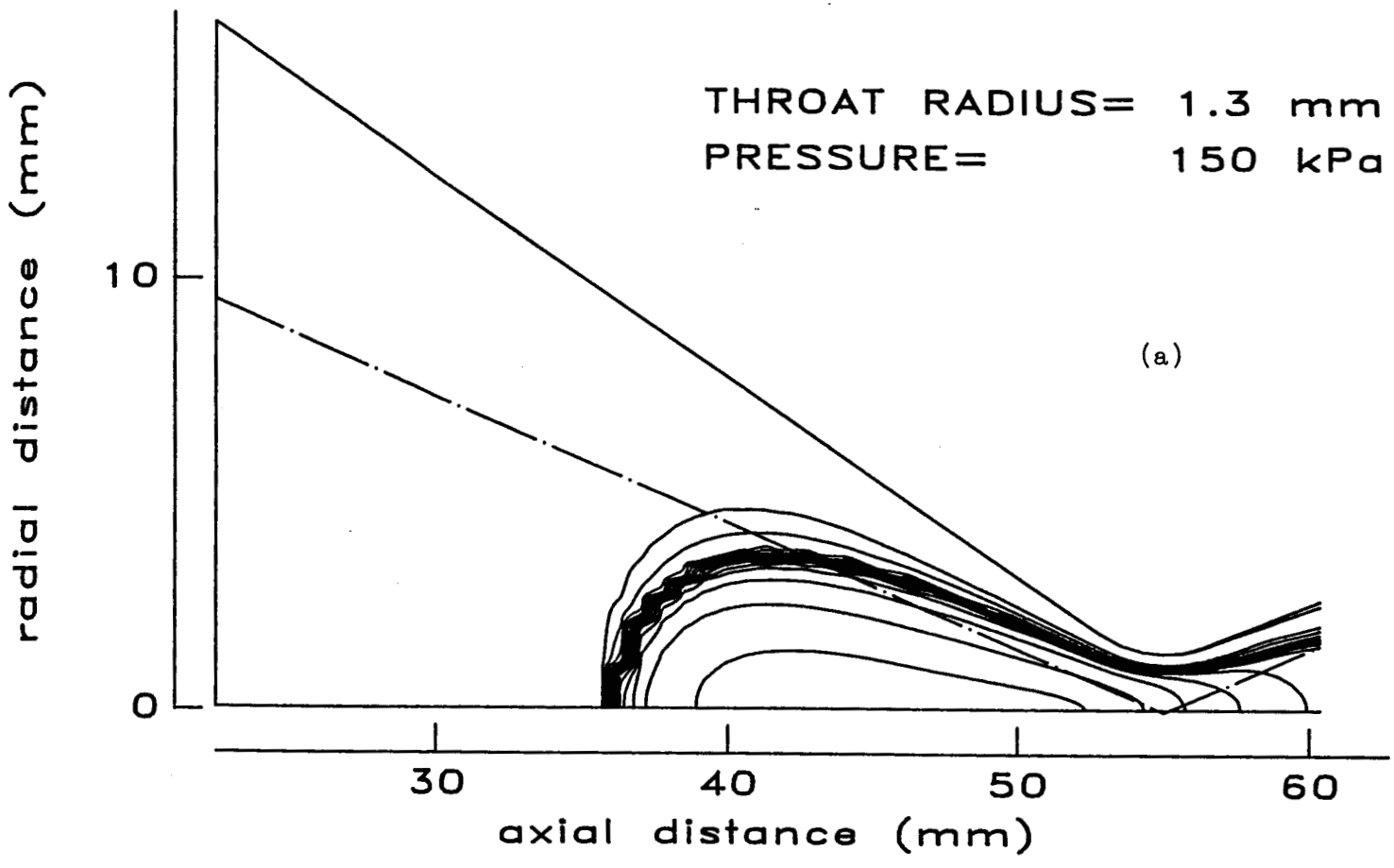

Figure 20-1. Isotherms for rocket (a) rocket No. 2 (b) rocket No. 3 (starting from 2,000 K to 15,000 K with 1,000 K increments)

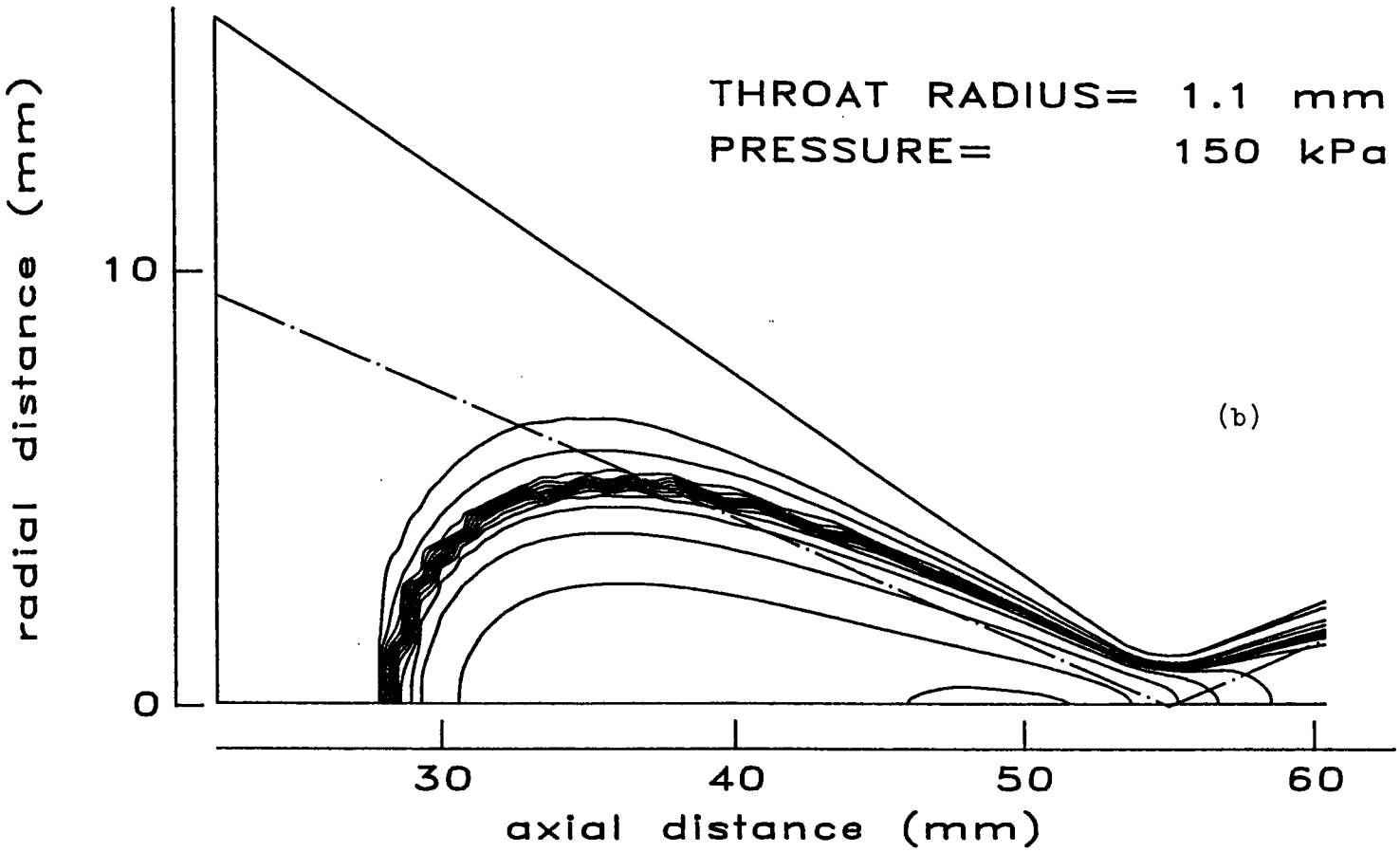

Figure 20-2. Isotherms for rocket (a) rocket No. 2 (b) rocket No. 3 (starting from 2,000 K to 15,000 K with 1,000 K increments)

are different. The mass flowrate, which is directly related to the throat size, is the major controlling factor for the plasma size and position. The mass flow rate of a constant total enthalpy fluid through a choked nozzle is proportional to the throat area. For the laser supported thruster, the propellant temperature and its distribution at the throat are other controlling factors for the mass flow rate. For a smaller throat thruster, a larger portion of the propellant at the throat has a high temperature and this will further reduce its critical mass flowrate. The calculated mass flow rate for cases 1-3, tabulated in Table 2, result from this effect. For a smaller throat thruster, the reduced axial velocity within the subsonic converging section of the thruster allows the plasma to move further upstream along the laser beam and to obtain a larger size, as shown in Figure 20. A detailed discussion of the interaction between the plasma structure and a forced convection flow can be found in References 2,7 and 8.

In the traditional chemical rocket, the total pressure has a minor effect on the expected value of specific impulse. However, in the laser-supported rocket the pressure has a substantial influence on the absorption and radiation processes which directly affect the available enthalpy of the propellant and the heat loading on the thruster wall. Figure 21 shows the isotherms for a 300 kPa inlet pressure thruster, rocket No 4. The absorption coefficient and optically thin thermal radiation for a hydrogen plasma are approximately proportional to the 1.5 power of pressure. With a higher absorption coefficient in this plasma, compared to those of rocket Nos. 1-3, only a very small amount of the laser power directly escapes from the thruster (see Table 2); however, the optically thin radiation from the plasma also increases. This results in a low conversion efficiency from laser power to available thermal power of the propellant. The higher absorption coefficient also results in a plasma which is positioned further upstream against the laser beam. Two local temperature maxima were predicted for this thruster. This results from two competitive processes which determine the local laser intensity: the attenuation by plasma absorption and the increase due to the converging laser beam. References 7-8 contain a detailed discussion of this subject.

The vacuum specific impulse variations with area expansion ratio for the four calculated thrusters are shown in Figure 22. The most advanced chemical rocket has an Isp of about 500 secs, and the calculated Isp for the four laser supported rockets are between 700 and 1020 secs. At the exit of these rockets the ratio between thermal energy and the kinetic energy of the propellant is still relatively high, and further expansion of these rockets will greatly enhance the rocket performance. Although the propellant within the expansion section is expected to be far away from chemical equilibrium, the reasonable Isp is expected to be around 1500 secs for higher expansion ratios using rockets Nos. 1 and 3. The highest Isp among the test cases is 1022 secs from rocket No. 3. As discussed before, this thruster has the propellant almost fully heated at the throat. Thruster No. 1 has a little larger throat than rocket No. 3. and has a very small cold propellant stream near the throat. The calculated Isp of this rocket is only 20 secs less than thruster No. 3. With further increase of throat size, the size of cold stream propellant increases, and the calculated Isp decreases rapidly. The Isp for thruster No. 2 is an example. Rocket No. 4

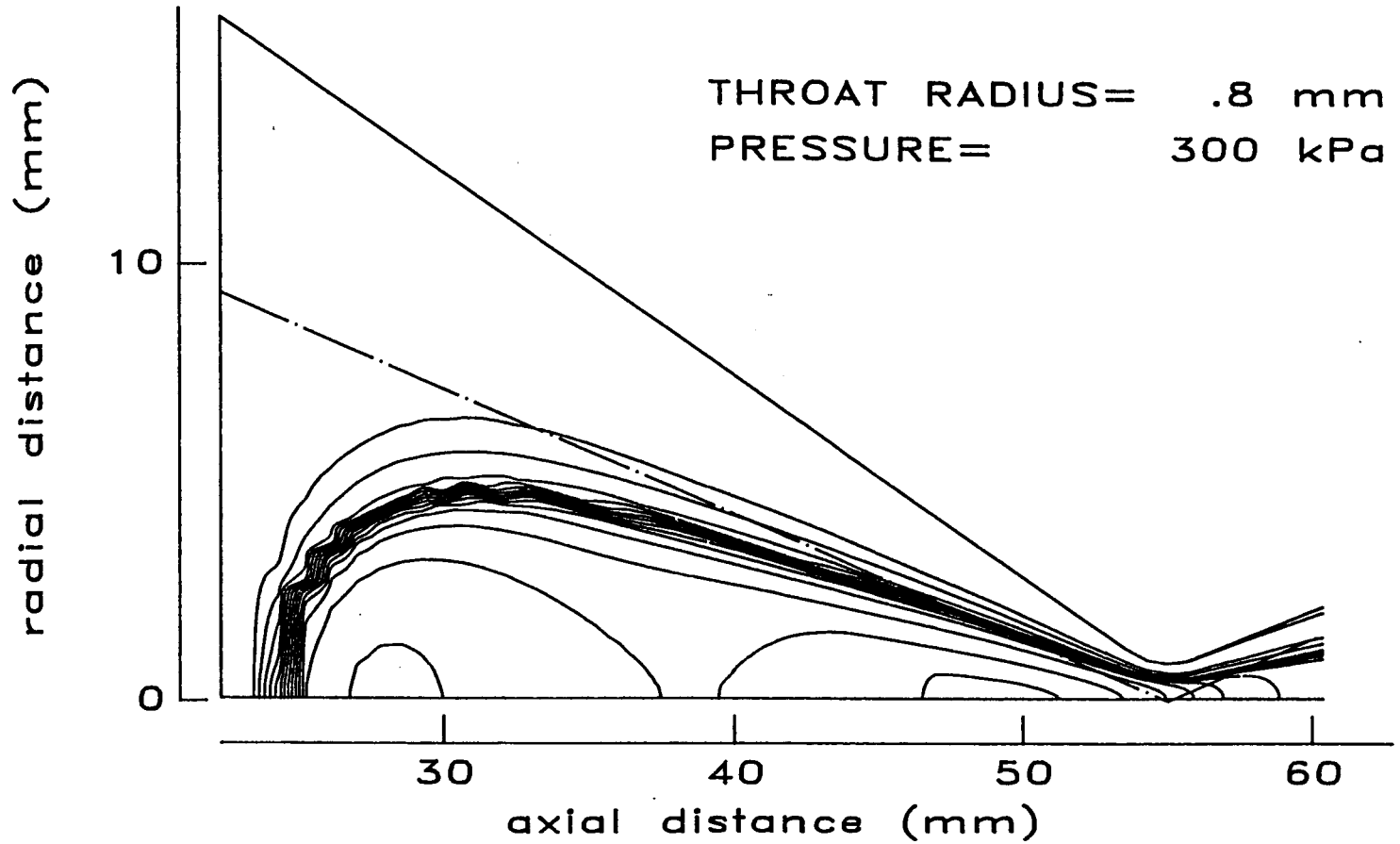

Figure 21. Isotherms for rocket No. 4 (starting from 2,000 K to 15,000 K with 1,000 K increments)

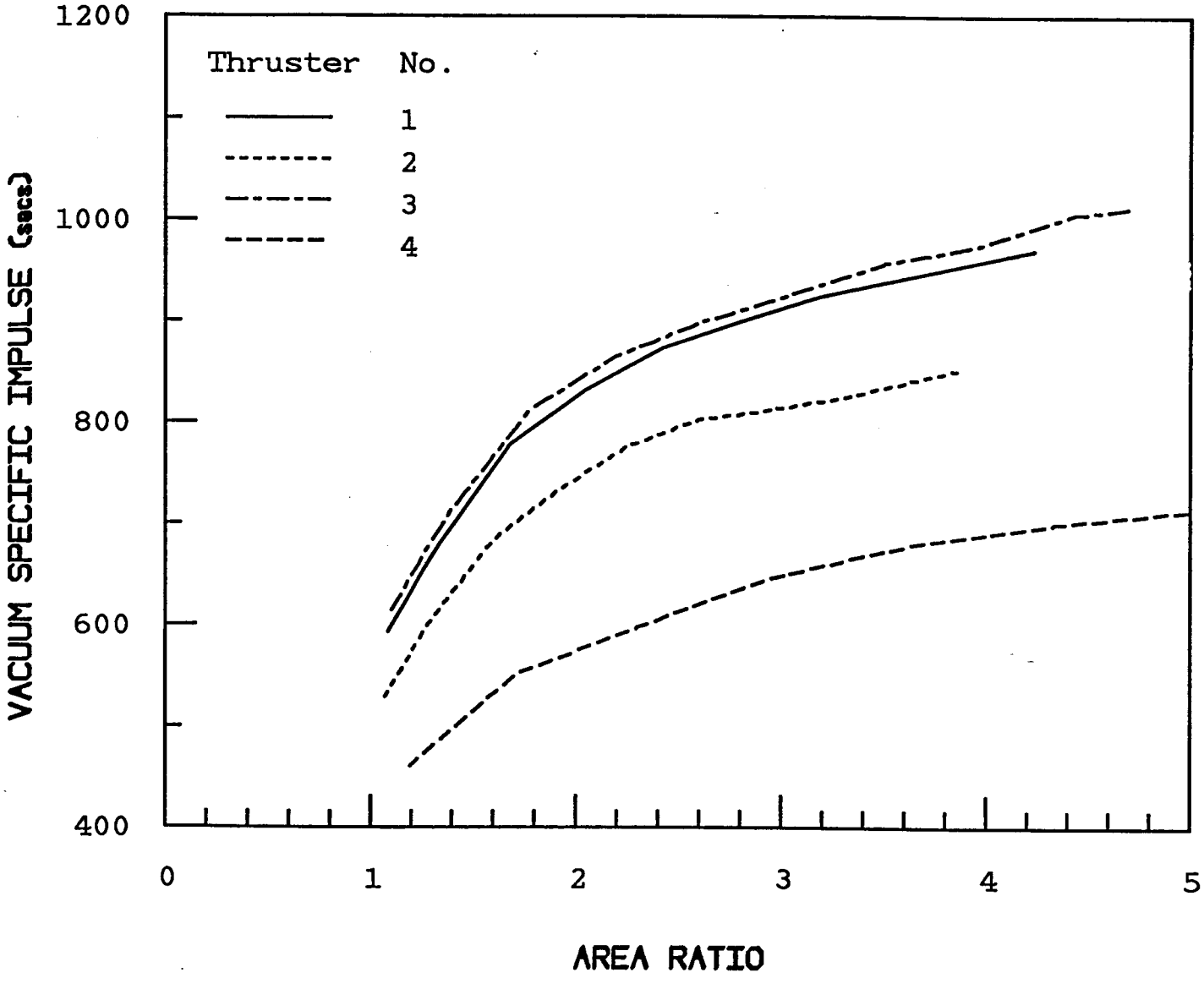

Figure 22. Vacuum specific impulse vs. area expansion ratio

operated at 300 kPa and the plasma occurs further away from the throat than the lower pressure thrusters. This results in a larger cold propellant stream around the throat and in a much lower Isp than the lower pressure thruster.

The heat loading on the inner wall of a good laser thruster should come from the plasma radiation, and a cold stream of propellant near the inner surface will reduce the heat flux through the wall. This heat flux is used to heat the propellant from its storage enthalpy up to the inlet enthalpy. The irradiation along the wall of the calculated rockets are shown in Figure 23. The irradiation first increases from the end of the thruster to where the hot plasma is located, and then decreases monotonically along the axial distance for all test rockets. The maximum irradiation on the wall for all the rockets is almost the same, although the 300 kPa rocket has much higher total irradiation flux on the wall (see Table 2). In order to estimate the radiation heat loading on the wall, the emissivity and absorptivity of the wall surface are needed. If absorptivity is unity, the irradiation will be equal to the wall heat loading. Generally, the absorptivity is less then one, and the radiation heat loading will be smaller and spatially smoothed. The calculated maximum irradiation represents an upper limit of the radiation heat loading, and all maxima are much less then the heat loading for chemical rockets.

Heat loading on the wall is also related to the thruster inlet propellant temperature which is regeneratively heated from the storage temperature. The propellant inlet temperature will influence the rocket performance as long as the cold stream of propellant exists near the wall at the nozzle. Rockets Nos. 1 and 3 have a very limited amount of unheated propellant at the throat, and the Isp for these rockets should not be strongly influenced by the inlet temperature. On the other hand, higher or lower inlet temperature will either increase or decrease the expected Isp significantly for rocket Nos. 2 and 4. An inlet temperature of 1500 K was used for the test rockets, and the expected inlet temperatures vs. three recovery efficiency of irradiation are tabulated in Table 3. Low pressure rockets Nos. 1 and 2 need the recovery efficiency of 30 and 52 percent, respectively, for the adopted inlet temperature, 1500 K. If the irradiation is fully converted to the propellant enthalpy through regenerative heating for these two thrusters, the inlet propellant temperatures will be 2810 K and 2390 K, respectively. For rockets Nos. 3 and 4, the inlet temperatures will be around 3400 K, which is not realistic in a practical device, and probably a radiator would be needed to dissipate the wall heat flux and lower the inlet propellant temperatures.

VII. EFFECTS OF CHEMICAL KINETICS

The developed computer code for the laser-supported thruster calculation only considers the chemically equilibrium conditions. The adopted numerical method is not computationally efficient for highly expanded supersonic flows either. The effect of finite rate chemistry on these rocket performance for maximum area expansion ratio of 25 was evaluated using the TDK code[20]. The adopted kinetics equations are the the same as that considered by McCay et al[21] for one-dimensional analysis. Six different options of the TDK code were considered in this study including two-dimensional equilibrium expansion, two-dimensional

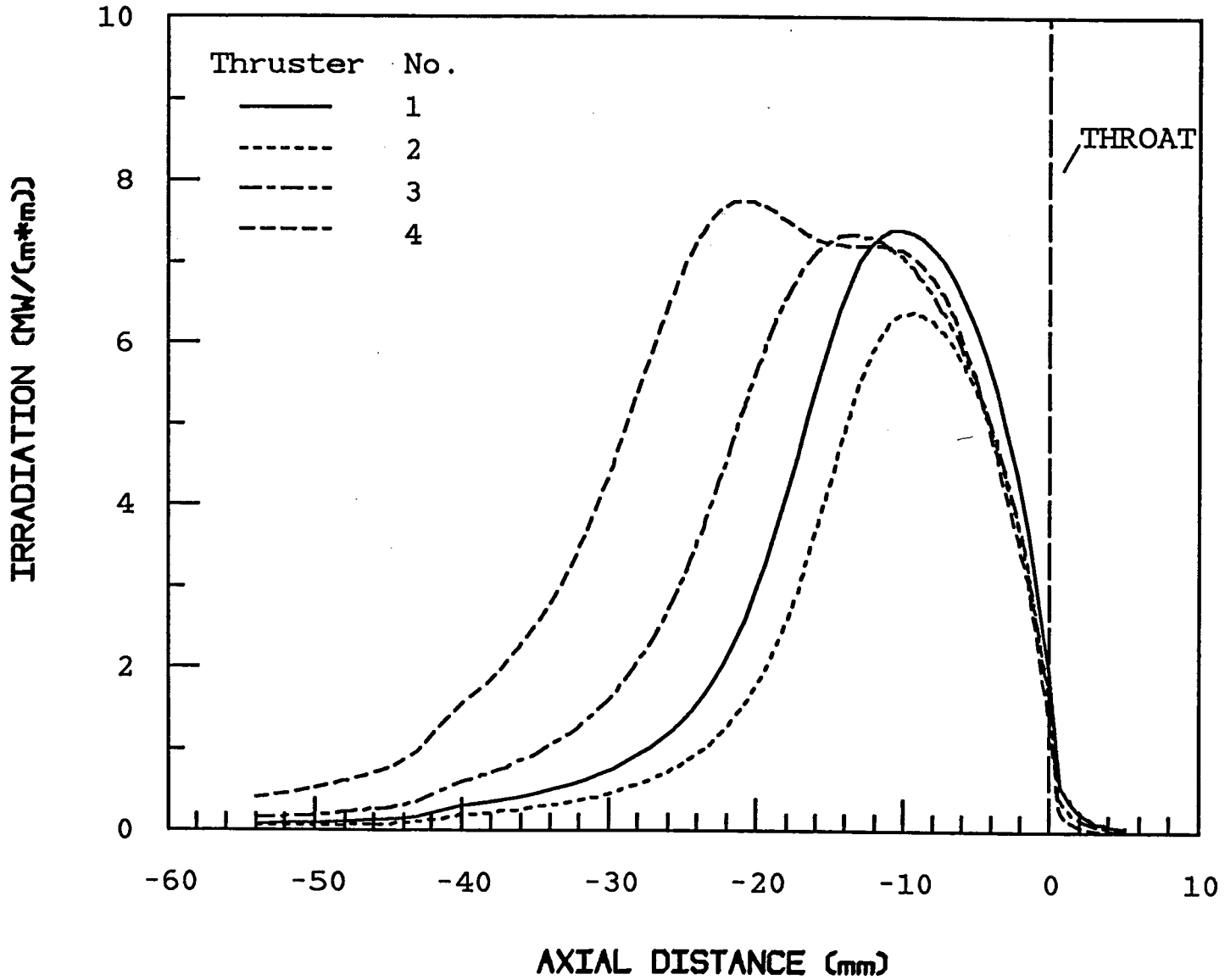

Figure 23. Irradiation along the thruster wall

TABLE II.
Performance of the Tested Rockets

ROCKET NO.	1	2	3	4
Transmitted Laser Power (kW)	4.9	5.7	4.2	0.8
Total Irradiation on Thruster (kW)	7.1	5.1	11.0	19.6
Mass Flow Rate (mg / sec)	90	118	73	121
Vacuum Specific Impulse* (sec)	960	859	980	686
Thrust* (N)	0.85	0.99	0.70	0.80

CG-0692

* at expansion area ratio of 4

TABLE III.
Expected Hydrogen Temperature vs. the Recovery Efficiency of Irradiation on Thruster

EFFICIENCY \ ROCKET NO.	1*	2*	3*	4**
100 %	2810 K	2390 K	3310 K	3430 K
50 %	2290 K	1420 K	2830 K	2950 K
25 %	1295 K	700 K	2220 K	2350 K

CG-0693

* at 150 kPa

** at 300 kPa

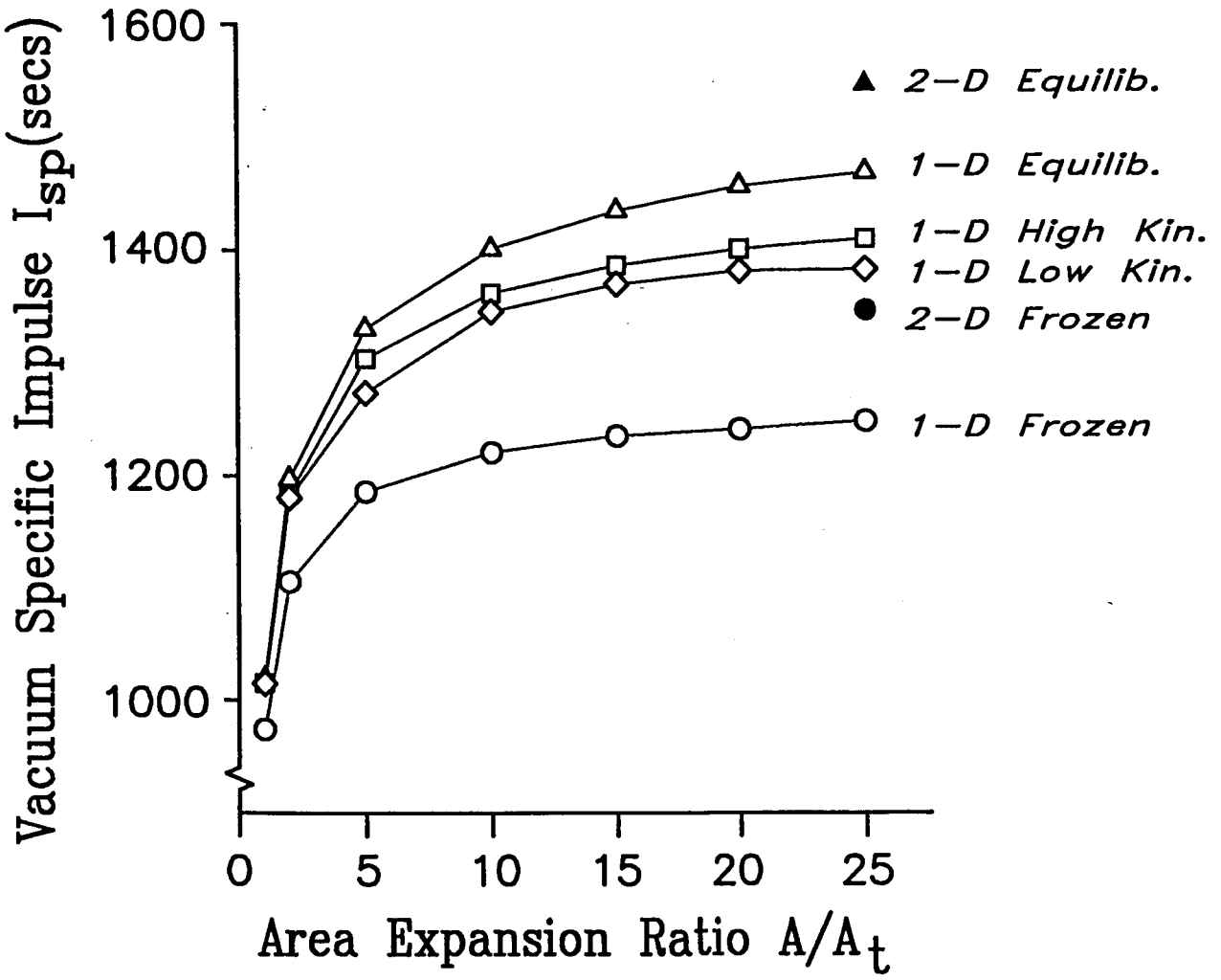

Figure 24. Effect of finite rate chemistry on rocket performance

frozen expansion, one-dimensional equilibrium expansion, one-dimensional frozen expansion, and one-dimensional kinetic expansion using two sets of rates compiled in Ref. 21. We experienced several difficulties during the practice of TDK calculations. For example, the TDK option of the TDK code fail to achieve a converge solution. It is because the fast chemical reaction rate under plasma conditions produces the numerical stiffness.

In order to extract the output from the developed code of laser thruster calculations to fit into the required format for TDK code, some reasonable assumptions are needed. The predicted temperature and velocity profile across the throat (normally 61 grid points) from the developed code was divided into 11 stream tubes. The stagnation enthalpy for each stream tube was calculated. Then this information and chamber stagnation pressure were fed into TDK code with different selected options for rocket performance calculations.

An example of this study for rocket no. 1 is shown in Figure 24. Since the predicted radial temperature profile at throat from the developed code is highly nonuniform and only eleven stream tube were used in the TDK code calculations, some errors may be introduced. The estimated inaccuracy for the above procedure in predicting the Isp value will be around 5 to 10 percent. The calculated values from two-dimensional options are always higher than the value calculated from one-dimensional analysis. The predictions considering finite rate chemistry do not differ too much from the equilibrium calculations. It is because that a large fraction of propellant at throat is in low temperature (between 2,000K to 8,000 K) and is not influenced by finite rate chemistry. The Isp from this thruster is bounded by 1350 and 1550 secs from TDF and TDE calculations.

VIII. SUMMARY AND CONCLUSIONS

The computer code has been developed for the laser-sustained plasma flows. The adopted numerical algorithm has demonstrated the capability to handle complicated flows within a thruster. The physical models have been evaluated using existing experimental data. Through the parametric study of LSP in a constant area pipe, the power conversion efficiency from laser to the propellant and plasma positions were found can be controlled by adjusting the forced convection level and optical arrangements. From this experience, the computer code has been extended for the realistic thruster calculations.

The performance of several realistic thrusters powered by a 30 kW laser has been studied. The results show that the laser supported rocket can have much higher vacuum specific impulse than the traditional chemical rocket. The Isp was in the range of 700 to 1020 secs for four calculated thrusters having an area expansion ratio of four. The irradiation from the plasma to the thruster wall was also calculated, and the estimated maximum heat loading on the thruster is within the range of the chemical rockets. Among four calculated rockets, rocket No. 1 was the best practical rocket. This rocket has nearly the highest vacuum specific impulse among the test rockets, and both the estimated thruster heat loading and the inlet propellant temperature are reasonable. The estimated Isp for this rocket at expansion ratio up to 25 were also considered, and the bound of Isp

is from 1350 to 1550 secs considering the frozen and equilibrium expansion, respectively.

REFERENCES

1. Raizer, Y. P., "Subsonic Propagation of a Light Spark and Threshold Conditions for the Maintenance of Plasma by Radiation," *Soviet Physics - JETP*, Vol. 31, 1970, pp. 1148-1154.
2. Jeng, S-M. and Keefer, D., "Theoretical Investigation of Laser-Sustained Argon Plasmas," Vol. 60, No. 7, pp. 2272-2279 *J. Applied Physics*, 1986.
3. Merkle, C. L., Molvik, G. A. and Choi, Y.-H., "A Two-Dimensional Analysis of Laser Heat Addition in a Constant Absorptivity Gas," *AIAA Journal*, Vol. 23, 1985, pp. 1053-1060.
4. Merkle, C. L., Molvik, G. A. and Shaw, E. J.-H., "Numerical Solution of Strong Radiation Gasdynamics Interactions in a Hydrogen-Seedant Mixture," AIAA Paper No. 85-1554, July, 1985.
5. Welle, R. P., Keefer, D. R. and Peters, C. E., "Energy Conversion Efficiency in High-Flow, Laser-Sustained Argon Plasmas," AIAA paper 86-1077.
6. Keefer, D., Welle, R. and Peters, C. E., "Power Absorption in Laser-Sustained Argon Plasma," *AIAA J.*, Vol.24, No.10, Oct. 1986, pp. 1663-1669.
7. Jeng, S-M. and Keefer, D., "Numerical Study of Laser-Sustained Hydrogen Plasmas in a Forced Convective Flow," *J. Power and Propulsion*, Vol.13, No.3, May-June, 1987, pp. 255-262.
8. Jeng, S-M., Keefer, D., Welle, R., and Peters, C., "Numerical Study of Laser-Sustained Argon Plasmas in a Forced Convective Flow," AIAA paper 86-1078, May, 1986.
9. Jeng, S-M. and Keefer, D., "Influence of Laser Beam Geometry and Wavelength on Laser-Sustained Plasmas," AIAA paper 87-1409, June, 1987.
10. Kemp, N. H. and Root, R. G., "Analytical Study of Laser-Supported Combustion Waves in Hydrogen," *Journal of Energy*, Vol. 3, 1979, pp. 40-49.
11. Caledonia, G. E., Wu, P. K. S. and Pirri, A. N., "Radiant Energy Absorption Studies for Laser Propagation," NASA CR-134809, 1975.
12. Shyy W, "A Numerical Study of Annular Dump Diffuser Flows," *Computer Methods In Applied Mechanics And Engineering*, Vol. 53, pp. 47-65, 1985.
13. Rhie, C. M., and Chow, W. L., "Numerical Study of the Turbulent Flow Past an Airfoil with Trailing Edge Separation," *AIAA J.*, Vol. 21, No. 11, pp. 1525-1532, Nov. 1983.
14. Rhie, C. M. "A Pressure Based Navier-Stokes Solver Using the Multigrid Method, " AIAA paper 86-0207, AIAA 24th Aerospace Sciences Meeting, Reno, Nevada, Jan. 1986.
15. Patankar, S. V., *Numerical Heat Transfer and Fluid Flow*, New Hemisphere, Washington, D.C., 1980.
16. Issa, R. I., "Solution of the implicitly Discretized Fluid Flow Equations by Operator-Splitting," *J. Computational Physics*, Vol. 62, pp. 40-65, 1986.
17. Issa, R. I., "Solution of the implicitly Discretised Fluid Flow Equations by Operator-Splitting," *J. Computational Physics*, Vol. 62, pp. 40-65, 1986.
    Issa, R. I., Gosman, A. D., and Watkins, A.P., "The Computation of Compressible and Incompressible Recirculating Flows by a Non-iterative Implicit Scheme," *J. Computational Physics*, Vol. 62, pp. 66-88, 1986.

19. Jeng, S-M. and Keefer, D., "A Theoretical Investigation of Laser-Sustained Plasmas Thruster," AIAA paper 87-0383, JAN., 1987.
20 Nickerson, G. R., Dang, L. D. and Coats, C. E., "The Two-Dimensional Kinetics (TDK) Reference Computer Program," Final Report for NASA contract no. NAS8-35931, 1985.
21 McCay, T. D. and Dexter, C. E., "Chemical Kinetic Performance Losses for a Hydrogen Laser Thermal Thruster," AIAA paper 85-0907, 1985.
22 Shamroth, S. J., McDonald, H., and Briley, W. R., " Prediction of Cascade Flow Fields Using the Averaged Navier-Stokes Equations," *J.Engr. for Gas Turbine and Power*, vol. 106, p383, 1989.

APPENDIX A

Numerical Method

APPENDIX A

A finite volume based computational scheme for a body-fitted coordinate system has been applied to the steady-state, axisymmetric transport equations in conservative form. The method employs a nonstaggered grid such that the velocity components and all variables are defined at common grid positions. A general transformation was used to transform the governing equations from the nonorthogonal, body-fitted, physical grid system to a new orthogonal grid mesh.

The development of the numerical scheme closely follows Rhie and Chow[13,14]. A generalized differential equation in cylindrical coordinates will be transformed to the computational grid and the results then applied to the specific conservation equations.

GENERAL FORMULATION

The generalized transport equation may be written as

$$\frac{\partial}{\partial t}(\rho\phi) + div(\rho\vec{V}\phi) = div(\Gamma_\phi\ grad\ \phi) + R_\phi(r,x) \qquad (A.1)$$

For steady-state conditions and axisymmetric, cylindrical coordinates, equation (A.1) becomes

$$\frac{\partial}{\partial x}(r\rho u\phi) + \frac{\partial}{\partial r}(r\rho v\phi) = \frac{\partial}{\partial x}(r\Gamma_\phi\frac{\partial\phi}{\partial x}) + \frac{\partial}{\partial r}(r\Gamma_\phi\frac{\partial\phi}{\partial r}) + rR_\phi(r,x) \qquad (A.2)$$

A general transformation to the orthogonal plane may be employed by introducing the new variables ξ and η (see Fig. 2) such that $\xi = \xi(r,x)$ and $\eta = \eta(r,x)$. It follows that the partial derivatives of any function f are transformed by the following relations.

$$f_x = (r_\eta f_\xi - r_\xi f_\eta)/J \qquad (A.3)$$

$$f_y = (-x_\eta f_\xi + x_\xi f_\eta)/J \qquad (A.4)$$

where J is the transformation Jacobian.

$$J = x_\xi r_\eta - x_\eta r_\xi \tag{A.5}$$

Introducing the relationships,

$$U = u r_\eta - v x_\eta \tag{A.6}$$

$$V = v x_\xi - v r_\xi \tag{A.7}$$

$$q_1 = x_\eta^2 + r_\eta^2 \tag{A.8}$$

$$q_2 = x_\xi x_\eta + r_\xi r_\eta \tag{A.9}$$

$$q_3 = x_\xi^2 + r_\xi^2 \tag{A.10}$$

produces the generalized equation in ξ and η coordinates.

$$\frac{1}{J}\frac{\partial}{\partial \xi}(r\rho U\phi) + \frac{1}{J}\frac{\partial}{\partial \eta}(r\rho V\phi) = \frac{1}{J}\frac{\partial}{\partial \xi}\left[\frac{\Gamma_\phi r}{J}(q_1\phi_\xi - q_2\phi_\eta)\right] + \frac{1}{J}\frac{\partial}{\partial \eta}\left[\frac{\Gamma_\phi r}{J}(-q_2\phi_\xi + q_3\phi_\eta)\right] + rS_\phi(\eta,\xi) \tag{A.11}$$

Integrating the transformed equation over a control volume shown in Fig. 2(b) gives

$$\int_w^e \int_s^n \int_o^{2\pi} \left\{\frac{1}{J}\frac{\partial}{\partial \xi}(r\rho U\phi) + \frac{1}{J}\frac{\partial}{\partial \eta}(r\rho V\phi) - \frac{1}{J}\frac{\partial}{\partial \xi}\left[\frac{\Gamma_\phi r}{J}(q_1\phi_\xi - q_2\phi_\eta)\right] - \frac{1}{J}\frac{\partial}{\partial \eta}\left[\frac{\Gamma_\phi r}{J}(-q_2\phi_\xi + q_3\phi_\eta)\right] - rS_\phi(\eta,\xi)\right\} d\eta d\xi d\zeta = 0 \tag{A.12}$$

where ζ represents the direction of rotation about the axis of symmetry. Carrying out the integration yields

$$\frac{1}{J}(r\rho U\phi)_e\Delta\eta - \frac{1}{J}(r\rho U\phi)_w\Delta\eta + \frac{1}{J}(r\rho V\phi)_n\Delta\xi - \frac{1}{J}(r\rho V\phi)_s\Delta\xi$$
$$-\frac{1}{J}\left[\frac{\Gamma_\phi r}{J}(q_1\phi_\xi - q_2\phi_\eta)\right]_e\Delta\eta + \frac{1}{J}\left[\frac{\Gamma_\phi r}{J}(q_1\phi_\xi - q_2\phi_\eta)\right]_w\Delta\eta$$
$$-\frac{1}{J}\left[\frac{\Gamma_\phi r}{J}(-q_2\phi_\xi + q_3\phi_\eta)\right]_n\Delta\xi + \frac{1}{J}\left[\frac{\Gamma_\phi r}{J}(-q_2\phi_\xi + q_3\phi_\eta)\right]_s\Delta\xi$$
$$-rS_\phi(\eta,\xi)\Delta\eta\Delta\xi = 0 \qquad (A.13)$$

Let $\Delta\eta = \Delta\xi = 1$ in the transformed plane for convenience and multiply through by J to get the finite difference approximation form for the integral conservation equation.

$$(r\rho U\phi)_w^e + (r\rho V\phi)_s^n = \left[\frac{\Gamma_\phi r}{J}(q_1\phi_\xi - q_2\phi_\eta)\right]_w^e$$
$$\left[\frac{\Gamma_\phi r}{J}(-q_2\phi_\xi + q_3\phi_\eta)\right]_s^n + rJS_\phi(\eta,\xi) \qquad (A.14)$$

In the preceding equation, the small letters e, w, n, s represent the control volume interfaces. The flow properties there must be interpolated from the known values at surrounding nodes denoted by capital letters. Assuming a piecewise-linear profile for ϕ between the nodes yields the following approximations.

$$(r\rho U\phi)_e \approx (r\rho U)_e\frac{1}{2}(\phi_E + \phi_P) \qquad (A.15)$$

$$(r\rho U\phi)_w \approx (r\rho U)_w\frac{1}{2}(\phi_P + \phi_W) \qquad (A.16)$$

$$(r\rho V\phi)_n \approx (r\rho V)_n\frac{1}{2}(\phi_N + \phi_P) \qquad (A.17)$$

$$(r\rho V\phi)_s \approx (r\rho V)_s\frac{1}{2}(\phi_P + \phi_S) \qquad (A.18)$$

Also,

$$\left(\frac{\Gamma_\phi r}{J}\right)_e (q_1\phi_\xi)_e \approx \left(\frac{\Gamma_\phi r}{J} q_1\right)_e \frac{(\phi_E - \phi_P)}{\Delta\xi} \qquad (A.19)$$

$$\left(\frac{\Gamma_\phi r}{J}\right)_w (q_1\phi_\xi)_e \approx \left(\frac{\Gamma_\phi r}{J} q_1\right)_e \frac{(\phi_P - \phi_W)}{\Delta\xi} \qquad (A.20)$$

$$\left(\frac{\Gamma_\phi r}{J}\right)_n (q_3\phi_\eta)_n \approx \left(\frac{\Gamma_\phi r}{J} q_3\right)_n \frac{(\phi_N - \phi_P)}{\Delta\eta} \qquad (A.21)$$

$$\left(\frac{\Gamma_\phi r}{J}\right)_s (q_3\phi_\eta)_s \approx \left(\frac{\Gamma_\phi r}{J} q_3\right)_s \frac{(\phi_P - \phi_S)}{\Delta\eta} \qquad (A.22)$$

Values for $(r\rho U)$, $(r\rho V)$, $(\Gamma_\phi r q_1/J)$ and, $(\Gamma_\phi r q_3/J)$ are obtained using a hybrid scheme which will be discussed. in the next section. The value of $1/2$ which arises in equations (A. 15) - (A.18) is the result of locating the cell interface midway between nodes.

Making the appropriate substitutions into equation (A.14) yields

$$\left(\frac{r\rho U}{2}\right)_e(\phi_E + \phi_P) - \left(\frac{r\rho U}{2}\right)_w(\phi_P + \phi_W) + \left(\frac{r\rho V}{2}\right)_n(\phi_N + \phi_P) - \left(\frac{r\rho V}{2}\right)_s(\phi_P + \phi_S)$$

$$= \left(\frac{\Gamma_\phi r q_1}{J}\right)_e(\phi_E - \phi_P) - \left(\frac{\Gamma_\phi r q_1}{J}\right)(\phi_P - \phi_W) + \left(\frac{\Gamma_\phi r q_3}{J}\right)_n(\phi_N - \phi_P) - \left(\frac{\Gamma_\phi r q_3}{J}\right)_s(\phi_P - \phi_S)$$

$$- \left[\left(\frac{\Gamma_\phi r q_2}{J}\phi_\eta\right)_w^e + \left(\frac{\Gamma_\phi r q_2}{J}\phi_\xi\right)_s^n\right] + rJS_\phi(\eta,\xi) \qquad (A.23)$$

By taking all terms involving ϕ_P to the left hand side of the equation and all other terms to the right hand side, a relationship between ϕ_P and its neighbors is obtained.

$$A_P\phi_P = A_E\phi_E + A_W\phi_W + A_N\phi_N + A_S\phi_S$$
$$- \left[\left(\frac{\Gamma_\phi r q_2}{J}\phi_\eta\right)_w^e + \left(\frac{\Gamma_\phi r q_2}{J}\phi_\xi\right)_s^n\right] + rJS_\phi(\eta,\xi) \qquad (A.24)$$

where

$$A_E = \left(\frac{\Gamma_\phi r q_1}{J}\right)_e - \left(\frac{r\rho U}{2}\right)_e \tag{A.25}$$

$$A_W = \left(\frac{\Gamma_\phi r q_1}{J}\right)_w + \left(\frac{r\rho U}{2}\right)_w \tag{A.26}$$

$$A_N = \left(\frac{\Gamma_\phi r q_3}{J}\right)_n - \left(\frac{r\rho V}{2}\right)_n \tag{A.27}$$

$$A_S = \left(\frac{\Gamma_\phi r q_3}{J}\right)_s + \left(\frac{r\rho V}{2}\right)_s \tag{A.28}$$

$$A_P = A_E + A_W + A_N + A_S + (r\rho U)_e - (r\rho U)_w + (r\rho V)_n - (r\rho V)_s \tag{A.29}$$

The quantities contained within the bracket in equation (A.24) result from the cross derivatives in the diffusion terms for the nonorthogonal coordinate system. Since these terms are small, they will be treated as known quantities and included with the source term. They may be evaluated through the following approximations.

$$\left(\frac{\Gamma_\phi r q_2}{J}\phi_\eta\right)_e \approx \left(\frac{\Gamma_\phi r q_2}{J}\right)_e \frac{1}{4}(\phi_{NE} - \phi_{SE} + \phi_N - \phi_S) \tag{A.30}$$

$$\left(\frac{\Gamma_\phi r q_2}{J}\phi_\eta\right)_w \approx \left(\frac{\Gamma_\phi r q_2}{J}\right)_w \frac{1}{4}(\phi_{NW} - \phi_{SW} + \phi_N - \phi_S) \tag{A.31}$$

$$\left(\frac{\Gamma_\phi r q_2}{J}\phi_\xi\right)_n \approx \left(\frac{\Gamma_\phi r q_2}{J}\right)_n \frac{1}{4}(\phi_{NE} - \phi_{NW} + \phi_E - \phi_W) \tag{A.32}$$

$$\left(\frac{\Gamma_\phi r q_2}{J}\phi_\xi\right)_s \approx \left(\frac{\Gamma_\phi r q_2}{J}\right)_s \frac{1}{4}(\phi_{SE} - \phi_{SW} + \phi_E - \phi_W) \tag{A.33}$$

Again, terms such as $(\Gamma_\phi r q_2/J)$ are evaluated by linear interpolation between nodes.

In transforming the source term $R_\phi(r,x)$ to the orthogonal coordinates $S_\phi(\eta,\xi)$, equations (A.3) and (A.4) should be applied in order to obtain the correct form. The source term may also be split to account for a linear dependence on the dependent variable ϕ.

$$\bar{S} = S_C + S_P \phi_p P \tag{A.34}$$

In equation (A.34), $\bar{S}$ is the average value of the source term through the control volume, S_C is considered to be the constant part of $\bar{S}$, and S_P becomes a coefficient of ϕ. Equation (A.24) takes the following form.

$$A_P \phi_P = A_E \phi_E + A_W \phi_W + A_N \phi_N + A_S \phi_S + S_C + S_P \phi_P \tag{A.35}$$

Here, S_C now contains the terms involving the cross derivatives in the diffusion terms for the nonorthogonal coordinate system in addition to the constant part of $\bar{S}$, and S_P must be negative to insure stability and to prevent physically unrealistic solutions.

HYBRID SCHEME

Special attention is also required concerning the evaluation of the A neighbor coefficients. Central differencing may be grossly inaccurate for these terms due to the non-linearities in the transport equations and because large convection terms mean that the ϕ-profile is far from linear between between nodes.

A suitable formulation for evaluating these coefficients is the hybrid scheme which is identically the central difference formulation when the cell Reynolds number is less than 2 but reproduces the first order upwind scheme for a cell Reynolds number greater than 2. See Patankar[15] for a detailed discussion. The hybrid scheme produces the following formulations.

$$A_E = max\left[\left(\frac{\Gamma r q_1}{J}\right)_e, \left(\frac{r\rho U}{2}\right)_e\right] - \left(\frac{r\rho U}{2}\right)_e \tag{A.36}$$

$$A_W = max\left[\left(\frac{\Gamma r q_1}{J}\right)_w, \left(\frac{r\rho U}{2}\right)_w\right] + \left(\frac{r\rho U}{2}\right)_w \tag{A.37}$$

$$A_N = max\left[\left(\frac{\Gamma r q_3}{J}\right)_n, \left(\frac{r\rho V}{2}\right)_n\right] - \left(\frac{r\rho V}{2}\right)_n \tag{A.38}$$

$$A_S = max\left[\left(\frac{\Gamma r q_3}{J}\right)_s, \left(\frac{r\rho V}{2}\right)_s\right] + \left(\frac{r\rho V}{2}\right)_s \qquad (A.39)$$

STABILITY

Stability considerations for the discretized equation must now be examined. From equation (A.29), it is apparent that the A_P coefficient depends on its neighbor coefficients and the net mass source over the control volume. At steady state, the net mass source should be zero in a converged solution, but during the iteration process this may not be true. Also, a situation could arise such that all the neighbor coefficients are zero. Thus, the combination of terms which determine A_P could at times become zero causing the finite difference solution for ϕ to become singular. Clearly, this must not be allowed to occur.

From inspection of equation (A.29), it is evident that, if the net mass source is positive, mass is being lost from the control volume and is carrying the property ϕ out of the cell. In this case, the net mass source may be set to zero, and a new term added corresponding to the mass flow rate out, carrying the old property (ϕ_P^*). For a negative net mass source, no adjustment is necessary. Introducing the above modification yields a new discretized equation.

$$A_P\phi_P = A_E\phi_E + A_W\phi_W + A_N\phi_N + A_S\phi_S + S_C + S_P\phi_P \qquad (A.40)$$

$$A_P = A_E + A_N + A_W + A_S \qquad (A.41)$$

$$S_C = max\left[\left\{(r\rho U)_e - (r\rho U)_w + (r\rho V)_n - (r\rho V)_s\right\}, O\right]\phi_P^* + S_C^{org} \qquad (A.42)$$

$$S_P = -max\left[\left\{(r\rho U)_e - (r\rho U)_w + (r\rho V)_n - (r\rho V)_s\right\}, O\right] + S_P^{org} \qquad (A.43)$$

The terms S_C^{org} and S_P^{org} correspond to the original source terms in equation (A.35), and ϕ_P^* corresponds to the previous iteration result for the dependent variable.

RELAXATION

The above algorithm will guarantee the convergence of linear differential equations, but this criterion may not be applied for nonlinear differential equations. To prevent divergence and to slow down the changes between iterations, underrelaxation of the dependent variable is employed. The discretization equation (A.40) is first reformulated to give

$$(A_P - S_P)\phi_P = \sum A\phi + S_C \tag{A.44}$$

where the sum of the product of the neighbor coefficient and dependent variable has been represented by the summation symbol. Dividing through by $(A_P - S_P)$,

$$\phi_P = \frac{\sum A\phi + S_C}{A_P - S_P} \tag{A.45}$$

Now, if ϕ_P^* is denoted as the old result from the previous iteration and added to and subtracted from the RHS of equation (A.45) the result is

$$\phi_P = \phi_P^* + \left(\frac{\sum A\phi + S_C}{A_P - S_P} - \phi_P^*\right) \tag{A.46}$$

Introducing a relaxation factor α gives

$$\phi_P = \phi_P^* + \alpha\left(\frac{\sum A\phi + S_C}{A_P - S_P} - \phi_P^*\right) \tag{A.47}$$

Multiply through by $(A_P - S_P)$.

$$(A_P - S_P)\phi_P = (A_P - S_P)\phi_P^* + \alpha\left[\sum A\phi + S_C - (A_P - S_P)\phi_P^*\right] \tag{A.48}$$

Finally, divide through by α and rearrange to get

$$\frac{(A_P - S_P)}{\alpha}\phi_P = \sum A\phi + S_C + (1-\alpha)\frac{(A_P - S_P)}{\alpha}\phi_P^* \tag{A.49}$$

This is the new discretization equation to be solved for ϕ_P. The general formulation has been completed and the results may now be applied to the governing transport equations.

EQUATIONS OF MOTION

The steady-state, laminar Navier-Stokes equations and the steady-state continuity equation are solved to determine the fluid motion. The momentum equation is expressed in general transport form and solved for the velocity components. The continuity equation, however, must be reformulated into a pressure correction equation which becomes appropriately coupled to the momentum equations.

The solution procedure used to solve these pressure coupled equations is a marriage between the algorithm developed by Rhie [14] and the PISO method of Issa[16–18]. The basic idea is to correct the mass flux obtained from the solution of the momentum equations such that the discretized pressure equation becomes a transport equation for compressible flow instead of a Poisson equation. The split operator concept of PISO is utilized to solve the pressure correction equation.

The development of the discretized momentum equations begins by writing them in cylindrical coordinates.

$$\frac{\partial}{\partial x}(r\rho uu) + \frac{\partial}{\partial r}(r\rho vu) = \frac{\partial}{\partial x}(r\mu\frac{\partial u}{\partial x}) + \frac{\partial}{\partial r}(r\mu\frac{\partial u}{\partial r}) - r\frac{\partial P}{\partial x} + rR_u(r,x) \qquad (A.50)$$

$$\frac{\partial}{\partial x}(r\rho uv) + \frac{\partial}{\partial r}(r\rho vv) = \frac{\partial}{\partial x}(r\mu\frac{\partial v}{\partial x}) + \frac{\partial}{\partial r}(r\mu\frac{\partial v}{\partial r}) - r\frac{\partial P}{\partial r} + rR_v(r,x) \qquad (A.51)$$

where the terms involving the pressure gradients are a part of the source term. From comparison with equation (A.2), the parameters for the ξ-direction momentum are $\phi = u$ and $\Gamma = \mu$, and the parameters for the η-direction momentum are, in a similar manner, $\phi = v$ and $\Gamma = \mu$.

Transforming to the orthogonal grid yields.

$$A_P u_P = \sum Au - \left[\left(\frac{\mu r q_2}{J}\frac{\partial u}{\partial \eta}\right)_e^w + \left(\frac{\mu r q_2}{J}\frac{\partial u}{\partial \xi}\right)_s^n\right] + \left[-r\frac{\partial r}{\partial \eta}\frac{\partial P}{\partial \xi} + r\frac{\partial r}{\partial \xi}\frac{\partial P}{\partial \eta}\right] + rJS_u(\eta,\xi) \qquad (A.52)$$

$$A_P v_P = \sum Av - \left[\left(\frac{\mu r q_2}{J}\frac{\partial v}{\partial \eta}\right)_e^w + \left(\frac{\mu r q_2}{J}\frac{\partial v}{\partial \xi}\right)_s^n\right]$$
$$+\left[r\frac{\partial x}{\partial \eta}\frac{\partial P}{\partial \xi} - r\frac{\partial x}{\partial \xi}\frac{\partial P}{\partial \eta}\right] + rJS_v(\eta,\xi) \qquad (A.53)$$

where the terms inside the brackets are considered constant and taken as part of the source term.

Following the formulation of equation (A.40) and employing the underrelaxation technique previously discussed, equations (A.52) and (A.53) take the following discretized form for the dependent variables u and v respectively.

$$\frac{(A_P - S_P)}{\alpha}u_P = \sum Au + S_C + (1-\alpha)\frac{(A_P - S_P)}{\alpha}u_P^* \qquad (A.54)$$

$$\frac{(A_P - S_P)}{\alpha}v_P = \sum Av + S_C + (1-\alpha)\frac{(A_P - S_P)}{\alpha}v_P^* \qquad (A.55)$$

Note that the coefficients and source terms in the above relationships are unique with respect to the dependent variable. The underrelaxation factors need not coincide either. The dependent variables u and v are solved for from the above discretization equations.

PRESSURE CORRECTION EQUATION

As previously stated, the split operator concept of Issa [16–18], as developed in the algorithm of Rhie [14,15], is implemented in this work to solve the coupled momentum and continuity equations. The fundamental approach is to correct the preliminary mass flux through the following perturbation relationship.

$$r\rho G_i = r(\rho^* + \rho')(G_i^* + G_i') \approx r\rho' G_i^* + r\rho^*(G_i^* + G_i') \qquad (A.56)$$

The variable G_i denotes the contravariant velocity, and the superscripts *, $'$ represent the intermediate iteration values and the correction increment, respectively. The perturbation relationship may then be combined with the continuity equation through a series of split operations producing a sequence of pressure correction equations in transport form; thus, the correction equations may be discretized in

the same manner as the previously developed method for the general, transport differential equation. The solution of these correction equations gives velocity and pressure fields which satisfy both the momentum and continuity equations. An important characteristic of this method is the ability to handle both incompressible and compressible flow regimes over the entire flow field. A formal derivation of the procedure follows.

First, recall relations (A.6) and (A.7) which relate the contravariant velocity components to the physical velocity components and substitute for u and v from the momentum equations (A.52) and (A.53). The results are

$$U = \left[H_\xi(u,v) - B_\xi \Delta_\xi P - C_\xi \Delta_\eta P + \bar{S}_\xi \right] \tag{A.57}$$

$$H_\xi(u,v) = \frac{\partial r}{\partial \eta} \frac{\sum Au}{A_p^u} - \frac{\partial x}{\partial \eta} \frac{\sum Av}{A_p^v} \tag{A.58}$$

$$B_\xi = \frac{r}{A_p^u} \frac{\partial r}{\partial \eta} \frac{\partial r}{\partial \eta} + \frac{r}{A_p^v} \frac{\partial x}{\partial \eta} \frac{\partial x}{\partial \eta} \tag{A.59}$$

$$C_\xi = -\frac{r}{A_p^u} \frac{\partial r}{\partial \xi} \frac{\partial r}{\partial \eta} - \frac{r}{A_p^v} \frac{\partial x}{\partial \xi} \frac{\partial x}{\partial \eta} \tag{A.60}$$

$$\bar{S}_\xi = \frac{\partial r}{\partial \eta} \frac{\bar{S}u}{A_p^u} - \frac{\partial x}{\partial \eta} \frac{\bar{S}}{A_p^v} \tag{A.61}$$

and

$$V = \left[H_\eta(u,v) - B_\eta \Delta_\eta P - C_\eta \Delta_\xi P + \bar{S}_\eta \right] \tag{A.62}$$

$$H_\eta(u,v) = \frac{\partial x}{\partial \xi} \frac{\sum Av}{A_p^v} - \frac{\partial r}{\partial \xi} \frac{\sum Au}{A_p^u} \tag{A.63}$$

$$B_\eta(u,v) = \frac{r}{A_p^v} \frac{\partial x}{\partial \xi} \frac{\partial x}{\partial \xi} + \frac{r}{A_p^u} \frac{\partial r}{\partial \xi} \frac{\partial r}{\partial \xi} \tag{A.64}$$

$$C_\eta(u,v) = -\frac{r}{A_p^v} \frac{\partial x}{\partial \eta} \frac{\partial x}{\partial \xi} - \frac{r}{A_p^u} \frac{\partial r}{\partial \eta} \frac{\partial r}{\partial \xi} \tag{A.65}$$

$$\bar{S}_\eta = \frac{\partial x}{\partial \xi}\frac{\bar{S}_v}{A_p^v} - \frac{\partial r}{\partial \xi}\frac{\bar{S}_u}{A_p^u} \qquad (A.66)$$

The Δ_i symbol represents the finite difference equivalent of $\partial/\partial x_i$. For ease of presentation, equations (A.57) and (A.62) may be written in indicial notation as

$$G_i = \left[H_i(u,v) - B_i\Delta_i P - C_i\Delta_j P + \bar{S}_i\right] \qquad (A.67)$$

If a preliminary pressure field is imposed, the mass fluxes across the control volume boundary are established yielding an initial predictor equation.

$$r\rho^* G_i^* = r\rho^*\left[H_i(u^*,v^*) - B_i\Delta_i P^* - C_i\Delta_j P^* + \bar{S}_i\right] \qquad (A.68)$$

Equation (A.68) is effectively a momentum equation for the contravariant velocities U and V. The P^* pressure field, however, will not normally allow the corresponding continuity equation to be satisfied throughout the flow field. The essence of the split-operator concept is to establish momentum and continuity satisfying velocity and pressure fields through a sequence of split operations using the perturbation relationship. Instead of correcting the pressure with one operation as in SIMPLE, new velocity and pressure fields are evolved through a succession of correction operations which attempt to update the field values in a step-wise manner. The procedure is to apply the perturbation relationship (A.56) - neglecting the product of the two perturbation variables - such that three correcting operations are formulated as follows:

(a) First Correcting Operation

$$r\rho^{**} G_i^{**} \approx r(\rho^{**} - \rho^*) G_i^*$$

$$+r\rho^*\left[H_i(u^*,v^*) - B_i\Delta_i P^{**} - C_i\Delta_j P^* + \bar{S}_i\right] \qquad (A.69)$$

(b) Second Correcting Operation

$$r\rho^{***}G_i^{***} \approx r(\rho^{***} - \rho^*)G_i^*$$

$$+r\rho^*\left[H_i(u^*, v^*) - B_i\Delta_i P^{***} - C_i\Delta_j P^{**} + \bar{S}_i\right] \qquad (A.70)$$

(c) Third Correcting Operation

$$r\rho^{****}G_i^{****} \approx r(\rho^{****} - \rho^*)$$

$$+r\rho^*\left[H_i(u^{***}, v^{***}) - B_i\Delta_i P^{****} - C_i\Delta_j P^{**} + \bar{S}_i\right] \qquad (A.71)$$

The number of $*$ superscripts denotes the intermediate iteration sequence. Note that several alternative approaches exist for operator-splitting and that the method presented here is only representative of Rhie's [14] algorithm. Another important point to remember is that each correcting operation acts as the predictor for the proceeding operation. There are three unknowns in each of the above equations – that is, the corrected velocity, pressure, and density; fortunately, the equation of state allows the density to be expressed as a function of pressure and temperature. If the temperature is assumed constant over each complete iterative cycle and then updated at the end of each cycle, the correcting operation equations contain only the corrected velocity and pressure as unknowns. Supposing that the new pressure field is obtained through some other means indicates that the corrected velocities may be calculated, explicitly. This is exactly the approach to be taken here.

The formulation of the desired pressure correction equations is accomplished by subtracting the predictor equation from its respective correcting operation equation, applying the equation of state, and enforcing continuity for the unknown corrected velocity. The density increment ρ', as expressed as a function of P' by the ideal gas law, is underrelaxed as follows:

$$\rho' = \frac{\beta}{RT^*}P' \qquad (A.72)$$

β is the underrelaxation factor; R is the gas constant; and T^* is the static temperature from the previous iterative cycle. The formulation procedure yields the pressure correction equations which follow:

(a) First Pressure Correction

$$\Delta_i \frac{r\beta}{RT^*} G_i^* (P^{**} - P^*) - \Delta_i r\rho^* B_i \Delta_i (P^{**} - P^*) = -\Delta_i r\rho^* G_i^* \qquad (A.73)$$

(b) Second Pressure Correction

$$\Delta_i \frac{r\beta}{RT^*} G_i^* (P^{***} - P^{**}) - \Delta_i r\rho^* B_i \Delta_i (P^{***} - P^{**})$$

$$= \Delta_i r\rho^* C_i \Delta_i (P^{**} - P^*) - \Delta_i r\rho^{**} G_i^{**} \qquad (A.74)$$

(c) Third Pressure Correction

$$\Delta_i \frac{r\beta}{RT^*} G_i^* (P^{****} - P^{***}) - \Delta_i r\rho^* B_i \Delta_i (P^{****} - P^{***})$$

$$= -\Delta_i r\rho^* \Big[H(u^{***}, v^{***}) - H(U^*, v^*) \Big] - \Delta_i r\rho^{***} G_i^{***} \qquad (A.75)$$

These correction equations are expressed in the form of the general differential equation. The first team on the LHS represents the convective part; the second term on the LHS represents the diffusive part; and the entire RHS is the source part. The correction equations are effectively the transport equations for compressible flow.

The physical implication of these equations is obtained by considering the grid cell Reynolds number. For convenience, let's assume that an orthogonal grid cell exists with a u component of velocity only. The grid cell Reynolds number for such a situation would be

$$Re_c = \frac{convection}{diffusion} = \beta \frac{u^2}{RT} = \beta\gamma M^2 = \omega M^2$$

Employing an upwind-difference scheme implies that the critical grid cell Reynolds number may be made to coincide with M = 0.3 by adjusting the value of ω. Such a method allows the convective terms to vanish in the incompressible flow limit and the same terms to dominate when the Mach number increases and the compressibility effects become consequential. For a nonorthogonal grid and multiple components

of velocity, the procedure is more complex, but the principle and physical correspondence still apply. At increasingly higher Mach numbers, artificial viscosity must be introduced to increase the smoothing properties of the correction equations and to suppress numerical oscillations. The term used by Rhie [14] as taken from Shamroth et al [21] may be implemented in the present work in the form

$$\mu_{art} = max\left[0.0, \frac{\rho U}{Re^c J(\xi_x^2 + \xi_p^2)} - \mu\right] \qquad (A.77)$$

Because a nonstaggered grid is used in this work, an oscillatory pressure field could result. To eliminate this possibility, the G_i^* value at the cell boundaries when evaluated for the RHS of equation (A.73) includes a fourth order pressure dissipation term. These flux terms are evaluated according to Rhie [14] in the form

$$U^*_{i+1/2} = (U_i^* + U^*_{i+1})/2.0 + \varepsilon_d\Big(P^*_{i+1/2} - 3P^*_{it1} + 3P_i^* - P^*_{i-1}\Big)/4 \qquad (A.78)$$

The coefficient ε_d is a function of A_P and the metric coefficients. The dissipation term allows the linearized flux and pressure gradient to become coupled.

The pressure correction equations are discretized in a form similar to the general transport equation. The pressure correction increment is solved for and substituted back into its respective correcting operation equation to determine the corresponding velocity components. Once this is done for all three correction equations, the energy transport equation is solved and all properties updated. The entire sequence is then repeated to convergence.

ENERGY EQUATION

The energy transport equation requires special consideration since a high temperature plasma is to be modeled. Radiation absorption from the laser power source and radiative heat loss must be incorporated into the physical model as described in the main body of the report.

Assuming that the flow is laminar, steady, axisymmetric, and has variable physical properties, the energy transport equation may be written in cylindrical coordinates as

$$\frac{\partial}{\partial x}(r\rho uh) + \frac{\partial}{\partial r}(r\rho vh) = \frac{\partial}{\partial x}\left(r\frac{K_{eff}}{C_p}\frac{\partial h}{\partial x}\right)$$

$$+\frac{\partial}{\partial r}\left(r\frac{K_{eff}}{C_p}\frac{\partial h}{\partial r}\right) + \sum \alpha I_i - \dot{q}_{rad} + rR(r,x) \qquad (A.79)$$

The last three terms are considered known from the previous iteration and comprise the total source term.

From comparison with the general transport equation, the dependent variable is seen to be $\phi = h$ and the diffusion coefficient is $\Gamma = K_{eff}/C_p$ where K_{eff}/C_p is compiled in a table as a function of pressure and temperature and is reevaluated at each iteration.

If equation (A.79) is transformed to the orthogonal grid, discretized, and formulated in the same manner as equation (A.40), the following form for the dependent variable h results.

$$\frac{(A_P - S_P)}{\alpha}h_P = \sum Ah + S_C + (1-\alpha)\frac{(A_P - S_P)}{\alpha}h_P^* \qquad (A.80)$$

BOUNDARY CONDITIONS

In the present numerical code, all boundaries coincide with the control volume sides. For the Dirichlet condition, the prescribed value of the dependent variable is specified at the control surface boundary; the correct convection and diffusion coefficients are calculated, and a new total coefficient and source term are obtained. For the Neumann conditions, the normal derivative to the boundary is specified by setting the appropriate neighbor coefficients to zero and marking the prescribed boundary flux into the source term. The specific boundary conditions for the present application are presented in the main body of the papers.

SOLUTION PROCEDURE

Due to the immense size of the matrices representing the systems of equations, direct solution techniques were considered impractical, and an iterative method was employed. Because a node point by node point Gauss-Siedel iterative scheme has slow convergency rate, a line by line method using the Tri-Diagonal Matrix Algorithm (TDMA) was implemented. A complete description of this method is given by Patakar [15]. It is important to remember that the iterative method requires several passes through the flow field to approach convergence. Of course, the system need not converge completed for intermediate steps, but it should converge enough to provide sufficiently reasonable value for the next step toward the final solution.

APPENDIX B

Publications

APPENDIX B

PUBLICATIONS LIST

D. Keefer, San-Mou Jeng and R. Welle, "Laser Thermal Propulsion Using Laser Sustained Plasmas". Acta Astronautica, Vol. 15, No. 6/7, pp. 367-376, 1987.

San-Mou Jeng and Dennis Keefer, "A Theoretical Investigation of Laser-Sustained Plasma Thruster". AIAA-87-0383, AIAA 25th Aerospace Sciences Meeting, Jan. 1987, Reno, NV.

San-Mou Jeng and Dennis Keefer, "A Theoretical Evaluation of Laser Sustained Plasma Thruster Performance". AIAA-87-2166, AIAA/SAE/ASME/ASEE 23rd Joint Propulsion Conference, Jun. 29- Jul. 2, 1987, San Diego, CA.

S.-M. Jeng, D. R. Keefer, R. Welle, C. E. Peters, "Laser-Sustained Plasmas in Forced Convective Argon Flow, Part II: Comparison of Numerical Model with Experiment". AIAA J., Vol. 25, No. 9, pp. 1224-1230, Sept. 1987.

Acta Astronautica Vol. 15, No. 6/7, pp. 367–376, 1987
Printed in Great Britain.

0094-5767/87 $3.00 + 0.00

LASER THERMAL PROPULSION USING LASER SUSTAINED PLASMAS†

D. KEEFER, SAN-MOU JENG and R. WELLE
Center for Laser Applications, The University of Tennessee Space Institute, Tullahoma, TN 37388, U.S.A.

(*Received* 6 *January* 1987)

Abstract—Laser thermal propulsion refers to a concept in which power from a laser is beamed to a vehicle, where it is absorbed and used to heat a propellent gas that produces thrust at high values of specific impulse. The success of the concept depends upon the ability to create laser sustained plasmas that are stable in the presence of a forced convection flow and that absorb essentially all of the incident laser radiation. In addition, the thermal radiation losses from the plasma must be controlled to realize high performance without the penalty of thermal radiators. Extensive experiments have been performed and analyzed utilizing plasmas sustained in flowing argon by a carbon dioxide laser of less than 1 kW incident power. Spatially detailed measurements of the temperature in the plasmas have resulted in a detailed understanding of the energy conversion processes occurring within the plasma. This understanding has provided an explanation of the limited range of pressure and power observed for stable operation of laser sustained plasmas and suggests the means by which that range can be extended. A computational model based on a Navier-Stokes description of the flow has been developed which utilizes ray tracing for the optical interaction and temperature dependent transport and thermodynamic properties for the plasma. This model has been verified using the detailed experimental results for the argon plasmas and has been extended to provide predictions for higher laser powers in hydrogen.

1. INTRODUCTION

Laser thermal propulsion refers to a concept in which power from a laser is beamed to a vehicle, where it is absorbed and used to heat a propellant gas that produces thrust at high values of specific impulse. This concept has the advantages that pure hydrogen can be used as the propellant and that the weight of the propulsion system can be small, since the power used to heat the propellent does not have to be carried aboard the vehicle. Several methods can be used to absorb the laser energy, but we shall restrict our discussion to the case where the energy is absorbed through the process of inverse bremsstrahlung in a high temperature plasma of the propellent gas. When pure hydrogen is used as the propellent gas, specific impulse values in the range of 1000–1500 s can be expected and significant improvements are obtained for the fractional payload that can be delivered from low earth orbit (LEO) to geosynchronous earth orbit (GEO)[1].

A schematic representation of the motor is shown in Fig. 1. The incoming laser beam is focused into the absorption chamber where it sustains a plasma at temperatures of approximately 16,000–20,000 K. In contrast to a normal combustion chamber, the high temperature plasma occupies only a small fraction of the chamber volume, and mixes with the incoming propellent to produce a flow having a bulk temperature of approximately 3000–5000 K that can be expanded through the nozzle to produce thrust. Due to the high temperature in the laser sustained plasma (LSP), a substantial portion of the absorbed power will be radiated from the LSP region and absorbed by the chamber walls. In order to utilize this radiated power effectively, the chamber walls are cooled by the incoming propellent in a regenerative cycle. If the power radiated from the plasma can be limited to that required to raise the propellent from storage temperature to an acceptable inlet temperature, then all of the absorbed power can be utilized to heat the propellent and no external radiator will be required. Sufficient mixing of the inlet propellent and the high temperature region within the LSP must be insured to produce the bulk temperature required for the nozzle inlet.

The fraction of absorbed laser power that is lost from the plasma as thermal radiation has a profound influence on the performance that can be achieved by the thruster. If the acceptable inlet temperature limits the enthalpy of the inlet flow to h_0, then the final bulk enthalpy will be limited to $h_T = h_0/\alpha_{RAD}$, where α_{RAD} is the fraction of the absorbed laser power that is radiated to the walls by thermal radiation. The bulk enthalpy, and therefore the impulse of the thruster, will be determined by the radiated fraction of the absorbed laser power that may be absorbed by regenerative cooling. It is clear that the success of this concept rests on the ability to sustain a stable plasma in a forced convective flow which can absorb substantially all of the incoming radiation and limits the fraction of the absorbed laser power that is lost from the plasma region through thermal radiation.

†Paper IAF-86-17S presented at the *37th Congress of the International Astronautical Federation*, Innsbruck, Austria, 4–11, October 1986.

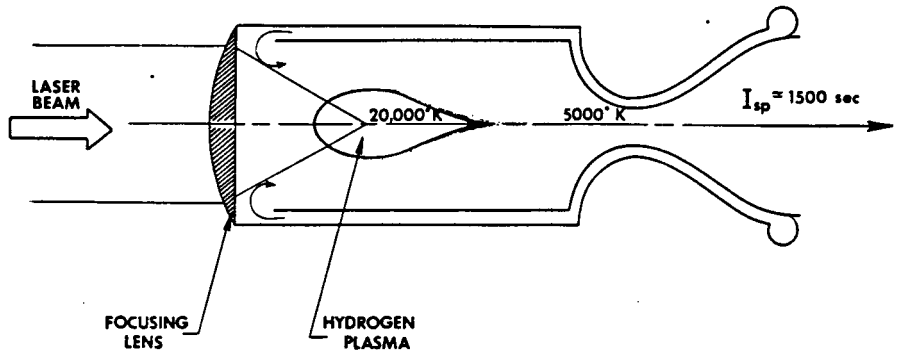

Fig. 1. Schematic representation of a rocket motor that operates by laser thermal propulsion.

Experimental studies of laser sustained plasmas have been conducted at The University of Tennessee Space Institute (UTSI) since 1983 to investigate their suitability for laser thermal propulsion. The objective of this research has been to understand the basic physical mechanisms of the LSP and determine their influence on stability, laser power absorption, and thermal radiation loss. The approach employed was to create the LSP in flowing argon at moderate carbon dioxide laser powers (less than 1.0 kW) and to obtain detailed measurements of the plasma temperature field using a modern digital image processing computer to acquire spectral images of the plasma emission. Using the measured temperature field, the laser power absorption and thermal plasma emission could be calculated at any point within the LSP to provide a detailed understanding of the energy conversion processes[2].

A computational model for the LSP in a forced convective flow has also been developed by Jeng and Keefer[3] to aid in the interpretation of the experimental results[4] and to provide a predictive capability for LSP's operating at higher power and in hydrogen[5]. This model for the LSP incorporates the temperature dependent thermodynamic and transport properties for the argon plasma within a Navier-Stokes model of the fluid mechanics. In addition, the model incorporates geometric ray-tracing for the optical configuration that permits the use of laser beam profiles of arbitrary power distribution and includes the effects of lens aberrations. The resulting model is solved numerically using a Spalding-Patanker SIMPLE algorithm.

2. EXPERIMENTAL INVESTIGATION

The primary objective of our experimental investigations has been to understand the physical mechanisms that determine the characteristics of the LSP in the regime where forced convection dominates the flow. In most previous experiments the LSP has been operated in a large chamber[6], or in the open air[7] where the flow is dominated by free thermal convection. The stability of the LSP was of particular interest to us, since stability is of crucial importance for propulsion and because it has been a subject of some discussion in the literature[8]. Our approach has been to sustain plasmas in argon using a relatively low power (1000 W) CO_2 laser and to obtain detailed spectroscopic measurements of plasma temperature for a variety of combinations of pressure, flowrate, laser power and focusing geometry. The measured temperature fields were then used to determine the detailed absorption and radiation processes that occur within the plasma.

2.1. Experimental procedure

The plasmas sustained in these experiments were contained in a 22 mm, inside diameter, cylindrical quartz flow tube which had a converging entrance section. A diagram of the experimental apparatus is shown in Fig. 2.

The laser power was provided by an axial-flow, electric discharge, carbon dioxide laser which provides a nominal 1 kW, continuous beam. The beam has an annular profile produced by an unstable oscillator of 1.5 magnification. The beam was approximately 54 mm in diameter with good axial symmetry, and was focused collinearly with the axis of symmetry of the flow tube. The apparatus was oriented with its symmetry axis in the vertical direction, with the laser beam propagating vertically upward, to avoid nonaxisymmetric buoyancy effects. This configuration generally produced a plasma with the good axial symmetry that is required for accurate diagnostics.

The primary measurements acquired from the experiments were digital images of the plasma. These images were obtained by a CID video camera whose spectral range was limited by a narrow bandpass interference filter. The filter was chosen to isolate a 1 nm wide region of the continuum radiation from the plasma, free of line radiation, and centered at 626.5 nm. The digital images were acquired by a digital image processing computer, which allowed images to be acquired at video frame rates (60/s) and averaged into memory. The entire image acquisition system was calibrated through direct substitution of a standard lamp of spectral radiance. Additional

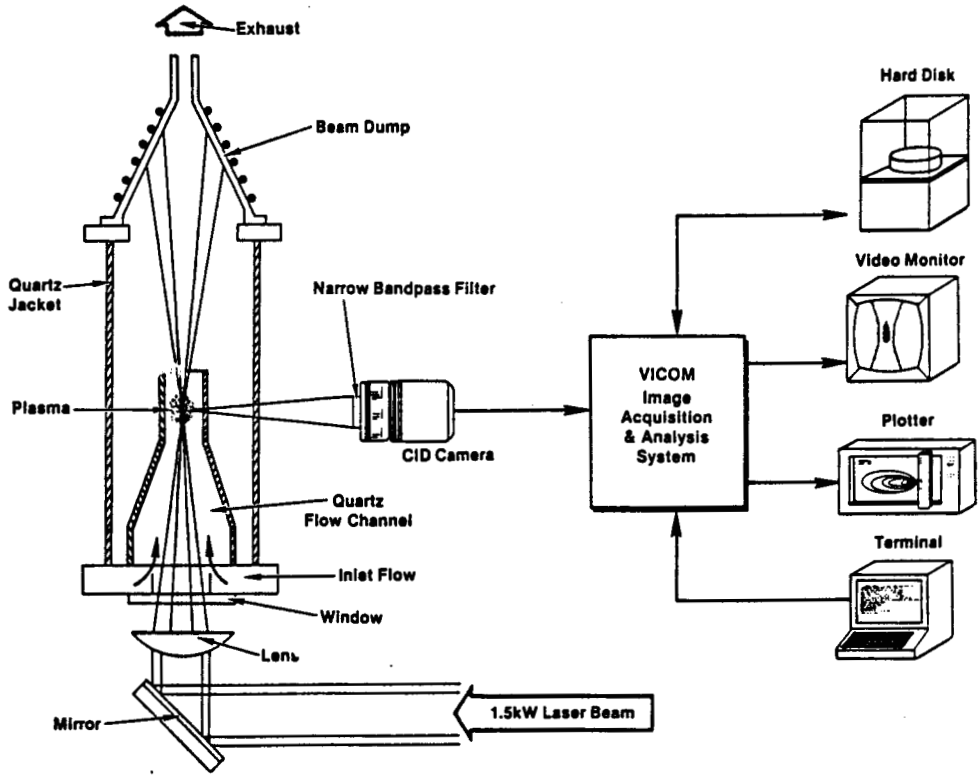

Fig. 2. Schematic diagram of the experimental apparatus.

details of the apparatus and experimental procedure have been described in earlier papers[2].

More than 125 different experiments have now been completed using lenses of two different focal lengths and a wide range of pressure, flow and power conditions. A new, transform domain method was developed to permit efficient and accurate Abel inversion of the large quantities of data that were obtained[9]. By applying appropriate calibration factors, the emission coefficient was obtained as a function of position in the plasma, and from this the temperature field within the plasma was obtained by interpolation in tabulated data published by Morris[10].

Detailed geometric ray tracing techniques were employed to calculate the spatial power absorption at each point in the plasma, using the measured temperature field to determine the laser absorption coefficient. To calculate power absorption within the plasma, the measured annular profile of the incoming laser beam was broken into discrete rays, each representing a fraction of the incident radiation. Each ray was traced, using geometric optics, through the sodium chloride focusing lens and window and then through a grid system superimposed on the measured temperature field of the plasma. The absorption coefficient at 10.6 μm was calculated according to the method described by Kemp and Lewis[11], using the thermodynamic data tabulated by Drellishak[12], and the Gaunt factors published by Karzas and Latter[13]. At each step through the grid, the power absorbed from each ray was subtracted from the ray and added to the plasma. This procedure gave both the spatial distribution of power absorption and the total power absorbed by the plasma.

It was also possible, using the measured temperature fields, to calculate the power lost from the plasma due to the optically thin portion of the thermal radiation. The thermal radiation losses from the plasma were determined using the relation published by Kozlov for optically thin radiation[8].

2.2. *Experimental results*

The objective of these experiments was to investigate the effect of high incident flow rates on the behavior of laser-sustained plasmas. At flow rates of less than approximately 30 cm/s, the position and shape of the plasma relative to the incident laser beam was essentially unaffected by the small forced convective flow. The plasma stabilized in the region of the focused beam where the incident intensity was just sufficient to balance the thermal radiation, conduction, and convection losses from the plasma. In general, this means that the plasma will stabilize at a position upstream of the focus that depends on the incident power, focusing geometry, and ambient pressure. The plasma tends to fill the beam at the position of stabilization, and therefore grows larger in diameter when it stabilizes at a position further up the beam. When the incident flow rate is increased significantly beyond 30 cm/s, convection becomes relatively more important in the energy balance and

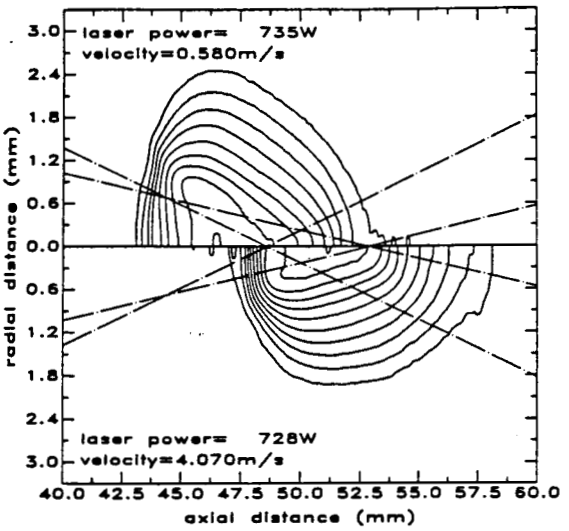

Fig. 3. Isothermal contour plots of two plasmas sustained using the 203 mm (8-in.) lens and a chamber pressure of 2.5 atm. The contour interval is 500 K, with the outer at 10,500 K.

tends to force the plasma to stabilize at a position further down the beam and closer to the focus. The plasma again tends to fill the beam, but because the beam is smaller in diameter near the focus, the plasma is also smaller in diameter and lies in a region of greater laser intensity.

Figure 3 shows an isothermal contour plot for the high temperature region of two plasmas sustained under similar conditions of pressure and laser power, but with substantially differing incident flow speeds. The contour interval is 500 K with the outer isotherm at 10,500 K, and the focal point of the laser (defined as the location of the circle of least confusion) is at the location labeled 50 mm on the x-axis. The flow is from left to right, and the laser beam is incident from the left. The path of the incident laser beam through the plasma is also illustrated in Fig. 3 where the lines represent the approximate boundaries of the annular beam in an unrefracted path through the plasma. For the low-flow case, the major portion of the plasma is upstream of the laser focus, and there is a local off-axis temperature maximum. The off-axis temperature maximum in this case occurs near the annular focus of the beam produced by spherical aberrations, as discussed in an earlier paper[14]. By comparison, the high-flow plasma stabilized with a significant fraction downstream of the focus, and has no significant off-axis temperature maximum. In addition, the maximum temperature of the high-flow plasma is higher than that for the low-flow case; 15,600 K compared to 14,600 K.

The path length of the beam through the two plasmas shown in Fig. 3 is comparable, but in the high-flow case the path traverses, on the average, a region of higher temperature and, therefore, a larger absorption coefficient, particularly in the region of highest laser intensity near the focus. This results in a significantly higher fractional absorption of the laser poser; 78% compared to 67%. At the same time, because the overall size of the high-flow plasma is smaller than the low-flow plasma and because the highest temperature region is confined to a smaller volume near the axis, the overall thermal radiation loss decreased from 53 to 45% of the incident laser power. As a result of the different spatial characteristics of the plasmas, the conversion from laser power to flow enthalpy increased from 14 to 32% as a result of the increase in flow.

The two sets of isotherms shown in Fig. 3 represent the endpoints of a series of different flow velocities. The data for fractional absorption of laser power and thermal radiation loss at the intermediate values are shown in Fig. 4.

The absorption fraction passes through a maximum near an incident flow velocity of 300 cm/s, while the fraction radiated reaches a maximum near 100 cm/s. The difference between the absorbed and radiated fractions represents the fraction of the incident laser power that is used to increase the enthalpy of the flow, and this quantity increases with flow up to a velocity of approximately 300 cm/s, after which it is nearly constant at 30%.

The focusing geometry used to sustain the plasma also has a strong influence on the power absorption and the stability characteristics of the LSP. We have conducted a series of experiments using two different focal length lenses: 203 mm, corresponding to an f/number of 3.8, and 305 mm, corresponding to an f/number of 5.6. Isothermal contour plots of plasmas sustained with the two lenses at a pressure of 2.5 atm are shown in Fig. 5.

Both plasmas were sustained at approximately 720 W and 4 m/s incident flow velocity in argon at a pressure of 2.5 atm. The f/3.8 (203 mm) plasma is centered about 2 mm downstream of the focus, and has a peak temperature of 15,600 K, while the f/5.6

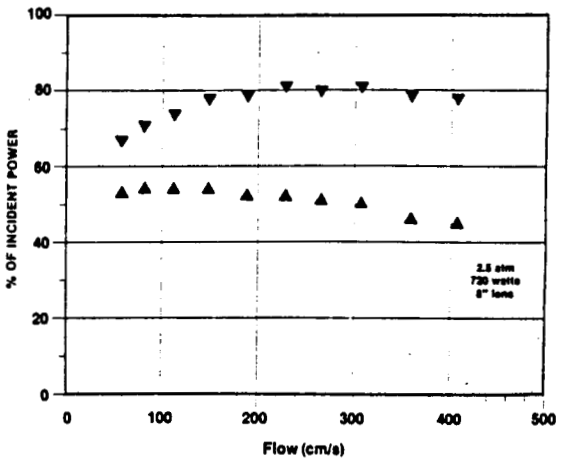

Fig. 4. Variation of the laser power absorption [▼] and thermal radiation loss [▲] with incident flow velocity for a chamber pressure of 2.5 atm using the 203 mm focal length lens. The powers are shown as a fraction of the 720 W incident laser power.

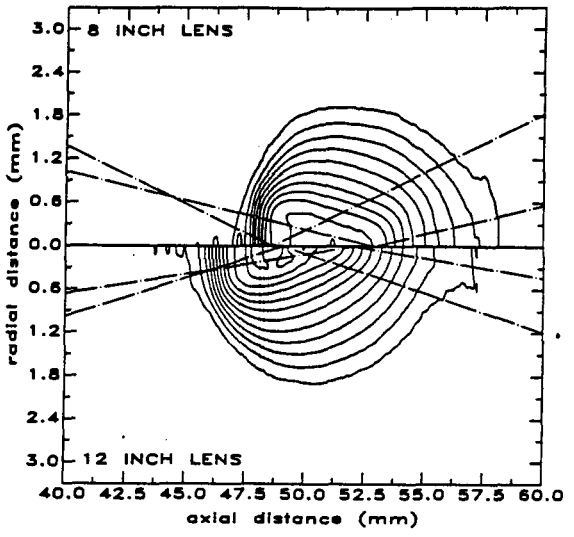

Fig. 5. Isothermal contour plots for two plasmas sustained at 2.5 atm in a 4 m/s incident flow with 720 W incident laser power using 203 mm (8-in.) and 305 mm (12-in.) focal length lenses. The contour interval is 500 K and the outer contour has a value of 10,500 K.

(305 mm) plasma is centered within 0.5 mm of the focal point, is just slightly smaller in diameter, and has a peak temperature of 16,200 K. Because of the narrower angle of convergence of the beam, the flow speed required to force the plasma into the downstream region of the focal zone, where the efficiency begins to deteriorate, is greater for the larger f/number lens. This suggests that stable plasmas may be sustained using very long focal length lenses, provided that the forced convective flow is sufficiently fast.

A comparison between the results of a series of experiments in argon at a pressure of 2.5 atm using both the 203 mm lens (f/3.8) and a similar series using the 305 mm lens (f/5.6), is shown in Fig. 6. Note that the fractional laser power absorption is greater for

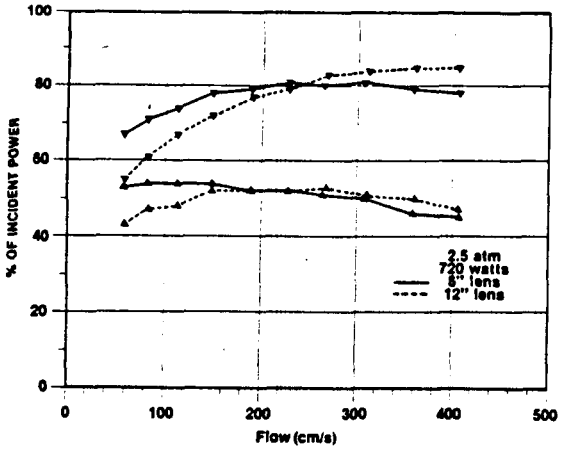

Fig. 6. The effect of incident flow velocity on laser power absorption [▼] and thermal radiation [▲] for plasmas sustained at a pressure of 2.5 atm using 203 mm (8-in.) and 305 mm (12-in.) focal length lenses.

the longer focal length lens at the higher incident flow velocities, but that it is smaller for the lower incident flows. It is also seen that the conversion of laser power to flow enthalpy is greater for the longer focal length lens at the higher flow velocities. For the longer focal length lens, the fractional laser absorption and the fractional thermal radiation losses are clearly tending toward the same value as the flow decreases, indicating that the plasma will become unstable in this flow region. In an earlier paper[14], we reported that we were unable to initiate or sustain a plasma at pressures greater than two atmospheres using the 305 mm focal length lens. The incident flow speed in that set of experiments was limited to less than 15 cm/s. As the pressure increased, at a constant mass flow rate, the plasma would move upstream until, at 2 atm, it became unstable. At the much higher flow speeds used in the later experiments, we had no difficulty initiating and sustaining plasmas with the 305 mm lens at pressures up to 3 atm. These results suggest that earlier experimental maps for regions of stability of the LSP[6] are not unique, but depend on the particular optical geometry employed.

The plasma position and shape also depend significantly on the pressure and incident laser power. At higher chamber pressures, the absorption coefficient is sufficiently large to allow the plasma to move upstream into a region of lower laser intensity. With the annular laser beam this can, in extreme cases, result in large diameter plasmas with strong off-axis temperature maxima. Because of the lower laser intensity in the annular focus relative to the axial focus, the magnitude of a typical off-axis temperature maximum is lower than one on the axis, and this results in a lower fractional power absorption. At the same time, the large plasma diameter ensures that the thermal radiation losses remain large. If the incident flow velocity is insufficient to hold the plasma near the focus, then the plasma will attempt to move far up the beam away from focus and become unstable.

The effect of incident laser power on the position and shape of the plasma is similar to that of pressure. For a given incident flow velocity, an increase in laser power causes the plasma to move up the beam to a new position of stability and a larger plasma diameter. If the plasma moves too far up the beam, the thermal radiation loss increases and, at the limit of stability, the radiation losses exceed the absorbed laser power. These positional effects would explain both the power instability and the pressure instability observed by Generalov *et al.*[6].

Detailed analysis of a large number of laser sustained plasmas has revealed the complex interactions between the flow and the energy conversion processes within the plasmas. These experiments also suggest that stable laser sustained plasmas may be operated over a wider range of conditions than previously reported by using appropriate combinations of optical geometry, pressure and incident flow velocity.

3. THEORETICAL ANALYSIS

The first theoretical model for the laser sustained plasma was developed by Raizer, who proposed a one-dimensional model based on an analogy to a subsonic combustion wave[15]. This model was extended by Jackson and Nielsen to include radiative transport[16], and by Kemp and Root to calculate hydrogen plasmas for laser propulsion[17]. Keefer *et al.* applied a different numerical method for solving the one-dimensional model that eliminated a problem with numerical convergence[18]. A quasi-two-dimensional model was proposed by Batteh and Keefer in which the flow and the laser beam were both assumed parallel to the axis and simple assumptions were made for the plasma properties to permit a closed form solution[19]. Glumb and Krier extended the quasi-two-dimensional model to include focusing of the laser beam and used a numerical solution to permit the inclusion of realistic thermodynamic and transport properties, but retained the axial flow, constant mass flux assumption[20].

A new model has been developed by Jeng and Keefer that is based on a laminar Navier-Stokes description of the flow and which utilizes geometric ray tracing to describe the optical interactions in the plasma[3]. This model has been verified by comparison with the detailed experiments described above[4], and has been extended to predict the properties of hydrogen at higher laser powers[5].

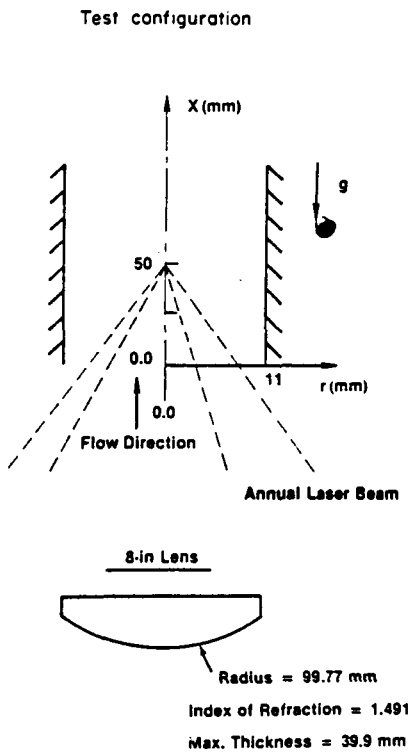

Fig. 7. Details of the solution domain used for the numerical calculations.

3.1. Numerical model

Ideally, the model would simulate the flow geometry shown in Fig. 1. However, in order to gain more understanding of the interactions between laser and plasma, the simple flow geometry as shown in Fig. 7 was adopted. It is assumed that this domain is axisymmetric, and a cylindrical coordinate system was employed. The incoming working fluid enters from the bottom, and the originally collimated 10.6 μm carbon dioxide laser beam is focused into the gas by an appropriate lens.

It was assumed that the flow is laminar, steady-state, axisymmetric and has variable physical properties. The pressure of the flow is relatively high, so that local thermodynamic equilibrium (LTE) can be assumed with little error. Therefore, the plasma can be described by a single temperature, and its physical properties are only a function of this temperature and pressure. Thermal radiation was divided into two parts: an optically thin portion in which all radiation escapes from the plasma; and an optically thick portion which can be described as a diffusion process. Since the mach number for the flow is small, the kinetic energy and viscous dissipation were neglected in the energy equation. Following the above assumptions and using incompressible flow viscous terms, the equations of conservation of mass, momentum and energy for the flow can be written as:

$$\frac{\partial(\rho u)}{\partial x}+\frac{1}{r}\frac{\partial(r\rho v)}{\partial r}=0 \tag{1}$$

$$\frac{\partial(\rho uu)}{\partial x}+\frac{1}{r}\frac{\partial(r\rho uv)}{\partial r}=-\frac{\partial p}{\partial x}-\rho g+\left[\frac{\partial}{\partial x}\left(\mu\frac{\partial u}{\partial x}\right)+\frac{1}{r}\frac{\partial}{\partial r}\left(\mu r\frac{\partial u}{\partial r}\right)\right] \tag{2}$$

$$\frac{\partial(\rho uv)}{\partial x}+\frac{1}{r}\frac{\partial(r\rho vv)}{\partial r}=-\frac{\partial p}{\partial r}+\left[\frac{\partial}{\partial x}\left(\mu\frac{\partial v}{\partial x}\right)+\frac{1}{r}\frac{\partial}{\partial r}\left(\mu r\frac{\partial v}{\partial r}\right)\right]-\frac{2\mu v}{r^2} \tag{3}$$

$$\frac{\partial(\rho uh)}{\partial x}+\frac{1}{r}\frac{\partial(\rho rvh)}{\partial r}=\frac{\partial}{\partial x}\left(\frac{k_{eff}}{c_p}\frac{\partial h}{\partial x}\right)+\frac{1}{r}\frac{\partial}{\partial r}\left(\frac{rk_{eff}}{c_p}\frac{\partial h}{\partial r}\right)+\sum\alpha I_i-\dot{q}_{rad} \tag{4}$$

where I_i is the local laser intensity described by the following equation

$$\frac{dI_i}{ds}=-\alpha I_i, \tag{5}$$

where s is the distance along the laser propagation direction. The laser beam path through the optical system was calculated by geometric ray tracing. Refraction of the individual rays due to the inhomogeneous refractive index within the plasma were neglected in the calculation. Since Welle *et al.*[2] had found that this assumption produced little error in the experimental results. Diffraction of the beam

when combined with lens aberrations can have a larger effect, as shown recently by Smith and Keefer[21], but these effects have been neglected in the current model.

The finite difference solution procedure employed in this work is an adaptation of the method described in detail by Patankar[22]. A detailed description of the numerical procedure used in the current calculation was given in[3]. The SIMPLE algorithm[22,23], which uses a conservative form of finite difference equation, primitive variables and staggered grids, was adopted to solve the coupled mass, momentum and energy conservation equations (1)–(4).

3.2. *Numerical results*

The validity of the present model was established by calculations for argon plasmas having a wide range of gas inlet velocities, gas static pressures and laser power, using two different lenses of 203 mm (8-in.) and 305 mm (12-in.) focal lengths. The flow conditions were varied over a range of static pressure from 1.3 to 4.0 atm, flow inlet velocity from 0.4 to 4.5 m/s and laser power from 261 to 967 W. The wall and gas inlet temperatures were assumed to be constant at 300 K, and the inlet velocity was assumed to be uniform for these calculations. The CO_2 laser operated at a wavelength 10.6 μm and the collimated laser intensity distribution was that used by Jeng and Keefer[3]. It is an annular beam with peak intensity at a radius of 25.5 mm. The dimensions of the 203 mm (8-in.) focal length lens are given in Fig. 7.

The semi-two-dimensional model of Glumb and Krier[20] assumes zero radial velocity which is equivalent to a constant axial mass flux assumption. However, the large temperature gradients within the LSP result in large density gradients and a very complex flow in the plasma. Figure 8 shows a typical calculated plasma from our two-dimensional model.

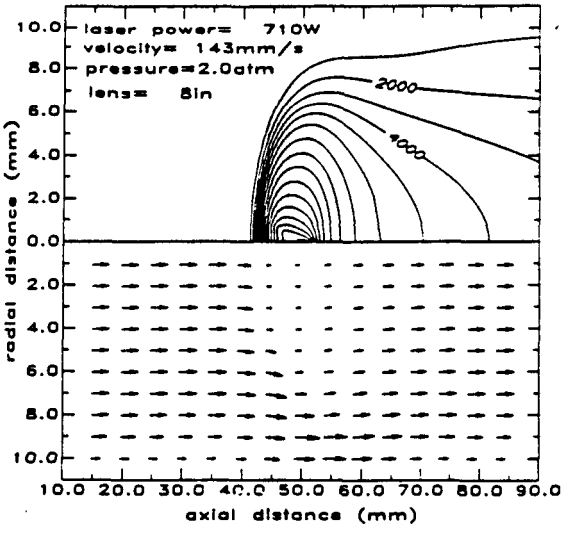

Fig. 8. Isothermal contours and mass flux vectors for a calculated plasma. The contour interval is 1000 K and the outer contour has a value of 1000 K.

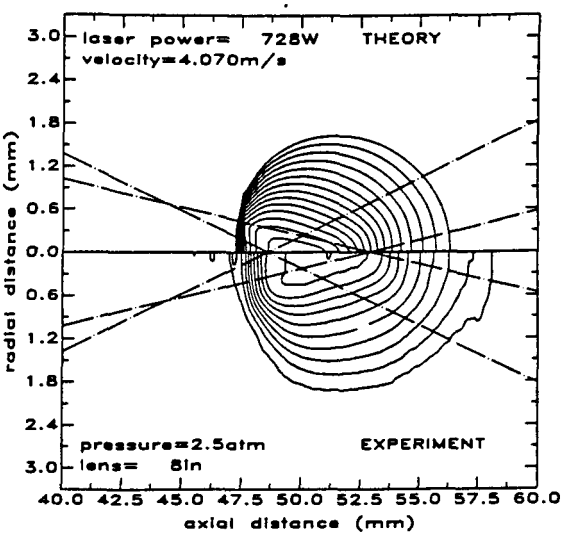

Fig. 9. Comparison of predicted and measured temperature contours for a high-velocity plasma. The contour interval is 1000 K and the outer contour has a value of 10,500 K.

The isotherms are shown in the top half of the figure, and the mass flux vectors are shown in the bottom half. The laser focal zone is located 50 mm from the inlet, and the direction and magnitude of the local mass flux, at the vector origins, is proportional to the direction and the length of the vectors.

The LSP is positioned near the laser focal zone, and the peak temperature is 16,390 K. In the high temperature region, where the axial velocities were much larger than elsewhere, the axial mass flux was very small compared to the inlet mass flux. It was found that a local high pressure zone was produced near the leading edge of the plasma that forced the flow to have outward radial velocities near the centerline. From this result, it is clear that the constant axial mass flux assumption is inadequate.

The model has been compared with a wide variety of experimental results given by Welle *et al.*[4] in order to learn the capability and limitations of the model. Since the spectroscopic measurements were limited to temperatures greater than 10,000 K, Figs 9 and 10 contain only those isotherms within that temperature range, and a limited portion of the calculation domain is plotted in order to gain a clearer comparison.

The performance of the model for two different inlet velocities, using the 203 mm (8-in.) focal length lens, is demonstrated in Figs 9 and 10. The static pressure and incident laser power of the two cases differ by less than 1%, but the inlet velocity of the LSP in Fig. 9 is about seven times that in Fig. 10. The model calculates the size and position of both plasmas well. As the inlet velocity increases, the radius of the plasma decreases, and the plasma stabilizes further downstream. The model predicts two local temperature maxima within the low-velocity LSP. One is on the laser path upstream of the focal zone, and another is at the focal zone. Both calculated max-

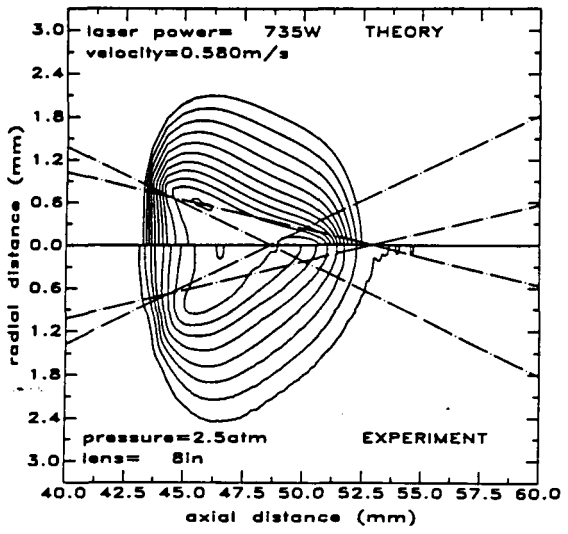

Fig. 10. Comparison of predicted and measured temperature contours for a low-velocity plasma. The contour interval is 1000 K and the outer contour has a value of 10,500 K.

imum temperatures are about 1000 K higher than the measured peak temperature (14,500 K). Only a single maximum temperature was measured, and it is located neither on the laser path nor at the focal zone.

The predicted local temperature maximum near the focal zone, which was not observed in the experiment, may result from the neglect of refraction of the laser beam. Although it has been demonstrated experimentally[2] that this assumption leads to only a small effect on the measured global laser power absorption, its local effect on the predictive model can be more serious, since the local temperature is strongly influenced by the local laser intensity. When refraction of the laser beam within the LSP is considered, it results in a larger focal spot size and reduced laser intensity. The spot size for the refracted beam is highly dependent on the LSP position and size. For a low-velocity LSP, most of the plasma is located upstream of the focal zone, and this makes the focal spot larger. When diffraction effects are combined with lens aberrations, the diffraction limited focal spot is approximately twice the size of that calculated from a geometric ray trace[21]. The combination of laser beam refraction and diffraction, and the longer absorption pathlength ahead of the focal zone, results in an actual laser intensity which is smaller near the laser focal zone than that which is predicted by the ray tracing model. Thus, the local temperature maximum will not occur as predicted in the low-velocity LSP. This may explain why the calculations do not agree with the experiments in this detail.

Since the size and temperature of these plasmas were well predicted, it is not surprising that the calculated thermal radiation power loss (316 and 445 W for high and low velocity, respectively) agreed with the experimental results (326 and 392 W for high and low velocity, respectively). The model prediction for the transmitted laser power in the high-velocity LSP also agrees reasonably well (110 and 159 W for prediction and experiment, respectively). However, the predicted transmitted laser power (91 W) in the low-velocity LSP is much smaller than the measurement (246 W). This is because the predicted second local maximum temperature near the focal zone absorbs an unrealistically large amount of additional laser power.

In general, the model predicted well the experimentally observed changes in LSP characteristics resulting from changes in pressure, optical geometry and incident laser power for the low power argon plasmas, as discussed at length by Jeng *et al.*[4]. Since the model was successful in predicting the behavior of low power argon plasmas, it was extended to permit the prediction of the higher power hydrogen plasmas that are of interest for applications in propulsion[5]. The model was modified to use the thermodynamic and transport properties of hydrogen and it was assumed that the laser beam incident on the lens had a Gaussian profile whose diameter could be varied. A parametric study was performed over the following range of flow and optical conditions: static pressure of the flow, 1–10 atm; flow inlet velocity, 5–100 m/s; laser power, 5–60 kW, and Gaussian laser beam diameter, 40–80 mm. Many examples of the model predictions can be found in[5], and a representative case is shown in Fig. 11.

Temperature contour lines range from 1000 to 16,000 K in 1000 K increments, and the maximum temperature of 16,804 K is located at $x = 37.4$ mm, which is well upstream of the laser focal point ($x = 52$ mm). The magnitude of the local mass flux, at the vector origins, is proportional to the vector lengths, and the flow direction is the same as the vector directions. Figure 12 is a close-up view of the same plasma where the beam boundary is also plot-

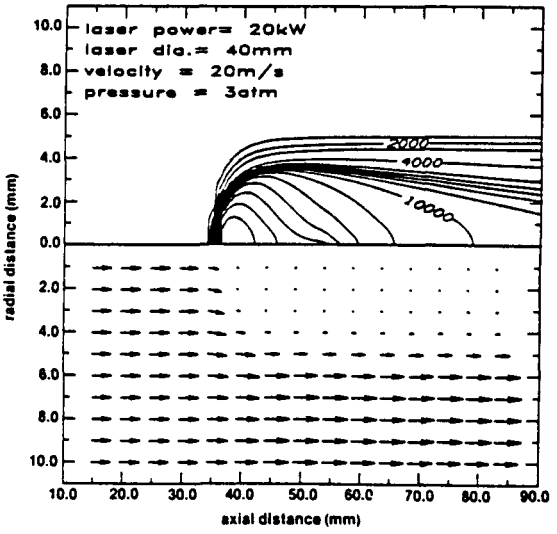

Fig. 11. Isothermal contours and mass flux vectors for a calculated hydrogen plasma.

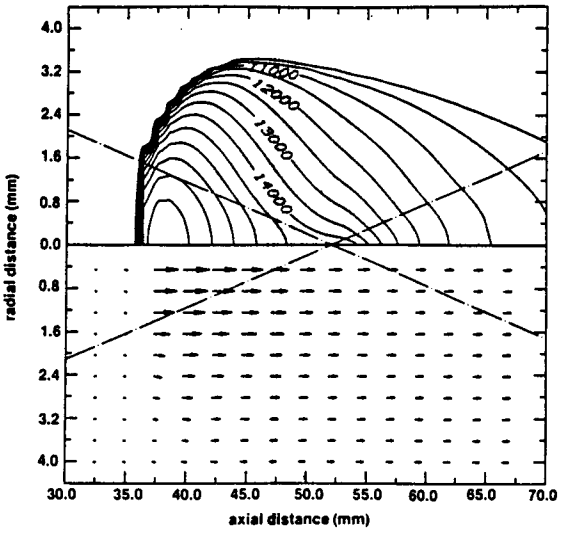

Fig. 12. Close-up view of the isotherms and the velocity vectors for the hydrogen plasma of Fig. 11.

ted. In the bottom half of this figure, the vectors represent the velocity vectors instead of mass flux vectors. Near the center axis, upstream of the maximum temperature, the directions of energy transfer by convection and conduction are opposite, so the axial temperature gradient is large in this region. On the other hand, the temperature gradient downstream of the maximum temperature, where the mixing between inner hot and outer cold flow occurs and laser heat addition is small, is much smaller than that in the upstream region.

The temperature ratio between the core region of the LSP and the inlet is as large as 50, the specific volume ratio can reach 150, and volumetric expansion is the dominant factor in the flow acceleration. In Fig. 12, the axial velocity increases from 20 m/s at the inlet to 255 m/s in the plasma core region, but the axial mass flux (see Fig. 11) is smaller in the high temperature region than at the inlet. Near the centerline upstream of the plasma, the axial mass flux decreases along the axial direction, so a small outward radial velocity develops (for example at $x = 35$ mm and $r = 3.0$ mm in Fig. 12). The axial mass flux within the high temperature region ($T > 6000$ K) is less than one-fifth of that at the inlet, and this indicates that the constant axial mass flux assumption used by quasi-two-dimensional models is not adequate.

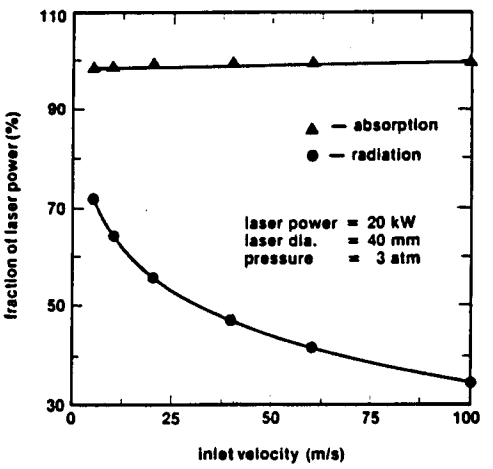

Fig. 13. Fractions of the incident laser power that are absorbed by and radiated from the hydrogen LSP as a function of inlet velocity. The incident laser power is 20 kW, the plasma pressure is 3 atm, and the Gaussian beam diameter is 40 mm.

The fractional power absorption and thermal radiation loss are shown as a function of inlet velocity in Fig. 13. The LSP absorbs most of the incident laser power and only a small fraction of laser power is transmitted (maximum fractional transmission is 1.7% at the lowest inlet velocity of 5 m/s). It was found that the fractional power absorption increases as the inlet velocity increases. This is because the plasma has a longer tail in the high-velocity cases which increases the total absorption pathlength. The fractional power lost from the plasma through thermal radiation decreases from 72% at 5 m/s to 34% at 100 m/s. For optically thin radiation, the radiated power is proportional to the volume of the plasma, and since the diameter of the high velocity plasma is smaller, the radiation power loss decreases with increasing velocity, as shown in Fig. 13. The difference between power absorbed and power radiated represents the net power converted from the laser directly to the flow. By increasing the inlet velocity, the net direct power conversion efficiency increases from 26 to 64%.

These results suggest that hydrogen plasmas sustained at higher laser powers with Gaussian beam profiles are capable of absorbing essentially all of the incident laser radiation, and that the thermal radiation losses can be limited to values that can be absorbed through the chamber walls in a regenerative cycle.

4. SUMMARY

Spatially detailed measurements have been obtained for a large number of plasmas sustained by a carbon dioxide laser in forced convection flows of argon. Analysis of these experiments have revealed the complex interactions between the flow, pressure and laser power that determine the stable operating regimes for these plasmas. It was found that the position of the plasma within the focal volume of the laser beam could be controlled with the incident flow velocity. Controlling the flow, together with the focusing geometry of the laser beam, permitted stable operation of the plasma with high fractional absorption of the incident laser beam and relatively small thermal radiation losses from the plasma. A numerical model that incorporates the complex energy conversion processes within the plasma has been developed and verified using the detailed experi-

mental measurements. This model was then extended to calculate hydrogen plasmas that were sustained by a higher power laser having a Gaussian beam profile. The results of these calculations indicate that hydrogen plasmas can be sustained that will absorb essentially all of the incident laser power and that lose only a small fraction of the absorbed power through thermal radiation.

The numerical studies for hydrogen plasmas indicate that, when higher power Gaussian laser beams are employed, the chamber walls can be adequately cooled by the propellent flow in an efficient regenerative cycle. No "fatal flaws" have been discovered by either the experimental or the theoretical investigations, and it appears that a practical, high specific impulse propulsion system could be based on the laser thermal propulsion concept if lasers having adequate power are developed and if suitable window materials can be found.

REFERENCES

1. D. Keefer, R. Elkins, C. Peters and L. Jones, Laser thermal propulsion. In *Orbit-Raising and Maneuvering Propulsion: Research Status and Needs* (Edited by Leonard H. Caveny), Vol. 89 of *Progress in Astronautics and Aeronautics* (1984).
2. R. Welle, D. Keefer and C. Peters, Energy conversion efficiency in high-flow laser-sustained plasmas. AIAA-86-1077, *AIAA/ASME 4th Fluid Mechanics, Plasma Dynamics and Lasers Conference*, Atlanta, May (1986).
3. S.-M. Jeng and D. Keefer, Theoretical investigation of laser-sustained argon plasmas. *J. Appl. Phys.* **60**, 2272–2279 (1986).
4. S.-M. Jeng, D. Keefer, R. Welle and C. Peters, Numerical study of laser-sustained argon plasmas in a forced convective flow. AIAA-86-1078, *AIAA/ASME 4th Fluid Mechanics, Plasma Dynamics and Lasers Conference*, Atlanta, May (1986).
5. S.-M. Jeng and D. Keefer, Numerical study of laser-sustained hydrogen plasmas in a forced convective flow. AIAA-86-1524, *AIAA/ASME/SAE/ASEE 22nd Joint Propulsion Conference*, Huntsville, June (1986).
6. N. A. Generalov, V. P. Ziniakov, G. I. Kozlov, V. A. Masyukov and Y. P. Raizer, Experimental investigation of a continuous optical discharge. *Soviet Phys.—JETP* **34**, 763–769 (1972).
7. D. R. Keefer, B. B. Henriksen and W. F. Braerman, Experimental study of a stationary laser-sustained air plasma. *J. Appl. Phys.* **46**, 1080–1083 (1975).
8. G. I. Kozlov, V. A. Kuznetsov and V. A. Masyukov, Radiative losses by argon plasma and the emissive model of a continuous optical discharge. *Soviet Phys.—JETP* **39**, 463–468 (1974).
9. S. I. Sudharsanan, The Abel inversion of noisy data using discrete integral transforms. Masters Thesis, The University of Tennessee, Knoxville, August (1986).
10. J. C. Morris and J. M. Yos, Radiation studies of arc heated plasmas. ARL 71-0317 (1971).
11. N. H. Kemp and P. F. Lewis, Laser-heated thruster interim report. NASA CR-161665 (PSI TR-205), Feb. (1980).
12. K. S. Drellishak, D. P. Aeschliman and A. B. Cambel, Tables of thermodynamic properties of argon, nitrogen and oxygen plasmas. AEDC-TR-64-12 (1964).
13. W. J. Karzas and R. Latter, Electron radiative transitions in a Coulomb field. *Astrophys. J., Supplement Series*, Supplement Number 55, Vol. **VI**, May, pp. 463–468 (1961).
14. D. R. Keefer, R. P. Welle and C. E. Peters, Power absorption processes in laser-sustained argon plasmas. *AIAA J.* **24**, 1663–1669 (1986).
15. Y. P. Raizer, Subsonic propagation of a light spark and threshold conditions for the maintenance of plasma by radiation. *Soviet Phys.—JETP* **31**, 1148–1154 (1970).
16. J. P. Jackson and P. E. Nielsen, Role of radiative transport in the propagation of laser-supported combustion waves. *AIAA J.* **12**, 1498–1501 (1974).
17. N. H. Kemp and R. G. Root, Analytical study of laser-supported combustion waves in hydrogen. *J. Energy* **3**, 40–49 (1979).
18. D. R. Keefer, C. E. Peters and H. L. Crowder, A reexamination of the laser supported combustion wave. *AIAA J.* **23**, 1208–1212 (1985).
19. J. H. Batteh and D. R. Keefer, Two-dimensional generalization of Raizer's analysis for the subsonic propagation of laser sparks. *IEEE Trans. Plasma Sci.* **PS-2**, 122–129 (1974).
20. R. J. Glumb and H. Krier, A two-dimensional model of laser-sustained plasmas in axisymmetric flow fields. AIAAA Paper No. 85-1553, July (1985).
21. L. M. Smith and D. R. Keefer, The Fourier optical analysis of aberrations in focused laser beams. *Proceedings of the SPIE*, Vol. 679, Current Developments in Optical Engineering and Diffraction Phenomena, August (1986).
22. S. V. Patankar, *Numerical Heat Transfer and Fluid Flow*. Hemisphere, Washington, D.C. (1980).
23. A. D. Gosman, W. M. Pun, A. K. Ruchal, D. B. Spalding and R. Wolfshstein, *Heat and Mass Transfer in Recirculating Flows*. Academic Press, London (1969).

AIAA'87

AIAA-87-0383
A Theoretical Investigation of Laser-Sustained Plasma Thruster

San - Mou Jeng and Dennis Keefer
The University of Tennessee Space Institute
Tullahoma, TN

AIAA 25th Aerospace Sciences Meeting

January 12-15, 1987/Reno, Nevada

A Theoretical Investigation of Laser-Sustained Plasma Thruster

San-Mou Jeng* and Dennis Keefer**

Center for Laser Applications
University of Tennessee Space Institute
Tullahoma, Tennessee 37388
(615) 455-0631 ext. 338

ABSTRACT

A numerical code has been successfully developed for the investigation of thruster performance using a laser-sustained hydrogen plasma as the propellant. The plasma was sustained using a 10.6μm CO_2 laser beam which is focused at different positions within the thruster. The physical model assumed that plasma is in thermodynamically equilibrium (LTE), and geometric ray tracing was adopted to describe the laser beam. The steady-state, axisymmetric, Navier-Stokes equations coupled with the laser power absorption process have been solved numerically. A pressure based Navier-Stokes numerical solver using body-fitted coordinates was used to calculate the laser-supported rocket flow which includes both subsonic and supersonic flow regions. From the limited parametric study, which did not try to optimize the rocket performance, it was found that better performance was obtained when the laser beam was focused closer to the rocket throat.

NOMENCLATURE

A	coefficient in difference equation for variable ϕ
I	laser ray intensity
J	Jacobian of inverse coordinate transformation
k	conductivity
p	pressure
q_1, q_2, q_3	geometric relations between coordinate systems
$\dot{q}$	emission coefficient for optically thin radiation
R, S, T	source term in equations 6, 7, 15, respectively
s	distance along laser ray
U, V	velocity component along $\varsigma-$ and $\eta-$axis, respectively
u, v	velocity component along $x-$ and $r-$axis, respectively
ς, η	axes of curvilinear coordinate system
ϕ	general dependent variable
ρ	density
Γ	effective diffusion coefficient
μ	viscosity
α	absorption coefficient

Subscript

E, W, N, S	four adjacent nodes to P
e, w, n, s	four surfaces of the control volume centered at P
i	laser ray i
P	nodal point to be solved in difference equation
rad	radiation
ς, η	partial derivative with respect to ς, η
ϕ	for dependent variable ϕ

Superscript

$*$	values based on given pressure field
$'$	corrected values according to corrected pressure field

INTRODUCTION

This paper describes the numerical calculations for a rocket using a laser-sustained plasma as the propellant for a propulsion device. The plasma is used to absorb and convert the power from a remote laser beam into the propellant which is expanded through a nozzle to generate the required thrust for a space vehicle. This kind of propulsion system is called laser-thermal propulsion. Several different modes of operating a laser-supported rocket have been proposed; for example, pulsed laser-supported detonation wave;[1] cw laser-sustained plasma (LSP).[2-4] In this paper, the discussion is limited to the numerical calculations of a rocket flow using a cw laser-sustained pure hydrogen plasma as the propellant.

A schematic of a proposed laser-supported rocket

---

* Assistant professor, Aerospace and Mechanical Engineering, Member AIAA

** Professor, Engineering Science and Mechanics, Member AIAA

thruster is shown in Figure 1. Laser power is absorbed by and sustains a high temperature plasma core (about 15,000-20,000 K), which mixes with the cold buffer flow of propellant downstream, heating the flow to the maximum temperature that the chamber wall material can tolerate. Then, the flow is accelerated through a conventional nozzle to produce the required thrust. Since the laser power absorption by a plasma is through inverse bremsstrahlung, any type of propellant can be used, and for propulsion purposes, the lowest molecular weight propellant, hydrogen, is the best candidate. The major advantages of this device, compared to chemical propulsion, are that the lowest molecular weight propellant can be used, and that the maximum temperature of the working fluid is not limited to the flame temperature of a combustion process. The combination of high temperature and a low molecular weight propellant results in a very high expected specific impulse. An estimated specific impulse for laser-sustained plasma propulsion using hydrogen propellant is in the range of 1000-1500 sec.,[5] which is about three times that of the most advanced chemical propulsion system.

The modeling of the LSP for propulsion began with the one-dimensional work of Raizer.[6] Several other studies[7,8] followed this analysis but used more sophisticated analytical and computational methods. Unfortunately, one-dimensional models have an inherent weakness. The LSP tends to be highly dependent on laser beam geometry, radial convection and radial diffusion transport of momentum and energy in the flow. Keefer and coworkers[9,10] developed a simplified semi-two-dimensional model which considered the radial energy diffusion but assumed that the laser beam and the streamlines were parallel. Later, Glumb and Krier[11] extended that model by using a converging laser beam, as well as using more realistic gas properties. However, their model still did not consider the momentum equations but, instead, assumed that the radial velocity was zero.

Merkle and coworkers[12,13] used a contemporary numerical method to attack the full two-dimensional problem. They succeeded in the calculation of a low temperature LSP (peak temperature about 4,000 K) in a low-mach number hydrogen flow seeded with cesium. It is feasible to extend their approach to a pure hydrogen plasma, but the higher peak temperature (about 16,000 K) and much stronger nonlinear optical properties of the pure hydrogen plasma can result in numerical stability problems.

Recently, Jeng and Keefer[14,15] obtained the numerical solutions for a rigorous two-dimensional model with realistic gas properties for the LSP in pure argon and pure hydrogen flows. Their results for the argon flows agree well with experimental data[16,17] in the prediction of plasma position, size, shape and peak temperature. Jeng et al[15,18,19] have also studied the effect of laser power, flow rate, static pressure and optical geometry on the LSP flows. Their work also indicated that there are no fatal errors in the laser propulsion concept, and the critical parameters of plasma size, position, radiation heat loss and energy conversion efficiency, can be controlled using an appropriate optical arrangement and a suitable flow configuration.

The objectives of the current study are to develop a new numerical code based on extended plasma model developed by Jeng and Keefer[14,15] for the real nozzle flow which includes both low and high mach number flows, and to conduct a preliminary parametric study of laser rocket performance. There was no attempt, in this paper, to determine the actual rocket performance. In the following section, the theoretical method used in the study is described. This is followed by a discussion of model calculations and some initial parametric studies.

THEORETICAL MODEL

LASER BEAM. Geometric optics were used to describe the laser beam which was assumed to be divided into a finite number of individual rays. Each ray path through the optical system to the plasma flow was calculated using real-ray tracing. Diffraction of the laser beam due to the finite aperture of the lens, and effects due to the inhomogeneous refractive index within the plasma were neglected in the calculation. The local intensity of each individual ray i was described by Beer's law written in the the following form.

$$\frac{dI_i}{ds_i} = -\alpha I_i \qquad (1)$$

where s_i is the distance along the laser propagation direction for ray i, and α is absorption coefficient at laser wavelength and depends on local plasma temperature and pressure.

PLASMA FLOW. The model assumed that the flow is laminar, steady-state, axisymmetric and has variable physical properties. The pressure of the plasma is relatively high so local thermodynamic equilibrium (LTE) for the plasma can be assumed with little error. Therefore, the plasma can be described by a single temperature, and its physical properties are only a function of this temperature and pressure. The model also considered the thermal radiation emitted from the plasma which included the contributions from free to free, free to bound, and bound to bound transitions. These radiation properties are a strong function of wavelength, and the current model adopted the simplified approach, developed by Kemp

et al[20] and Caledonia et al.[21] to solve the hydrogen plasma radiation transport equations. Radiation transport was divided into two parts depending on wavelength: for wavelengths longer than 0.095 μm, the optical depth is long and an optically thin approximation, in which all radiation escapes from the plasma, was used; and in other wavelength regions, the optical depth is short and an optically thick approximation, which can be described as a diffusion process, was assumed. Following the above assumptions, the equations of conservation of mass, momentum and energy for the flow can be written as :

$$\frac{\partial(\rho u)}{\partial x}+\frac{1}{r}\frac{\partial(r\rho v)}{\partial r}=0, \tag{2}$$

$$\frac{\partial(\rho uu)}{\partial x}+\frac{1}{r}\frac{\partial(r\rho uv)}{\partial r}=-\frac{\partial p}{\partial x}+\frac{\partial}{\partial x}\left(\mu\frac{\partial u}{\partial x}\right)$$
$$+\frac{1}{r}\frac{\partial}{\partial r}\left(\mu r\frac{\partial u}{\partial r}\right)+\frac{\partial}{\partial x}\left(\mu\frac{\partial u}{\partial x}\right)+\frac{1}{r}\frac{\partial}{\partial r}\left(\mu r\frac{\partial v}{\partial x}\right)$$
$$-\frac{\partial}{\partial x}\left[\frac{2\mu}{3}\left(\frac{\partial u}{\partial x}+\frac{1}{r}\frac{\partial(rv)}{\partial r}\right)\right], \tag{3}$$

$$\frac{\partial(\rho uv)}{\partial x}+\frac{1}{r}\frac{\partial(r\rho vv)}{\partial r}=-\frac{\partial p}{\partial r}+\frac{\partial}{\partial x}\left(\mu\frac{\partial v}{\partial x}\right)$$
$$+\frac{1}{r}\frac{\partial}{\partial r}\left(\mu r\frac{\partial v}{\partial r}\right)+\frac{\partial}{\partial x}\left(\mu\frac{\partial u}{\partial r}\right)+\frac{1}{r}\frac{\partial}{\partial r}\left(\mu r\frac{\partial v}{\partial r}\right)-\frac{2\mu v}{r^2}$$
$$-\frac{1}{r}\frac{\partial}{\partial r}\left[\frac{2\mu r}{3}\left(\frac{\partial u}{\partial x}+\frac{1}{r}\frac{\partial(rv)}{\partial r}\right)\right]+\frac{2\mu}{3r}\left(\frac{\partial u}{\partial x}+\frac{1}{r}\frac{\partial(rv)}{\partial r}\right), \tag{4}$$

$$\frac{\partial(\rho uh)}{\partial x}+\frac{1}{r}\frac{\partial(r\rho vh)}{\partial r}=\frac{\partial}{\partial x}\left(\frac{k_{eff}}{c_p}\frac{\partial h}{\partial x}\right)$$
$$+\frac{1}{r}\frac{\partial}{\partial r}\left(\frac{rk_{eff}}{c_p}\frac{\partial h}{\partial r}\right)-\frac{\partial\left(\rho u\left(\frac{1}{2}u^2+\frac{1}{2}v^2\right)\right)}{\partial x}$$
$$-\frac{\partial\left(r\rho v\left(\frac{1}{2}u^2+\frac{1}{2}v^2\right)\right)}{r\partial r}+\frac{4}{3}\mu\left(\left(\frac{\partial u}{\partial x}\right)^2+\left(\frac{\partial v}{\partial r}\right)^2\right)$$
$$+\mu\left(\left(\frac{\partial v}{\partial x}\right)^2+\left(\frac{\partial u}{\partial r}\right)^2\right)+\frac{4}{3}\mu\frac{\partial u}{\partial x}\frac{\partial v}{\partial r}+2\mu\frac{\partial v}{\partial x}\frac{\partial u}{\partial r}$$
$$+\frac{1}{r}\left(\frac{4}{3}\mu\frac{v^2}{r}-\frac{4}{3}\mu v\left(\frac{\partial v}{\partial x}+\frac{\partial v}{\partial r}\right)\right)$$
$$+\sum\alpha I_i-\dot{q}_{rad}, \tag{5}$$

where k_{eff} is the sum of molecular thermal conductivity and radiation-induced thermal conductivity in the optically thick limit; $\dot{q}_{rad}$ is radiative heat loss in the optically thin limit; $\alpha\Sigma I_i$ represents the local power addition from the laser beam to the flow; and as mentioned before, the physical properties involved in equations (2-5) are a function of the local temperatures and pressures. Reference 15 has a detailed description of the thermophysical and optical properties sources used in this work.

In the calculations, adiabatic, nonslip and zero emissivity conditions were assigned at the thruster wall. Total pressure, total temperature and zero radial velocity were specified at the inlet, and upstream running Riemann invariants extrapolation plus the isentropic relations were used to calculate other properties. At the exit, the properties were linearly extrapolated from the interior flow domain.

METHOD OF COMPUTATION

COORDINATE TRANSFORMATION. The set of transport equations (3-5) can be written in the cylindrical system coordinates for the dependent variable, ϕ, in the following generalized form:

$$\frac{\partial}{\partial x}(r\rho u\phi)+\frac{\partial}{\partial r}(r\rho v\phi)=\frac{\partial}{\partial x}(\Gamma^{\phi}r\frac{\partial\phi}{\partial x})$$
$$+\frac{\partial}{\partial r}(\Gamma^{\phi}r\frac{\partial\phi}{\partial r})$$
$$+r\cdot R^{\phi}(x,r), \tag{6}$$

where Γ^{ϕ}_{eff} is the effective diffusion coefficient and $R^{\phi}(x,r)$ is the source term. The source term for the momentum equations (3,4) also includes the diffusion terms from the dilation effect. When new independent variables ς and η are introduced, Eq. (6) changes according to the general transformation ς and η. A schematic illustration of the relations between the physical domain and the transformed domain is shown in Figure 2. Equation (6) is rewritten in ς and η coordinates as follows:

$$\frac{1}{J}\frac{\partial}{\partial\xi}(r\rho U\phi)+\frac{1}{J}\frac{\partial}{\partial\eta}(r\rho V\phi)=$$
$$\frac{1}{J}\frac{\partial}{\partial\xi}\left[\frac{\Gamma^{\phi}r}{J}(q_1\phi_\xi-q_2\phi_\eta)\right]+\frac{1}{J}\frac{\partial}{\partial\eta}\left[\frac{\Gamma^{\phi}r}{J}(-q_2\phi_\xi+q_3\phi_\eta)\right]$$
$$+r\cdot S^{\phi}(\xi,\eta) \tag{7}$$

where

$$U=ur_\eta-vx_\eta, \tag{8}$$

$$V=vx_\xi-ur_\xi, \tag{9}$$

$$q_1 = x_\eta^2 + r_\eta^2, \tag{10}$$

$$q_2 = x_\xi x_\eta + r_\xi r_\eta, \tag{11}$$

$$q_3 = x_\xi^2 + y_\xi^2, \tag{12}$$

$$J = x_\xi r_\eta - x_\eta r_\xi, \tag{13}$$

and $S^\phi(\varsigma, \eta)$ is the source term in the ς and η coordinates.

NUMERICAL ALGORITHM A nonstaggered grid system, as shown in Figure 2, is adopted in the calculations. For a typical grid node P are enclosed in its cell and surrounded by its neighbors N, S, E, and W. The integral of Eq. 7 over its control volume, by arbitrary taking $\Delta\varsigma = 1$ and $\Delta\eta = 1$, becomes

$$\begin{aligned}
&(r\rho U\phi)_e - (r\rho U\phi)_w + (r\rho V\phi)_n - (r\rho V\phi)_s \\
&= \left[\frac{r\Gamma^\phi}{J}(q_1\phi_\xi - q_2\phi_\eta)\right]_e - \left[\frac{r\Gamma^\phi}{J}(q_1\phi_\xi - q_2\phi_\eta)\right]_w \\
&+ \left[\frac{r\Gamma^\phi}{J}(-q_2\phi_\xi + q_3\phi_\eta)\right]_n - \left[\frac{r\Gamma^\phi}{J}(-q_2\phi_\xi + q_3\phi_\eta)\right]_s \\
&+ r \cdot J \cdot S^\phi(\varsigma, \eta),
\end{aligned} \tag{14}$$

Second-order center differencing is used to discretize the above equation, except for the convective terms when the cell Reynolds number is greater than 2. In that case, first order upwind differencing is used for the convective terms. A staggered grid system, for body-fitted coordinates, has been widely used,[22] and it has been known that an oscillatory field will be produced using the nonstaggered grid system. The artificial viscosity term proposed by Rhie and Chow[23] to cure the problem was also implemented in this study. The cross derivatives in the diffusion terms of Eq. (14) are the results of the nonorthogonal coordinate system and are usually small. In order to use the solution procedure for the five-point unknowns, these terms are combined with the source term and treated as known quantities and the resulting relation between ϕ_P and the neighboring values can be written as :

$$\begin{aligned}
A_p\phi_p &= A_E\phi_E + A_W\phi_W + A_N\phi_N + A_S\phi_S \\
&+ r \cdot J \cdot T^\phi(\varsigma, \eta),
\end{aligned} \tag{15}$$

where the coefficients A involve the flow properties of convection, diffusion, area, etc., and $T^\phi(\varsigma, \eta)$ includes the source term $S^\phi(\varsigma, \eta)$ and the cross derivatives in the diffusion terms.

PRESSURE CORRECTION PROCEDURE. While the general transport equation, Eq. (15), was used to solved momentum and energy equations, the pressure field must be solved using the continuity equation. The procedure used in this work is an adoption of algorithm developed by Rhie,[24] and only a brief discussion is presented in this section. The pressure equation used in the adopted procedure is similar to that of SIMPLER[25] and PISO,[26,27] except that the density term is treated implicitly for the compressible flow. The basic idea is to use the following relations to correct the mass flux obtained from momentum equations

$$\rho u = \rho^* u^* + \rho' u^* + \rho^* u' \tag{16}$$

$$\rho v = \rho^* v^* + \rho' v^* + \rho^* v' \tag{17}$$

and the discretized pressure equation becomes a transport equation for compressible flow instead of Poisson equation. The ratio of diffusion term to convection term is dependent on Mach number, and as Mach number increases, the convection term becomes dominant. The split operator concept similar to PISO was also adopted in the current study to solve the pressure correction equation.

RESULTS AND DISUCSSION

Figure 3 shows the thruster dimensions used in the calculations. It includes a cylindrical section upstream of the convergent-divergent nozzle. The throat and cylindrical diameters are 6 and 40.74 mm respectively, and the exit to throat area ratio is 6. The coordinate origin used to present the calculated results is at the center of the throat. Although Figure 1 shows that the hydrogen flows into the chamber radially, in the calculations reported here the inlet flow direction was assumed axial. The total pressure and total temperature were specified at the inlet. In the traditional chemical rocket, the total pressure has a minor effect on the expected value of the specific impulse, but in the laser-supported rocket, the pressure has a substantial influence on the absorption and radiation processes that directly affect the available enthalpy of the propellant and the specific impulse of the thruster. Based on our previous parametric studies[15] for laser-sustained hydrogen plasmas in a constant area pipe flow, it was found that 3 atm total pressure was adequate for the thruster upstream condition, and this value was used in the calculations. The total temperature at the inlet was specified as 1500K in the calculations, based on the expected use of a regenerative cycle to recover the optically thin radiation from plasma.

The focusing lens used in the calculations has a nominal focal length 203 mm, and References 14 and 15 has detailed discussion of this lens geometry. The actual dimensions of this lens were adopted in the ray

tracing for the laser beam, so the spherical aberration of the lens was also included in the calculations. The laser was assumed to have 10.6 μm wavelength and a collimated, 40 mm diameter Gaussian beam incident on the lens. The only preliminary parametric study of the rocket performance reported in this paper was to focus the laser beam at different axial locations using the same lens arrangement. Table 1 lists the operating conditions, including one case without laser power addition.

In the calculations, nonuniformly spaced grids in the physical space were transformed into uniformly spaced grids in both radial and axial directions in the transformed space, as illustrated in Figure 4. From previous studies [14,15,18,19] of LSP within a constant diameter pipe, the position of the high temperature plasma zone was found to be highly dependent on the flow configurations and the optical arrangements, and it was not easy to prelocate the region in the physical plane where a dense grid distribution was needed to accommodate the high temperature gradients. Therefore, a preliminary calculation was first performed for each case to locate the high temperature zone, then the grid distribution was refined and used for the final calculation.

The newly developed computer code was first used to calculate the thruster flow without considering laser heat addition, and the results were used to check the behavior of the computer program and to serve as benchmark to compare with the other calculated cases which included the laser heat addition. The Mach number contours for case no. 1 are shown in Figure 5. Because the nozzle expansion angle is only 6°, the contours outside of the wall where diffusion transport is not important, are almost straight, and are similar to one-dimensional nozzle calculations. Since the nonslip condition was applied in the calculations, the Mach number near the wall is smaller than that near the centerline at the same axial location. This demonstrates that the newly developed computer program can also handle the boundary layer in supersonic flow. In this test case, there were only a few grids within the boundary, and we made no special attempt to resolve the boundary layer to good numerical accuracy. If needed, more grids can be included in that region and a more accurate solution can be obtained.

Figure 6 shows isotherms for case no. 2, and the outer laser beam boundary was also plotted in the figure as a dashed line. The plasma core is located upstream of the laser focus, and the distance between the laser focus and the high temperature plasma core, which depends on flow configurations and optical arrangements as discussed in the early section of this paper, is 10 mm. Downstream of the laser focus, the mixing process quickly reduces the centerline temperature. In the throat region, only a small portion of the hydrogen flow near the axis is heated, and a major portion of the flow is still unheated. For an optimized rocket, one of the design criteria is to have a uniformly distributed temperature at the throat in order to reduce the two-dimensional losses. In the calculated case, this condition was not satisfied. Near the wall of the nozzle exit, there is a local hot spot which is due to the viscous dissipation effect within the boundary layer.

Laser-sustained plasmas, operated at 30 kW laser power, absorb almost all of the incoming laser beam power. In the calculated case no. 2, only 397 W of laser power was transmitted through the plasma which either reached the thruster wall or was transmitted through the throat. The wall material could easily withstand this small level of transmitted power density. The optically thin radiation from the plasma is also an important factor for a laser-supported rocket design. It represents the portion of laser power that is not directly converted into the flow power. However, this radiation power, like a part of the transmitted laser power, will be absorbed by the wall, and by using a regenerative cycle, part of this energy can be recovered and used to heat the hydrogen from its storage temperature up to the propellant inlet temperature of the thruster. For case no. 2, the optically thin radiation was 17.9 kW which was only 30 % of the energy needed to heat hydrogen to the assigned inlet temperature, 1500 K.

Pressure and Mach number contours for case no. 2 are shown in Figure. 7 and Figure. 8, respectively. Pressure contours downstream of the laser focus in Figure 7 are similar to the calculated results for case no. 1. Those have only a very small radial variation and imply that the nonuniformly distributed temperature field has little effect on the pressure field. However, a high pressure zone, even higher than the inlet static pressure of the thruster ($3x10^5 N/m^2$), occurs ahead the high temperature plasma zone. The Mach number at the inlet is about 0.019 and the maximum calculated Mach number is 2.605 at the nozzle exit. The Mach number contours in the supersonic region are very complicated, compared to that of case. no. 1 in Figure 5, although the velocity monotonically increased from the wall to the centerline. The Mach number at the centerline is always smaller than away from the centerline, since the temperature, as well as sonic speed, is higher at the centerline. The unheated region still has very straight Mach number contours similar to those shown in Figure 5 for case no. 1. The mixing region between hot center flow and the colder unheated flow shows very complicated contours. Mixing in that region, which implies variations of sonic speed due to different temperature, molecular weight, and specific heat, are the major factors. The Mach

number near the wall is smallest due to the boundary effect, and the Mach number on the centerline is always smaller than that away from the centerline in the subsonic portion of the flow.

In the previous studies[15,16], it was found that laser heat addition to the flow will generate a very complicated velocity field, even in a constant area pipe. The same behavior was also observed in the current results. Figure 9 shows the radial velocity contours for case no. 2. Near the high temperature plasma core region, both positive and negative radial velocity occurs. In the supersonic region, a local minimum exists in the mixing zone between heated and unheated flow for case no. 2, and the radial velocity increases from the centerline up to the edge of the boundary for the unheated case no. 1. Nonuniformly distributed temperature at the throat is the main cause for the above results.

Figure 10(a) and 10(b) show isotherms for cases no.4 and no. 5, respectively. Their laser focuses are closer to the throat than case no. 2, and the focus is within the nozzle contracting section for case no. 5. As the laser focus moves closer to the throat, the size of the plasma becomes smaller. Since the optically thin radiation is proportional to the plasma size, the radiation loss for case no. 5, 9.9 kW, is much smaller than 15.9 kW and 18.6 kW for cases no.4 and no. 2, respectively. Because the transmitted laser power is small and similar for all cases, the energy directly converted to the flow is highest for case no. 5. The laser beam also heats a larger portion of the flow at the throat in case no. 5 than other cases, and this produces better thruster performance.

Table 2 lists the calculated properties for the five test cases. The optically thin radiation heat loss ranges from 61 % to 33 % of the laser power, and the transmitted laser power is relatively small by comparison. The peak axial velocity, which is always located on the centerline at the exit, increases from 4763 m/sec for the unheated thruster to 18957 m/sec for case no. 5. The maximum temperature of the plasma shows little dependence on the variation of laser focal position among the test cases. The peak Mach number at the exit plane is located within the unheated flow for all test cases, and it increases as the laser focal point moves downstream. The mass flow rate decreases as the laser focal point moves toward the throat.

SUMMARY AND CONCLUSIONS

The flow within a laser-sustained plasma rocket thruster has been successfully calculated. The physical model was based on steady-state two-dimensional Navier-Stokes equations for the flow and geometric real-ray tracing for the laser beam. Realistic thermophysic and optical properties based on locally thermodynamical equilibrium assumptions were incorporated into the calculations, and radiation heat transfer from the plasma was simplified using optically thin and optically thick assumptions. The governing equations were first transformed into body-fitted coordinates and were solved numerically. A pressure-based Navier-Stokes solver with a split operator concept was used for the numerical procedure.

Several laser propulsion cases were calculated using the newly developed computer code. The nozzle geometry, flow configuration and optical arrangements were not optimized for rocket performance. However, some useful information was obtained from these preliminary test cases. The performance of the rocket is highly dependent on the laser focal position. The maximum velocity is larger when laser focal point moves closer to the throat. Generally speaking, the laser beam only heated a small portion of the hydrogen propellant, and the best thruster performance will not be achieved due to the two-dimensional losses. In the future, an extensive parametric study will be required to optimize the rocket performance, and one of the major goals of the study is to design the rocket to produce a more uniformly distributed temperature at the throat.

ACKNOWLEDGEMENT

The authors acknowledge Dr. C. Peters and Mr. R. Rhodes for providing valuable discussion, and Mr. J. White and Mr. M. Smith for preparing the graphs. This work has been partially supported by NASA Marshell Flight Center under Contract NAS8-36620 monitored by Mr. R. Eskridge, and Air Force Office of Scientific Research under Grant AFOSR-86-0317 monitored by Dr. R. Vondra.

REFERENCES

1. Simons, G. A., and Pirri, A. N., " The Fluid Mechanics of Pulsed Laser Propulsion," *AIAA J.*, Vol. 15, June 1977, pp. 835-842.
2. Keefer, D. R., Elkins, R., Peters, C. and Jones, L., "Laser Thermal Propulsion," in *Orbit-Raising and Maneuvering Propulsion: Research Status and Needs*, edited by L. H. Caveny, (American Institute of Aeronautics and Astronautics Inc., New York), pp. 129-148, 1984.
3. Kemp, N. H. and Root, R. G., "Analytical Study of Laser-Supported Combustion Waves in Hydrogen," *Journal of Energy*, Vol. 3, 1979, pp. 40-49.
4 Glumb, R. J. and Krier, H., "Concept and Status of Laser-Supported Rocket Propulsion," *J. Spacecraft*, Vol. 21, No.3, pp. 70-79, 1983.

5. McCay, T. D. and Dexter, C. E., "Chemical Kinetic Performance Losses for a Hydrogen Laser Thermal Thruster," AIAA paper 85-0907, June, 1985.

6. Raizer, Y. P., "Subsonic Propagation of a Light Spark and Threshold Conditions for the Maintenance of Plasma by Radiation," *Soviet Physics - JETP*, Vol. 31, 1970, pp. 1148-1154.

7 Jackson, J. P., and Nielsen, P. E., "Role of Radiative Transport in the Propagation of Laser-Supported Combustion Waves," *AIAA Journal*, Vol. 12, 1974, pp. 1498-1501.

8. Keefer, D. R., Peters, C. E. and Crowder, H. L., "A Reexamination of the Laser Supported Combustion Wave," *AIAA Journal*, Vol. 23, 1985, pp. 1208-1212.

9. Batteh, J. H. and Keefer, D. R., "Two-Dimensional Generalization of Raizer's Analysis for the Subsonic Propagation of Laser Sparks," *IEEE Transactions on Plasma Science*, vol. PS-2, 1974, pp. 122-129.

10. Keefer, D. R., Crowder, H. L. and Elkins, R., "A Two-Dimensional Model of the Hydrogen Plasma for a Laser Powered Rocket," AIAA Paper No. 82-0404, January, 1982.

11. Glumb, R. J. and Krier, H., "A Two-Dimensional Model of Laser-Sustained plasmas in Axisymmetric Flow fields," AIAA Paper No. 85-1553, July, 1985.

12. Merkle, C. L., Molvik, G. A. and Choi, Y.-H., "A Two-Dimensional Analysis of Laser Heat Addition in a Constant Absorptivity Gas," *AIAA Journal*, Vol. 23, 1985, pp. 1053-1060.

13. Merkle, C. L., Molvik, G. A. and Shaw, E. J.-H., "Numerical Solution of Strong Radiation Gasdynamic Interactions in a Hydrogen-Seedant Mixture," AIAA Paper No. 85-1554, July, 1985.

14. Jeng, S-M. and Keefer, D., "Theoretical Investigation of Laser-Sustained Argon Plasmas," Vol. 60, No. 7, pp. 2272-2279 *J. Applied Physics*, 1986.

15. Jeng, S-M. and Keefer, D., "Numerical Study of Laser-Sustained Hydrogen Plasmas in a Forced Convective Flow," AIAA paper 86-1524, May, 1986.

16. Welle, R. P., Keefer, D. R. and Peters, C. E., "Energy Conversion Efficiency in High-Flow, Laser-Sustained Argon Plasmas," AIAA paper 86-1078.

17. Keefer, D.R., Crowder H.L., and Peters, C.E., "Laser-Sustained Argon Plasmas in a Forced Convection Flows," AIAA paper No. 85-0388, January, 1985.

18. Jeng, S-M., Keefer, D., Welle, R., and Peters, C., "Numerical Study of Laser-Sustained Argon Plasmas in a Forced Convective Flow," AIAA-86-1078, May, 1986.

19. Keefer, D., Jeng, S.-M., and Welle, R., "Laser Thermal Propulsion Using Laser Sustained Plasmas," IAF-86-175, 37th Congress of the International Astronautical Federation, Innsbruck, Austria, Oct. 4-11,1986.

20. Kemp, N. H. and Root, R. G., "Analytical Study of Laser-Supported Combustion Waves in Hydrogen," NASA CR-135349, 1977.

21. Caledonia, G. E., Wu, P. K. S. and Pirri, A. N., "Radiant Energy Absorption Studies for Laser Propagation," NASA CR-134809, 1975.

22. Shyy W, "A Numerical Study of Annular Dump Diffuser Flows," *Computer Methods In Applied Mechanics And Engineering*, Vol. 53, pp. 47-65, 1985.

23. Rhie, C. M., and Chow, W. L., "Numerical Study of the Turbulent Flow Past an Airfoil with Trailing Edge Separation," *AIAA J.*, Vol. 21, No. 11, pp. 1525-1532, Nov. 1983.

24. Rhie, C. M. "A Pressure Based Navier-Stokes Slover Using the Multigrid Method, " AIAA paper 86-0207, AIAA 24th Aerospace Sciences Meeting, Reno, Nevada, Jan. 1986.

25. Patankar, S. V., *Numerical Heat Transfer and Fluid Flow*, New Hemisphere, Washington, D.C., 1980.

26. Issa, R. I., "Solution of the implicitly Discretized Fluid Flow Equations by Operator-Splitting," *J. Computational Physics*, Vol. 62, pp. 40-65, 1986.

27. Issa, R. I., Gosman, A. D., and Watkins, A.P., "The Computation of Compressible and Incompressible Recirculating Flows by a Non-iterative Implicit Scheme," *J. Computational Physics*, Vol. 62, pp. 66-88, 1986.

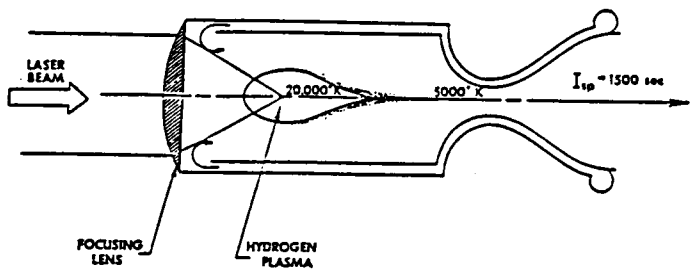

Figure 1. Schematic of a laser-sustained plasma propulsion thruster chamber.

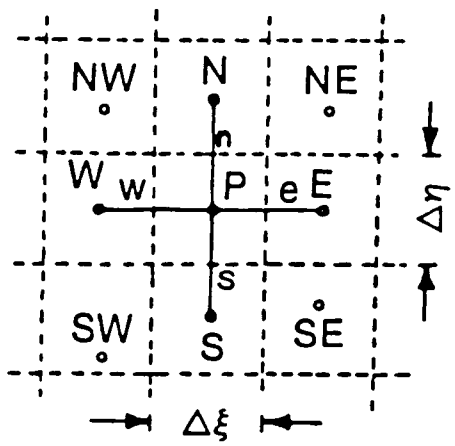

(b)

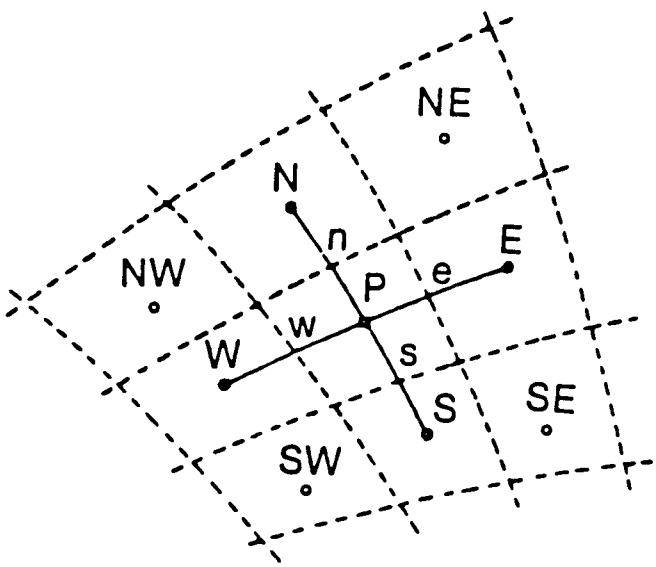

(a)

Figure 2. Finite-difference grid representation: (a) physical plane, (b) transformed plane.

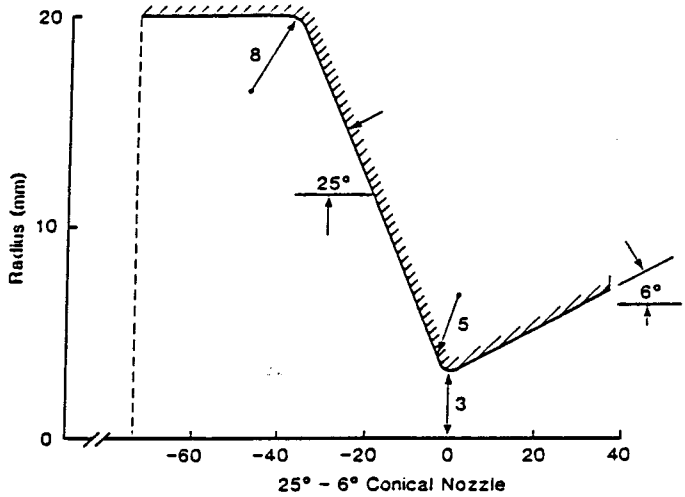

Figure 3. Conical nozzle geometry.

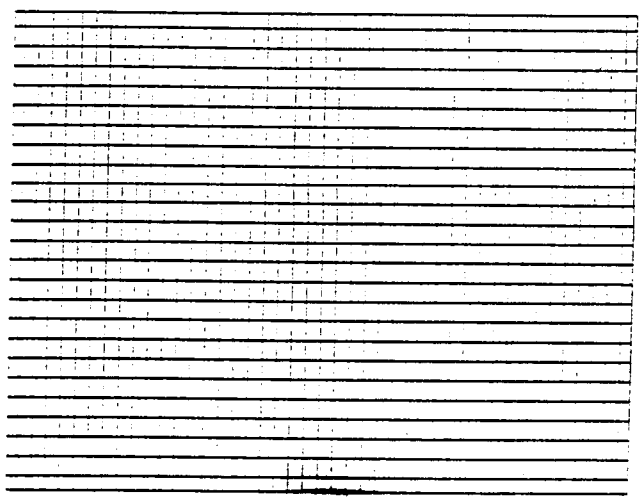

(b)

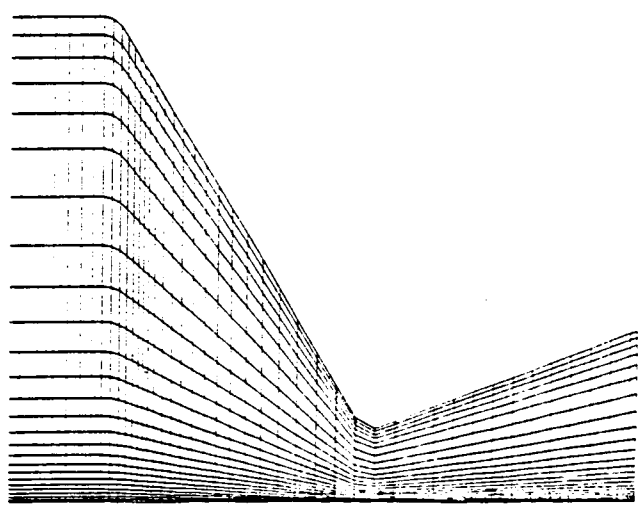

(a)

Figure 4. Schematic of grid transformation (a) physical plane, (b) transformed plane.

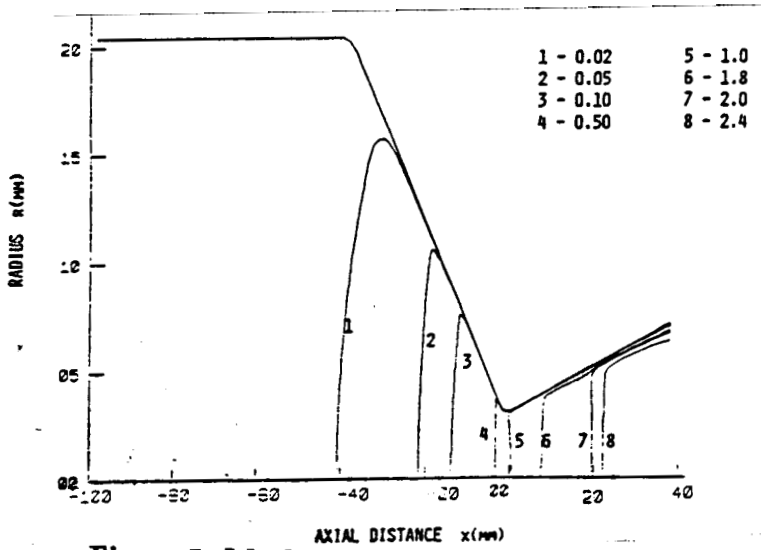

Figure 5. Mach number contours for case number 1.

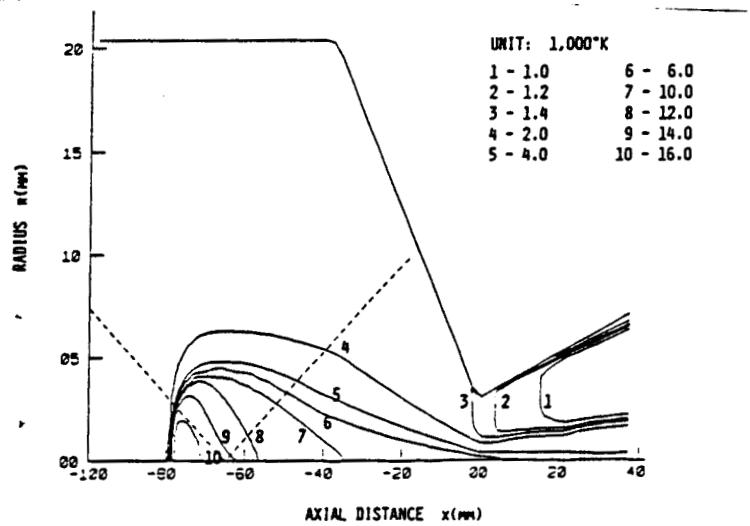

Figure 6. Temperature contours for case number 2.

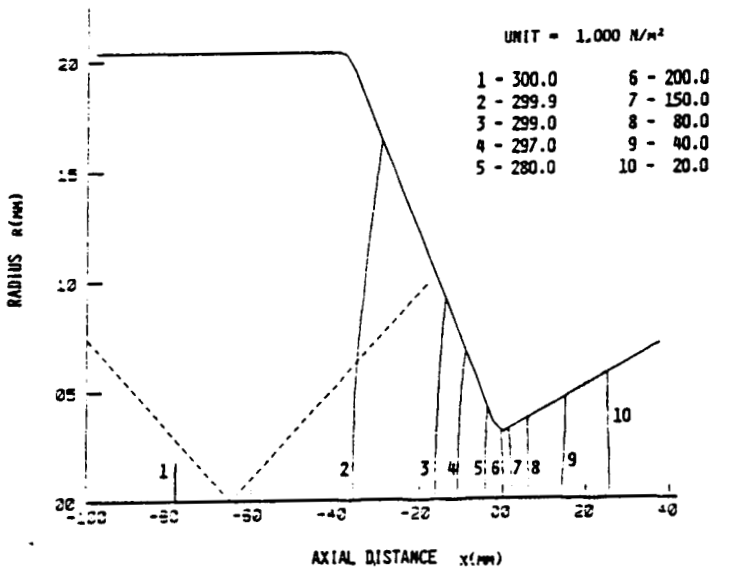

Figure 7. Pressure contours for case number 2.

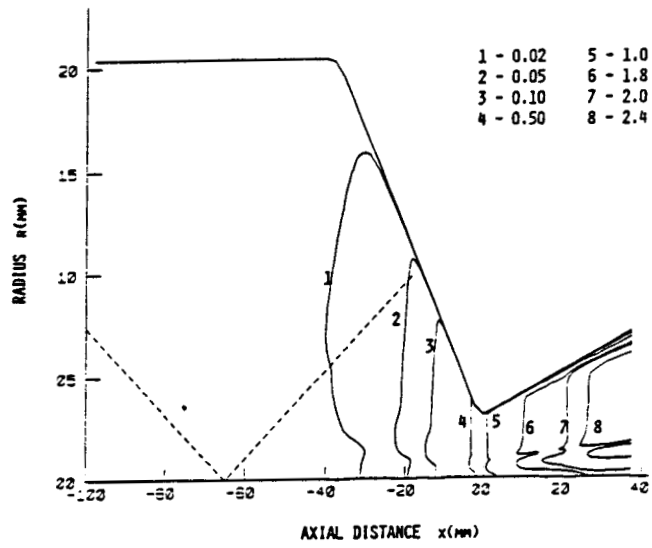

Figure 8. Mach number contours for case number 2.

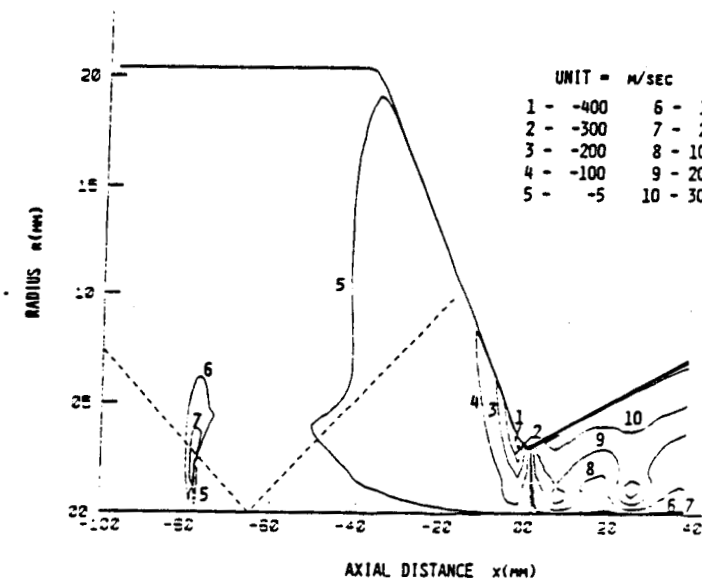

Figure 9. Radial velocity contours for case number 2.

ORIGINAL PAGE IS
OF POOR QUALITY

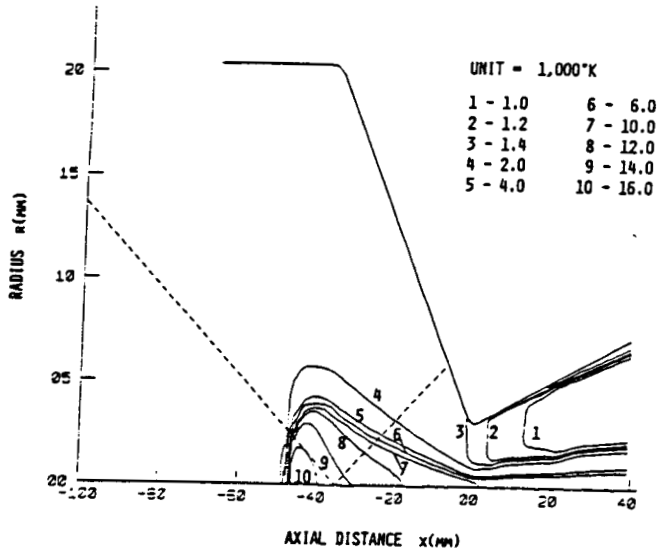

(a)

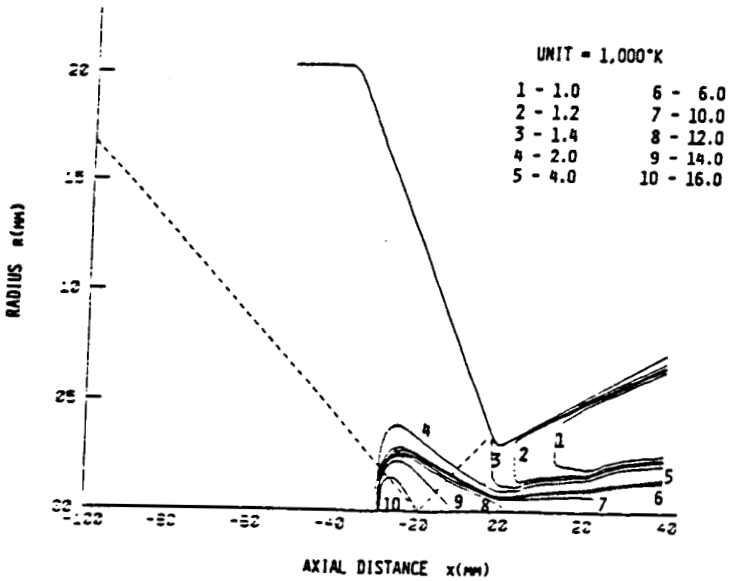

(b)

Figure 10. Temperature contours: (a) case number 4, (b) case number 5.

Table 1: Test Conditions

Case no.	Laser power (kW)	focus (mm)
1	0	
2	30	-65
3	30	-50
4	30	-35
5	30	-20

Table 2: Calculated properties for five test cases

Case no.	1	2	3	4	5
Optically thin. rad. (kW)	0.	18.6	17.9	16.0	9.9
Transmitted power (W)	0.	397	395	330	320
Max. axial vel. (m/sec)	4783	12513	13403	15643	18957
Max. temperature (K)	1500	16854	16872	16878	17293
Max. mach number	2.50	2.61	2.64	2.68	2.78
Mass flow rate (g/sec)	2.88	2.82	2.74	2.69	2.66

AIAA'87

AIAA - 87 - 2166

A Theoretical Evaluation of Laser Sustained Plasma Thruster Performance

San-Mou Jeng and Dennis Keefer
Center for Laser Applications
The University of Tennessee Space Institute
Tullahoma, TN 37388

AIAA/SAE/ASME/ASEE 23rd Joint Propulsion Conference

June 29-July 2, 1987/San Diego, California

A Theoretical Evaluation of Laser-Sustained Plasma Thruster Performance

San-Mou Jeng* and Dennis Keefer**

Center for Laser Applications

University of Tennessee Space Institute

Tullahoma, Tennessee 37388

(615) 455-0631 ext. 338

ABSTRACT

An extensive numerical experiment has been conducted to evaluate rocket thruster performance using a laser-sustained hydrogen plasma as the propellant. The plasma was sustained using a 30 kW CO_2 laser beam operated at 10.6 μm focused inside the thruster. The steady-state Navier-Stokes equations coupled with the laser power absorption process have been solved numerically. A pressure based Navier-Stokes solver using body-fitted coordinate was used to calculate the laser-supported rocket flow which included both recirculating and transonic flow regions. The local thermodynamic equilibrium (LTE) assumption was used for the plasma thermophysical and optical properties. Geometric ray tracing was adopted to describe the laser beam. Several different throat size thrusters operated at 150 and 300 kPa chamber stagnation pressure were studied. It was found that the thruster performance (vacuum specific impulse) was highly dependent on the operating conditions, and a properly designed laser supported thruster can attain a specific impulse around 1500 secs. The heat loading on the thruster wall was also estimated and was in the range of that for a conventional chemical rocket.

NOMENCLATURE

I	local laser ray intensity
k	conductivity
p	pressure
$\dot{q}$	optically thin radiation
s	distance along laser ray
u, v	velocity component along $x-$ and $r-$axis, respectively
ρ	density
α	absorption coefficient

Subscript

i	for laser ray i
rad	radiation

INTRODUCTION

A propulsion system supported by a laser-sustained plasma (LSP) has been the subject of many studies. A schematic of a continuously laser supported thruster is shown in Figure 1. The high power laser beam from a remote site is focused into the thruster. The plasma is ignited and continuously sustained near the laser focus. The plasma is used to absorb the power from the laser beam and convert it into propellant enthalpy. Since the focusing lens is positioned at the end of the thruster, the propellant flows into chamber radially through annular slots. The concept of two separated propellant inlets are used for the rocket shown in the Figure 1. The propellant flowing through the slot near the lens is relatively cold and serves to cool the lens. The major propellant flow enters the thruster through the other slot and has a relatively high temperature. This temperature is dependent on the regenerative heat from the thruster wall to heat the propellant which was originally at storage temperature. Within the thruster, the flow convects high enthalpy plasma downstream and mixes with other propellant to obtain a more uniform radial temperature distribution. Then the propellant thermal energy is converted to kinetic energy and produces the required thrust for the rocket through a converging and diverging nozzle. The major advantage of the laser thruster, compared to the chemical thruster, is higher specific impulse (about 1000-2000 secs) since the lowest molecular weight propellant (hydrogen) and a higher propellant temperature (not limited to the flame temperature of a combustion process) can be used.

---

* Assistant professor, Aerospace and Mechanical Engineering, Member AIAA

** Professor, Engineering Science and Mechanics, Member AIAA

The modeling of the LSP for propulsion began with the one-dimensional work of Raizer.[1] Jeng and Keefer[2] have extensively reviewed the early analytical work using one-dimensional and semi-two-dimensional models. A full two-dimensional model on the LSP was first numerically solved by Merkle and coworkers.[3,4] The objective of their work was to demonstrate the capability of the developed numerical method, and part of the governing process of LSP model was simplified. For example, the plasma radiation process was neglected in their model. They succeeded in the calculation of a low temperature LSP (peak temperature about 4,000 K) in a hydrogen flow seeded with cesium. They adopted a rocket geometry, but the calculations were limited to the subsonic flow region. It is feasible to extend their approach to a pure hydrogen plasma, but the higher peak temperature (about 16,000 K) and much stronger nonlinear optical properties of the pure hydrogen plasma can result in numerical stability problems.

Jeng and Keefer[2] obtained the numerical solutions for a rigorous two-dimensional model with realistic gas properties for the LSP in pure argon subsonic pipe flow. Their results for the argon flows agree well with experimental data[5,6] in the prediction of plasma position, size, shape and peak temperature. Jeng and Keefer[7,8] also extended the model for the LSP in pure hydrogen subsonic flows and studied the effect of laser power, flow rate, static pressure and optical geometry on the LSP structures. A study using different laser beam profiles and wavelengths was also investigated recently[9]. Their work indicated that there are no fatal errors in the laser propulsion concept, and the critical parameters, for example plasma size, position, radiation heat loss and energy conversion efficiency, can be controlled using an appropriate optical arrangement and a suitable flow configuration.

Recently, Jeng and Keefer[10] developed a numerical method to solve the laser supported rocket. They have successfully calculated a hydrogen LSP in the transonic flow region. They considered an axial inflowing propellant, but only a limited number of rockets were investigated. Although they did not optimize to the rocket design, the predicted rocket performance is rather promising.

The objectives of the current study are to extend the developed numerical code for calculating realistic rocket thrusters, and to perform extensive numerical experiments for an optimized rocket design powered by a 30 kW CO_2 laser. The calculated flow structure, rocket performance (vacuum specific impulse and thrust) and the heat loading on the thruster wall will be discussed. In the following section, the theoretical method used in the study is described.

THEORETICAL MODEL AND METHOD OF COMPUTATION

An extensive discussion of the theoretical model and numerical approach can be found in References 7-10. Only a brief description of the model and numerical method is presented in this section.

LASER BEAM. Geometric optics were used to describe the laser beam which was assumed to consist of a finite number of individual laser rays. Each laser ray path through the optical system to the plasma flow was calculated using real-ray tracing. Diffraction of the laser beam due to the finite aperture of the lens, and effects due to the inhomogeneous refractive index within the plasma were neglected in the calculation. Beer's law was used to calculate the local intensity for each individual ray:

$$\frac{dI_i}{ds_i} = -\alpha I_i \qquad (1)$$

PLASMA PROPERTIES. Since the calculated rocket has a relatively high pressure, local thermodynamic equilibrium (LTE) for the plasma can be assumed with little error. Therefore, the plasma can be described by a single temperature, and its physical properties are only a function of this temperature and pressure. Reference 7 has a detailed description of the thermophysical and optical properties used in this work.

FLUID FLOW. It was assumed that the flow is steady-state, laminar and axisymmetric. The conservation of mass and Navier-Stokes equations for compressible and variable properties flow were used in the analysis. These equations are similar to those used in typical fluid mechanics analysis and are discussed in the previous work.[10]

One of the major interactions between a high power laser beam and plasma is the energy absorption process. The energy equation, EQ. [2], used in the calculations is listed below, and the $\sum \alpha I_i$ term represented the local heat addition from the laser to the fluid.

$$\frac{\partial(\rho u h)}{\partial x} + \frac{1}{r}\frac{\partial(r\rho v h)}{\partial r} = \frac{\partial}{\partial x}\left(\frac{k_{eff}}{c_p}\frac{\partial h}{\partial x}\right)$$

$$+\frac{1}{r}\frac{\partial}{\partial r}\left(\frac{r k_{eff}}{c_p}\frac{\partial h}{\partial r}\right) - \frac{\partial\left(\rho u(\frac{1}{2}u^2 + \frac{1}{2}v^2)\right)}{\partial x}$$

$$-\frac{\partial\left(r\rho v(\frac{1}{2}u^2 + \frac{1}{2}v^2)\right)}{r\partial r} + DISS.$$

$$+\sum \alpha I_i - \dot{q}_{rad} \qquad (2)$$

This equation also included the thermal radiation emitted from the plasma and included the contributions from free to free, free to bound, and bound to bound transitions. These radiation properties are a strong function of wavelength, and the current model adopted the simplified approach, developed by Kemp et al[11] and Caledonia et al.[12] to solve the hydrogen plasma radiation transport equations. Radiation transport was divided into two parts depending on wavelength: for wavelengths longer than 0.095 μm, the optical depth is long, and an optically thin approximation in which all radiation escapes from the plasma, was used; and in the short wavelength region, the optical depth is short and an optically thick approximation, which can be described as a diffusion process, was assumed. The $\dot{q}_{rad}$ term in Equation [2] is radiative heat loss in the optically thin limit, and the k_{eff} is the sum of molecular thermal conductivity and radiation-induced thermal conductivity in the optically thick limit. The viscous dissipation is represented by $DISS$ in Equation [2].

NUMERICAL METHOD. The set of transport equations for fluid flow written in the conservative form and in the cylindrical system coordinates was first transformed to the generalized curvilinear coordinate system.[10] A nonstaggered grid system is adopted in the calculations for the set of the transport equations. For the transport equations of momentum and energy, second-order central differencing is used to discretize the equations except for the convective terms when the cell Reynolds number is greater than 2. In that case, first order upwind differencing is used. The staggered grid system in body-fitted coordinates has been widely used in the literature,[13] and it has been known that an oscillatory field will be produced using the nonstaggered grid system. The artificial viscosity term, proposed by Rhie and Chow[14] to cure the problem, was also implemented in this study.

While the above numerical algorithm was used to solve the momentum and energy equations, the pressure field must be solved using the continuity equation. The procedure used in this work is an adoption of the algorithm developed by Rhie.[15] This algorithm is similar to that of SIMPLE[16] and PISO,[17,18] except the density term is treated implicitly for compressible flow. The split operator concept similar to PISO was also adopted in the current study to solve the pressure correction equation.

RESULTS AND DISUCSSION

Figure 2 shows the thruster dimensions used in the calculations. As discussed in the previous section of this paper, the propellant temperature and flowrate of each inlet slot of the two-slot thruster shown in the Figure 1, are different and will depend on the requirements for lens cooling and the regenerative heating efficiency. This information is not well known yet, so the one-slot thruster shown in Figure 2 was chosen for the computation. The cylindrical section of the thruster has a 20 mm radius, which is the same as the lens and incoming laser beam radius, and 25° and 15° were used for the thruster converging and diverging angles, respectively. The other parameters used for the calculated rockets are tabulated in Table 1. The lens had a 54.5 mm nominal focal length and focused the incoming gaussian distributed 30 kW laser beam to 0.5 mm upstream of the throat.

Nonuniformly spaced grids, 70 by 44 grids, were used in the calculation, and the same procedure used in the previous work[10] to locate a dense grid distribution around the high temperature gradient zone was also implemented. The total pressure, total temperature and flow vector were specified at the interface between the slot and thruster chamber as the boundary conditions for the computations. Either 300 kPa or 150 kPa inlet total pressure was used for the parametric study, and zero inlet axial velocity was used. The total propellant temperature at the inlet is not easy to determine. It is influenced by the thruster wall material (emissivity), regenerative system performance and thruster internal heat transfer (convection and radiation). The total temperature of the inlet propellant was specified as 1500K in the calculations. This was based on the maximum expected use of a regenerative cycle to recover the optically thin radiation from plasma and the practical temperature limitation of the thruster wall material. The thruster wall temperature was also assigned as uniformly distributed 1500 K in the calculations.

The calculated isotherms and normalized streamlines for rocket No. 1 are shown in Figure 3 and Figure 4, respectively. The plasma is positioned near the throat with a peak temperature of 15,800 K upstream of the laser focus. Most of the propellant within the thruster is not directly heated by the laser beam. However, nearly all of the propellant mixes with the hot plasma and raises the propellant bulk temperature up to approximately 10,000 K before it enters the diverging section of the thruster. Eighty four percent of laser power (25 kW) is absorbed by the propellant, and most of the remaining laser power is transmitted through the throat, except for a very small portion that reaches the thruster wall.

C-2

Since the propellant enters the chamber radially through a slot away from the lens, part of the propellant is expected to recirculate within the thruster. As shown in Figure 4, two recirculation zones occur in this thruster. A large one exists near the focusing lens, and the other one is near the thruster wall downstream of the inlet slot. The streamlines near the centerline upstream of the plasma indicate the flow has an outward direction. This is because the downstream hot plasma propellant (low density) generates a locally unfavorable axial pressure gradient in the flow. This phenomena was also observed in the previous work[2,7,8] for the LSP within a constant area pipe.

An enlarged view of the isotherms and constant axial velocity contours around the throat are shown in Figure 5 and Figure 6, respectively. The leading edge of the LSP is 11 mm upstream of the throat. The axial temperature gradient at the leading edge is very high since the axial heat transfer of convection and conduction is in opposite directions. The detailed discussion of how LSP structures are influenced by forced convection and optical geometry can be found in the previous work.[2,7,8] At the throat the propellant is very hot, approximately 13,500 K on the centerline. The temperature decreases radially from the centerline and reachs a value near 1250 K, which corresponds to the sonic temperature of the adiabatic (without heat addition from the laser beam) propellant. Then the temperature increases due to the wall heat transfer and viscous dissipation effects.

The traditional chemical rockets are preferred to have a uniform temperature distribution at the throat to minimize the two-dimensional loss of thruster performance (Isp). For rockets supported by a laser beam, the spatial distribution of heat addition is highly nonuniform, and a nonuniform temperature distribution is likely to exit at the throat as shown in Figure 5. Actually, it is required to have some kind of nonuniform temperature distribution around the throat for a practical high performance laser supported thruster (around 10,000 K propellant temperature at the throat), or the thruster wall will be damaged. The heat loading on the thruster wall, which will be discussed later in this paper, is primary due to irradiation from the plasma. A stream of cold propellant near the wall as shown in Figure 5, which results in some loss of rocket performance, is required to cool the wall.

Upstream of the leading edge of the plasma a local minimum in the axial velocity occurs on the centerline where the propellant is unheated by the laser beam. The radial distribution of the axial velocity within the center plasma core region is relatively uniform with the peak axial velocity on the centerline. Large radial variations of the axial velocity is found near the thruster wall where the large radial temperature gradient is also located. The exit temperature and axial velocity on the centerline are 10,700 K and 25,300 m/s, respectively. The predicted vacuum specific impulse for this rocket, with exit area expansion ratio of 4, is 960 secs. With further expansion of this rocket, the estimated specific impulse of this rocket can be approximately 1500 secs.

The isotherms for two other throat radius thrusters operated at 150 kPa pressure, rockets Nos. 2 and 3, are shown in Figure 7. The leading edge and size of these plasmas are different. The mass flowrate, which is directly related to the throat size, is the major controlling factor for the plasma size and position. The mass flow rate of a constant total enthalpy fluid through a choked nozzle is proportional to the throat area. For the laser supported thruster, the propellant temperature and its distribution at the throat are other controlling factors for the mass flow rate. For a smaller throat thruster, a larger portion of the propellant at the throat has a high temperature and this will further reduce its critical mass flowrate. The calculated mass flow rate for cases 1-3, tabulated in TABLE 2, result from this effect. For a smaller throat thruster, the reduced axial velocity within the subsonic converging section of the thruster allows the plasma to move further upstream along the laser beam and to obtain a larger size, as shown in Figure 7. A detailed discussion of the interaction between the plasma structure and a forced convection flow can be found in References 2,7 and 8.

In the traditional chemical rocket, the total pressure has a minor effect on the expected value of specific impulse. However, in the laser-supported rocket the pressure has a substantial influence on the absorption and radiation processes which directly affect the available enthalpy of the propellant and the heat loading on the thruster wall. Figure 8 shows the isotherms for a 300 kPa inlet pressure thruster, rocket No 4. The absorption coefficient and optically thin thermal radiation for a hydrogen plasma are approximately proportional to the 1.5 power of pressure. With a higher absorption coefficient in this plasma, compared to those of rocket Nos. 1-3, only a very small amount of the laser power directly escapes from the thruster (see Table 2); however, the optically thin radiation from the plasma also increases. This results in a low conversion efficiency from laser power to available thermal power of the propellant. The higher absorption coefficient also results in a plasma which is positioned further upstream against the laser beam. Two local temperature maxima were predicted for this thruster. This results from two competitive processes which determine the local laser intensity: the attenuation by /p /vfill /eject /nd plasma absorption and the increase due to the converging laser

beam. References 7-8 contain a detailed discussion of this subject.

The vacuum specific impulse variations with area expansion ratio for the four calculated thrusters are shown in Figure 9. The most advanced chemical rocket has an Isp of about 500 secs, and the calculated Isp for the four laser supported rockets are between 700 and 1020 secs. At the exit of these rockets the ratio between thermal energy and the kinetic energy of the propellant is still relatively high, and further expansion of these rockets will greatly enhance the rocket performance. Although the propellant within the expansion section is expected to be far away from chemical equilibrium, the reasonable Isp is expected to be around 1500 secs for higher expansion ratios using rockets Nos. 1 and 3. The highest Isp among the test cases is 1022 secs from rocket No. 3. As discussed before, this thruster has the propellant almost fully heated at the throat. Thruster No. 1 has a little larger throat than rocket No. 3. and has a very small cold propellant stream near the throat. The calculated Isp of this rocket is only 20 secs less than thruster No. 3. With further increase of throat size, the size of cold stream propellant increases, and the calculated Isp decreases rapidly. The Isp for thruster No. 2 is an example. Rocket No. 4 operated at 300 kPa and the plasma occurs further away from the throat than the lower pressure thrusters. This results in a larger cold propellant stream around the throat and in a much lower Isp than the lower pressure thruster.

The heat loading on the inner wall of a good laser thruster should come from the plasma radiation, and a cold stream of propellant near the inner surface will reduce the heat flux through the wall. This heat flux is used to heat the propellant from its storage enthalpy up to the inlet enthalpy. The irradiation along the wall of the calculated rockets are shown in Figure 10. The irradiation first increases from the end of the thruster to where the hot plasma is located, and then decreases monotonically along the axial distance for all test rockets. The maximum irradiation on the wall for all the rockets is almost the same, although the 300 kPa rocket has much higher total irradiation flux on the wall (see Table 2). In order to estimate the radiation heat loading on the wall, the emissivity and absorptivity of the wall surface are needed. If absorptivity is unity, the irradiation will be equal to the wall heat loading. Generally, the absorptivity is less then one, and the radiation heat loading will be smaller and spatially smoothed. The calculated maximum irradiation represents an upper limit of the radiation heat loading, and all maxima are much less then the heat loading for chemical rockets.

Heat loading on the wall is also related to the thruster inlet propellant temperature which is regeneratively heated from the storage temperature. The propellant inlet temperature will influence the rocket performance as long as the cold stream of propellant exists near the wall at the nozzle. Rockets Nos. 1 and 3 have a very limited amount of unheated propellant at the throat, and the Isp for these rockets should not be strongly influenced by the inlet temperature. On the other hand, higher or lower inlet temperature will either increase or decrease the expected Isp significantly for rocket Nos. 2 and 4. An inlet temperature of 1500 K was used for the test rockets, and the expected inlet temperatures vs. three recovery efficiency of irradiation are tabulated in Table 3. Low pressure rockets Nos. 1 and 2 need the recovery efficiency of 30 and 52 percent, respectively, for the adopted inlet temperature, 1500 K. If the irradiation is fully converted to the propellant enthalpy through regenerative heating for these two thrusters, the inlet propellant temperatures will be 2810 K and 2390 K, respectively. For rockets Nos. 3 and 4, the inlet temperatures will be around 3400 K, which is not realistic in a practical device, and probably a radiator would be needed to dissipate the wall heat flux and lower the inlet propellant temperatures.

SUMMARY AND CONCLUSIONS

The flow within a laser-sustained plasma rocket thruster has been successfully calculated based on a previously verified physical model[2,7,8,10]. The adopted numerical algorithm has demonstrated the capability to handle complicated flows within a thruster. The performance of several realistic thrusters powered by a 30 kW laser has been studied. The results show that the laser supported rocket can have much higher vacuum specific impulse than the traditional chemical rocket. The Isp was in the range of 700 to 1020 secs for four calculated thrusters having an area expansion ratio of four. The irradiation from the plasma to the thruster wall was also calculated, and the estimated maximum heat loading on the thruster is within the range of the chemical rockets. Among four calculated rockets, rocket No. 1 was the best practical rocket. This rocket has nearly the highest vacuum specific impulse among the test rockets, and both the estimated thruster heat loading and the inlet propellant temperature are reasonable.

ACKNOWLEDGEMENT

This work has been partially supported by NASA Marshall Flight Center under Contract NAS8-36220 monitored by Mr. R. Eskridge, and Air Force Office of Scientific Research under Grant AFOSR-86-0317 monitored by Dr. J. Tishkoff.

REFERENCES

1. Raizer, Y. P., "Subsonic Propagation of a Light Spark and Threshold Conditions for the Maintenance of Plasma by Radiation," *Soviet Physics - JETP*, Vol. 31, 1970, pp. 1148-1154.
2. Jeng, S-M. and Keefer, D., "Theoretical Investigation of Laser-Sustained Argon Plasmas," Vol. 60, No. 7, pp. 2272-2279 *J. Applied Physics*, 1986.
3. Merkle, C. L., Molvik, G. A. and Choi, Y.-H., "A Two-Dimensional Analysis of Laser Heat Addition in a Constant Absorptivity Gas," *AIAA Journal*, Vol. 23, 1985, pp. 1053-1060.
4. Merkle, C. L., Molvik, G. A. and Shaw, E. J.-H., "Numerical Solution of Strong Radiation Gasdynamic Interactions in a Hydrogen-Seedant Mixture," AIAA Paper No. 85-1554, July, 1985.
5. Welle, R. P., Keefer, D. R. and Peters, C. E., "Energy Conversion Efficiency in High-Flow, Laser-Sustained Argon Plasmas," AIAA paper 86-1077.
6. Keefer, D., Welle, R. and Peters, C. E., "Power Absorption in Laser-Sustained Argon Plasma," *AIAA J.*, Vol.24, No.10, Oct. 1986, pp. 1663-1669.
7. Jeng, S-M. and Keefer, D., "Numerical Study of Laser-Sustained Hydrogen Plasmas in a Forced Convective Flow," *J. Power and Propulsion*, Vol.13, No.3, May-June, 1987, pp. 255-262.
8. Jeng, S-M., Keefer, D., Welle, R., and Peters, C., "Numerical Study of Laser-Sustained Argon Plasmas in a Forced Convective Flow," AIAA paper 86-1078, May, 1986.
9. Jeng, S-M. and Keefer, D., "Influence of Laser Beam Geometry and Wavelength on Laser-Sustained Plasmas," AIAA paper 87-1409, June, 1987.
10. Jeng, S-M. and Keefer, D., "A Theoretical Investigation of Laser-Sustained Plasmas Thruster," AIAA paper 87-0383, JAN., 1987.
11. Kemp, N. H. and Root, R. G., "Analytical Study of Laser-Supported Combustion Waves in Hydrogen," *Journal of Energy*, Vol. 3, 1979, pp. 40-49.
12. Caledonia, G. E., Wu, P. K. S. and Pirri, A. N., "Radiant Energy Absorption Studies for Laser Propagation," NASA CR-134809, 1975.
13. Shyy W, "A Numerical Study of Annular Dump Diffuser Flows," *Computer Methods In Applied Mechanics And Engineering*, Vol. 53, pp. 47-65, 1985.
14. Rhie, C. M., and Chow, W. L., "Numerical Study of the Turbulent Flow Past an Airfoil with Trailing Edge Separation," *AIAA J.*, Vol. 21, No. 11, pp. 1525-1532, Nov. 1983.
15. Rhie, C. M. "A Pressure Based Navier-Stokes Solver Using the Multigrid Method, " AIAA paper 86-0207, AIAA 24th Aerospace Sciences Meeting, Reno, Nevada, Jan. 1986.
16. Patankar, S. V., *Numerical Heat Transfer and Fluid Flow*, New Hemisphere, Washington, D.C., 1980.
17. Issa, R. I., "Solution of the implicitly Discretized Fluid Flow Equations by Operator-Splitting," *J. Computational Physics*, Vol. 62, pp. 40-65, 1986.
18. Issa, R. I., Gosman, A. D., and Watkins, A.P., "The Computation of Compressible and Incompressible Recirculating Flows by a Non-iterative Implicit Scheme," *J. Computational Physics*, Vol. 62, pp. 66-88, 1986.

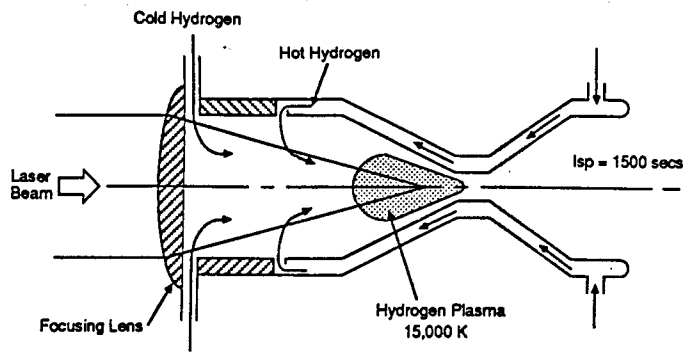

Figure 1. Schematic of laser-sustained plasma thruster

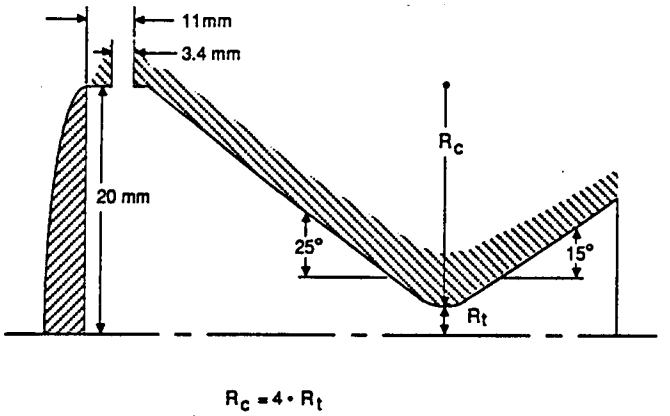

Figure 2. Thruster geometry adopted for the computation

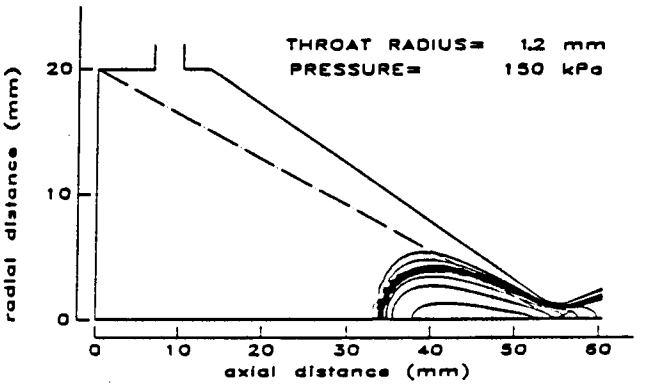

Figure 3. Isotherms for rocket No. 1 (starting from 2,000 K to 15,000 K with 1,000 K increments)

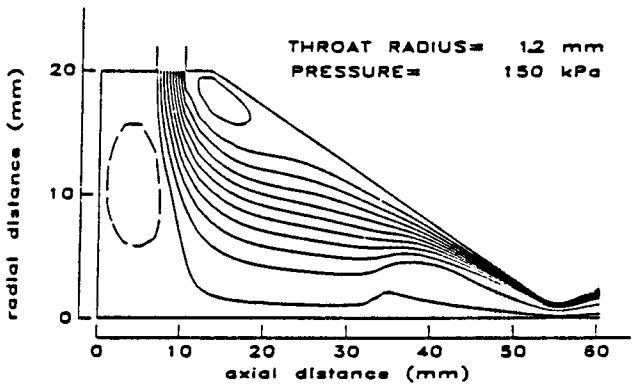

Figure 4. Normalized streamlines for rocket No. 1 (starting from -0.09 to 1.01 with 0.1 increments)

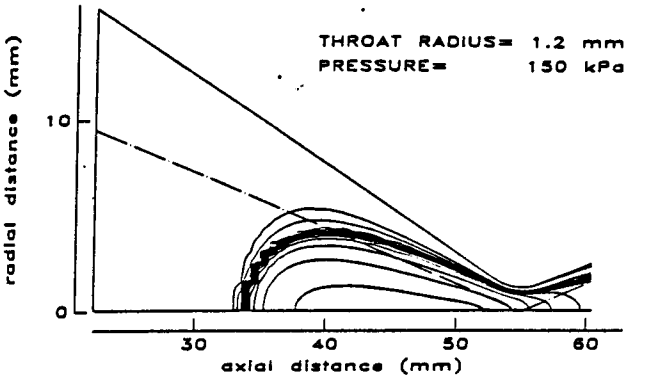

Figure 5. Enlarged view of isotherms for rocket No. 1 (starting from 2,000 K to 15,000 K with 1,000 K increments)

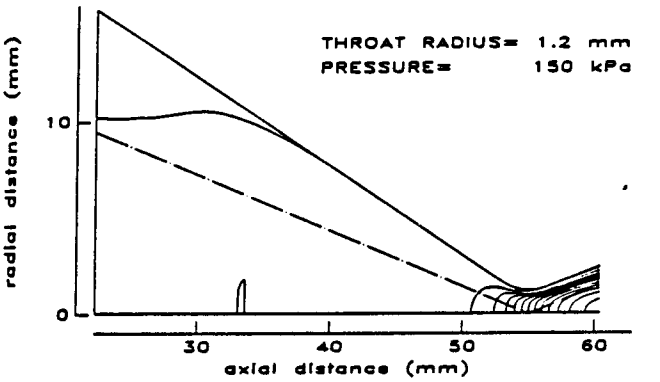

Figure 6. Axial velocity contours for rocket No. 1 (starting from 50 m/s to 24,050 m/s with 2,000 m/s increments)

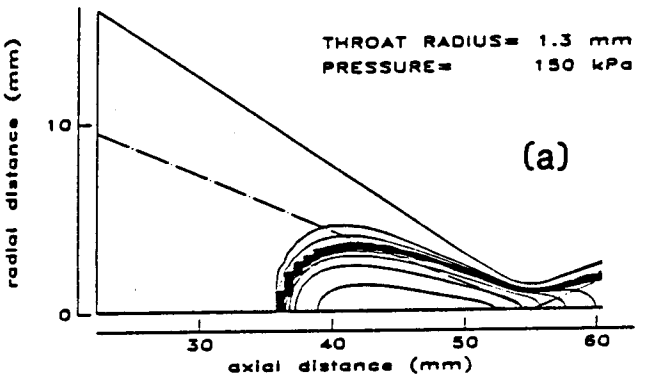

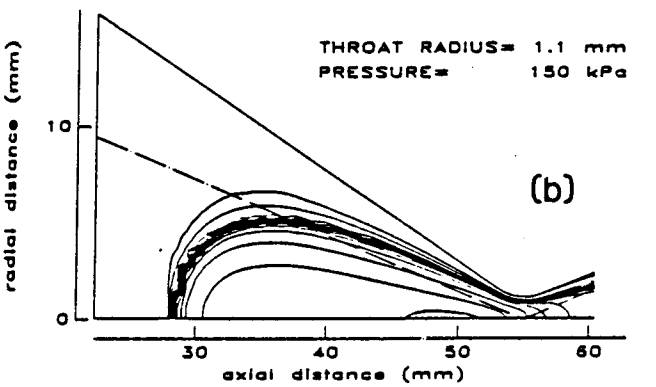

Figure 7. Isotherms for rocket (a) rocket No. 2, (b) rocket No. 3 (starting from 2,000 K to 15,000 K with 1,000 K increments)

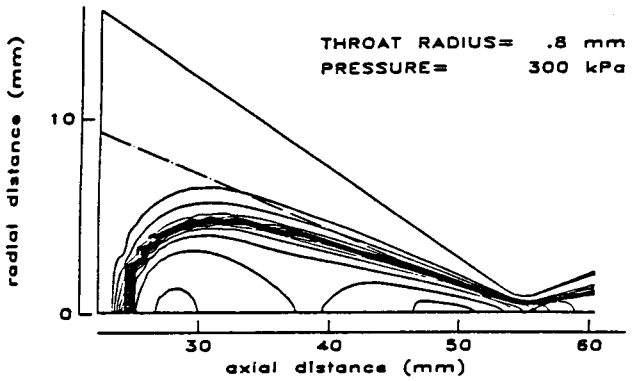

Figure 8. Isotherms for rocket No. 4 (starting from 2,000 K to 15,000 K with 1,000 K increments)

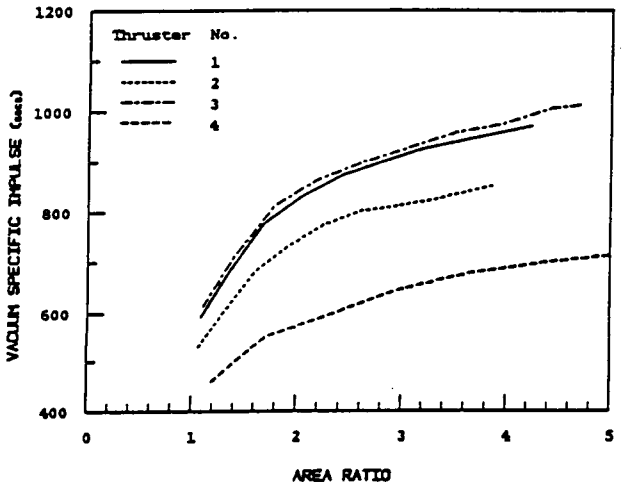

Figure 9. Vacuum specific impulse vs. area expansion ratio

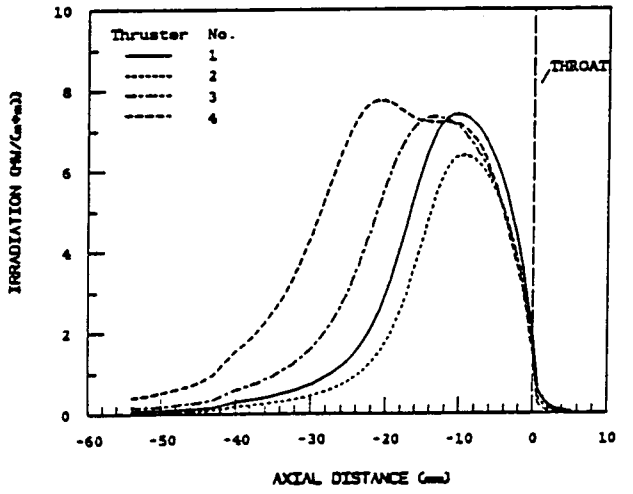

Figure 10. Irradiation along the thruster wall

TABLE I.
Test Conditions

ROCKET NO.	1	2	3	4
Throat Radius (mm)	1.2	1.3	1.1	0.8
Inlet Pressure (kPa)	150	150	150	300

TABLE II.
Performance of the Tested Rockets

ROCKET NO.	1	2	3	4
Transmitted Laser Power (kW)	4.9	5.7	4.2	0.8
Total Irradiation on Thruster (kW)	7.1	5.1	11.0	19.6
Mass Flow Rate (mg / sec)	90	118	73	121
Vacuum Specific Impulse* (sec)	960	859	980	686
Thrust* (N)	0.85	0.99	0.70	0.80

* at expansion area ratio of 4

TABLE III.
Expected Hydrogen Temperature vs. the Recovery Efficiency of Irradiation on Thruster

EFFICIENCY \ ROCKET NO.	1*	2*	3*	4**
100 %	2810 K	2390 K	3310 K	3430 K
50 %	2290 K	1420 K	2830 K	2950 K
25 %	1295 K	700 K	2220 K	2350 K

* at 150 kPa
** at 300 kPa

Laser-Sustained Plasmas in Forced Convective Argon Flow, Part II: Comparison of Numerical Model with Experiment

S.-M. Jeng, D. R. Keefer, R. Welle, C. E. Peters

Reprinted from

AIAA Journal Volume 25, Number 9, September 1987, Page 1224

AMERICAN INSTITUTE OF AERONAUTICS AND ASTRONAUTICS • 1633 BROADWAY • NEW YORK, N.Y. 10019

Laser-Sustained Plasmas in Forced Convective Argon Flow, Part II: Comparison of Numerical Model with Experiment

San-Mou Jeng,* Dennis R. Keefer,† Richard Welle,‡ and Carroll E. Peters§
University of Tennessee Space Institute, Tullahoma, Tennessee

A two-dimensional laser-sustained plasma model, which is based on the laminar, Navier-Stokes equations for the flow and geometric ray tracing for the laser beam, has been evaluated and compared with existing experimental results for a wide range of forced convective argon flows. The influence of gas inlet velocity, gas pressure, laser power, and focusing geometry on the structure of the plasma was examined. The model agreed well with the existing experimental data in both global structure and detailed temperature distribution, particularly for static pressures greater than 2 atm. It was found that the diffusion approximation for the optically thick portion of the thermal radiation was not adequate for low-pressure (less than 2 atm) plasmas and that the radiation-induced thermal conductivity had to be adjusted in order to obtain agreement between the model calculations and experimental results. The present model calculations were also compared with a recently published semi-two-dimensional model and the results indicate that the existing one-dimensional and semi-two-dimensional models do not provide adequate solutions for the laser-sustained plasma.

Nomenclature

c_p = specific heat at constant pressure, J/kg·K
h = specific enthalpy, J/kg
I = laser intensity, W/m^2
k = intrinsic thermal conductivity, W/m·K
k_{eff} = effective thermal conductivity, W/m·K
k_{rad} = radiation-induced thermal conductivity, W/m·K
$\dot{q}_{rad}$ = radiation heat loss, J/m^3·s
r = radius, m
s = distance along the laser ray, m
u = axial velocity, m/s
v = radial velocity, m/s
x = axial distance, m
y = radial distance, m
α = absorption coefficient at 10.6 μm wavelength, 1/m
μ = viscosity, kg/m·s
ρ = density, kg/m^3

Introduction

THE main objective of the present investigation was to evaluate a proposed new model[1] for predicting both the global and detailed structure of laser-sustained plasmas (LSP) under various flow conditions and optical geometries. Although the low-molecular-weight hydrogen is the best propellant for laser thermal propulsion, there is very little hydrogen LSP data available at present. Therefore, this investigation was limited to axisymmetric LSP in flowing argon, since we have made detailed measurements of their structure in our laboratory.[2,3] A separate theoretical study, using a similar model, for the hydrogen LSP can be found in Ref. 4.

It has been pointed out[5,6] that a basic understanding of the interaction between a high-power laser beam and a plasma is needed and that the following questions must be answered before designing a laser thermal propulsion thruster. How can the position and size of the LSP, which are clearly related to the size and shape of the absorption chamber, be controlled? How can the power conversion efficiency from laser energy to propellant thermal energy be maximized? How can damage to the absorption chamber from the high-power laser beam and the high-temperature plasma be avoided? In order to answer these questions, experiments with laboratory-sized LSP under various flow conditions and optical geometries have been performed.[2,3] However, a theoretical model, which can accurately predict the properties of the laboratory-sized LSP, is needed in order to fill the gap between the laboratory-sized LSP and the larger LSP that would be required for a practical propulsion device.

Since the LSP has highly nonlinear thermodynamic, transport, and optical properties and an extremely large absorption of laser energy by the flow, a solution of this problem is not easily achieved. The modeling of the LSP began with the one-dimensional work of Raizer.[7] Several other studies[8-10] followed this analysis, but used more sophisticated analytical and computational methods. Unfortunately, one-dimensional models have an inherent weakness. The LSP tends to be highly dependent on laser beam geometry, radial convection, and radial diffusion transport of momentum and energy in the flow. Keefer and his co-workers[11,12] developed a simplified semi-two-dimensional model that considered the radial energy diffusion, but assumed that the laser beam and the streamlines were parallel. Later, Glumb and Krier[13] extended that model by using a converging laser beam as well as more realistic gas properties. However, their model still did not consider the momentum equations, but instead assumed a known velocity field. Merkle and his co-workers[14,15] used a contemporary numerical method to attack the full two-dimensional problem. They succeeded in the calculation of a low-temperature LSP (peak temperature about 4000 K) in a hydrogen flow seeded with cesium. It is feasible to extend their approach to a pure hydrogen plasma,

Presented as Paper 86-1078 at the AIAA/ASME Fourth Fluid Mechanics, Plasma Dynamics and Lasers Conference, Atlanta, GA, May 12-14, 1986; received May 21, 1986; revision received Jan. 27, 1987.

*Assistant Professor, Mechanical and Aerospace Engineering, Center for Laser Applications. Member AIAA.

†Professor, Engineering Science and Mechanics, Center for Laser Applications. Member AIAA.

‡Predoctoral Fellow, Center for Laser Applications (presently Member of the Technical Staff, The Aerospace Corporation, El Segundo, CA). Student Member AIAA.

§Professor, Mechanical and Aerospace Engineering, Center for Laser Applications. Member AIAA.

but the higher peak temperature (about 16,000 K) and much stronger nonlinear optical properties of the pure hydrogen and argon plasma can result in numerical stability problems.

Recently, Jeng and Keefer[1] obtained a numerical solution for a rigorous two-dimensional model with realistic gas properties for the LSP in an argon flow. Their results agree well with the experimental data[2,3] in the prediction of plasma position, size, shape, and peak temperature. Jeng and Keefer[4] have also studied the effect of laser power, flow rate, static pressure, and optical geometry on the hydrogen LSP. They found that the zero radial velocity assumption used by Glumb and Krier[13] is not adequate for this problem. Their work also indicated that there are no fatal errors in the laser propulsion concept and that the critical parameters, e.g., plasma size, position, radiation heat loss, and energy conversion efficiency, can be controlled using an appropriate optical arrangement and a suitable flow configuration.

The purposes of this work were to evaluate the full two-dimensional laser-sustained plasma model developed by Jeng and Keefer[1] against experimental results from Welle et al.[3] to compare this model prediction with that from the constant axial mass flux, zero radial velocity, laser-sustained plasma model proposed by Glumb and Krier[13] (referred to in this paper as the "quasi-two-dimensional" model), and to explore possible future model improvement. In the following section, the theoretical method used in the study is briefly described. This is followed by discussions of model calculations and of comparisons between the model calculations and experimental results. Additional details concerning the theoretical method can be found in Ref. 1.

Theoretical Model

The object of this work was the verification of the full two-dimensional model, and the simple flow geometry as shown in Fig. 1 was adopted. The domain is axisymmetric, and a cylindrical coordinate system was employed in the model. The argon enters from the bottom with a uniform velocity and temperature distribution and an originally collimated 10.6 μm CO_2 annular laser beam is focused into the gas by an appropriate lens.

It is assumed that the flow is laminar, low Mach number, steady state and axisymmetric and has variable thermophysical and optical properties. The pressure of the flow is relatively high, so that local thermodynamic equilibrium (LTE) can be assumed with little error. Therefore, the plasma can be described by a single temperature and its intrinsic properties are only a function of this temperature and pressure. Thermal radiation is divided into two parts: an optically thin portion in which all radiation escapes from the plasma and an optically thick portion that can be described as a diffusion process. Since the Mach number for the flow is small, the kinetic energy and viscous dissipation are neglected in the energy equation. Following these assumptions, the equations of conservation of mass, momentum, and energy for the flow can be written as

$$\frac{\partial(\rho u)}{\partial x}+\frac{1}{r}\frac{\partial(r\rho v)}{\partial r}=0 \tag{1}$$

$$\frac{\partial(\rho uu)}{\partial x}+\frac{1}{r}\frac{\partial(r\rho uv)}{\partial r}=-\frac{\partial p}{\partial x}-\rho g + \left[\frac{\partial}{\partial x}\left(\mu\frac{\partial u}{\partial x}\right)+\frac{1}{r}\frac{\partial}{\partial r}\left(\mu r\frac{\partial u}{\partial r}\right)\right] \tag{2}$$

$$\frac{\partial(\rho uv)}{\partial x}+\frac{1}{r}\frac{\partial(r\rho vv)}{\partial r}=-\frac{\partial p}{\partial r} + \left[\frac{\partial}{\partial x}\left(\mu\frac{\partial v}{\partial x}\right)+\frac{1}{r}\frac{\partial}{\partial r}\left(\mu r\frac{\partial v}{\partial r}\right)\right]-\frac{2\mu v}{r^2} \tag{3}$$

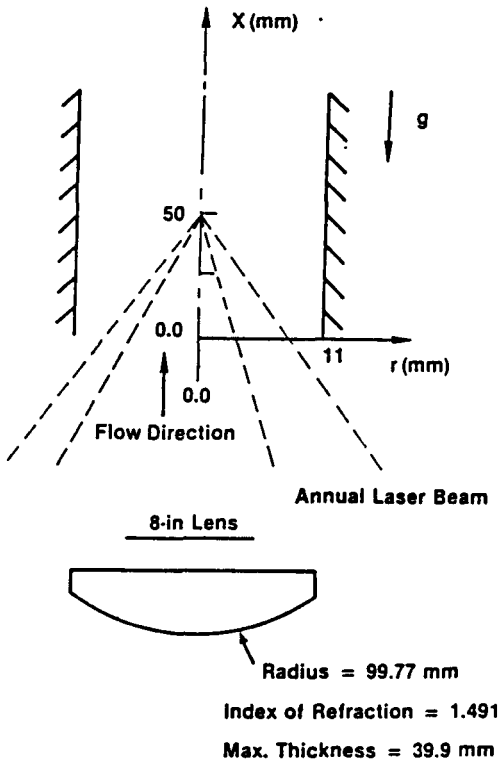

Fig. 1 Sketch of the test configuration.

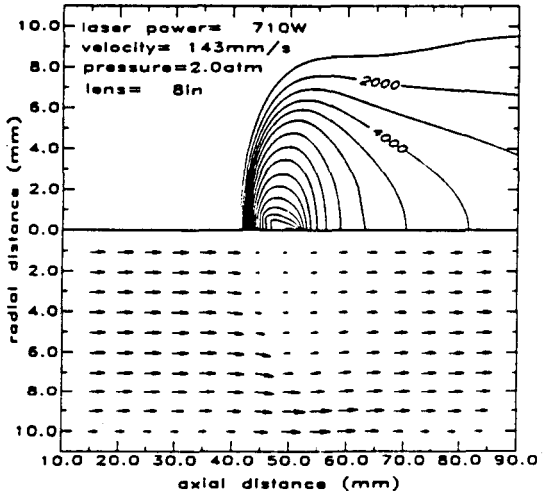

Fig. 2 Isothermal contour plot and mass flux vector plot of a calculated plasma (isothermal lines starting from 1000 K with 1000 K increments).

$$\frac{\partial(\rho uh)}{\partial x}+\frac{1}{r}\frac{\partial(r\rho vh)}{\partial r}=\frac{\partial}{\partial x}\left(\frac{k_{\text{eff}}}{c_p}\frac{\partial h}{\partial x}\right) + \frac{1}{r}\frac{\partial}{\partial r}\left(\frac{rk_{\text{eff}}}{c_p}\frac{\partial h}{\partial r}\right)+\sum\alpha I_i-\dot{q}_{\text{rad}} \tag{4}$$

where I_i is the local laser intensity described by

$$\frac{dI_i}{ds_i}=-\alpha I_i \tag{5}$$

and s_i is the distance along the laser ray propagation direction. The laser beam path through the optical system was

calculated by geometric ray tracing. The diffraction of the laser beam due to the finite aperture of the lens and the effects due to the inhomogeneous refractive index within the plasma are neglected in the calculations.

In Eqs. (2) and (3), the viscous term related to dilation has been omitted for computational efficiency. A few computations were made with the dilation term included and the influence of this term on the computed flowfield was found to be negligible.

The following properties of argon were used in the analysis. Thermodynamic properties (enthalpy, specific heat at constant pressure, and density) were interpolated from the tabulated values given by Drellishak et al.[16] The viscosity between 5000 and 20,000 K was obtained from De Voto[17,18] and below 5000 K the viscosity was interpolated from the graph given by Vargaftik and Filippov.[19] The value of the intrinsic thermal conductivity for temperatures above 5000 K was adopted from De Veto[17,18] and for the low temperature region, it was obtained from Vargaftik.[20] The absorption coefficient at 10.6 μm was calculated using the expression given by Kemp and Lewis,[21] whose analysis included photoionization as well as electron-ion and electron-neutral inverse Brehmstrahlung using the Gaunt factors given by Karzas and Latter.[22] The expressions for radiation loss were obtained from Kozlov et al.,[23] who considered both line and continuum emission in the optically thin limit as a function of temperature and density.

The use of the diffusion approximation for the radiation transport is not trivial; it is not a gas property and it depends upon the actual size and detailed temperature field of the plasma. If, according to the study of Kopainsky,[24] the size of the argon plasma is greater than 5 mm and the pressure is higher than 3 atm, then the radiation contribution below 200 nm represents a true optically thick case and the radiation-induced thermal conductivity no longer depends on the size of the plasma. The size and pressure of the plasmas under consideration are comparable to these limits. The theoretically calculated value of radiation-induced thermal conductivity[24] was used for static pressures greater than 3 atm, and an interpolated value between the experimental results[25] at 1 atm and the theoretical calculations[24] at 3 and 5 atm were used for low-pressure (< 3 atm) flows.

Finite-Difference Solution

The finite-difference solution procedure employed in this work is an adaptation of the method described in detail by Patankar.[26] The detailed description of the numerical procedure used in the current calculations is discussed by Jeng and Keefer[1] and only a brief description is presented in this section. The SIMPLE[26,27] algorithm, which uses a conservative form of finite-difference equation, primitive variables, and staggered grids, was adopted to solve the coupled mass, momentum, and energy conservation equations [Eqs. (1-4)].

At a temperature of 300 K, argon is transparent to the laser irradiation, and the flow will absorb no energy. If the numerical calculation starts with a 300 K initial temperature distribution, a flow with uniform 300 K temperature will result. This solution is trivial and no plasma will be predicted. To obtain a (stable) LSP, an initial high-temperature zone around the focal point was assigned (resembling a spark ignition) where the size, position, and temperature of the "spark" were chosen by trial and error.

The computer code used in this study is similar to that of Jeng et al.[1,4] Generally, the convergence of the numerical solution was achieved in 2000 iterations and the CPU time requirements are approximately 40 s for each iteration on a Masscomp-500 computer.

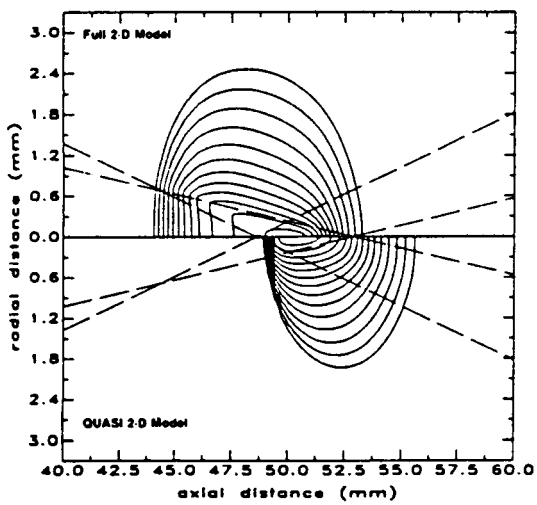

Fig. 3 Comparison of the calculated temperature contour between full two-dimensional and quasi-two-dimensional model (contour lines starting from 10,500 K with 500 K increments).

Results and Discussions

In the calculations, the wall and gas inlet temperature were assumed to be constant at 300 K and the inlet velocity to be uniform. The CO_2 laser operated at a wavelength of 10.6 μm and the collimated laser intensity distribution was that used by Jeng and Keefer.[1] It is an annular beam with peak intensity at a radius of 25.5 mm. The dimensions of the 8 in. focal length lens, which is one of two lenses used in the calculations, are shown in Fig. 1. Another lens of 12 in. focal length is similar to the 8 in. focal length lens, except for a maximum thickness of 39.9 mm and a radius of curvature of 143.2 mm.

The fundamental physical processes occurring within the LSP have been discussed by Jeng and Keefer.[1] The validity of the present model was established by calculations for two typical LSP's. The calculation included the interaction between the laser beam and the plasma, thermal radiation transport, and fluid convection. In the present paper, the verification of the model has been extended to a wider range of gas inlet velocities, gas static pressures, and laser power using two different lenses of 8 and 12 in. focal lengths. The flow conditions were varied at a static pressure of 1.3-4.0 atm, the flow inlet velocity at 0.4-4.5 m/s, and the laser power at 261-967 W.

Full Two-Dimensional and Quasi-Two-Dimensional Model Calculations

The temperature gradient within an LSP is very large, resulting in very high-density gradients and thus a very complex flow in the plasma. The most sophisticated quasi-two-dimensional model assumes a zero radial velocity, leading to a constant axial mass flux assumption. This simplifies the coupled nonlinear momentum and mass conservation differential equations so that the energy equation is the only differential equation to be solved numerically and the stability of the numerical solution is easily achieved. From the results of this work, the CPU time required for the quasi-two-dimensional model is at least of an order of magnitude less than that required for the full two-dimensional model. Figure 2 shows a typical calculated plasma from the full two-dimensional model. The isotherms are shown in the top half of the figure and the mass flux vectors in the bottom half. The laser focal zone is located 50 mm from the inlet and the directions and the magnitudes of the local mass flux, at the vector origins, is proportional to the directions and lengths of the vectors. The detailed heat-transfer and momentum transfer mechanisms for this LSP have been discussed by Jeng and Keefer,[1] so only a brief discussion is presented here. The LSP is positioned near the laser focal zone, and the peak temperature is 16,390 K. In the high-temperature region, where the aixal velocities were much larger than

elsewhere, the axial mass flux was very small compared with the inlet mass flux. It was found that the plasma produced a local high-pressure zone near the leading edge of the plasma, which forced the flow to have outward radial velocities near the centerline. From this result, it is clear that the constant axial mass flux assumption in the quasi-two-dimensional model is inadequate.

A comparison of the temperature distribution calculated using the full two-dimensional and the quasi-two-dimensional models is shown in Fig. 3. The figure shows only a portion of the calculation domains near the laser focal zone and isotherms with temperature higher than 10,500 K. The innermost and outermost laser rays are also plotted in the figure. It was demonstrated in the earlier paper[1] that the calculations from the present model agreed well with the experimental data with regard to LSP position, size, and temperature distribution. The quasi-two-dimensional model, compared with the present model, predicts a smaller size for the plasma and a higher peak temperature. Although the location of the predicted maximum temperature is the same for both models, the detailed temperature distributions are considerably different. The quasi-two-dimensional model calculated a very steep temperature gradient and a short high-temperature zone upstream of the laser focal zone and most of the plasma was positioned downstream of the focal point. From the mass flux distribution shown in Fig. 2, it is clear that the quasi-two-dimensional model overestimated the axial mass flux in the high-temperature zone. In this case, the calculated plasma using the quasi-two-dimensional model is similar to the predictions that would be obtained with the full two-dimensional model having increased inlet velocity.

Model Verification

The model has been compared with a wide variety of experimental results given by Welle and his co-workers[2,3] in order to learn the capability and limitations of the model. Since the spectroscopic measurements were limited to temperatures greater than 10,000 K, the following figures contain only those isotherms within that temperature range, and a limited portion of the calculation domain is plotted in order to gain a clearer comparison. Due to space limitations, only a few typical comparisons are presented in this section.

Inlet Velocity Effect

The performance of the model for two different inlet velocities, using the 8 in. focal length lens, is demonstrated in Figs. 4 and 5, respectively. The static pressure and laser power of these two LSP's differ by less than 1% and the inlet velocity of the LSP in Fig. 4 is about seven times that in Fig. 5. The model calculates the size and position of both plasmas well. As the inlet velocity increases, the radius of the plasma decreases, and the plasma is located further downstream. The local maximum temperatures within the low-velocity LSP are predicted by the model. One is on the laser path upstream of the focal zone and another is at the focal zone. Both calculated maximum temperatures are about 1000 K higher than the measured peak temperature (14,500 K). Only a single maximum temperature was measured, which was located neither on the laser path nor at the focal zone. The predicted local peak temperature at the focal zone, which was not observed in the experiment, may result from the neglect of the diffraction and refraction of the laser beam. Although it has been demonstrated experimentally[2,3] that this assumption leads to only a small effect on the measured global laser power absorption, the predictive model can suffer more serious effects. If the refraction of the laser beam within the LSP is considered, it results in a larger focal spot size and reduced laser intensity. The spot size for the refracted beam is highly dependent on the LSP position and size. For a low-velocity LSP, most of the plasma is located upstream of the focal zone, making the focal spot larger. When diffraction is also considered, the

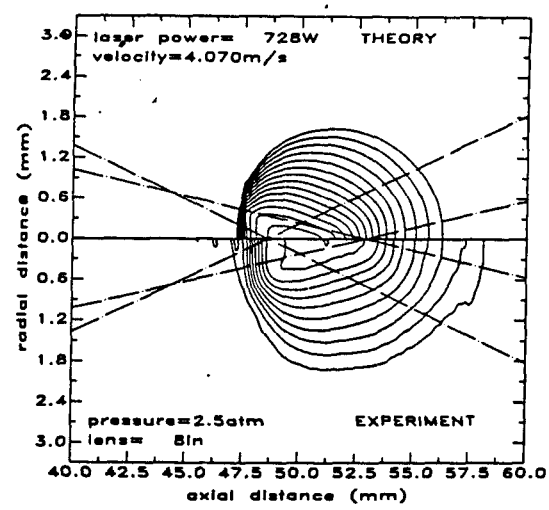

Fig. 4 Temperature contour plot of a high-velocity plasma (contour lines starting from 10,500 K with 500 K increments).

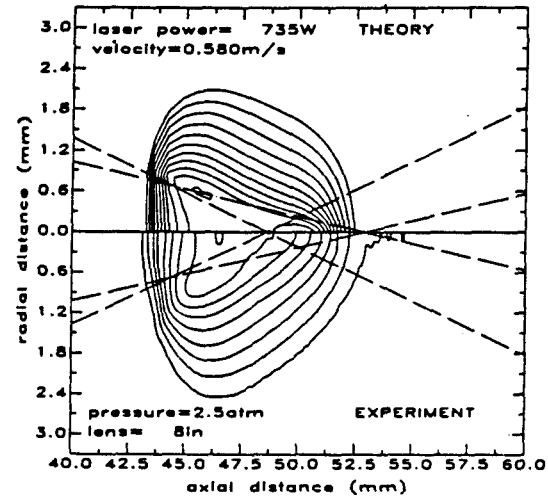

Fig. 5 Temperature contour plot of a low-velocity plasma (contour lines starting from 10,500 K with 500 K increments).

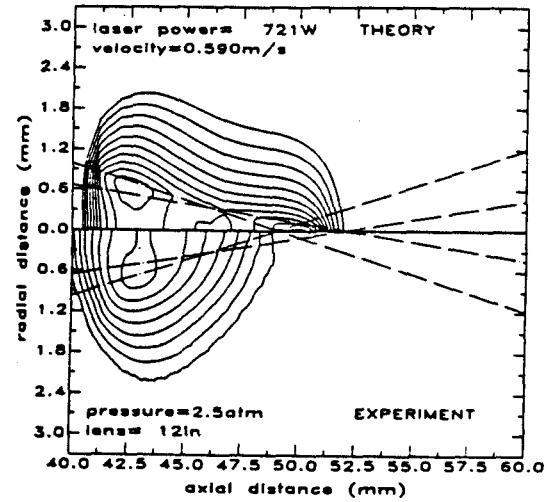

Fig. 6 Temperature contour plot of a low-velocity plasma with the 12 in. focal length lens (contour lines starting from 10,500 K with 500 K increments).

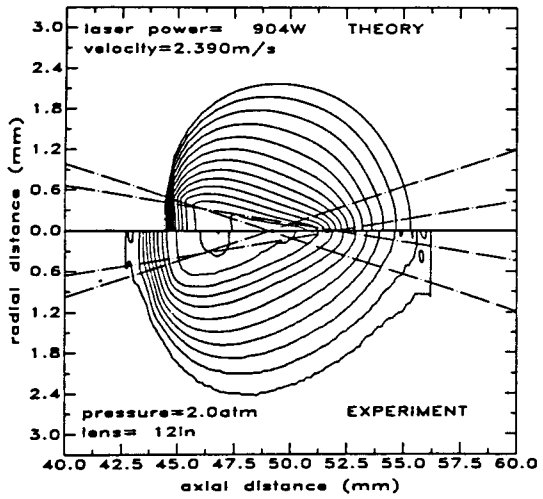

Fig. 7 Temperature contour plot of a plasma with high laser power (contour lines starting from 10,500 K with 500 K increments).

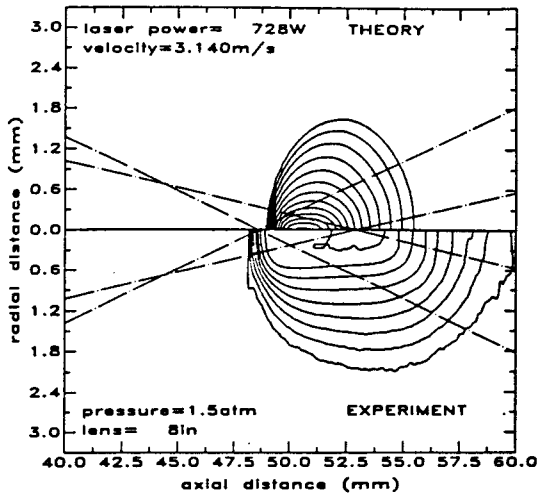

Fig. 9 Temperature contour plot of a low-pressure (1.5 atm) plasma (contour lines starting from 10,500 K with 500 K increments).

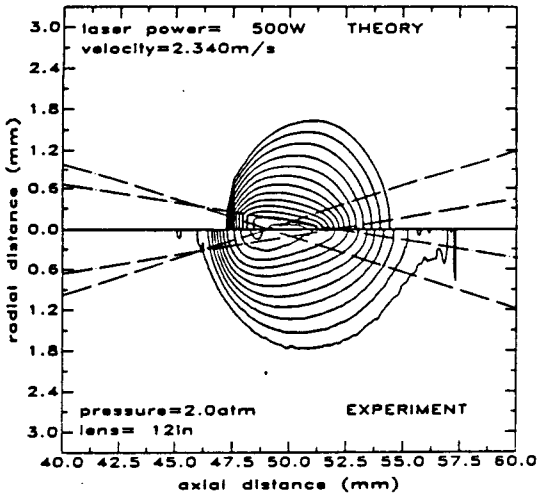

Fig. 8 Temperature contour plot of a plasma with low laser power.

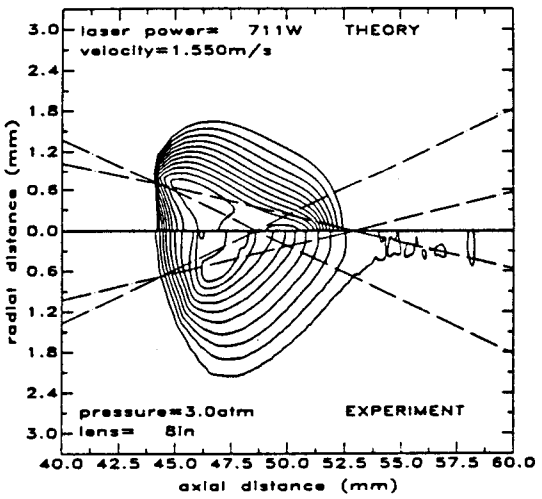

Fig. 10 Temperature contour plot of a high-pressure (3.0 atm) plasma (contour lines starting from 10,500 K with 500 K increments).

diffraction limited focal spot is approximately twice the size of that calculated from a geometric ray trace. The combination of laser beam refraction and diffraction and the longer absorption pathlength ahead of the focal zone result in an actual laser intensity that is smaller near the laser focal zone than that which is predicted by the model. Thus, the local temperature maximum will not be generated there in the low-velocity LSP. This may explain why the calculations are not consistent with the experiments in this detail.

Since the size and temperature of these LSP were well predicted, it is not surprising that the calculated thermal radiation power loss (316 and 445 W for high- and low-velocity, respectively) agreed with the experimental results (326 and 392 W for high- and low-velocity, respectively). The model prediction for the transmitted laser power in the high-velocity LSP also agrees reasonably well (110 and 159 W for prediction and experiment, respectively). However, the predicted transmitted laser power (91 W) in the low-velocity LSP is much smaller than the measurement (246 W). This is because the predicted second local maximum temperature near the focal zone absorbs an unrealistically large amount of additional laser power.

Lens Effect

Isotherms are shown in Fig. 6 for an LSP with operating conditions similar to those of Fig. 5 except for the use of the 12 in. focal length lens instead of the 8 in. lens. Both calculation and experiment show that the plasma moves further upstream than in Fig. 5 and the model predicted the upstream position and the radius of the plasma well. Again, the model predicts a local maximum temperature near the focal zone, which was not measured in the experiment. The effect of laser beam refraction and diffraction, which was discussed in the last section, is probably responsible. Similar to the 8 in. LSP, the thermal radiation from the LSP is well predicted and the transmitted laser power is underestimated.

Laser Power Effect

Figures 7 and 8 show the effect of laser power on the structure of the plasma. Both cases use the 12 in. focal length lens with similar flow conditions. The calculations are quite consistent with the experiments. As laser power increases, the plasma becomes larger and moves upstream. For the 10,500 K isotherms, the model underpredicted the length. However, the experimental results exhibit more noise in these isotherms than in the higher-temperature isotherms; if the 11,500 K isotherms are used, then the model predicts the length of this isotherm within 10%. The calculated positions of both plasmas are about 1 mm downstream of the experiments. After carefully reviewing the experimental data, it

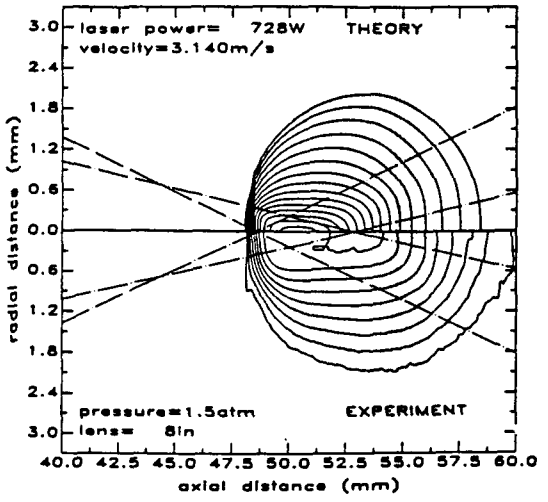

Fig. 11 Temperature contour plot of a low-pressure (1.5 atm) plasma using 50% of radiation-induced thermal conductivity (contour lines starting from 10,500 K with 500 K increments).

was found that the on-axis maximum temperatures are not on the laser beam path (using real ray tracing and neglecting the inhomogeneous refractive index effect). If the experimental results are shifted downstream by 1 mm, which is within the accuracy claimed by Welle et al.,[3] the peak temperatures are located on the laser path. In this case, the model predictions agree well with the experimental LSP positions. The predicted global properties are also in reasonable agreement with the experiments: the transmitted laser power is within 10%, and the thermal radiation from the LSP is underpredicted within 30%.

Static Pressure Effect

All the LSP's shown in the previous sections have either 2.0 or 2.5 atm static pressure and the model performed well at these pressures. In this section, the effects of the static pressure are presented. The intrinsic properties of plasmas are highly pressure dependent, especially the optical properties. The absorption coefficient of the plasma at the laser wavelength and the thermal radiation from the plasma are approximately proportional to $p^{1.5}$. Figures 9 and 10 show the plasmas at 3.0 and 1.5 atm, respectively. Both plasmas have similar laser power levels and inlet mass flow rates (but different inlet velocities). In the low-pressure case, the predicted plasma size is much smaller than the experiment. In the 3 atm case, the model provides an excellent prediction.

After reviewing the model assumptions, we concluded that the treatment of the optically thick thermal radiation was the weakest link and was probably responsible for the failure of the model in the low-pressure case. As mentioned before, the validity of the diffusion approximation for short-range radiation is dependent on pressure and the size of the plasma. As the pressure decreases, the required size of the plasma increases. For the present calculation, the size of the 1.5 atm plasma is below the minimum size required for the valid use of the diffusion approximation found by Kopainsky.[24] Although the diffusion approximation for short-range thermal radiation is not valid for the low-pressure plasma, a sensitivity study using this approximation was performed to investigate the sensitivity of the solutions to radiative transport. For small, low-pressure plasmas, the radiation-induced thermal conductivity should be smaller than that for a large, low-pressure plasma.

A calculated result, where the radiation-induced thermal conductivity was reduced to 50% of the value used for the calculation in Fig. 9, is illustrated in Fig. 11. The size of this plasma is much larger than the previous calculation and agrees well with the experimental results. The role of a change in thermal conductivity on the results can be understood qualitatively. As conductivity decreases, the conduction heat-transfer loss from the portion of the plasma along the laser path is reduced, which increases the plasma temperature along the laser path. Due to this increased temperature, the absorption coefficient at the laser wavelength increases and the plasma absorbs more laser power, which in turn generates a larger plasma. Because the exact solution of radiation heat transport will not be easy to achieve in the near future, the optically thin and thick approximations for the radiative transport process should be retained for the near term. Although in some pressure and dimension ranges the optically thick approximation is not quite valid, this concept can still be utilized with some adjustment for the magnitude of the radiation-induced thermal conductivity.

Conclusions

A full two-dimensional model for laser-sustained plasmas has been numerically solved for a wide range of argon flows. The calculations were compared with experimental temperature distributions and it was found that the model performed well at static pressures greater than 2 atm. The plasma position and size are well predicted and the behavior of the predicted plasma structure using different inlet velocity, focusing lenses, and laser power agreed well with experimental results.[3]

At lower pressures, the model underpredicts the plasma size. It was recognized that the diffusion approximation for short-range thermal radiation is probably responsible. When 50% of the optically thick, radiation-induced thermal conductivity at a pressure of 1.5 atm is used, the calculations are in reasonable agreement with experiments.

The global thermal radiation heat loss from the LSP and transmitted laser power are well calculated except for two LSP's. In these two LSP's, two local maximum temperatures were predicted. However, the experiment did not show the same two maxima. We concluded that neglecting the laser beam refraction and diffraction is responsible and recommend that the model should include these effects in future studies.

A comparison of calculations from the present model and those from a constant axial mass flux model was also performed. The axial mass flux field calculated from the present model differs considerably from the constant axial mass flux assumption in the simplified model. The characteristics of the temperature fields calculated with these two models are different and the results of the simplified model are similar to the calculated results from the present model using a much higher inlet velocity.

Acknowledgment

This work was partially supported by U.S. Air Force Office of Scientific Research Grant AFOSR-83-0043, the Program Manager was Dr. Robert Vondra.

References

[1]Jeng, S-M. and Keefer, D. R., "Theoretical Investigation of Laser-Sustained Argon Plasmas," *Journal of Applied Physics*, Vol. 60, Oct. 1986, pp. 2272-2279.

[2]Keefer, D. R., Welle, R. P., and Peters, C. E., "Power Absorption in Laser-Sustained Argon Plasmas," *AIAA Journal*, Vol. 24, Oct. 1986, pp. 1663-1669.

[3]Welle, R. P., Keefer, D. R., and Peters, C. E., "Laser-Sustained Plasmas in Forced Convective Argon Flow, Part 1: Experimental Studies," *AIAA Journal*, Vol. 25, August 1987, pp. 1093-1099.

[4]Jeng, S-M. and Keefer, D. R., "Numerical Study of Laser-Sustained Hydrogen Plasmas in a Forced Convective Flow," AIAA Paper 86-1524, June 1986.

[5]Merkle, C. L., "Laser Radiation to Supply Energy for Propulsion," *AIAA Progress in Astronautics and Aeronautics: Orbit-Raising and Maneuvering Propulsion: Research Status and Needs*, Vol. 89, edited by L. H. Caveny, AIAA, NY, 1984, pp. 73-94.

[6]Keefer, D. R., Elkins, R., Peters, C., and Jones, L., "Laser Thermal Propulsion," *AIAA Progress in Astronautics and Aeronautics: Orbit-Raising and Maneuvering Propulsion: Research Status and Needs*, Vol. 89, edited by L. H. Caveny, AIAA, NY, 1984, pp. 129-148.

[7]Raizer, Y. P., "Subsonic Propagation of a Light Spark and Threshold Conditions for the Maintenance of Plasma by Radiation," *Soviet Physics—JETP*, Vol. 31, 1970, pp. 1148-1154.

[8]Jackson, J. P. and Nielsen, P. E., "Role of Radiative Transport in the Propagation of Laser-Supported Combustion Waves," *AIAA Journal*, Vol. 12, 1974, pp. 1498-1501.

[9]Kemp, N. H. and Root, R. G., "Analytical Study of Laser-Supported Combustion Waves in Hydrogen," *Journal of Energy*, Vol. 3, 1979, pp. 40-49.

[10]Keefer, D. R., Peters, C.E., and Crowder, H. L., "A Reexamination of the Laser Supported Combustion Wave," *AIAA Journal*, Vol. 23, 1985, pp. 1208-1212.

[11]Batteh, J. H. and Keefer, D. R., "Two-Dimensional Generalization of Raizer's Analysis for the Subsonic Propagation of Laser Sparks," *IEEE Transactions on Plasma Science*, Vol. PS-2, 1974, pp. 122-129.

[12]Keefer, D. R., Crowder, H. L., and Elkins, R., "A Two-Dimensional Model of the Hydrogen Plasma for a Laser Powered Rocket," AIAA Paper 82-0404, Jan. 1982.

[13]Glumb, R. J. and Krier, H., "A Two-Dimensional Model of Laser-Sustained Plasmas in Axisymmetric Flowfields," AIAA Paper 85-1553, July 1985.

[14]Merkle, C. L., Molvik, G. A., and Choi, Y.-H., "A Two-Dimensional Analysis of Laser Heat Addition in a Constant Absorptivity Gas," *AIAA Journal*, Vol. 23, 1985, pp. 1053-1060.

[15]Merkle, C. L., Molvik, G. A., and Shaw, E. J.-H., "Numerical Solution of Strong Radiation Gasdynamic Interactions in a Hydrogen-Seedant Mixture," AIAA Paper 85-1554, July 1985.

[16]Drellishak, K. S., Aeschliman, D. P., and Cambel, A. B., "Tables of Thermodynamics Properties of Argon, Nitrogen, and Oxygen Plasmas," AEDC-TR-64-12, 1964.

[17]DeVoto, R. S., "The Transport Properties of a Partially Ionized Monatomic Gas," Ph.D. Thesis, Stanford University, Stanford, CA, 1965.

[18]DeVoto, R. S., "Transport Properties of Ionized Monatomic Gases," *The Physics of Fluids*, Vol. 165, 1973, pp. 615-623.

[19]Vargaftik, N. B. and Filippov, L. P., *Thermal Conductivity of Gases and Liquids (Data Book)*, Standards Press, Cincinnati, 1970.

[20]Vargaftik, N. B., *Tables on the Thermophysical Properties of Liquids and Gases*, Hemisphere Publishing, Washington, DC, 1975.

[21]Kemp, N. H. and Lewis, P. F., "Laser-Heated Thruster Interim Report," NASA CR-161665, 1980.

[22]Karzas, W. J. and Latter, R., "Electron Radiative Transitions in a Coulomb Field," *Astrophysical Journal Supplement Series*, Supp. 55, Vol. VI, May 1961.

[23]Kozlov, G. I., Kuznetsov, V. A., and Masyukov, V. A., "Radiative Losses by Argon Plasma in the Emissive Model of a Continuous Optical Discharge," *Soviet Physics—JETP*, Vol. 39, 1974, pp. 463-468.

[24]Kopainsky, J., "Strahlungstransportmechanismus und Transportkoeffizienten im Ar-Hochdruckbogen," *Zeitschrift für Physik*, Vol. 248, 1971, pp. 417-432.

[25]Bues, J., Patt, H. J., Richter, J., "Uber die Elektrische Leitfahigkeit und die Warmeleitfahigkeit des Argons bei Hohen Temperaturen," *Zeitschrift für Angewandte Physik*, Vol. 22, 1967, p. 345.

[26]Patankar, S. V., *Numerical Heat Transfer and Fluid Flow*, Hemisphere Publishing, Washington, DC, 1980.

[27]Gosman, A. D., Pun, W. M., Ruchal, A. K., Spalding, D. B., and Wolfshstein, R., *Heat and Mass Transfer in Recirculating Flows*, Academic Press, London, 1969.

APPENDIX C

Computer Code

```
      SUBROUTINE BOUND
        DOUBLE PRECISION ZZA,ZZB,ZZC,ZZD
C       INCLUDE 'DIMENSION1'
C       INCLUDE 'DIMENSION'
C       IMPLICIT REAL*8 (A-H,O-Z)
        PARAMETER (IT=100,JT=60,LMAX=500)
        CHARACTER*8 PFOR1,PUFOR1,FILIN,FILOUT
        CHARACTER*8 PFOR2,PUFOR2
        CHARACTER*8 PFOR3,PUFOR3
        CHARACTER*8 PFOR4,PUFOR4
       COMMON /FNAME1/PFOR1,PUFOR1,FILIN,FILOUT
       COMMON /FNAME2/PFOR2,PUFOR2,PFOR3,PUFOR3
       COMMON /FNAME3/PP1,PP2,PP3,PP4,MPL,MPL1
       COMMON /FNAME4/PFOR4,PUFOR4
       COMMON /COEFF/Q1P(IT,JT),Q2P(IT,JT),Q3P(IT,JT),COB(IT,JT)
     1    ,SEW(IT,JT),YSEW(IT,JT),SNS(IT,JT),XSNS(IT,JT)
     2    ,DU(IT,J1),DU1(IT,JT),DV(IT,JT),DV1(IT,JT)
     3    ,AP(IT,JT),AN(IT,JT),AS(IT,JT),AE(IT,JT),AW(IT,JT),SU(IT,JT)
     1    ,SP(IT,JT)
       COMMON /POS/ YPOS(IT,JT),XPOS(IT,JT),R(IT,JT)
       COMMON /VAR/ U(IT,JT),V(IT,JT),P(IT,JT),TM(IT,JT),PP(IT,JT)
     1    ,UDUMMY(IT,JT),VDUMMY(IT,JT)
     2    ,TVIS(IT,JT),TCON(IT,JT),DEN(IT,JT),DISS(IT,JT)
       COMMON
     1    /UVEL/RESORU,NSWPU,URFU,SD
     1    /VVEL/RESORV,NSWPV,URFV
     1    /PCOR/RESORM,NSWPP,URFP,IPREF,JPREF
     1    /TMP/RESORT,NSWPT,URFT
       COMMON/INPUT/NI,NJ,NIM1,NJM1,GREAT,INDCOS,INDSM
     1             ,DATAR,DATAW,IFORM,ILASER,CLASIN,NRAYS
     2             ,FOCUS,IFOCUS,BDIAM,ITRACE,ISUPER
     3             ,ANGI,ANGE,RCI,RCT,RT,RI,XEXIT,XI,RTIOY1
       COMMON/IINPUT/
     4             RTIOX1,RTIOX2,XDENSE,JS1,JS2,IS1,IS2
     5             ,URSUP,URVIS,IDENSE,JDENSE,YENRAT,RTIOY2
     6             ,NCONST,XCONST
     6             ,INITP,INITER,SCALE
       COMMON/COND/CCN(IT,JT),CCE(IT,JT),DDN(IT,JT),DDE(IT,JT)
     1     ,DDN1(IT,JT),DDE1(IT,JT)
       COMMON/LASER/QINP(IT,JT),GRA(IT,JT),TRANS(IT,JT),CAB(IT,JT)
     1     ,TNG(LMAX),ING(LMAX,IT)
     2     ,POWER(LMAX),QRA(IT,JT),TH(IT,JT)
       COMMON/LASER2/HT(3000,4),HMU(400,4),HDEN(400,4)
     1     ,HCCP(400,4),HCAB(400,4),HRA(400,4)
       COMMON /ADD8/ANU(IT,JT),ASU(IT,JT),AEU(IT,JT),AWU(IT,JT)
       COMMON /ADD9/ANV(IT,JT),ASV(IT,JT),AEV(IT,JT),AWV(IT,JT)
       COMMON /ADD10/AAN(IT,JT),AAE(IT,JT),COEF(IT),UTEMP(IT,JT),
     1               VTEMP(IT,JT),DYDX(IT),XP(IT)
       COMMON/EXTRA/HINLET
     1        /EXTRA1/UINLET,TBOUND
     1/MMAIN/MAXIT,JMON,IMON,INDPRI,SOLPAT
     1/ADD5/NITER
     1/ADD6/SORMAX,TRSMT,RDL
       COMMON/PROP/PTL,TTL,GAMMA,RG,WGHT,WGHT1,RATIO
       COMMON/EXTRA/PDUMMY(IT,JT)
       COMMON/PLUS/LROAT,NVS,NVS1,NVE,NVE1
```



```
       COMMON/MACHO/MAEX(JT),PEX(JT)
       DIMENSION AMASS(IT),ADD1(IT),AFLUX(IT),BFLUX(IT)
C
C
                    ENTRY BUNDXR
C ***************** EXIT BOUNDARY CONDITIONS (I=NI)***************
C ***************** SUPERSONIC BOUNDARY CONDITION ****************
       NIM2=NI-2
       NIM3=NI-3
       DO 604 J=1,NJ
       PTE=-.2*PTL
       IF(P(NI,J).GE.PTE) P(NI,J)=PTE
C      PEX(J)=-.98*PTL*.5+.5*P(NI,J)
       AAA=XPOS(NIM1,J)-XPOS(NI-2,J)
       BBB=XPOS(NI,J)-XPOS(NIM1,J)
       AAA=1.
       BBB=0.5
       U(NI,J)=U(NIM1,J)+(U(NIM1,J)-U(NI-2,J))*BBB/AAA
       V(NI,J)=V(NIM1,J)+(V(NIM1,J)-V(NI-2,J))*BBB/AAA
       TH(NI,J)=TH(NIM1,J)+(TH(NIM1,J)-TH(NI-2,J))*BBB/AAA
C       IF(U(NI,J).LE.U(NIM1,J)) U(NI,J)=U(NIM1,J)
       IF(U(NI,J).LT.0.) U(NI,J)=1.
       IF(P(NIM2,J).LE.P(NIM1,J)) P(NIM1,J)=P(NIM2,J)
       IF(P(NIM2,J).LE.P(NIM1,J)) TH(NIM1,J)=TH(NIM2,J)
       IF(P(NIM1,J).GE.PTE) P(NIM1,J)=PTE
       P(NI,J)=P(NIM1,J)+(P(NIM1,J)-P(NI-2,J))*BBB/AAA
       IF(P(NI,J).GE.P(NIM1,J)) P(NI,J)=P(NIM1,J)
       IF(P(NI,J).GE.PTE) P(NI,J)=PTE
       IF(P(NI,J).GE.P(NIM1,J)) TH(NI,J)=TH(NIM1,J)
       PEX(J)=(PTL+P(NI,2))*.97-PTL
C      IF(MAEX(J).EQ.0.AND.J.GE.44) P(NI,J)=PEX(J)
       IF(P(NI,J).GE.PTE) P(NI,J)=PTE
C ************ CHECK THE LOWER PRESSURE AND TEMPERATURE BOUND *********
       PLLL=-.99*PTL
       IF(P(NI,J).LE.PLLL) P(NI,J)=PLLL
       TLLL=0.05*TH(1,2)
       TH(NI,J)=TH(NIM1,J)+(TH(NIM1,J)-TH(NI-2,J))*BBB/AAA
       IF(TH(NI,J).LE.TLLL) TH(NI,J)=TLLL
       DO 605 I=NIM3,NI
       AAA=ABS(U(I,J))
       IF(AAA.GE.30000.) U(I,J)=30000.
       BBB=ABS(V(I,J))
       CCC=1.
       IF(BBB.LE.0.) CCC=-1.
       IF(BBB.GE.13000.) V(I,J)=13000.
       IF(V(I,J).GE.13000.) V(I,J)=13000.
605    CONTINUE
604    CONTINUE
       RETURN
C
C
                ENTRY BUNDYT
C
C ***************** SLIP WALL BOUNDARY CONDITIONS ***************
C
       NJM2=NJ-2
```

```
      NJM3=NJ-3
      DO 185 I=NVE1,NIM1
      U(I,NJ)=0.
      V(I,NJ)=0.
      IF(COEF(I).GE.0.)
     1 P(I,NJ)=P(I,NJM1)*COEF(I)+(1.-COEF(I))*P(I+1,NJM1)
      IF(COEF(I).LE.0.)
     1 P(I,NJ)=-P(I,NJM1)*COEF(I)+(1.+COEF(I))*P(I-1,NJM1)
      IF(COEF(I).GE.0.)
     1 PP(I,NJ)=PP(I,NJM1)*COEF(I)+(1.-COEF(I))*PP(I+1,NJM1)
      IF(COEF(I).LE.0.)
     1 PP(I,NJ)=-PP(I,NJM1)*COEF(I)+(1.+COEF(I))*PP(I-1,NJM1)
C      IF(I.GE.15) TH(I,NJ)=31.
C      IF(I.LT.15.AND.I.GE.NVE1) TH(I,NJ)=TH(11,NJM1)
      TH(I,NJ)=TH(NVS,NJ)
185   CONTINUE
      U(1,NJ)=0.
      U(NI,NJ)=0.
      V(1,NJ)=0.
      V(NI,NJ)=0.
      P(1,NJ)=P(1,NJM1)
      P(NI,NJ)=P(NI,NJM1)
      PP(1,NJ)=PP(1,NJM1)
      PP(NI,NJ)=PP(NI,NJM1)
      DO 557 I=NVS,NVE
      IF(V(I,NJM1).GE.0.) V(I,NJM1)=-1.E-2
      IF(V(I,NJM2).GE.0.) V(I,NJM2)=-1.E-2
      IF(V(I,NJM3).GE.0.) V(I,NJM3)=-1.E-2
557   CONTINUE
      AMASS6=0.
      DO 949 J=2,NJM1
      AREA=DEN(LROAT,J)*R(LROAT,J)*SNS(LROAT,J)
      AMASS6=AMASS6+AREA*U(LROAT,J)
949   CONTINUE
      DO 998 I=2,NI
      AMASS7=0.
      DO 999 J=2,NJM1
      AREA=DEN(I,J)*R(I,J)*SNS(I,J)
      AMASS7=AMASS6+AREA*U(I,J)
999   CONTINUE
C     PRINT *,'I=',I,AMASS7
998   CONTINUE
      AREA1=0.
      DO 948 I=NVS,NVE
      AREA1=AREA1+DEN(I,NJ)*YPOS(I,NJ)*SEW(I,NJ)
948   CONTINUE
      TTEMP=-1.*AMASS6/AREA1
      PRINT *,TTEMP
C     DO 558 I=NVS,NVE
C     V(I,NJ)=TTEMP*.20+.80*V(I,NJ)
C558  CONTINUE
      DO 457 I=NVS,NVE
      RG=(P(I,NJM1)+PTL)/DEN(I,NJM1)/TM(I,NJM1)/100.
      II=TH(I,NJM1)
      AAA=HT(II,4)
      BBB=HT(II+1,4)
```



```
      CCC=RG*(BBB-AAA)*100./SCALE
C     PP1=P(I,NJ)+PTL
C     IF(PP1.GE.1.E5) KK1=4
C     IF(PP1.GE.0.3E5.and.PP1.LE.1.E5) KK1=3
      GAMMA=1./(1.-CCC)
CC    PRINT *,'AT 2',GAMMA,RG
      IF(V(I,NJM1).GT.0.) V(I,NJM1)=0.
      IF(V(I,NJM2).GT.0.) V(I,NJM2)=0.
      IF(V(I,NJ).GT.0.) V(I,NJ)=0.
C      AMASS(I)=(U(I,NJM1)**2+V(I,NJM1)**2)**.5
C    1-(2.*(GAMMA*RG*TM(I,NJM1)*100.)**.5)/(GAMMA-1.)
      AMASS(I)=(U(I,NJM1)**2+V(I,NJM1)**2+1.e-30)**.5
     1-(2.*(GAMMA*RG*TM(I,NJM1)*100.)**.5)/(GAMMA-1.)
C     PRINT *,'I=',I,' V=',V(I,NJ),' AMASS(I)=',AMASS(I),TM(I,NJM1)
      ADD1(I)=(U(I,NJM2)**2+V(I,NJM2)**2+1.e-30)**.5
     1-(2.*(GAMMA*RG*TM(I,NJM2)*100.)**.5)/(GAMMA-1.)
      ZZA=U(I,NJM1)**2+V(I,NJM1)**2+1.D-30
      ZZA=ZZA**.5
      ZZB=GAMMA*RG*TM(I,NJM1)*100.
      ZZB=ZZB**.5
      ZZB=2.*ZZB/(GAMMA-1.)
      AMASS(I)=ZZA-ZZB
C     PRINT *,'NI=',I,'   V=',V(I,NJ),'    AMASS(I)=',AMASS(I)
C     AMASS(I)=(YPOS(I,NJM1)-YPOS(I,NJ))/(YPOS(I,NJM2)
C    1+YPOS(I,NJM1)-2.*YPOS(I,NJ))*ADD1(I)
C    1+(YPOS(I,NJM2)-YPOS(I,NJ))/(YPOS(I,NJM2)
C    1+YPOS(I,NJM1)-2.*YPOS(I,NJ))*AMASS(I)
      AAA=V(I,NJ)
      BBB=TM(I,NJ)
      CCC=TH(I,NJ)
      V(I,NJ)=(GAMMA-1.)*AMASS(I)+(4.*(GAMMA+1)*RG*GAMMA/(GAMMA-1.)
     1*TTL-
     12.*(GAMMA-1.)*AMASS(I)**2)**.5
C     PRINT *,'VNI=',I,'   V=',V(I,NJ)
      ZZA=(GAMMA-1.)*AMASS(I)
      ZZB=4.*(GAMMA+1.)*RG*GAMMA/(GAMMA-1.)*TTL
      ZZC=2.*(GAMMA-1.)*AMASS(I)**2
      ZZD=ZZB-ZZC
      IF(ZZD.LE.0.D0) ZZD=1.D-30
      V(I,NJ)=ZZA+ZZD**.5
C     PRINT *,'VNI=',I,'   V=',V(I,NJ)
      V(I,NJ)=V(I,NJ)/(GAMMA+1.)
C     PRINT *,I,'VE',V(I,NJ)
      V(I,NJ)=-V(I,NJ)
      IF(V(I,NJ).GE.0.) V(I,NJ)=-0.001
      VV1=.2*TTEMP
      VV2=5.*TTEMP
      IF(P(I,NJM1).GE.0.) V(I,NJ)=-.001
      IF(P(I,NJM1).GE.0.) P(I,NJ)=0.
      IF(V(I,NJ).GE.VV1) V(I,NJ)=VV1
      IF(V(I,NJ).LE.VV2) V(I,NJ)=VV2
      PRINT *, V(I,NJ)
      V(I,NJ)=AAA*0.90+V(I,NJ)*.10
C     IF(V(I,NJ).GE.0.) V(I,NJ)=-0.001
C     IF(V(I,NJ).LE.-100.) V(I,NJ)=-100.
      BBB=TM(I,NJ)
```

```
        CCC=TH(I,NJ)
        TM(I,NJ)=(TTL-.5*V(I,NJ)**2/RG/GAMMA*(GAMMA-1.))*1.
        ZZB=TTL
        ZZC=.5*V(I,NJ)**2/RG/GAMMA*(GAMMA-1.)
C ######################################################
        ABCD=((TM(I,NJ)/TTL)**(GAMMA/(GAMMA-1.))-1.)*PTL
        ZZA=ZZB-ZZC
C       PRINT *,ZZA
        ZZB=TTL
        ZZC=GAMMA/(GAMMA-1.)
        ZZD=(ZZA/ZZB)**ZZC-1.
        ZZD=ZZD*PTL
C       PRINT *, 'DOU.= ',ZZD, '     SIN.=',ABCD
        ABCD=ZZD
        PP(I,NJ)=(ABCD-P(I,NJ))*.0
C       PRINT *,'PRE.  I=  ',I,P(I,NJM1),P(I,NJM2),P(I,NJ)
        P(I,NJ)=ABCD
C       PRINT *,'PRESS',P(I,NJ),ZZD
C       P(I,NJM1)=P(I,NJ)*.9+P(I,NJM1)*.1
C       PRINT *,'PRE1.  I=  ',I,P(I,NJM1),P(I,NJM2),P(I,NJ)
        DEN(I,NJ)=(P(I,NJ)+PTL)/TM(I,NJ)/RG
        TH(I,NJ)=(TM(I,NJ)-BBB*100.)*RG*GAMMA/(-1.+GAMMA)/SCALE+CCC
        TM(I,NJ)=TM(I,NJ)/100.
C       PP(I,NJ)=0.
457     CONTINUE
        AAAA=0.
        DO 757 I=NVS,NVE
        AAAA=V(I,NJ)+AAAA
757     CONTINUE
        AAAA=AAAA/(NVE-NVS+1)
        DO 758 I=NVS,NVE
C       V(I,NJ)=V(I,NJ)-.1*(AAAA-TTEMP)
        IF(V(I,NJ).GE.0.) V(I,NJ)=1.E-3
C       V(I,NJ)=10.
C        PRINT *, V(I,NJ)
758     CONTINUE
        DO 947 I=1,NVS1
        P(I,NJ)=P(I,NJM1)
        PP(I,NJ)=PP(I,NJM1)
        TM(I,NJ)=TM(I,NJM1)
        DEN(I,NJ)=DEN(I,NJM1)
        TH(I,NJ)=TH(I,NJM1)
        V(I,NJ)=0.
        U(I,NJ)=0.
947     CONTINUE
        DO 103 J=1,NJM1
C       U(1,J)=U(1,J)+.1*(U(2,J)-U(1,J))
C       P(1,J)=P(2,J)
C       TH(1,J)=TH(2,J)
C       DEN(1,J)=DEN(2,J)
103     CONTINUE
        V(1,NJ)=0.
        PLO=-.005*PTL
        PLO1=.01*PTL
        NVE3=NVE+3
        DO 179 I=1,NVS
```



```
        DO 179 J=1,NJ
        IF(U(I,J).GE.500.) U(I,J)=500.
        IF(V(I,J).GE.500.) V(I,J)=500.
        IF(V(I,J).LE.-500.) V(I,J)=-500.
        IF(U(I,J).LE.-500.) U(I,J)=-500.
        IF(P(I,J).GE.PLO1) P(I,J)=PLO1
        IF(P(I,J).LE.PLO) P(I,J)=PLO
179     CONTINUE
        RETURN
C
C
              ENTRY BUNDYB
        DO 200 I=1,NI
        U(I,1)=U(I,2)
        V(I,1)=0.
        P(I,1)=P(I,2)
      - PP(I,1)=PP(I,2)
        TH(I,1)=TH(I,2)
200     CONTINUE
        RETURN
C
C
        ENTRY BUNDXL
C
C ********************IF ISUP.EQ.1 , NO TOTAL MASS FLUX CORRECTION**
C
        DO 301 J=1,NJ
        U(1,J)=0.
        V(1,J)=0.
        P(1,J)=P(2,J)
        PP(1,J)=PP(2,J)
        TH(1,J)=TH(2,NJ)
301     CONTINUE
        PLO=0.005*PTL
        DO 288 I=1,NI
        DO 288 J=1,NJ
C        IF(P(I,J).GE.PLO) P(I,J)=PLO
288     CONTINUE
C       PRINT *, 'NJ=',NJ
C       PRINT *,'PRESS1', P(1,40),P(2,40),P(1,45),P(2,45)
        DO 302 J=1,45
C       PRINT *,'J=J',J
        P(1,J)=P(2,J)
C       PRINT *,'J=J1',J
302     CONTINUE
C       PRINT *,'PRESS', P(1,40),P(2,40),P(1,45),P(2,45)
C       PRINT *,'PRESS',P(1,50),P(2,50),P(6,50),P(7,50),P(30,50)
        RETURN
                ENTRY BNDYT1
C
C ***************** SLIP WALL BOUNDARY CONDITIONS ********************
C
        NJM2=NJ-2
        NJM3=NJ-3
        DO 585 I=NVE1,NIM1
        IF(COEF(I).GE.0.)
```

```
     1  PP(I,NJ)=PP(I,NJM1)*COEF(I)+(1.-COEF(I))*PP(I+1,NJM1)
        IF(COEF(I).LE.0.)
     1  PP(I,NJ)=-PP(I,NJM1)*COEF(I)+(1.+COEF(I))*PP(I-1,NJM1)
C         IF(I.GE.15) TH(I,NJ)=31.
C         IF(I.LT.15.AND.I.GE.NVE1)
        U(I,NJ)=0.
        V(I,NJ)=0.
        TH(I,NJ)=TH(NVS,NJ)
585     CONTINUE
        U(1,NJ)=0.
        U(NI,NJ)=0.
        V(1,NJ)=0.
        V(NI,NJ)=0.
        P(1,NJ)=P(1,NJM1)
        P(NI,NJ)=P(NI,NJM1)
        PP(1,NJ)=PP(1,NJM1)
        PP(NI,NJ)=PP(NI,NJM1)
        DO 586 I=1,NVS1
        P(I,NJ)=P(I,NJM1)
        PP(I,NJ)=PP(I,NJM1)
        TM(I,NJ)=TM(I,NJM1)
        DEN(I,NJ)=DEN(I,NJM1)
        TH(I,NJ)=TH(I,NJM1)
        V(I,NJ)=0.
        U(I,NJ)=0.
586     CONTINUE
        RETURN
        END
       SUBROUTINE CALCP
C       INCLUDE 'DIMENSION1'
C       INCLUDE 'DIMENSION'
C       IMPLICIT REAL*8 (A-H,O-Z)
        PARAMETER (IT=100,JT=60,LMAX=500)
        CHARACTER*8 PFOR1,PUFOR1,FILIN,FILOUT
        CHARACTER*8 PFOR2,PUFOR2
        CHARACTER*8 PFOR3,PUFOR3
        CHARACTER*8 PFOR4,PUFOR4
     COMMON /FNAME1/PFOR1,PUFOR1,FILIN,FILOUT
     COMMON /FNAME2/PFOR2,PUFOR2,PFOR3,PUFOR3
     COMMON /FNAME3/PP1,PP2,PP3,PP4,MPL,MPL1
     COMMON /FNAME4/PFOR4,PUFOR4
     COMMON /COEFF/Q1P(IT,JT),Q2P(IT,JT),Q3P(IT,JT),COB(IT,JT)
    1    ,SEW(IT,JT),YSEW(IT,JT),SNS(IT,JT),XSNS(IT,JT)
    2    ,DU(IT,JT),DU1(IT,JT),DV(IT,JT),DV1(IT,JT)
    3    ,AP(IT,JT),AN(IT,JT),AS(IT,JT),AE(IT,JT),AW(IT,JT),SU(IT,JT)
    1    ,SP(IT,JT)
     COMMON /POS/ YPOS(IT,JT),XPOS(IT,JT),R(IT,JT)
     COMMON /VAR/ U(IT,JT),V(IT,JT),P(IT,JT),TM(IT,JT),PP(IT,JT)
    1    ,UDUMMY(IT,JT),VDUMMY(IT,JT)
    2    ,TVIS(IT,JT),TCON(IT,JT),DEN(IT,JT),DISS(IT,JT)
     COMMON
    1    /UVEL/RESORU,NSWPU,URFU,SD
    1    /VVEL/RESORV,NSWPV,URFV
    1    /PCOR/RESORM,NSWPP,URFP,IPREF,JPREF
    1    /TMP/RESORT,NSWPT,URFT
     COMMON/INPUT/NI,NJ,NIM1,NJM1,GREAT,INDCOS,INDSM
```



```
    1            ,DATAR,DATAW,IFORM,ILASER,CLASIN,NRAYS
    2            ,FOCUS,IFOCUS,BDIAM,ITRACE,ISUPER
    3            ,ANGI,ANGE,RCI,RCT,RT,RI,XEXIT,XI,RTIOY1
     COMMON/IINPUT/
    4            RTIOX1,RTIOX2,XDENSE,JS1,JS2,IS1,IS2
    5            ,URSUP,URVIS,IDENSE,JDENSE,YENRAT,RTIOY2
    6            ,NCONST,XCONST
    6            ,INITP,INITER,SCALE
     COMMON/COND/CCN(IT,JT),CCE(IT,JT),DDN(IT,JT),DDE(IT,JT)
    1    ,DDN1(IT,JT),DDE1(IT,JT)
     COMMON/LASER/QINP(IT,JT),GRA(IT,JT),TRANS(IT,JT),CAB(IT,JT)
    1    ,TNG(LMAX),ING(LMAX,IT)
    2    ,POWER(LMAX),QRA(IT,JT),TH(IT,JT)
     COMMON/LASER2/HT(3000,4),HMU(400,4),HDEN(400,4)
    1    ,HCCP(400,4),HCAB(400,4),HRA(400,4)
       COMMON /ADD8/ANU(IT,JT),ASU(IT,JT),AEU(IT,JT),AWU(IT,JT)
       COMMON /ADD9/ANV(IT,JT),ASV(IT,JT),AEV(IT,JT),AWV(IT,JT)
       COMMON /ADD10/AAN(IT,JT),AAE(IT,JT),COEF(IT),UTEMP(IT,JT),
    1             VTEMP(IT,JT),DYDX(IT),XP(IT)
       COMMON/EXTRA/HINLET
    1       /EXTRA1/UINLET,TBOUND
    1/MMAIN/MAXIT,JMON,IMON,INDPRI,SOLPAT
    1/ADD5/NITER
    1/ADD6/SORMAX,TRSMT,RDL
       COMMON/PROP/PTL,TTL,GAMMA,RG,WGHT,WGHT1,RATIO
       COMMON/EXTRA/PDUMMY(IT,JT)
       COMMON/PLUS/LROAT,NVS,NVS1,NVE,NVE1
       COMMON/MACHO/MAEX(JT),PEX(JT)
C       DIMENSION AAN(IT,JT),AAE(IT,JT)
       DIMENSION UCOEFF(IT,JT),VCOEFF(IT,JT)
C
                              CALL CONUVT
       DO 599 I=1,NI
       DO 599 J=1,NJ
       UTEMP(I,J)=0.
       VTEMP(I,J)=0.
599    CONTINUE
       DO 102 I=1,NIM1
       DO 102 J=1,NJM1
     DENN=0.5*(DEN(I,J)+DEN(I,J+1))
     DENE=0.5*(DEN(I,J)+DEN(I+1,J))
     AN1=DENN*(R(I,J+1)+R(I,J))*(DV(I,J+1)+DV(I,J))*.25*(SEW(I,J)
    1+SEW(I,J+1))*.5
     AN2=DENN*(R(I,J+1)+R(I,J))*(DU1(I,J+1)+DU1(I,J))*.25*(YSEW(I,J)
    1+YSEW(I,J+1))*.5
       IF(J.EQ.1)
    1AN1=DEN(I,J)*R(I,J)*DV(I,J)*SEW(I,J)
       IF(J.EQ.1)
    2AN2=DEN(I,J)*R(I,J)*DU1(I,J)*YSEW(I,J)
       IF(J.EQ.NJM1)
    1AN1=DEN(I,J+1)*R(I,J+1)*DV(I,J)*SEW(I,J+1)*1.
       IF(J.EQ.NJM1)
    2AN2=DEN(I,J+1)*R(I,J+1)*DU1(I,J)*YSEW(I,J+1)*1.
     AE1=DENE*(R(I,J)+R(I+1,J))*(DU(I+1,J)+DU(I,J))*.25*(SNS(I,J)+
    1SNS(I+1,J))*.5
     AE2=DENE*(R(I,J)+R(I+1,J))*(DV1(I+1,J)+DV1(I,J))*.25*(XSNS(I,J)+
```

```
     1XSNS(I+1,J))*.5
        IF(I.EQ.1)
     1AE1=DEN(I,J)*R(I,J)*DU(I+1,J)*SNS(I+1,J)*1.
        IF(I.EQ.1)
     1AE2=DEN(I,J)*R(I,J)*DV1(I+1,J)*XSNS(I+1,J)*1.
        IF(I.EQ.NIM1)
     1AE1=DEN(I+1,J)*R(I+1,J)*DU(I+1,J)*SNS(I+1,J)
        IF(I.EQ.NIM1)
     1AE2=DEN(I+1,J)*R(I+1,J)*DV1(I+1,J)*XSNS(I+1,J)
        AAN(I,J)=AN1-AN2
        AAE(I,J)=AE1-AE2
        IF(I.EQ.1) AAE(I,J)=0.
        IF(I.EQ.NIM1) AAE(I,J)=0.
C?        IF(J.EQ.NJM1.AND.I.GE.NVE1) AAN(I,J)=0.
C?        IF(J.EQ.NJM1.AND.I.LE.NVS1) AAN(I,J)=0.
        IF(J.EQ.NJM1) AAN(I,J)=0.
        IF(J.EQ.1) AAN(I,J)=0.
102     CONTINUE
        DO 100 I=2,NIM1
        DO 100 J=2,NJM1
        CN=CCN(I,J)/((P(I,J)+P(I,J+1))/2.+PTL)
     1*URSUP
        IF(J.EQ.NJM1) CN=CCN(I,J)/(P(I,J+1)+PTL)*URSUP
C        IF(J.EQ.NJM1.AND.I.EQ.7) PRINT *, CN,AAN(7,50)
        CS=CCN(I,J-1)/((P(I,J-1)+P(I,J))/2.+PTL)
     1*URSUP
        IF(J.EQ.2) CS=CCN(I,J-1)/(P(I,J-1)+PTL)*URSUP
        CE=CCE(I,J)/((P(I,J)+P(I+1,J))/2.+PTL)
     1*URSUP
        IF(I.EQ.NIM1) CE=CCE(I,J)/(P(I+1,J)+PTL)*URSUP
        CW=CCE(I-1,J)/((P(I-1,J)+P(I,J))/2.+PTL)
     1*URSUP
        IF(I.EQ.2) CW=CCE(I-1,J)/(P(I-1,J)+PTL)*URSUP
        AN(I,J)=MAX(ABS(0.5*CN),AAN(I,J))-0.5*CN
        AS(I,J)=MAX(ABS(0.5*CS),AAN(I,J-1))+0.5*CS
        AE(I,J)=MAX(ABS(0.5*CE),AAE(I,J))-0.5*CE
        AW(I,J)=MAX(ABS(0.5*CW),AAE(I-1,J))+0.5*CW
100     CONTINUE
      RESORM=0.0
C
C*************** CALCULATE SOURCE TERMS *******************************
C
        DO 359 I=2,NIM1
        DO 359 J=2,NJM1
                SMP=CCN(I,J)-CCN(I,J-1)+CCE(I,J)-CCE(I-1,J)
                SP(I,J)=0.0
                SU(I,J)=-SMP
                RESORM=RESORM+ABS(SMP)
  359 CONTINUE
      CALL MODP
C
      DO 300 I=2,NIM1
      DO 300 J=2,NJM1
           AP(I,J)=AN(I,J)+AS(I,J)+AE(I,J)+AW(I,J)-SP(I,J)
        IF(AP(I,J).EQ.0.0) PRINT *,'AP IN P', I,J,AP(I,J)
        IF(AP(I,J).EQ.0.0) AP(I,J)=1.E-30
```



```
  300 CONTINUE
C
C
      IF(SD)51,50,50
   51 DO 510 N=1,NSWPP
  510 CALL LISOLH(2,2,NI,NJ,PP)
      GO TO 600
   50 DO 400 N=1,NSWPP
  400 CALL LISOLV(2,2,NI,NJ,PP)
  600 CONTINUE
C               CALL PRINT(1,1,NI,NJ,PP,HEDP,IS1,JS1)
C       PRINT *, 'PP',PP(2,30),PP(2,50),PP(3,30),PP(3,50)
C
      PPREF=PP(IPREF,JPREF)
C
C *************************** EXIT BOUNDARY CONDITIONS ************
C
           CALL BUNDXR
           CALL BNDYT1
           CALL BUNDYB
           CALL BUNDXL
C              CALL PRINT(1,1,NI,NJ,PP,HEDP,IS1,JS1)
C
C ********************** UPDATE PRESSURE FIELD *********************
        PTTTL=-.9999*PTL
C
      DO 504 I=1,NI
      DO 504 J=1,NJM1
       P(I,J)=P(I,J)+URFP*PP(I,J)
        IF(P(I,J).LE.PTTTL) P(I,J)=PTTTL
  504 CONTINUE
        NIM2=NIM1-1
      DO 500 I=2,NIM1
      DO 501 J=2,NJM1
        AAA=(PP(I-1,J)-PP(I+1,J))/2.
        BBB=(PP(I,J-1)-PP(I,J+1))/2.
        IF(I.EQ.2)
     1AAA=(4.*PP(I-1,J)-PP(I+1,J)-3.*PP(I,J))/3.
        IF(I.EQ.NIM1)
     1AAA=-1.*(4.*PP(I+1,J)-PP(I-1,J)-3.*PP(I,J))/3.
        IF(J.EQ.2)
     1BBB=(4.*PP(I,J-1)-PP(I,J+1)-3.*PP(I,J))/3.
        IF(J.EQ.NJM1)
     1BBB=-1.*(4.*PP(I,J+1)-PP(I,J-1)-3.*PP(I,J))/3.
       UTEMP(I,J)=DU(I,J)*AAA
     1+DU1(I,J)*BBB
       VTEMP(I,J)=DV(I,J)*BBB
     1+DV1(I,J)*AAA
        U(I,J)=U(I,J)+UTEMP(I,J)
        V(I,J)=V(I,J)+VTEMP(I,J)
  501 CONTINUE
  500 CONTINUE
      CALL BUNDXR
      CALL BNDYT1
      CALL BUNDYB
         CALL BUNDXL
```

```
      DO 853 I=1,NI
      DO 853 J=1,NJM1
853   PP(I,J)=0.
      DO 899 I=2,NIM1
      DO 898 J=2,NJM1
      UCOEFF(I,J)=AEU(I,J)*UTEMP(I+1,J)+AWU(I,J)*UTEMP(I-1,J)
     1+ANU(I,J)*UTEMP(I,J+1)+ASU(I,J)*UTEMP(I,J-1)
      VCOEFF(I,J)=AEV(I,J)*VTEMP(I+1,J)+AWV(I,J)*VTEMP(I-1,J)
     1+ANV(I,J)*VTEMP(I,J+1)+ASV(I,J)*VTEMP(I,J-1)
898   CONTINUE
899   CONTINUE
      DO 897 I=2,NIM1
      DO 896 J=2,NJM1
      GE=(UCOEFF(I,J)+UCOEFF(I+1,J))*(SNS(I,J)+SNS(I+1,J))
     1-(VCOEFF(I,J)+VCOEFF(I+1,J))*(XSNS(I,J)+XSNS(I+1,J))
      GE=GE*(R(I+1,J)+R(I,J))*(DEN(I,J)+DEN(I+1,J))/16.
      IF(I.EQ.NIM1)
     1  GE=(UCOEFF(I+1,J)*SNS(I+1,J)-VCOEFF(I+1,J)*XSNS(I+1,J))
     2  *R(I+1,J)*DEN(I+1,J)
      GW=(UCOEFF(I,J)+UCOEFF(I-1,J))*(SNS(I,J)+SNS(I-1,J))
     1-(VCOEFF(I,J)+VCOEFF(I-1,J))*(XSNS(I,J)+XSNS(I-1,J))
      GW=GW*(R(I-1,J)+R(I,J))*(DEN(I,J)+DEN(I-1,J))/16.
      IF(I.EQ.2)
     1  GW=(UCOEFF(I-1,J)*SNS(I-1,J)-VCOEFF(I-1,J)*XSNS(I-1,J))
     2  *R(I-1,J)*DEN(I-1,J)
      GN=(VCOEFF(I,J)+VCOEFF(I,J+1))*(SEW(I,J)+SEW(I,J+1))
     1-(UCOEFF(I,J)+UCOEFF(I,J+1))*(YSEW(I,J)+YSEW(I,J+1))
      GN=GN*(R(I,J+1)+R(I,J))*(DEN(I,J)+DEN(I,J+1))/16.
      IF(J.EQ.NJM1)
     1  GN=(VCOEFF(I,J+1)*SEW(I,J+1)-UCOEFF(I,J+1)*YSEW(I,J+1))
     2  *R(I,J+1)*DEN(I,J+1)
      GS=(VCOEFF(I,J)+VCOEFF(I,J-1))*(SEW(I,J)+SEW(I,J-1))
     1-(UCOEFF(I,J)+UCOEFF(I,J-1))*(YSEW(I,J)+YSEW(I,J-1))
      GS=GS*(R(I,J-1)+R(I,J))*(DEN(I,J)+DEN(I,J-1))/16.
      IF(J.EQ.2)
     1  GS=(VCOEFF(I,J-1)*SEW(I,J-1)-UCOEFF(I,J-1)*YSEW(I,J-1))
     2  *R(I,J-1)*DEN(I,J-1)
C#####################
      IF(I.EQ.NIM1) GE=0.
      IF(I.EQ.2) GW=0.
      IF(J.EQ.2) GS=0.
      IF(J.EQ.NJM1) GN=0.
      SMP=GN-GS+GE-GW
      SP(I,J)=0.
      SU(I,J)=-SMP
896   CONTINUE
897   CONTINUE
     IF(SD)151,150,150
 151 DO 511 N=1,NSWPP
 511 CALL LISOLH(2,2,NI,NJ,PP)
     GO TO 601
 150 DO 401 N=1,NSWPP
  401 CALL LISOLV(2,2,NI,NJ,PP)
  601 CONTINUE
C
C ************ CENTERLINE BOUNDARY CONDITIONS ******************
```



```
C ***********  WALL SLIP CONDITIONS ****************************
C
C       BTEMP=0.
C       DO 713 I=2,NIM1
C       U(I,1)=U(I,2)
C       P(I,1)=P(I,2)
C       IF(COEF(I).GE.BTEMP)
C     1 P(I,NJ)=P(I,NJM1)*COEF(I)+(1.-COEF(I))*P(I+1,NJM1)
C       IF(COEF(I).LE.BTEMP)
C     1 P(I,NJ)=-P(I,NJM1)*COEF(I)+(1.+COEF(I))*P(I-1,NJM1)
C       PP(I,1)=PP(I,2)
C       IF(COEF(I).GE.BTEMP)
C     1 PP(I,NJ)=PP(I,NJM1)*COEF(I)+(1.-COEF(I))*PP(I+1,NJM1)
C       IF(COEF(I).LE.BTEMP)
C     1 PP(I,NJ)=-PP(I,NJM1)*COEF(I)+(1.+COEF(I))*PP(I-1,NJM1)
C       U(I,NJ)=0.
C       V(I,NJ)=U(I,NJ)/SEW(I,NJ)*YSEW(I,NJ)
C713    CONTINUE
C
        CALL BUNDXR
        CALL BNDYT1
        CALL BUNDYB
           CALL BUNDXL
        DO 859 I=2,NIM1
        DO 859 J=2,NJM1
        AAA=(PP(I-1,J)-PP(I+1,J))/2.
        BBB=(PP(I,J-1)-PP(I,J+1))/2.
        IF(I.EQ.2)
     1AAA=(4.*PP(I-1,J)-PP(I+1,J)-3.*PP(I,J))/3.
        IF(I.EQ.NIM1)
     1AAA=-1.*(4.*PP(I+1,J)-PP(I-1,J)-3.*PP(I,J))/3.
        IF(J.EQ.2)
     1BBB=(4.*PP(I,J-1)-PP(I,J+1)-3.*PP(I,J))/3.
        IF(J.EQ.NJM1)
     1BBB=-1.*(4.*PP(I,J+1)-PP(I,J-1)-3.*PP(I,J))/3.
       UTEMP(I,J)=DU(I,J)*AAA
     1+DU1(I,J)*BBB
       VTEMP(I,J)=DV(I,J)*BBB
     1+DV1(I,J)*AAA
        U(I,J)=U(I,J)
     1+(UTEMP(I,J)+UCOEFF(I,J))*1.
        V(I,J)=V(I,J)
     1+(VTEMP(I,J)+VCOEFF(I,J))*1.
859     CONTINUE
      PPREF=PP(IPREF,JPREF)
        PTTTL=-.9999*PTL
          DO 502 I=1,NI
       DO 503 J=1,NJM1
       P(I,J)=P(I,J)+URFP*PP(I,J)
        IF(P(I,J).LE.PTTTL) P(I,J)=PTTTL
       PP(I,J)=0.0
  503 CONTINUE
  502 CONTINUE
        RETURN
        END
      SUBROUTINE CALCU
```

```
C       INCLUDE 'DIMENSION1'
C       INCLUDE 'DIMENSION'
C       IMPLICIT REAL*8 (A-H,O-Z)
        PARAMETER (IT=100,JT=60,LMAX=500)
        CHARACTER*8 PFOR1,PUFOR1,FILIN,FILOUT
        CHARACTER*8 PFOR2,PUFOR2
        CHARACTER*8 PFOR3,PUFOR3
        CHARACTER*8 PFOR4,PUFOR4
      COMMON /FNAME1/PFOR1,PUFOR1,FILIN,FILOUT
      COMMON /FNAME2/PFOR2,PUFOR2,PFOR3,PUFOR3
      COMMON /FNAME3/PP1,PP2,PP3,PP4,MPL,MPL1
      COMMON /FNAME4/PFOR4,PUFOR4
      COMMON /COEFF/Q1P(IT,JT),Q2P(IT,JT),Q3P(IT,JT),COB(IT,JT)
     1    ,SEW(IT,JT),YSEW(IT,JT),SNS(IT,JT),XSNS(IT,JT)
     2    ,DU(IT,JT),DU1(IT,JT),DV(IT,JT),DV1(IT,JT)
     3    ,AP(IT,JT),AN(IT,JT),AS(IT,JT),AE(IT,JT),AW(IT,JT),SU(IT,JT)
     1    ,SP(IT,JT)
      COMMON /POS/ YPOS(IT,JT),XPOS(IT,JT),R(IT,JT)
      COMMON /VAR/ U(IT,JT),V(IT,JT),P(IT,JT),TM(IT,JT),PP(IT,JT)
     1    ,UDUMMY(IT,JT),VDUMMY(IT,JT)
     2    ,TVIS(IT,JT),TCON(IT,JT),DEN(IT,JT),DISS(IT,JT)
      COMMON
     1    /UVEL/RESORU,NSWPU,URFU,SD
     1    /VVEL/RESORV,NSWPV,URFV
     1    /PCOR/RESORM,NSWPP,URFP,IPREF,JPREF
     1    /TMP/RESORT,NSWPT,URFT
      COMMON/INPUT/NI,NJ,NIM1,NJM1,GREAT,INDCOS,INDSM
     1             ,DATAR,DATAW,IFORM,ILASER,CLASIN,NRAYS
     2             ,FOCUS,IFOCUS,BDIAM,ITRACE,ISUPER
     3             ,ANGI,ANGE,RCI,RCT,RT,RI,XEXIT,XI,RTIOY1
      COMMON/IINPUT/
     4            RTIOX1,RTIOX2,XDENSE,JS1,JS2,IS1,IS2
     5             ,URSUP,URVIS,IDENSE,JDENSE,YENRAT,RTIOY2
     6             ,NCONST,XCONST
     6             ,INITP,INITER,SCALE
      COMMON/COND/CCN(IT,JT),CCE(IT,JT),DDN(IT,JT),DDE(IT,JT)
     1    ,DDN1(IT,JT),DDE1(IT,JT)
      COMMON/LASER/QINP(IT,JT),GRA(IT,JT),TRANS(IT,JT),CAB(IT,JT)
     1    ,TNG(LMAX),ING(LMAX,IT)
     2    ,POWER(LMAX),QRA(IT,JT),TH(IT,JT)
      COMMON/LASER2/HT(3000,4),HMU(400,4),HDEN(400,4)
     1    ,HCCP(400,4),HCAB(400,4),HRA(400,4)
      COMMON /ADD8/ANU(IT,JT),ASU(IT,JT),AEU(IT,JT),AWU(IT,JT)
      COMMON /ADD9/ANV(IT,JT),ASV(IT,JT),AEV(IT,JT),AWV(IT,JT)
      COMMON /ADD10/AAN(IT,JT),AAE(IT,JT),COEF(IT),UTEMP(IT,JT),
     1              VTEMP(IT,JT),DYDX(IT),XP(IT)
      COMMON/EXTRA/HINLET
     1       /EXTRA1/UINLET,TBOUND
     1/MMAIN/MAXIT,JMON,IMON,INDPRI,SOLPAT
     1/ADD5/NITER
     1/ADD6/FORMAX,TRSMT,RDL
      COMMON/PROP/PTL,TTL,GAMMA,RG,WGHT,WGHT1,RATIO
      COMMON/EXTRA/PDUMMY(IT,JT)
      COMMON/PLUS/LROAT,NVS,NVS1,NVE,NVE1
                          CALL CONUVT
                          CALL DIFUV
```



```
      DO 100 I=2,NIM1
      DO 101 J=2,NJM1
C
        DN1=DDN1(I,J)*.25*(U(I+1,J+1)+U(I+1,J)-U(I-1,J+1)-U(I-1,J))
        DS1=DDN1(I,J-1)*.25*(U(I+1,J-1)+U(I+1,J)
     1  -U(I-1,J-1)-U(I-1,J))
        DE1=DDE1(I,J)*.25*(U(I,J+1)+U(I+1,J+1)-U(I,J-1)-U(I+1,J-1))
        DW1=DDE1(I-1,J)*.25*(U(I,J+1)+U(I-1,J+1)
     1  -U(I,J-1)-U(I-1,J-1))
        IF(J.EQ.NJM1) DN1=DDN1(I,J)*.5*(U(I+1,J+1)-U(I-1,J+1))
        IF(J.EQ.2) DS1=DDN1(I,J-1)*.5*(U(I+1,J-1)-U(I-1,J-1))
        IF(I.EQ.2) DW1=DDE1(I-1,J)*.5*(U(I-1,J+1)-U(I-1,J-1))
        IF(I.EQ.NIM1) DE1=DDE1(I,J)*.5*(U(I+1,J+1)-U(I+1,J-1))
C
C******** CALCULATE COEFFICIENTS OF SOURCE TERMS *****************
C
      SMP=CCN(I,J)-CCN(I,J-1)+CCE(I,J)-CCE(I-1,J)
      CP=MAX(0.0,SMP)
      CPO=CP
C
C********** ASSEMBLE MAIN COEFFICIENTS ****************************
C
      AN(I,J)=MAX(ABS(0.5*CCN(I,J)),DDN(I,J))-0.5*CCN(I,J)
      AS(I,J)=MAX(ABS(0.5*CCN(I,J-1)),DDN(I,J-1))+0.5*CCN(I,J-1)
      AE(I,J)=MAX(ABS(0.5*CCE(I,J)),DDE(I,J))-0.5*CCE(I,J)
      AW(I,J)=MAX(ABS(0.5*CCE(I-1,J)),DDE(I-1,J))+0.5*CCE(I-1,J)
      DU(I,J)=R(I,J)*SNS(I,J)
      DU1(I,J)=-1.*R(I,J)*YSEW(I,J)
      AAA=DU(I,J)*(P(I-1,J)-P(I+1,J))/2.
      BBB=DU1(I,J)*(P(I,J-1)-P(I,J+1))/2.
        IF(I.EQ.2)
     1AAA=DU(I,J)*(4.*P(I-1,J)-P(I+1,J)-3.*P(I,J))/3.
        IF(I.EQ.NIM1)
     1AAA=-1.*DU(I,J)*(4.*P(I+1,J)-P(I-1,J)-3.*P(I,J))/3.
        IF(J.EQ.2)
     1BBB=DU1(I,J)*(4.*P(I,J-1)-P(I,J+1)-3.*P(I,J))/3.
        IF(J.EQ.NJM1)
     1BBB=-1.*DU1(I,J)*(4.*P(I,J+1)-P(I,J-1)-3.*P(I,J))/3.
      SU(I,J)=CPO*U(I,J)+AAA
     1+BBB
     2+DN1+DE1-DS1-DW1
      SP(I,J)=-CP
  101 CONTINUE
  100 CONTINUE
C
      CALL MODU
C
      RESORU=0.0
      DO 300 I=2,NIM1
      DO 301 J=2,NJM1
      AP(I,J)=AN(I,J)+AS(I,J)+AE(I,J)+AW(I,J)-SP(I,J)
        IF(AP(I,J).LE.0.) PRINT *,'AP IN U', I,J,AP(I,J)
        IF(AP(I,J).LE.0.) AP(I,J)=1.E-30
      DU(I,J)=DU(I,J)/AP(I,J)
      DU1(I,J)=DU1(I,J)/AP(I,J)
      RESOR=AN(I,J)*U(I,J+1)+AS(I,J)*U(I,J-1)+AE(I,J)*U(I+1,J)
```

```
     1     +AW(I,J)*U(I-1,J)-AP(I,J)*U(I,J)+SU(I,J)
      RESORU=RESORU+ABS(RESOR)
C
C******** UNDER-RELAXATION  ******************************
      AP(I,J)=AP(I,J)/URFU
      SU(I,J)=SU(I,J)+(1.-URFU)*AP(I,J)*U(I,J)
      DU(I,J)=DU(I,J)*URFU
      DU1(I,J)=DU1(I,J)*URFU
        ANU(I,J)=AN(I,J)/AP(I,J)
        ASU(I,J)=AS(I,J)/AP(I,J)
        AEU(I,J)=AE(I,J)/AP(I,J)
        AWU(I,J)=AW(I,J)/AP(I,J)
  301 CONTINUE
  300 CONTINUE
C
C
       IF(SD) 51,50,50
   51  DO 500 N=1,NSWPU
  500  CALL LISOLH(2,2,NI,NJ,U)
       GO TO 600
   50  DO 400 N=1,NSWPU
  400  CALL LISOLV(2,2,NI,NJ,U)
  600   CONTINUE
      RETURN
      END
      SUBROUTINE CALCV
C       INCLUDE 'DIMENSION1'
C       INCLUDE 'DIMENSION'
C       IMPLICIT REAL*8 (A-H,O-Z)
        PARAMETER (IT=100,JT=60,LMAX=500)
        CHARACTER*8 PFOR1,PUFOR1,FILIN,FILOUT
        CHARACTER*8 PFOR2,PUFOR2
        CHARACTER*8 PFOR3,PUFOR3
        CHARACTER*8 PFOR4,PUFOR4
      COMMON /FNAME1/PFOR1,PUFOR1,FILIN,FILOUT
      COMMON /FNAME2/PFOR2,PUFOR2,PFOR3,PUFOR3
      COMMON /FNAME3/PP1,PP2,PP3,PP4,MPL,MPL1
      COMMON /FNAME4/PFOR4,PUFOR4
      COMMON /COEFF/Q1P(IT,JT),Q2P(IT,JT),Q3P(IT,JT),COB(IT,JT)
     1   ,SEW(IT,JT),YSEW(IT,JT),SNS(IT,JT),XSNS(IT,JT)
     2   ,DU(IT,JT),DU1(IT,JT),DV(IT,JT),DV1(IT,JT)
     3   ,AP(IT,JT),AN(IT,JT),AS(IT,JT),AE(IT,JT),AW(IT,JT),SU(IT,JT)
     1   ,SP(IT,JT)
      COMMON /POS/ YPOS(IT,JT),XPOS(IT,JT),R(IT,JT)
      COMMON /VAR/ U(IT,JT),V(IT,JT),P(IT,JT),TM(IT,JT),PP(IT,JT)
     1   ,UDUMMY(IT,JT),VDUMMY(IT,JT)
     2   ,TVIS(IT,JT),TCON(IT,JT),DEN(IT,JT),DISS(IT,JT)
      COMMON
     1   /UVEL/RESORU,NSWPU,URFU,SD
     1   /VVEL/RESORV,NSWPV,URFV
     1   /PCOR/RESORM,NSWPP,URFP,IPREF,JPREF
     1   /TMP/RESORT,NSWPT,URFT
      COMMON/INPUT/NI,NJ,NIM1,NJM1,GREAT,INDCOS,INDSM
     1            ,DATAR,DATAW,IFORM,ILASER,CLASIN,NRAYS
     2            ,FOCUS,IFOCUS,BDIAM,ITRACE,ISUPER
     3            ,ANGI,ANGE,RCI,RCT,RT,RI,XEXIT,XI,RTIOY1
```



```
      COMMON/IINPUT/
     4            RTIOX1,RTIOX2,XDENSE,JS1,JS2,IS1,IS2
     5            ,URSUP,URVIS,IDENSE,JDENSE,YENRAT,RTIOY2
     6            ,NCONST,XCONST
     6            ,INITP,INITER,SCALE
      COMMON/COND/CCN(IT,JT),CCE(IT,JT),DDN(IT,JT),DDE(IT,JT)
     1    ,DDN1(IT,JT),DDE1(IT,JT)
      COMMON/LASER/QINP(IT,JT),GRA(IT,JT),TRANS(IT,JT),CAB(IT,JT)
     1    ,TNG(LMAX),ING(LMAX,IT)
     2    ,POWER(LMAX),QRA(IT,JT),TH(IT,JT)
      COMMON/LASER2/HT(3000,4),HMU(400,4),HDEN(400,4)
     1    ,HCCP(400,4),HCAB(400,4),HRA(400,4)
        COMMON /ADD8/ANU(IT,JT),ASU(IT,JT),AEU(IT,JT),AWU(IT,JT)
        COMMON /ADD9/ANV(IT,JT),ASV(IT,JT),AEV(IT,JT),AWV(IT,JT)
        COMMON /ADD10/AAN(IT,JT),AAE(IT,JT),COEF(IT),UTEMP(IT,JT),
     1              VTEMP(IT,JT),DYDX(IT),XP(IT)
        COMMON/EXTRA/HINLET
     1       /EXTRA1/UINLET,TBOUND
     1/MMAIN/MAXIT,JMON,IMON,INDPRI,SOLPAT
     1/ADD5/NITER
     1/ADD6/SORMAX,TRSMT,RDL
        COMMON/PROP/PTL,TTL,GAMMA,RG,WGHT,WGHT1,RATIO
        COMMON/EXTRA/PDUMMY(IT,JT)
        COMMON/PLUS/LROAT,NVS,NVS1,NVE,NVE1
                              CALL CONUVT
      DO 100 I=2,NIM1
      DO 101 J=2,NJM1
        DN1=DDN1(I,J)*.25*(V(I+1,J)+V(I+1,J+1)-V(I-1,J)-V(I-1,J+1))
        DS1=DDN1(I,J-1)*.25*(V(I+1,J)+V(I+1,J-1)
     1  -V(I-1,J)-V(I-1,J-1))
        DE1=DDE1(I,J)*.25*(V(I+1,J+1)+V(I,J+1)-V(I+1,J-1)-V(I,J-1))
        DW1=DDE1(I-1,J)*.25*(V(I-1,J+1)+V(I,J+1)
     1  -V(I-1,J-1)-V(I,J-1))
        IF(J.EQ.NJM1) DN1=DDN1(I,J)*.5*(V(I+1,J+1)-V(I-1,J+1))
        IF(J.EQ.2) DS1=DDN1(I,J-1)*.5*(V(I+1,J-1)-V(I-1,J-1))
        IF(I.EQ.2) DW1=DDE1(I-1,J)*.5*(V(I-1,J+1)-V(I-1,J-1))
        IF(I.EQ.NIM1) DE1=DDE1(I,J)*.5*(V(I+1,J+1)-V(I+1,J-1))
C
C********** CALCULATE COEFFICIENTS OF SOURCE TERMS *****************
      SMP=CCN(I,J)-CCN(I,J-1)+CCE(I,J)-CCE(I-1,J)
      CP=MAX(0.0,SMP)
      CPO=CP
C
C************* ASSEMBLE MAIN COEFFICIENTS ************************
C
      AN(I,J)=MAX(ABS(0.5*CCN(I,J)),DDN(I,J))-0.5*CCN(I,J)
      AS(I,J)=MAX(ABS(0.5*CCN(I,J-1)),DDN(I,J-1))+0.5*CCN(I,J-1)
      AE(I,J)=MAX(ABS(0.5*CCE(I,J)),DDE(I,J))-0.5*CCE(I,J)
      AW(I,J)=MAX(ABS(0.5*CCE(I-1,J)),DDE(I-1,J))+0.5*CCE(I-1,J)
      DV(I,J)=R(I,J)*SEW(I,J)
      DV1(I,J)=-1.*R(I,J)*XSNS(I,J)
      AAA=DV(I,J)*(P(I,J-1)-P(I,J+1))/2.
      BBB=DV1(I,J)*(P(I-1,J)-P(I+1,J))/2.
        IF(I.EQ.2)
     1BBB=DV1(I,J)*(4.*P(I-1,J)-P(I+1,J)-3.*P(I,J))/3.
        IF(I.EQ.NIM1)
```

```
     1BBB=-1.*DV1(I,J)*(4.*P(I+1,J)-P(I-1,J)-3.*P(I,J))/3.
        IF(J.EQ.2)
     1AAA=DV(I,J)*(4.*P(I,J-1)-P(I,J+1)-3.*P(I,J))/3.
        IF(J.EQ.NJM1)
     1AAA=-1.*DV(I,J)*(4.*P(I,J+1)-P(I,J-1)-3.*P(I,J))/3.
      SU(I,J)=CPO*V(I,J)+AAA
     1+BBB
     2+DN1-DS1+DE1-DW1
       SP(I,J)=-CP
C     IF(INDCOS.EQ.2) SP(I,J)=SP(I,J)-TVIS(I,J)*DV(I,J)/RV(J)**2
  101 CONTINUE
  100 CONTINUE
C
      CALL MODV
C
      RESORV=0.0
      DO 300 I=2,NIM1
      DO 301 J=2,NJM1
      AP(I,J)=AN(I,J)+AS(I,J)+AE(I,J)+AW(I,J)-SP(I,J)
        IF(AP(I,J).LE.0.) PRINT *, 'AP in V', I,J, AP(I,J)
        IF(AP(I,J).LE.0.) AP(I,J)=1.E-30
      DV(I,J)=DV(I,J)/AP(I,J)
      DV1(I,J)=DV1(I,J)/AP(I,J)
      RESOR=AN(I,J)*V(I,J+1)+AS(I,J)*V(I,J-1)+AE(I,J)*V(I+1,J)
     1     +AW(I,J)*V(I-1,J)-AP(I,J)*V(I,J)+SU(I,J)
      RESORV=RESORV+ABS(RESOR)
C
C******************** UNDER-RELAXATION ************************
      AP(I,J)=AP(I,J)/URFV
        ANV(I,J)=AN(I,J)/AP(I,J)
        ASV(I,J)=AS(I,J)/AP(I,J)
        AEV(I,J)=AE(I,J)/AP(I,J)
        AWV(I,J)=AW(I,J)/AP(I,J)
      SU(I,J)=SU(I,J)+(1.-URFV)*AP(I,J)*V(I,J)
      DV(I,J)=DV(I,J)*URFV
      DV1(I,J)=DV1(I,J)*URFV
  301 CONTINUE
  300 CONTINUE
C
      IF(SD)51,50,50
   51 DO 500   N=1,NSWPV
  500 CALL LISOLH(2,2,NI,NJ,V)
      GO TO 600
   50 DO 400 N=1, NSWPV
  400 CALL LISOLV(2,2,NI,NJ,V)
  600 CONTINUE
      RETURN
      END
      SUBROUTINE CALTM
C       INCLUDE 'DIMENSION1'
C       INCLUDE 'DIMENSION'
C       IMPLICIT REAL*8 (A-H,O-Z)
        PARAMETER (IT=100,JT=60,LMAX=500)
        CHARACTER*8 PFOR1,PUFOR1,FILIN,FILOUT
        CHARACTER*8 PFOR2,PUFOR2
        CHARACTER*8 PFOR3,PUFOR3
```



```
        CHARACTER*8 PFOR4,PUFOR4
      COMMON /FNAME1/PFOR1,PUFOR1,FILIN,FILOUT
      COMMON /FNAME2/PFOR2,PUFOR2,PFOR3,PUFOR3
      COMMON /FNAME3/PP1,PP2,PP3,PP4,MPL,MPL1
      COMMON /FNAME4/PFOR4,PUFOR4
      COMMON /COEFF/Q1P(IT,JT),Q2P(IT,JT),Q3P(IT,JT),COB(IT,JT)
     1    ,SEW(IT,JT),YSEW(IT,JT),SNS(IT,JT),XSNS(IT,JT)
     2    ,DU(IT,JT),DU1(IT,JT),DV(IT,JT),DV1(IT,JT)
     3    ,AP(IT,JT),AN(IT,JT),AS(IT,JT),AE(IT,JT),AW(IT,JT),SU(IT,JT)
     1    ,SP(IT,JT)
      COMMON /POS/ YPOS(IT,JT),XPOS(IT,JT),R(IT,JT)
      COMMON /VAR/ U(IT,JT),V(IT,JT),P(IT,JT),TM(IT,JT),PP(IT,JT)
     1    ,UDUMMY(IT,JT),VDUMMY(IT,JT)
     2    ,TVIS(IT,JT),TCON(IT,JT),DEN(IT,JT),DISS(IT,JT)
      COMMON
     1    /UVEL/RESORU,NSWPU,URFU,SD
     1    /VVEL/RESORV,NSWPV,URFV
     1    /PCOR/RESORM,NSWPP,URFP,IPREF,JPREF
     1    /TMP/RESORT,NSWPT,URFT
      COMMON/INPUT/NI,NJ,NIM1,NJM1,GREAT,INDCOS,INDSM
     1             ,DATAR,DATAW,IFORM,ILASER,CLASIN,NRAYS
     2             ,FOCUS,IFOCUS,BDIAM,ITRACE,ISUPER
     3             ,ANGI,ANGE,RCI,RCT,RT,RI,XEXIT,XI,RTIOY1
      COMMON/IINPUT/
     4             RTIOX1,RTIOX2,XDENSE,JS1,JS2,IS1,IS2
     5             ,URSUP,URVIS,IDENSE,JDENSE,YENRAT,RTIOY2
     6             ,NCONST,XCONST
     6             ,INITP,INITER,SCALE
      COMMON/COND/CCN(IT,JT),CCE(IT,JT),DDN(IT,JT),DDE(IT,JT)
     1    ,DDN1(IT,JT),DDE1(IT,JT)
      COMMON/LASER/QINP(IT,JT),GRA(IT,JT),TRANS(IT,JT),CAB(IT,JT)
     1    ,TNG(LMAX),ING(LMAX,IT)
     2    ,POWER(LMAX),QRA(IT,JT),TH(IT,JT)
      COMMON/LASER2/HT(3000,4),HMU(400,4),HDEN(400,4)
     1    ,HCCP(400,4),HCAB(400,4),HRA(400,4)
        COMMON /ADD8/ANU(IT,JT),ASU(IT,JT),AEU(IT,JT),AWU(IT,JT)
        COMMON /ADD9/ANV(IT,JT),ASV(IT,JT),AEV(IT,JT),AWV(IT,JT)
        COMMON /ADD10/AAN(IT,JT),AAE(IT,JT),COEF(IT),UTEMP(IT,JT),
     1              VTEMP(IT,JT),DYDX(IT),XP(IT)
        COMMON/EXTRA/HINLET
     1       /EXTRA1/UINLET,TBOUND
     1/MMAIN/MAXIT,JMON,IMON,INDPRI,SOLPAT
     1/ADD5/NITER
     1/ADD6/SORMAX,TRSMT,RDL
        COMMON/PROP/PTL,TTL,GAMMA,RG,WGHT,WGHT1,RATIO
        COMMON/EXTRA/PDUMMY(IT,JT)
        COMMON/PLUS/LROAT,NVS,NVS1,NVE,NVE1
C
                              CALL DISSIP
                              CALL CONUVT
                              CALL DIFT
        TRAD=0.
        CPP=1.
      DO 100 I=2,NIM1
      DO 101 J=2,NJM1
        DN1=DDN1(I,J)*.25*(TH(I+1,J+1)+TH(I+1,J)-TH(I-1,J+1)-TH(I-1,J))
```

```
      DS1=DDN1(I,J-1)*.25*(TH(I+1,J-1)+TH(I+1,J)
     1  -TH(I-1,J-1)-TH(I-1,J))
      DE1=DDE1(I,J)*.25*(TH(I,J+1)+TH(I+1,J+1)-TH(I,J-1)-TH(I+1,J-1))
      DW1=DDE1(I-1,J)*.25*(TH(I,J+1)+TH(I-1,J+1)
     1  -TH(I,J-1)-TH(I-1,J-1))
      IF(J.EQ.NJM1) DN1=DDN1(I,J)*.5*(TH(I+1,J+1)-TH(I-1,J+1))
      IF(J.EQ.2) DS1=DDN1(I,J-1)*.5*(TH(I+1,J-1)-TH(I-1,J-1))
      IF(I.EQ.2) DW1=DDE1(I-1,J)*.5*(TH(I-1,J+1)-TH(I-1,J-1))
      IF(I.EQ.NIM1) DE1=DDE1(I,J)*.5*(TH(I+1,J+1)-TH(I+1,J-1))
C
C******* CALCULATE COEFFICIENTS OF SOURCE TERMS ****************
C
      SMP=CN-CS+CE-CW
      CP=MAX(0.0,SMP)
      CPO=CP
C********* ASSEMBLE MAIN COEFFICIENTS ***************************
C
      AN(I,J)=MAX(ABS(0.5*CCN(I,J)),DDN(I,J))-0.5*CCN(I,J)
      AS(I,J)=MAX(ABS(0.5*CCN(I,J-1)),DDN(I,J-1))+0.5*CCN(I,J-1)
      AE(I,J)=MAX(ABS(0.5*CCE(I,J)),DDE(I,J))-0.5*CCE(I,J)
      AW(I,J)=MAX(ABS(0.5*CCE(I-1,J)),DDE(I-1,J))+0.5*CCE(I-1,J)
C       CPP=RG/(GAMMA-1.)*GAMMA
        CPP=1.
      SU(I,J)=CPO*TH(I,J)
     2+DN1-DS1-DW1+DE1
        ZAE=(U(I+1,J)+U(I,J))**2+(V(I+1,J)+V(I,J))**2
        IF(I.EQ.NIM1) ZAE=4.*(U(I+1,J)**2+V(I+1,J)**2)
        ZAW=(U(I-1,J)+U(I,J))**2+(V(I-1,J)+V(I,J))**2
        IF(I.EQ.2) ZAE=4.*(U(I-1,J)**2+V(I-1,J)**2)
        ZAN=(U(I,J+1)+U(I,J))**2+(V(I,J+1)+V(I,J))**2
        IF(J.EQ.NJM1) ZAN=4.*(U(I,J+1)**2+V(I,J+1)**2)
        ZAS=(U(I,J-1)+U(I,J))**2+(V(I,J-1)+V(I,J))**2
        IF(J.EQ.2) ZAS=4.*(U(I,J-1)**2+V(I,J-1)**2)
      RSIDUE=(CCE(I,J)*ZAE-CCE(I-1,J)*ZAW
     1+CCN(I,J)*ZAN-CCN(I,J-1)*ZAS)/8.
        SP(I,J)=-CP-RSIDUE/TH(I,J)/SCALE
        IF(ILASER.EQ.0) GO TO 200
      VOL=R(I,J)*COB(I,J)
C       QRA(I,J)=QRA(I,J)*VOL
        SU(I,J)=QINP(I,J)-QRA(I,J)*VOL+SU(I,J)
     1+DISS(I,J)
        TRAD=TRAD+QRA(I,J)*VOL
  200 CONTINUE
  101 CONTINUE
  100 CONTINUE
        RDL=TRAD*6.28
C
      CALL MODT
C
      RESORT=0.0
      DO 300 I=2,NIM1
      DO 301 J=2,NJM1
      AP(I,J)=AN(I,J)+AS(I,J)+AE(I,J)+AW(I,J)-SP(I,J)
        IF(AP(I,J).LE.0.) PRINT *,'AP IN T', I,J,AP(I,J)
        IF(AP(I,J).LE.0.) AP(I,J)=1.E-30
      RESOR=AN(I,J)*TH(I,J+1)+AS(I,J)*TH(I,J-1)+AE(I,J)*TH(I+1,J)
```



```
     1      +AW(I,J)*TH(I-1,J)-AP(I,J)*TH(I,J)+SU(I,J)
      RESORT=RESORT+ABS(RESOR)
C-----UNDER-RELAXATION
      AP(I,J)=AP(I,J)/URFT
      SU(I,J)=SU(I,J)+(1.-URFT)*AP(I,J)*TH(I,J)
  301 CONTINUE
  300 CONTINUE
C
      IF(SD)51,50,50
   51 DO 500 N=1,NSWPT
  500 CALL LISOLH(2,2,NI,NJ,TH)
      GO TO 600
   50 DO 400 N=1,NSWPT
  400 CALL LISOLV(2,2,NI,NJ,TH)
  600 CONTINUE
        DO 183 I=1,NI.
C ??????????????????????????????
        TH(I,1)=TH(I,2)
C        IF(I.GE.15) TH(I,NJ)=31.
C        IF(I.LT.15.AND.I.GE.NVE1) TH(I,NJ)=TH(NVE1,NJM1)
        TH(I,NJ)=TH(NVS,NJ)
C        IF(I.LT.NVS) TH(I,NJ)=TH(I,NJM1)
C       TH(I,NJ)=TH(I,NJM1)
  183   CONTINUE
        PPTL=-.99*PTL
        TTTL=.05*TH(2,2)
        DO 187 I=60,NIM1
        DO 187 J=1,NJ
  187   CONTINUE
        NJ5=NJ-12
        DO 185 I=1,NI
        U(I,NJ)=0.
C       V(I,NJ)=U(I,NJ)/SEW(I,NJ)*YSEW(I,NJ)
        DO 186 J=1,NJ
        IF(P(I,J).LE.PPTL) P(I,J)=PPTL
C       IF(P(I,J).LE.PPTL.AND.I.NE.NI) PRINT *, 'PRESS LOWER LIMIT',I,J
        IF(TH(I,J).LE.TTTL) TH(I,J)=TTTL
C       IF(TH(I,J).LE.TTTL) PRINT *, 'TEMP LOWER LIMIT',I,J
  186   CONTINUE
  185   CONTINUE
      RETURN
      END
      SUBROUTINE CONDIF
C       INCLUDE 'DIMENSION1'
C       INCLUDE 'DIMENSION'
C       IMPLICIT REAL*8 (A-H,O-Z)
        PARAMETER (IT=100,JT=60,LMAX=500)
        CHARACTER*8 PFOR1,PUFOR1,FILIN,FILOUT
        CHARACTER*8 PFOR2,PUFOR2
        CHARACTER*8 PFOR3,PUFOR3
        CHARACTER*8 PFOR4,PUFOR4
      COMMON /FNAME1/PFOR1,PUFOR1,FILIN,FILOUT
      COMMON /FNAME2/PFOR2,PUFOR2,PFOR3,PUFOR3
      COMMON /FNAME3/PP1,PP2,PP3,PP4,MPL,MPL1
      COMMON /FNAME4/PFOR4,PUFOR4
      COMMON /COEFF/Q1P(IT,JT),Q2P(IT,JT),Q3P(IT,JT),COB(IT,JT)
```

```
     1    ,SEW(IT,JT),YSEW(IT,JT),SNS(IT,JT),XSNS(IT,JT)
     2    ,DU(IT,JT),DU1(IT,JT),DV(IT,JT),DV1(IT,JT)
     3    ,AP(IT,JT),AN(IT,JT),AS(IT,JT),AE(IT,JT),AW(IT,JT),SU(IT,JT)
     1    ,SP(IT,JT)
      COMMON /POS/ YPOS(IT,JT),XPOS(IT,JT),R(IT,JT)
      COMMON /VAR/ U(IT,JT),V(IT,JT),P(IT,JT),TM(IT,JT),PP(IT,JT)
     1    ,UDUMMY(IT,JT),VDUMMY(IT,JT)
     2    ,TVIS(IT,JT),TCON(IT,JT),DEN(IT,JT),DISS(IT,JT)
      COMMON
     1    /UVEL/RESORU,NSWPU,URFU,SD
     1    /VVEL/RESORV,NSWPV,URFV
     1    /PCOR/RESORM,NSWPP,URFP,IPREF,JPREF
     1    /TMP/RESORT,NSWPT,URFT
      COMMON/INPUT/NI,NJ,NIM1,NJM1,GREAT,INDCOS,INDSM
     1            ,DATAR,DATAW,IFORM,ILASER,CLASIN,NRAYS
     2            ,FOCUS,IFOCUS,BDIAM,ITRACE,ISUPER
     3            ,ANGI,ANGE,RCI,RCT,RT,RI,XEXIT,XI,RTIOY1
      COMMON/IINPUT/
     4            RTIOX1,RTIOX2,XDENSE,JS1,JS2,IS1,IS2
     5            ,URSUP,URVIS,IDENSE,JDENSE,YENRAT,RTIOY2
     6            ,NCONST,XCONST
     6            ,INITP,INITER,SCALE
      COMMON/COND/CCN(IT,JT),CCE(IT,JT),DDN(IT,JT),DDE(IT,JT)
     1     ,DDN1(IT,JT),DDE1(IT,JT)
      COMMON/LASER/QINP(IT,JT),GRA(IT,JT),TRANS(IT,JT),CAB(IT,JT)
     1     ,TNG(LMAX),ING(LMAX,IT)
     2     ,POWER(LMAX),QRA(IT,JT),TH(IT,JT)
      COMMON/LASER2/HT(3000,4),HMU(400,4),HDEN(400,4)
     1     ,HCCP(400,4),HCAB(400,4),HRA(400,4)
        COMMON /ADD8/ANU(IT,JT),ASU(IT,JT),AEU(IT,JT),AWU(IT,JT)
        COMMON /ADD9/ANV(IT,JT),ASV(IT,JT),AEV(IT,JT),AWV(IT,JT)
        COMMON /ADD10/AAN(IT,JT),AAE(IT,JT),COEF(IT),UTEMP(IT,JT),
     1               VTEMP(IT,JT),DYDX(IT),XP(IT)
        COMMON/EXTRA/HINLET
     1         /EXTRA1/UINLET,TBOUND
     1/MMAIN/MAXIT,JMON,IMON,INDPRI,SOLPAT
     1/ADD5/NITER
     1/ADD6/SORMAX,TRSMT,RDL
        COMMON/PROP/PTL,TTL,GAMMA,RG,WGHT,WGHT1,RATIO
        COMMON/EXTRA/PDUMMY(IT,JT)
        COMMON/PLUS/LROAT,NVS,NVS1,NVE,NVE1
C
C
        ENTRY CONUVT
        DO 692 I=1,NI
        DO 692 J=1,NJ
        UDUMMY(I,J)=U(I,J)*SNS(I,J)-V(I,J)*XSNS(I,J)
        VDUMMY(I,J)=V(I,J)*SEW(I,J)-U(I,J)*YSEW(I,J)
692     CONTINUE
        NJM2=NJM1-1
        NIM2=NIM1-1
      DO 100 I=1,NIM1
      DO 100 J=1,NJM1
      CCN(I,J)=0.25*(DEN(I,J+1)+DEN(I,J))*(VDUMMY(I,J+1)+VDUMMY(I,J))
      IF(J.EQ.1) CCN(I,J)=DEN(I,J)*VDUMMY(I,J)
      IF(J.EQ.NJM1) CCN(I,J)=DEN(I,NJ)*VDUMMY(I,NJ)
```



```
      CCE(I,J)=0.25*(DEN(I+1,J)+DEN(I,J))*(UDUMMY(I,J)+UDUMMY(I+1,J))
      IF(I.EQ.1) CCE(I,J)=DEN(I,J)*UDUMMY(I,J)
      IF(I.EQ.NIM1) CCE(I,J)=DEN(NI,J)*UDUMMY(NI,J)
C
C ******** MOD. ADD DAMPING *********************************
C
c       AND.J.NE.NJM2)
C       AND.I.NE.NIM2)
        IF(J.NE.1.AND.J.NE.NJM1)
     1CCN(I,J)=CCN(I,J)+(P(I,J+2)-3.*P(I,J+1)+3.*P(I,J)-P(I,J-1))*
     1 ((DV(I,J)*SEW(I,J)-DU1(I,J)*YSEW(I,J))
     2+(DV(I,J+1)*SEW(I,J+1)-DU1(I,J+1)*YSEW(I,J+1)))/2./8.
     3*(DEN(I,J+1)+DEN(I,J))*URVIS/URFV
        IF(I.NE.1.AND.I.NE.NIM1)
     1CCE(I,J)=CCE(I,J)+(P(I+2,J)-3.*P(I+1,J)+3.*P(I,J)-P(I-1,J))*
     1 ((DU(I,J)*SNS(I,J)-DV1(I,J)*XSNS(I,J))
     2+(DU(I+1,J)*SNS(I+1,J)-DV1(I+1,J)*XSNS(I+1,J)))/2./8.
     3*(DEN(I+1,J)+DEN(I,J))*URVIS/URFU
C
C************** AXIS SYMMETRIC ****************************************
C
      RN=.5*(R(I,J)+R(I,J+1))
      RE=.5*(R(I,J)+R(I+1,J))
      IF(I.EQ.1) RE=R(I,J)
      IF(I.EQ.NIM1) RE=R(NI,J)
      IF(J.EQ.1) RN=R(I,J)
      IF(J.EQ.NJM1) RN=R(I,NJ)
        CCN(I,J)=CCN(I,J)*RN
        CCE(I,J)=CCE(I,J)*RE
100     CONTINUE
        RETURN
C
C
        ENTRY DIFUV
        DO 105 I=1,NIM1
        DO 105 J=1,NJM1
C
C******** CALCULATE DIFFUSION COEFFICIENTS **********************
      TVISN=0.5*(TVIS(I,J)+TVIS(I,J+1))
      TVISE=0.5*(TVIS(I+1,J)+TVIS(I,J))
      IF(I.EQ.1) TVISE=TVIS(I,J)
      IF(I.EQ.NIM1) TVISE=TVIS(NI,J)
      IF(J.EQ.1) TVISN=TVIS(I,J)
      IF(J.EQ.NJM1) TVISN=TVIS(I,NJ)
      DDN(I,J)=TVISN/(COB(I,J)+COB(I,J+1))*
     1(Q3P(I,J)+Q3P(I,J+1))
      DDN1(I,J)=-1.*TVISN/(COB(I,J)+COB(I,J+1))*
     1(Q2P(I,J)+Q2P(I,J+1))
      DDE(I,J)=TVISE/(COB(I,J)+COB(I+1,J))*
     1(Q1P(I+1,J)+Q1P(I,J))
      DDE1(I,J)=-1.*TVISE/(COB(I,J)+COB(I+1,J))*
     1(Q2P(I+1,J)+Q2P(I,J))
        IF(J.EQ.1)    DDN(I,J)=TVISN/COB(I,J)*Q3P(I,J)
        IF(J.EQ.NJM1) DDN(I,J)=TVISN/COB(I,NJ)*Q3P(I,NJ)
        IF(J.EQ.1)    DDN1(I,J)=-1.*TVISN/COB(I,J)*Q2P(I,J)
        IF(J.EQ.NJM1) DDN1(I,J)=-1.*TVISN/COB(I,NJ)*Q2P(I,NJ)
```

```
        IF(I.EQ.1)     DDE(I,J)=TVISE/COB(I,J)*Q1P(I,J)
        IF(I.EQ.NIM1) DDE(I,J)=TVISE/COB(NI,J)*Q1P(NI,J)
        IF(I.EQ.1)     DDE1(I,J)=-1.*TVISE/COB(I,J)*Q2P(I,J)
        IF(I.EQ.NIM1) DDE1(I,J)=-1.*TVISE/COB(NI,J)*Q2P(NI,J)
C
C********** AXIS SYMMETRIC ****************************************
C
      RN=.5*(R(I,J)+R(I,J+1))
      RE=.5*(R(I,J)+R(I+1,J))
      IF(I.EQ.1) RE=R(I,J)
      IF(I.EQ.NIM1) RE=R(NI,J)
      IF(J.EQ.1) RN=R(I,J)
      IF(J.EQ.NJM1) RN=R(I,NJ)
        DDN(I,J)=DDN(I,J)*RN
        DDE(I,J)=DDE(I,J)*RE
        DDN1(I,J)=DDN1(I,J)*RN
        DDE1(I,J)=DDE1(I,J)*RE
105     CONTINUE
        RETURN
C
        ENTRY DIFT
        DO 109 I=1,NIM1
        DO 109 J=1,NJM1
C
C******** CALCULATE DIFFUSION COEFFICIENTS ***********************
      TVISN=0.5*(TRANS(I,J)+TRANS(I,J+1))
      TVISE=0.5*(TRANS(I+1,J)+TRANS(I,J))
      IF(I.EQ.1) TVISE=TRANS(I,J)
      IF(I.EQ.NIM1) TVISE=TRANS(NI,J)
      IF(J.EQ.1) TVISN=TRANS(I,J)
      IF(J.EQ.NJM1) TVISN=TRANS(I,NJ)
      DDN(I,J)=TVISN/(COB(I,J)+COB(I,J+1))*
     1(Q3P(I,J)+Q3P(I,J+1))
      DDN1(I,J)=-1.*TVISN/(COB(I,J)+COB(I,J+1))*
     1(Q2P(I,J)+Q2P(I,J+1))
      DDE(I,J)=TVISE/(COB(I,J)+COB(I+1,J))*
     1(Q1P(I+1,J)+Q1P(I,J))
      DDE1(I,J)=-1.*TVISE/(COB(I,J)+COB(I+1,J))*
     1(Q2P(I+1,J)+Q2P(I,J))
        IF(J.EQ.1)     DDN(I,J)=TVISN/COB(I,J)*Q3P(I,J)
        IF(J.EQ.NJM1) DDN(I,J)=TVISN/COB(I,NJ)*Q3P(I,NJ)
        IF(J.EQ.1)     DDN1(I,J)=-1.*TVISN/COB(I,J)*Q2P(I,J)
        IF(J.EQ.NJM1) DDN1(I,J)=-1.*TVISN/COB(I,NJ)*Q2P(I,NJ)
        IF(I.EQ.1)     DDE(I,J)=TVISE/COB(I,J)*Q1P(I,J)
        IF(I.EQ.NIM1) DDE(I,J)=TVISE/COB(NI,J)*Q1P(NI,J)
        IF(I.EQ.1)     DDE1(I,J)=-1.*TVISE/COB(I,J)*Q2P(I,J)
        IF(I.EQ.NIM1) DDE1(I,J)=-1.*TVISE/COB(NI,J)*Q2P(NI,J)
C
C********** AXIS SYMMETRIC ****************************************
C
      RN=.5*(R(I,J)+R(I,J+1))
      RE=.5*(R(I,J)+R(I+1,J))
      IF(I.EQ.1) RE=R(I,J)
      IF(I.EQ.NIM1) RE=R(NI,J)
      IF(J.EQ.1) RN=R(I,J)
      IF(J.EQ.NJM1) RN=R(I,NJ)
```



```
        DDN(I,J)=DDN(I,J)*RN
        DDE(I,J)=DDE(I,J)*RE
        DDN1(I,J)=DDN1(I,J)*RN
        DDE1(I,J)=DDE1(I,J)*RE
109     CONTINUE
        RETURN
        END
      SUBROUTINE GEOM
C
C     ******************************************************************
C
C     THIS SUBROUTINE CALCULATES THE WALL RADIUS AND SLOPE
C
C     ******************************************************************
C
C       INCLUDE 'DIMENSION1'
C       INCLUDE 'DIMENSION'
C       IMPLICIT REAL*8 (A-H,O-Z)
        PARAMETER (IT=100,JT=60,LMAX=500)
        CHARACTER*8 PFOR1,PUFOR1,FILIN,FILOUT
        CHARACTER*8 PFOR2,PUFOR2
        CHARACTER*8 PFOR3,PUFOR3
        CHARACTER*8 PFOR4,PUFOR4
       COMMON /FNAME1/PFOR1,PUFOR1,FILIN,FILOUT
       COMMON /FNAME2/PFOR2,PUFOR2,PFOR3,PUFOR3
       COMMON /FNAME3/PP1,PP2,PP3,PP4,MPL,MPL1
       COMMON /FNAME4/PFOR4,PUFOR4
       COMMON /COEFF/Q1P(IT,JT),Q2P(IT,JT),Q3P(IT,JT),COB(IT,JT)
      1   ,SEW(IT,JT),YSEW(IT,JT),SNS(IT,JT),XSNS(IT,JT)
      2   ,DU(IT,JT),DU1(IT,JT),DV(IT,JT),DV1(IT,JT)
      3   ,AP(IT,JT),AN(IT,JT),AS(IT,JT),AE(IT,JT),AW(IT,JT),SU(IT,JT)
      1   ,SP(IT,JT)
       COMMON /POS/ YPOS(IT,JT),XPOS(IT,JT),R(IT,JT)
       COMMON /VAR/ U(IT,JT),V(IT,JT),P(IT,JT),TM(IT,JT),PP(IT,JT)
      1   ,UDUMMY(IT,JT),VDUMMY(IT,JT)
      2   ,TVIS(IT,JT),TCON(IT,JT),DEN(IT,JT),DISS(IT,JT)
       COMMON
      1   /UVEL/RESORU,NSWPU,URFU,SD
      1   /VVEL/RESORV,NSWPV,URFV
      1   /PCOR/RESORM,NSWPP,URFP,IPREF,JPREF
      1   /TMP/RESORT,NSWPT,URFT
       COMMON/INPUT/NI,NJ,NIM1,NJM1,GREAT,INDCOS,INDSM
      1            ,DATAR,DATAW,IFORM,ILASER,CLASIN,NRAYS
      2            ,FOCUS,IFOCUS,BDIAM,ITRACE,ISUPER
      3            ,ANGI,ANGE,RCI,RCT,RT,RI,XEXIT,XI,RTIOY1
       COMMON/IINPUT/
      4            RTIOX1,RTIOX2,XDENSE,JS1,JS2,IS1,IS2
      5            ,URSUP,URVIS,IDENSE,JDENSE,YENRAT,RTIOY2
      6            ,NCONST,XCONST
      6            ,INITP,INITER,SCALE
       COMMON/COND/CCN(IT,JT),CCE(IT,JT),DDN(IT,JT),DDE(IT,JT)
      1    ,DDN1(IT,JT),DDE1(IT,JT)
       COMMON/LASER/QINP(IT,JT),GRA(IT,JT),TRANS(IT,JT),CAB(IT,JT)
      1    ,TNG(LMAX),ING(LMAX,IT)
      2    ,POWER(LMAX),QRA(IT,JT),TH(IT,JT)
       COMMON/LASER2/HT(3000,4),HMU(400,4),HDEN(400,4)
```

```
     1    ,HCCP(400,4),HCAB(400,4),HRA(400,4)
          COMMON /ADD8/ANU(IT,JT),ASU(IT,JT),AEU(IT,JT),AWU(IT,JT)
          COMMON /ADD9/ANV(IT,JT),ASV(IT,JT),AEV(IT,JT),AWV(IT,JT)
          COMMON /ADD10/AAN(IT,JT),AAE(IT,JT),COEF(IT),UTEMP(IT,JT),
     1                 VTEMP(IT,JT),DYDX(IT),XP(IT)
          COMMON/EXTRA/HINLET
     1         /EXTRA1/UINLET,TBOUND
     1/MMAIN/MAXIT,JMON,IMON,INDPRI,SOLPAT
     1/ADD5/NITER
     1/ADD6/SORMAX,TRSMT,RDL
          COMMON/PROP/PTL,TTL,GAMMA,RG,WGHT,WGHT1,RATIO
          COMMON/EXTRA/PDUMMY(IT,JT)
          COMMON/PLUS/LROAT,NVS,NVS1,NVE,NVE1
C
C ***************** CALCULATE X-COORDINATE ***************************
C
          NIM2=NIM1-1
          NIM3=NIM1-2
          NJM2=NJM1-1
          NJM3=NJM1-2
          NCOST1=NCONST-1
C
          XP(IDENSE)=XDENSE
          AAA=XDENSE*(1.-RTIOX1)/(1.-RTIOX1**(IDENSE-2)*1.5+.5*
     1RTIOX1**(IDENSE-3))
          IDEN1=IDENSE-1
        DO 101 I=1,IDEN1
          III=IDENSE-I+1
          XP(IDENSE-I)=XP(III)-AAA*RTIOX1**(I-1)
101     CONTINUE
          AAA=(XCONST-XDENSE)*(1.-RTIOX2)/(1.-RTIOX2**
     1(NCONST-IDENSE))
        DO 102 I=IDENSE,NCOST1
          XP(I+1)=XP(I)+AAA*RTIOX2**(I-IDENSE)
102     CONTINUE
          XP(1)=XP(2)-.5*(XP(3)-XP(2))
C          DIST=(XEXIT-XP(NCONST))/(NI-NCONST)
          DIST=XP(NCONST)-XP(NCOST1)
          DO 201 I=NCONST,NIM1
C201       XP(I+1)=XP(NCONST)+(I-NCONST+1)*DIST
201       XP(I+1)=XP(I)+DIST*XEXIT**(I-NCOST1)
          XP(NIM1)=XP(NIM2)+1.*(XP(NIM2)-XP(NIM3))
          XP(NI)=XP(NIM1)+.5*(XP(NIM2)-XP(NIM3))
C
C ***************** END OF X COORDINATE CALCULATE*********************
C
C ***************** BEGIN OF Y COORDINATE CALCULATION ****************
C
          BTEMP=0.
        IF (RCI.EQ.BTEMP.OR.RCT.EQ.BTEMP) GO TO 200
        ANI=ANGI*3.141593/180.0
        ANE=ANGE*3.141593/180.0
        XTAN=XI+RCI*SIN(ANI)
        RTAN=RI+RCI*(COS(ANI)-1.0)
        RT1=RT-RCT*(COS(ANI)-1.0)
        XT1=XTAN+(RTAN-RT1)/TAN(ANI)
```



```
        IF (XT1.GE.XTAN) GO TO 40
        XT1=XTAN
        RT1=RTAN
   40 XT=XT1+RCT*SIN(ANI)
        XT2=XT+RCT*SIN(ANE)
        RT2=RT+RCT*(1.0-COS(ANE))
        RE=RT2+(XE-XT2)*TAN(ANE)
        LROAT=1
        XTII=XT
        XT=XCONST
        XI=XI+XCONST-XTII
        XTAN=XTAN+XCONST-XTII
        XT1=XT1+XCONST-XTII
        XT2=XT2+XCONST-XTII
        DO 110 L=1,NI
        IF (XP(L).LE.XI) GO TO 41
        IF (XP(L).LE.XTAN) GO TO 50
        IF (XP(L).GT.XTAN.AND.XP(L).LE.XT1) GO TO 60
        IF (XP(L).GT.XT1.AND.XP(L).LE.XT) GO TO 70
        IF (XP(L).GT.XT.AND.XP(L).LE.XT2) GO TO 80
        GO TO 90
C
   41 YPOS(L,NJ)=RI
        DYDX(L)=0.
        GO TO 100
   50 YPOS(L,NJ)=RI+RCI*(COS(ASIN((XP(L)-XI)/RCI))-1.0)
        DYDX(L)=-(XP(L)-XI)/(YPOS(L,NJ)-RI+RCI)
        GO TO 100
C
   60 YPOS(L,NJ)=RT1+(XT1-XP(L))*TAN(ANI)
        DYDX(L)=-TAN(ANI)
        GO TO 100
C
   70 YPOS(L,NJ)=RT+RCT*(1.0-COS(ASIN((XT-XP(L))/RCT)))
        DYDX(L)=-(XT-XP(L))/(RCT+RT-YPOS(L,NJ))
        GO TO 100
C
   80 YPOS(L,NJ)=RT+RCT*(1.0-COS(ASIN((XP(L)-XT)/RCT)))
        DYDX(L)=-(XT-XP(L))/(RCT+RT-YPOS(L,NJ))
        GO TO 100
C
   90 YPOS(L,NJ)=RT2+(XP(L)-XT2)*TAN(ANE)
        DYDX(L)=TAN(ANE)
C
  100 IF (L.EQ.1) GO TO 110
        IF (YPOS(L,NJ).LT.YPOS(LROAT,NJ)) LROAT=L
  110 CONTINUE
C
C ****************STRETCH OF THE Y-COORDINATE ********************
C
        DO 301 I=66,NIM1
C       XP(I)=XP(I-1)+0.000024
C       YPOS(I,NJ)=YPOS(I-1,NJ)+0.000006
301     CONTINUE
C       XP(NI)=XP(NIM1)+0.000008
C       YPOS(NI,NJ)=YPOS(NIM1,NJ)+0.000002
```

```
        DO 2 I=1,NI
        YPOS(I,1)=0.
        YPOS(I,JDENSE)=YPOS(I,NJ)*YENRAT
        YDENSE=YPOS(I,JDENSE)
        AAA=YDENSE*(1.-RTIOY1)/(1.-RTIOY1**(JDENSE-2)*1.5+0.5*
     1RTIOY1**(JDENSE-3))
        JDEN1=JDENSE-1
      DO 501 J=1,JDEN1
        III=JDENSE-J+1
        YPOS(I,JDENSE-J)=YPOS(I,III)-AAA*RTIOY1**(J-1)
501    CONTINUE
        YPOS(I,1)=0.
        AAA=(YPOS(I,NJ)-YDENSE)*(1.-RTIOY2)/(1.-RTIOY2**
     1(NJ-JDENSE-1)*1.5+.5*RTIOY2**(NJ-JDENSE-2))
        NJM2=NJM1-1
      DO 502 J=JDENSE,NJM2
        YPOS(I,J+1)=YPOS(I,J)+AAA*RTIOY2**(J-JDENSE)
502    CONTINUE
        DO 2 J=1,NJ
        XPOS(I,J)=XP(I)
2       CONTINUE
C
C ***************** END OF Y COORDINATE CALCULATION *****************
C
C ***************** CALCULATE THE RELATIONSHIP BETWEEN NJ AND NJM1
C *************** GRID POINTS ***************************************
C
        RHROAT=RT
        XHROAT=XT
        COEF(1)=1.
        COEF(NI)=1.
        BTEMP=1.E-15
        DO 900 I=2,NIM1
        AAA=YPOS(I+1,NJ)-YPOS(I-1,NJ)
        IF(ABS(AAA).LE.BTEMP) AAA=1.D-20
        IF(ABS(AAA).LE.BTEMP) COEF(I)=1.
        IF(ABS(AAA).LE.BTEMP) GO TO 900
        BC=-1.*(XPOS(I+1,NJ)-XPOS(I-1,NJ))/AAA
        IF(ABS(BC).LE.BTEMP) BC=1.D-20
        BC=-1./BC
        CC=-1.*XPOS(I,NJ)-BC*YPOS(I,NJ)
        AAA=YPOS(I+1,NJM1)-YPOS(I,NJM1)
        IF(ABS(AAA).LE.BTEMP) AAA=1.D-20
        BC1=-1.*(XPOS(I+1,NJM1)-XPOS(I,NJM1))/AAA
        CC1=-1.*XPOS(I,NJM1)-BC1*YPOS(I,NJM1)
        BB2=BC-BC1
        IF(ABS(BB2).LE.BTEMP) BB2=1.D-20
        PXP=(BC1*CC-BC*CC1)/BB2
        IF(PXP.GE.XPOS(I,NJM1)) THEN
        COEF(I)=(XPOS(I+1,NJM1)-PXP)/(XPOS(I+1,NJM1)-XPOS(I,NJM1))
        BTEMP=0.
        IF(COEF(I).LT.BTEMP) COEF(I)=1.
        IF(COEF(I).LT.BTEMP) PRINT *, 'ERROR IN COEF 111'
        ELSE
        AAA=YPOS(I,NJM1)-YPOS(I-1,NJM1)
                BTEMP=1.E-15
```



```
        IF(ABS(AAA).LE.BTEMP) AAA=1.D-20
        BC1=-1.*(XPOS(I,NJM1)-XPOS(I-1,NJM1))/AAA
        CC1=-1.*XPOS(I,NJM1)-BC1*YPOS(I,NJM1)
        BB2=BC-BC1
        IF(ABS(BB2).LE.BTEMP) BB2=1.D-20
        PXP=(BC1*CC-BC*CC1)/BB2
        IF(PXP.LE.XPOS(I,NJM1)) THEN
        COEF(I)=-1.*(XPOS(I-1,NJM1)-PXP)/(XPOS(I-1,NJM1)-XPOS(I,NJM1))
        BTEMP=0.
        IF(COEF(I).GT.BTEMP) PRINT *, 'ERROR IN COEF 222'
        ELSE
        PRINT *,'ERROR IN COEF 333'
        END IF
        END IF
C        PRINT *,'COEF',I,COEF(I)
900     CONTINUE
        DO 901 I=1,NI
        IF(COEF(I).GE.1.) COEF(I)=1.
        IF(COEF(I).LE.-1.) COEF(I)=-1.
901     CONTINUE
        WRITE (6,280) XI,RI,RT,XE,RCI,RCT,ANGI,ANGE,XT,RE
        DO 230 I=1,NI
C        DO 230 J=1,NJ
        WRITE(6,380) I,XP(I),YPOS(I,NJ),DYDX(I)
230     CONTINUE
      RETURN
200     PRINT *, 'ERROR IN ONEDIM SUB'
        STOP
C
C     FORMAT STATEMENTS
C
  280 FORMAT (1H0,20X,'A CIRCULAR-ARC, CONICAL NOZZLE HAS BEEN SPECIFI
     1ED BY XI=',F8.4,' (M), RI=',F8.4,' (M)'/,21X,'RT=',F8.4,' (
     2M), XE=',F8.4,' (M), RCI=',F8.4,' (M), RCT=',F8.4,' (M), ANG
     3I=',F6.2,' (DEG)'/,21X,'AND ANGE=',F6.2,' (DEG). THE COMPUTED V
     4ALUES ARE XT=',F8.4,' (M) AND RE=',F8.4,' (M).')
380     FORMAT(1X,'I= ',I5,' X POS= ',F13.6,' Y WALL= ',F13.6,
     1' SLOPE= ',F13.6)
      END
        SUBROUTINE HEAT
C       INCLUDE 'DIMENSION1'
C       INCLUDE 'DIMENSION'
C       IMPLICIT REAL*8 (A-H,O-Z)
        PARAMETER (IT=100,JT=60,LMAX=500)
        CHARACTER*8 PFOR1,PUFOR1,FILIN,FILOUT
        CHARACTER*8 PFOR2,PUFOR2
        CHARACTER*8 PFOR3,PUFOR3
        CHARACTER*8 PFOR4,PUFOR4
      COMMON /FNAME1/PFOR1,PUFOR1,FILIN,FILOUT
      COMMON /FNAME2/PFOR2,PUFOR2,PFOR3,PUFOR3
      COMMON /FNAME3/PP1,PP2,PP3,PP4,MPL,MPL1
      COMMON /FNAME4/PFOR4,PUFOR4
      COMMON /COEFF/Q1P(IT,JT),Q2P(IT,JT),Q3P(IT,JT),COB(IT,JT)
     1   ,SEW(IT,JT),YSEW(IT,JT),SNS(IT,JT),XSNS(IT,JT)
     2   ,DU(IT,JT),DU1(IT,JT),DV(IT,JT),DV1(IT,JT)
     3   ,AP(IT,JT),AN(IT,JT),AS(IT,JT),AE(IT,JT),AW(IT,JT),SU(IT,JT)
```

```
     1   ,SP(IT,JT)
      COMMON /POS/ YPOS(IT,JT),XPOS(IT,JT),R(IT,JT)
      COMMON /VAR/ U(IT,JT),V(IT,JT),P(IT,JT),TM(IT,JT),PP(IT,JT)
     1   ,UDUMMY(IT,JT),VDUMMY(IT,JT)
     2   ,TVIS(IT,JT),TCON(IT,JT),DEN(IT,JT),DISS(IT,JT)
      COMMON
     1   /UVEL/RESORU,NSWPU,URFU,SD
     1   /VVEL/RESORV,NSWPV,URFV
     1   /PCOR/RESORM,NSWPP,URFP,IPREF,JPREF
     1   /TMP/RESORT,NSWPT,URFT
      COMMON/INPUT/NI,NJ,NIM1,NJM1,GREAT,INDCOS,INDSM
     1            ,DATAR,DATAW,IFORM,ILASER,CLASIN,NRAYS
     2            ,FOCUS,IFOCUS,BDIAM,ITRACE,ISUPER
     3            ,ANGI,ANGE,RCI,RCT,RT,RI,XEXIT,XI,RTIOY1
      COMMON/IINPUT/
     4            RTIOX1,RTIOX2,XDENSE,JS1,JS2,IS1,IS2
     5            ,URSUP,URVIS,IDENSE,JDENSE,YENRAT,RTIOY2
     6            ,NCONST,XCONST
     6            ,INITP,INITER,SCALE
      COMMON/COND/CCN(IT,JT),CCE(IT,JT),DDN(IT,JT),DDE(IT,JT)
     1    ,DDN1(IT,JT),DDE1(IT,JT)
      COMMON/LASER/QINP(IT,JT),GRA(IT,JT),TRANS(IT,JT),CAB(IT,JT)
     1    ,TNG(LMAX),ING(LMAX,IT)
     2    ,POWER(LMAX),QRA(IT,JT),TH(IT,JT)
      COMMON/LASER2/HT(3000,4),HMU(400,4),HDEN(400,4)
     1    ,HCCP(400,4),HCAB(400,4),HRA(400,4)
         COMMON /ADD8/ANU(IT,JT),ASU(IT,JT),AEU(IT,JT),AWU(IT,JT)
         COMMON /ADD9/ANV(IT,JT),ASV(IT,JT),AEV(IT,JT),AWV(IT,JT)
         COMMON /ADD10/AAN(IT,JT),AAE(IT,JT),COEF(IT),UTEMP(IT,JT),
     1               VTEMP(IT,JT),DYDX(IT),XP(IT)
         COMMON/EXTRA/HINLET
     1        /EXTRA1/UINLET,TBOUND
     1/MMAIN/MAXIT,JMON,IMON,INDPRI,SOLPAT
     1/ADD5/NITER
     1/ADD6/SORMAX,TRSMT,RDL
         COMMON/PROP/PTL,TTL,GAMMA,RG,WGHT,WGHT1,RATIO
         COMMON/EXTRA/PDUMMY(IT,JT)
         COMMON/PLUS/LROAT,NVS,NVS1,NVE,NVE1
         DIMENSION TR(IT),TW(IT),TGRAD(IT)
C        QLENSE,QOUT,TGRAD,CP
         DO 999 I=1,NI
         DO 999 J=1,NJ
         TCON(I,J)=QRA(I,J)*R(I,J)*COB(I,J)*6.28
999      CONTINUE
         OPEN(UNIT=20,FILE='RAD.ORG',FORM='UNFORMAT')
         WRITE(20) ((XPOS(I,J),I=1,NI),J=1,NJ)
     1           ,((YPOS(I,J),I=1,NI),J=1,NJ)
     1           ,((TCON(I,J),I=1,NI),J=1,NJ)
         CLOSE(UNIT=20)
         NJM2=NJM1-1
         NJM3=NJM1-2
         CP=1.4E4
         QLENSE=0.
         QOUT=0.
         QIN=0.
         LROAT1=LROAT-1
```



```
         LROAT2=LROAT-2
         PRINT *,LROAT,LROAT1
         AI=YPOS(1,NJ)**2
         AO=YPOS(LROAT,NJ)**2
         DO 1 I=2,LROAT1
         DI=(XPOS(I,1)-XPOS(1,1))**2
         DO=(XPOS(I,1)-XPOS(LROAT,1))**2
         DO 1 J=2,NJM1
         B=YPOS(I,J)**2
         FI=(1.-(B+DI-AI)/(B**2+2.*(DI-AI)*B+(DI+AI)**2)**.5)/4.
         FO=(1.-(B+DO-AO)/(B**2+2.*(DO-AO)*B+(DO+AO)**2)**.5)/4.
         QLENSE=QLENSE+FI*QRA(I,J)*R(I,J)*COB(I,J)*6.28
         QOUT=QOUT+FO*QRA(I,J)*R(I,J)*COB(I,J)*6.28
         QIN=QIN+QRA(I,J)*R(I,J)*COB(I,J)*6.28
1        CONTINUE
C ********************RDL NEEDED TO BE CHANGED **************
         HWALL=RDL-QLENSE-QOUT
         HWALL=QIN-QLENSE-QOUT
C        CALCULATE WALL AREA
         AREA=0.
         DO 2 I=NVE1,LROAT
         AREA=AREA+6.28*R(I,NJ)*((R(I+1,NJ)-R I-1,NJ))**2+
     1   (XPOS(I+1,NJ)-XPOS(I-1,NJ))**2.)**.5/2.
2        CONTINUE
C        HEAT DENSITY
         HATRAD=HWALL/AREA*1.E6
         DO 3 I=NVE1,NIM1
         AA1=(-YPOS(I,NJM1)-YPOS(I,NJM2))
     1/(YPOS(I,NJM1)*YPOS(I,NJM2))
         AA2=-YPOS(I,NJM2)/(YPOS(I,NJM1)
     1*(YPOS(I,NJM1)-YPOS(I,NJM2)))
         AA3=-YPOS(I,NJM1)/(YPOS(I,NJM2)
     1*(YPOS(I,NJM2)-YPOS(I,NJM1)))
         TTCON=(AA1*TM(I,NJ)+AA2*TM(I,NJM1)+AA3*TM(I,NJM2))
     1   *TRANS(I,NJ)*CP
         IF(I.LE.LROAT) TGRAD(I)=-TTCON+HATRAD
         IF(I.GE.LROAT) TGRAD(I)=-TTCON
3        CONTINUE
         AMASS6=0.
         DO 4 J=2,NJM1
         AREA=DEN(LROAT,J)*R(LROAT,J)*SNS(LROAT,J)
         AMASS6=AMASS6+AREA*U(LROAT,J)
4        CONTINUE
         AMASS6=AMASS6*6.28
         TR(NI)=1.
         TW(NI)=1.
         DO 5 I=NVE1,NIM1
         AREA=6.28*R(I,NJ)*((R(I+1,NJ)-R(I-1,NJ))**2+
     1   (XPOS(I+1,NJ)-XPOS(I-1,NJ))**2.)**.5/2.
         ABC=TGRAD(NI-I+NVE)
     1/AMASS6/CP*AREA/100.
C        PRINT *, 'ABC',ABC
         TR(NI-I+NVE)=TR(NI-I+NVE+1)+ABC
         TW(NI-I+NVE)=TGRAD(NI-I+NVE)/100./100.+TR(NI-I+NVE)
5        CONTINUE
         PRINT *, 'RADIATION POWER ON LENSE (MW)= ', QLENSE
```

```
      PRINT *, 'RADIATION THROUGH THROAT (MW)= ', QOUT
      PRINT *, 'RADIATION ON THE WALL (MW)= ', HWALL
      PRINT *, 'AVERGED RADIATION FLUX ON THE WALL (W/M**2)= '
     1  ,HATRAD
      PRINT *,'I HEAT FLUX(W/M**2)  FLUID TEMP(100K) WALL TEMP(100K)'
      DO 6 I=1,NI
      PRINT *,I,TGRAD(I),TR(I),TW(I)
6     CONTINUE
      RETURN
      END
      SUBROUTINE LENSE
      PARAMETER (IT=100,JT=60,LMAX=500)
      CHARACTER*8 PFOR1,PUFOR1,FILIN,FILOUT
      CHARACTER*8 PFOR2,PUFOR2
      CHARACTER*8 PFOR3,PUFOR3
      CHARACTER*8 PFOR4,PUFOR4
      COMMON /FNAME1/PFOR1,PUFOR1,FILIN,FILOUT
      COMMON /FNAME2/PFOR2,PUFOR2,PFOR3,PUFOR3
      COMMON /FNAME3/PP1,PP2,PP3,PP4,MPL,MPL1
      COMMON /FNAME4/PFOR4,PUFOR4
      COMMON /COEFF/Q1P(IT,JT),Q2P(IT,JT),Q3P(IT,JT),COB(IT,JT)
     1   ,SEW(IT,JT),YSEW(IT,JT),SNS(IT,JT),XSNS(IT,JT)
     2   ,AU(IT,JT),DU1(IT,JT),DV(IT,JT),DV1(IT,JT)
     3   ,AP(IT,JT),AN(IT,JT),AS(IT,JT),AE(IT,JT),AW(IT,JT),SU(IT,JT)
     1   ,SP(IT,JT)
      COMMON /POS/ YPOS(IT,JT),XPOS(IT,JT),R(IT,JT)
      COMMON /VAR/ U(IT,JT),V(IT,JT),P(IT,JT),TM(IT,JT),PP(IT,JT)
     1   ,UDUMMY(IT,JT),VDUMMY(IT,JT)
     2   ,TVIS(IT,JT),TCON(IT,JT),DEN(IT,JT),DISS(IT,JT)
      COMMON
     1   /UVEL/RESORU,NSWPU,URFU,SD
     1   /VVEL/RESORV,NSWPV,URFV
     1   /PCOR/RESORM,NSWPP,URFP,IPREF,JPREF
     1   /TMP/RESORT,NSWPT,URFT
      COMMON/INPUT/NI,NJ,NIM1,NJM1,GREAT,INDCOS,INDSM
     1            ,DATAR,DATAW,IFORM,ILASER,CLASIN,NRAYS
     2            ,FOCUS,IFOCUS,BDIAM,ITRACE,ISUPER
     3            ,ANGI,ANGE,RCI,RCT,RT,RI,XEXIT,XI,RTIOY1
      COMMON/IINPUT/
     4            RTIOX1,RTIOX2,XDENSE,JS1,JS2,IS1,IS2
     5            ,URSUP,URVIS,IDENSE,JDENSE,YENRAT,RTIOY2
     6            ,NCONST,XCONST
     6            ,INITP,INITER,SCALE
      COMMON/COND/CCN(IT,JT),CCE(IT,JT),DDN(IT,JT),DDE(IT,JT)
     1    ,DDN1(IT,JT),DDE1(IT,JT)
      COMMON/LASER/QINP(IT,JT),GRA(IT,JT),TRANS(IT,JT),CAB(IT,JT)
     1    ,TNG(LMAX),ING(LMAX,IT)
     2    ,POWER(LMAX),QRA(IT,JT),TH(IT,JT)
      COMMON/LASER2/HT(3000,4),HMU(400,4),HDEN(400,4)
     1    ,HCCP(400,4),HCAB(400,4),HRA(400,4)
      COMMON /ADD8/ANU(IT,JT),ASU(IT,JT),AEU(IT,JT),AWU(IT,JT)
      COMMON /ADD9/ANV(IT,JT),ASV(IT,JT),AEV(IT,JT),AWV(IT,JT)
      COMMON /ADD10/AAN(IT,JT),AAE(IT,JT),COEF(IT),UTEMP(IT,JT),
     1             VTEMP(IT,JT),DYDX(IT),XP(IT)
      COMMON/EXTRA/HINLET
     1       /EXTRA1/UINLET,TBOUND
```



```
      1/MMAIN/MAXIT,JMON,IMON,INDPRI,SOLPAT
      1/ADD5/NITER
      1/ADD6/SORMAX,TRSMT,RDL
        COMMON/PROP/PTL,TTL,GAMMA,RG,WGHT,WGHT1,RATIO
        COMMON/EXTRA/PDUMMY(IT,JT)
        COMMON/PLUS/LROAT,NVS,NVS1,NVE,NVE1
C       INCLUDE 'DIMENSION1'
C       INCLUDE 'DIMENSION'
        TEMP=0.
        R1=.0*BDIAM
        R2=BDIAM
        RLAS=R2/2.
        DRN=(R2-R1)/NRAYS
        RO=1.403*25.4*2.5/1000.
        UUU=2.403
        TP=30./1000.
        DO 333 N=1,NRAYS
        RR=R1+(N-1)*DRN
        XXX=(RR-R1)/(R2-R1)
        STH=RR/RO
        STHP=STH/UUU
        TH2=ASIN(STH)-ASIN(STHP)
        Q=RO-SQRT(RO*RO-RR*RR)
        TT=TP-Q
        R3=RR-TT*TAN(TH2)
        TH3=ASIN(UUU*SIN(TH2))
        TTH3=TAN(TH3)
        DO 332 I=1,NI
        ZO=XPOS(I,1)
        RIO=R3-ZO*TTH3+.000
        DO 40 J=2,NJM1
        AA=.5*(YPOS(I,J)+YPOS(I,J+1))
        IF(ABS(RIO).LE.AA) GO TO 41
        ING(N,I)=NJ
        INI=I
C       IF(J.EQ.NJM1) GO TO 334
40      CONTINUE
        GO TO 334
41      ING(N,I)=J
332     CONTINUE
        GO TO 336
334     DO 335 I=INI,NI
        ING(N,I)=NJ
335     CONTINUE
336     CONTINUE
        TNG(N)=1./COS(TH3)
        PTEMP=1.-EXP(-(RR+.5*DRN)**2/RLAS**2)
        POWER(N)=PTEMP-PTEMP1
        PTEMP1=PTEMP
        TEMP=POWER(N)+TEMP
333     CONTINUE
        CONST=1./TEMP
        DO 103 N=1,NRAYS
        POWER(N)=CLASIN*POWER(N)/6.28*CONST
        IF(ITRACE.EQ.1 )
     1  WRITE(6,987)N,POWER(N),TNG(N),(ING(N,I),I=1,NIM1)
```

```
987     FORMAT(1X,I3,2E13.6/1x,20I3/1x,20I3/1x,20I3/1x,20I3)
103     CONTINUE
        RETURN
        END
      SUBROUTINE STREAM
C       INCLUDE 'DIMENSION1'
C       INCLUDE 'DIMENSION'
C       IMPLICIT REAL*8 (A-H,O-Z)
        PARAMETER (IT=100,JT=60,LMAX=500)
        CHARACTER*8 PFOR1,PUFOR1,FILIN,FILOUT
        CHARACTER*8 PFOR2,PUFOR2
        CHARACTER*8 PFOR3,PUFOR3
        CHARACTER*8 PFOR4,PUFOR4
      COMMON /FNAME1/PFOR1,PUFOR1,FILIN,FILOUT
      COMMON /FNAME2/PFOR2,PUFOR2,PFOR3,PUFOR3
      COMMON /FNAME3/PP1,PP2,PP3,PP4,MPL,MPL1
      COMMON /FNAME4/PFOR4,PUFOR4
      COMMON /COEFF/Q1P(IT,JT),Q2P(IT,JT),Q3P(IT,JT),COB(IT,JT)
     1   ,SEW(IT,JT),YSEW(IT,JT),SNS(IT,JT),XSNS(IT,JT)
     2   ,DU(IT,JT),DU1(IT,JT),DV(IT,JT),DV1(IT,JT)
     3   ,AP(IT,JT),AN(IT,JT),AS(IT,JT),AE(IT,JT),AW(IT,JT),SU(IT,JT)
     1   ,SP(IT,JT)
      COMMON /POS/ YPOS(IT,JT),XPOS(IT,JT),R(IT,JT)
      COMMON /VAR/ U(IT,JT),V(IT,JT),P(IT,JT),TM(IT,JT),PP(IT,JT)
     1   ,UDUMMY(IT,JT),VDUMMY(IT,JT)
     2   ,TVIS(IT,JT),TCON(IT,JT),DEN(IT,JT),DISS(IT,JT)
      COMMON
     1   /UVEL/RESORU,NSWPU,URFU,SD
     1   /VVEL/RESORV,NSWPV,URFV
     1   /PCOR/RESORM,NSWPP,URFP,IPREF,JPREF
     1   /TMP/RESORT,NSWPT,URFT
      COMMON/INPUT/NI,NJ,NIM1,NJM1,GREAT,INDCOS,INDSM
     1            ,DATAR,DATAW,IFORM,ILASER,CLASIN,NRAYS
     2            ,FOCUS,IFOCUS,BDIAM,ITRACE,ISUPER
     3            ,ANGI,ANGE,RCI,RCT,RT,RI,XEXIT,XI,RTIOY1
      COMMON/IINPUT/
     4            RTIOX1,RTIOX2,XDENSE,JS1,JS2,IS1,IS2
     5            ,URSUP,URVIS,IDENSE,JDENSE,YENRAT,RTIOY2
     6            ,NCONST,XCONST
     6            ,INITP,INITER,SCALE
      COMMON/COND/CCN(IT,JT),CCE(IT,JT),DDN(IT,JT),DDE(IT,JT)
     1    ,DDN1(IT,JT),DDE1(IT,JT)
      COMMON/LASER/QINP(IT,JT),GRA(IT,JT),TRANS(IT,JT),CAB(IT,JT)
     1    ,TNG(LMAX),ING(LMAX,IT)
     2    ,POWER(LMAX),QRA(IT,JT),TH(IT,JT)
      COMMON/LASER2/HT(3000,4),HMU(400,4),HDEN(400,4)
     1    ,HCCP(400,4),HCAB(400,4),HRA(400,4)
      COMMON /ADD8/ANU(IT,JT),ASU(IT,JT),AEU(IT,JT),AWU(IT,JT)
      COMMON /ADD9/ANV(IT,JT),ASV(IT,JT),AEV(IT,JT),AWV(IT,JT)
      COMMON /ADD10/AAN(IT,JT),AAE(IT,JT),COEF(IT),UTEMP(IT,JT),
     1             VTEMP(IT,JT),DYDX(IT),XP(IT)
      COMMON/EXTRA/HINLET
     1       /EXTRA1/UINLET,TBOUND
     1/MMAIN/MAXIT,JMON,IMON,INDPRI,SOLPAT
     1/ADD5/NITER
     1/ADD6/SORMAX,TRSMT,RDL
```



```
      COMMON/PROP/PTL,TTL,GAMMA,RG,WGHT,WGHT1,RATIO
      COMMON/EXTRA/PDUMMY(IT,JT)
      COMMON/PLUS/LROAT,NVS,NVS1,NVE,NVE1
      COMMON/MACHO/MAEX(JT),PEX(JT)
      NIM2=NI-2
      NIM3=NI-3
      NVEM1=NVE-1
      NVSM1=NVS-1
      DO 185 I=NVE1,NI
      AAN(I,NJ)=1.
      AAE(I,NJ)=1.
185   CONTINUE
      DO 186 I=1,NVS1
      AAN(I,NJ)=0.
      AAE(I,NJ)=0.
186   CONTINUE
      AMASS=0.
      DO 187 I=NVS,NVE
      AMASS=AMASS+R(I,NJ)*SEW(I,NJ)*DEN(I,NJ)*V(I,NJ)
187   CONTINUE
      PRINT *, ' INLET MASS FLOW', AMASS
      AAN(NVS,NJ)=R(NVS,NJ)*SEW(NVS,NJ)*DEN(NVS,NJ)*V(NVS,NJ)
     1 /AMASS
      AAE(NVS,NJ)=AAN(NVS,NJ)
      DO 188 I=NVS,NVEM1
      AAN(I+1,NJ)=AAN(I,NJ)+
     1 SEW(I+1,NJ)*R(I+1,NJ)*
     1 DEN(I+1,NJ)*V(I+1,NJ)/AMASS
      AAE(I+1,NJ)=AAN(I+1,NJ)
188   CONTINUE
      DO 189 I=1,NI
      AAE(I,1)=0.
189   AAN(I,1)=0.
      DO 190 J=1,NJ
      AAE(1,J)=0.
190   AAN(1,J)=0.
      DO 193 I=NVS,NIM1
      AMASS6=0.
      AMASS9=0.
      DO 191 J=2,NJM1
      AREA=DEN(I,J)*R(I,J)*SNS(I,J)
      AMASS6=AMASS6+AREA*U(I,J)
      AMASS9=AMASS9+CCE(I,J)
191   CONTINUE
      PRINT *, 'I=', I, 'MASS FLOW', AMASS6,AMASS9
      DO 192 J=2,NJ
      AREA=(DEN(I,J)+DEN(I,J-1))*(R(I,J)+R(I,J-1))*(SNS(I,J)+
     1 +SNS(I,J-1))*(U(I,J)+U(I,J-1))
C      AREA=DEN(I,J)*R(I,J)*SNS(I,J)*U(I,J)
C     1 +DEN(I,J-1)*R(I,J-1)*SNS(I,J-1)*U(I,J-1)
      AAN(I,J)=AAN(I,J-1)+CCE(I,J)
192   CONTINUE
      DO 393 J=2,NJ
      AAN(I,J)=AAN(I,J)/AAN(I,NJ)*AAE(I,NJ)
393   CONTINUE
193   CONTINUE
```

```
      DO 493 J=1,NJ
493   AAN(NI,J)=AAN(NIM1,J)
      DO 29. I=2,NVSM1
      AMASS6=0.
      AMASS9=0.
      DO 291 J=2,NJM1
      AREA=DEN(I,J)*R(I,J)*SNS(I,J)
      AMASS6=AMASS6+AREA*U(I,J)
      AMASS9=AMASS9+CCE(I,J)
291   CONTINUE
      DO 292 J=2,NJ
      AREA=(DEN(I,J)+DEN(I,J-1))*(R(I,J)+R(I,J-1))*(SNS(I,J)+
     1  +SNS(I,J-1))*(U(I,J)+U(I,J-1))/16.
C      AREA=DEN(I,J)*R(I,J)*SNS(I,J)*U(I,J)
C     1  +DEN(I,J-1)*R(I,J-1)*SNS(I,J-1)*U(I,J-1)
      AAN(I,J)=AAN(I,J-1)-CCE(I,J)/AMASS
292   CONTINUE
      DO 392 J=2,NJ
C     AAN(I,J)=AAN(I,J)-AAN(I,NJ)/(NJ-1.)*(J-1.)
392   CONTINUE
293   CONTINUE
      OPEN (UNIT=30,FILE='STREAM.OUT',FORM='UNFORMATTED')
      WRITE(30) ((AAN(I,J),I=1,NI), J=1,NJ)
      CLOSE (UNIT=30)
      RETURN
      END
    SUBROUTINE ONEDIM
C
C     ****************************************************************
C
C     THIS SUBROUTINE CALCULATES THE 1-D INITIAL-DATA SURFACE
C
C     ****************************************************************
C
C       INCLUDE 'DIMENSION1'
C       INCLUDE 'DIMENSION'
C       IMPLICIT REAL*8 (A-H,O-Z)
      PARAMETER (IT=100,JT=60,LMAX=500)
      CHARACTER*8 PFOR1,PUFOR1,FILIN,FILOUT
      CHARACTER*8 PFOR2,PUFOR2
      CHARACTER*8 PFOR3,PUFOR3
      CHARACTER*8 PFOR4,PUFOR4
    COMMON /FNAME1/PFOR1,PUFOR1,FILIN,FILOUT
    COMMON /FNAME2/PFOR2,PUFOR2,PFOR3,PUFOR3
    COMMON /FNAME3/PP1,PP2,PP3,PP4,MPL,MPL1
    COMMON /FNAME4/PFOR4,PUFOR4
    COMMON /COEFF/Q1P(IT,JT),Q2P(IT,JT),Q3P(IT,JT),COB(IT,JT)
   1   ,SEW(IT,JT),YSEW(IT,JT),SNS(IT,JT),XSNS(IT,JT)
   2   ,DU(IT,JT),DU1(IT,JT),DV(IT,JT),DV1(IT,JT)
   3   ,AP(IT,JT),AN(IT,JT),AS(IT,JT),AE(IT,JT),AW(IT,JT),SU(IT,JT)
   1   ,SP(IT,JT)
    COMMON /POS/ YPOS(IT,JT),XPOS(IT,JT),R(IT,JT)
    COMMON /VAR/ U(IT,JT),V(IT,JT),P(IT,JT),TM(IT,JT),PP(IT,JT)
   1   ,UDUMMY(IT,JT),VDUMMY(IT,JT)
   2   ,TVIS(IT,JT),TCON(IT,JT),DEN(IT,JT),DISS(IT,JT)
    COMMON
```



```
   1   /UVEL/RESORU,NSWPU,URFU,SD
   1   /VVEL/RESORV,NSWPV,URFV
   1   /PCOR/RESORM,NSWPP,URFP,IPREF,JPREF
   1   /TMP/RESORT,NSWPT,URFT
    COMMON/INPUT/NI,NJ,NIM1,NJM1,GREAT,INDCOS,INDSM
   1            ,DATAR,DATAW,IFORM,ILASER,CLASIN,NRAYS
   2            ,FOCUS,IFOCUS,BDIAM,ITRACE,ISUPER
   3            ,ANGI,ANGE,RCI,RCT,RT,RI,XEXIT,XI,RTIOY1
    COMMON/IINPUT/
   4            RTIOX1,RTIOX2,XDENSE,JS1,JS2,IS1,IS2
   5            ,URSUP,URVIS,IDENSE,JDENSE,YENRAT,RTIOY2
   6            ,NCONST,XCONST
   6            ,INITP,INITER,SCALE
    COMMON/COND/CCN(IT,JT),CCE(IT,JT),DDN(IT,JT),DDE(IT,JT)
   1    ,DDN1(IT,JT),DDE1(IT,JT)
    COMMON/LASER/QINP(IT,JT),GRA(IT,JT),TRANS(IT,JT),CAB(IT,JT)
   1    ,TNG(LMAX),ING(LMAX,IT)
   2    ,POWER(LMAX),QRA(IT,JT),TH(IT,JT)
    COMMON/LASER2/HT(3000,4),HMU(400,4),HDEN(400,4)
   1    ,HCCP(400,4),HCAB(400,4),HRA(400,4)
      COMMON /ADD8/ANU(IT,JT),ASU(IT,JT),AEU(IT,JT),AWU(IT,JT)
      COMMON /ADD9/ANV(IT,JT),ASV(IT,JT),AEV(IT,JT),AWV(IT,JT)
      COMMON /ADD10/AAN(IT,JT),AAE(IT,JT),COEF(IT),UTEMP(IT,JT),
   1              VTEMP(IT,JT),DYDX(IT),XP(IT)
      COMMON/EXTRA/HINLET
   1       /EXTRA1/UINLET,TBOUND
   1/MMAIN/MAXIT,JMON,IMON,INDPRI,SOLPAT
   1/ADD5/NITER
   1/ADD6/SORMAX,TRSMT,RDL
      COMMON/PROP/PTL,TTL,GAMMA,RG,WGHT,WGHT1,RATIO
      COMMON/EXTRA/PDUMMY(IT,JT)
      COMMON/PLUS/LROAT,NVS,NVS1,NVE,NVE1
       REAL*8 MN3
      II=TTL/100.
      AII=TTL/100.
      AT=TTL/100.-II
      IF(II.GE.348) II=348
      IF(II.GE.348) AT=1.
      AT1=1.-AT
      IJ=II+1
      DENN=HDEN(II,4)*AT1+HDEN(IJ,4)*AT
      DENN=DENN*PTL/PP4
      RG=+PTL/DENN/TTL
      DO 123 I=1,300
      II=I
      IF(HT(I,3).GE.AII) GO TO 124
123   CONTINUE
124   II=II-1
      AAA=HT(II,3)
      BBB=HT(II+1,3)
      CCC=RG*(BBB-AAA)*100./SCALE
      GAMMA=1./(1.-CCC)
C     RG=4.6666E3
      PRINT *, 'UNIVERS. CONST. =',RG,'GAMMA =',GAMMA
      IF(ISUPER.NE.1) GO TO 310
      N1D=1
```

```
        MN3=0.001
        NXCK=0
       GAM1=GAMMA/(GAMMA-1.)
       GAM2=(GAMMA-1.)/2.
       ACOEF=2.0/(GAMMA+1.0)
       BCOEF=(GAMMA-1.0)/(GAMMA+1.0)
       CCOEF=(GAMMA+1.0)/2.0/(GAMMA-1.0)
C
C     OVERALL LOOP
C
      RSTAR=RT
      RSTARS=RT*RT
      DO 180 L=1,NI
      IF (L.LT.LROAT) GO TO 60
      IF (L.GT.LROAT) GO TO 50
      MN3=1.0
      GO TO 110
   50 IF (NXCK.EQ.1) GO TO 60
      IF (N1D.EQ.1) MN3=1.1
      IF (N1D.EQ.2) MN3=0.9
      NXCK=1
   60 IF (INDCOS.EQ.2) GO TO 70
      RAD=YPOS(L,NJ)
      ARATIO=RAD/RSTAR
      GO TO 80
   70 RADS=YPOS(L,NJ)**2
      ARATIO=RADS/RSTARS
C
C     NEWTON-RAPHSON ITERATION LOOP
C
   80 DO 100 ITER=1,100
      ABM=ACOEF+BCOEF*MN3*MN3
      ABMC=ABM**CCOEF
      FM=ABMC/MN3-ARATIO
      FPM=ABMC*(2.0*BCOEF*CCOEF/ABM-1.0/(MN3*MN3))
      OMN3=MN3
      MN3=OMN3-FM/FPM
        ATEMP=.99
        BTEMP=1.01
      IF (OMN3.GT.ATEMP.AND.OMN3.LT.BTEMP) MN3=0.5*(OMN3+MN3)
        CTEMP=1.
      IF (MN3.GT.CTEMP.AND.OMN3.LT.CTEMP) MN3=0.99
      IF (MN3.LT.CTEMP.AND.OMN3.GT.CTEMP) MN3=1.01
        DTEMP=50.
      IF (MN3.GT.DTEMP) MN3=50.0
        EDEMP=0.
      IF (MN3.GE.ETEMP) GO TO 90
      MN3=-MN3
        IF(MN3.GE.ATEMP) MN3=-.99
      GO TO 100
   90 FTEMP=0.0005
        IF (ABS(MN3-OMN3)/OMN3.LE.FTEMP) GO TO 110
  100 CONTINUE
        MN3=1./ARATIO
      WRITE (6,190) L
C
```



```
C     FILL IN 2-D ARRAYS LOOP
C
999     CONTINUE
  110 LDFS=0
      DEM=1.0+GAM2*MN3*MN3
      DEMP=DEM**GAM1
      DNXNY=DYDX(L)/FLOAT(NJM1)
  120 DO 170 M=1,NJ
      DNXNY1=DNXNY*FLOAT(M-1)
      P(L,M)=PTL/DEMP
      TM(L,M)=TTL/DEM
      DEN(L,M)=P(L,M)/(RG*TM(L,M))
      QQ=MN3*SQRT(GAMMA*P(L,M)/DEN(L,M))
      U(L,M)=QQ/SQRT(1.+DNXNY1*DNXNY1)
      V(L,M)=U(L,M)*DNXNY1
        P(L,M)=P(L,M)-PTL
        AII=TM(L,M)/100.
        IF (AII.LE.HT(2,3)) GO TO 139
        DO 127 I=1,300
        II=I
        IF(HT(I,3).GE.AII) GO TO 126
127     CONTINUE
139     TH(L,M)=AII/HT(2,3)*2.
        GO TO 170
126     II=II-1
        AAA=HT(II,3)
        BBB=HT(II+1,3)
        TH(L,M)=II+(AII-AAA)/(BBB-AAA)
  170 CONTINUE
  180 CONTINUE
        GO TO 400
  310   CONTINUE
C
C ********************** ????????????????
C
        INCOS=2
        DO 311 I=1,NI
        DO 311 J=1,NJ
        U(I,J)=UINLET*(YPOS(1,NJ)/YPOS(I,NJ))**INCOS
        V(I,J)=0.
        P(I,J)=0.
        TH(I,J)=HINLET
311     CONTINUE
400     CALL PROPS(1,1,NI,NJ)
        DO  179 L=1,NI
        DO  179 M=1,NJ
C       WRITE(6,200) L,M,HINLET,P(L,M),TH(L,M),TM(L,M),U(L,M),V(L,M)
C       WRITE(6,200) L,M,MN3,P(L,M),TH(L,M),TM(L,M),U(L,M),V(L,M)
179     CONTINUE
      RETURN
C
C     FORMAT STATEMENTS
C
  200 FORMAT(1X,2I5,6(1X,E13.6))
  190 FORMAT (1H0,10X,47H***** THE 1-D SOLUTION FOR THE INITIAL-DATA SUR
     1 ,47HFACE FAILED TO CONVERGE IN 100 ITERATIONS AT L=,I2,6H *****)
```

```
      END
      SUBROUTINE PRINT(ISTART,JSTART,NI,NJ,PHI,HEAD,ISKIP,JSKIP)
C       INCLUDE 'DIMENSION1'
C       IMPLICIT REAL*8 (A-H,O-Z)
        PARAMETER (IT=100,JT=60,LMAX=500)
        CHARACTER*20 HEAD
      CHARACTER*4 F,F4,HI,HY
      DIMENSION PHI(IT,JT)        ,STORE(IT)
      DIMENSION F(7),F4(11)
      DATA F/4H(1H ,4H,A4,,4HI3, ,4H11I ,4H10, ,4H7X, ,
     14HA6) /
      DATA F4/4H 1I ,4H 2I ,4H 3I ,4H 4I ,4H 5I ,4H 6I ,
     1        4H 7I ,4H 8I ,4H 9I ,4H10I ,4H11I /
      DATA HI,HY/4H  I=,4H Y =/
      WRITE(6,110)HEAD
      ISTA=ISTART-12
  100 CONTINUE
      ISTA=ISTA+12
      IEND=ISTA+11
      IEND=MIN0(NI,IEND)
      F(4)=F4(IEND-ISTA)
      WRITE(6,F) HI, (I,I=ISTA,IEND,ISKIP)
      WRITE(6,112)
      DO 101 JJ=JSTART,NJ,JSKIP
      J=JSTART+NJ-JJ
      DO 120 I=ISTA,IEND
      A=PHI(I,J)
        BTEMP=1.E-20
      IF(ABS(A).LT.BTEMP) A=0.0
  120 STORE(I)=A
  101 WRITE(6,113) J,(STORE(I),I=ISTA,IEND,ISKIP)
C-----------------------------------------------------------------
      IF(IEND.LT.NI)GO TO 100
      RETURN
  110 FORMAT(1H0,20(2H*-),7X,A20,7X,20(2H-*))
  112 FORMAT(3H  J)
  113 FORMAT(1H ,I3,1P12E10.2,0PF7.3)
  114 FORMAT(6H0X=    ,F7.3,11F10.3)
      END
      SUBROUTINE PROMOD
C       INCLUDE 'DIMENSION1'
C       INCLUDE 'DIMENSION'
C       IMPLICIT REAL*8 (A-H,O-Z)
        PARAMETER (IT=100,JT=60,LMAX=500)
        CHARACTER*8 PFOR1,PUFOR1,FILIN,FILOUT
        CHARACTER*8 PFOR2,PUFOR2
        CHARACTER*8 PFOR3,PUFOR3
        CHARACTER*8 PFOR4,PUFOR4
      COMMON /FNAME1/PFOR1,PUFOR1,FILIN,FILOUT
      COMMON /FNAME2/PFOR2,PUFOR2,PFOR3,PUFOR3
      COMMON /FNAME3/PP1,PP2,PP3,PP4,MPL,MPL1
      COMMON /FNAME4/PFOR4,PUFOR4
      COMMON /COEFF/Q1P(IT,JT),Q2P(IT,JT),Q3P(IT,JT),COB(IT,JT)
     1   ,SEW(IT,JT),YSEW(IT,JT),SNS(IT,JT),XSNS(IT,JT)
     2   ,DU(IT,JT),DU1(IT,JT),DV(IT,JT),DV1(IT,JT)
     3   ,AP(IT,JT),AN(IT,JT),AS(IT,JT),AE(IT,JT),AW(IT,JT),SU(IT,JT)
```



```
     1   ,SP(IT,JT)
      COMMON /POS/ YPOS(IT,JT),XPOS(IT,JT),R(IT,JT)
      COMMON /VAR/ U(IT,JT),V(IT,JT),P(IT,JT),TM(IT,JT),PP(IT,JT)
     1   ,UDUMMY(IT,JT),VDUMMY(IT,JT)
     2   ,TVIS(IT,JT),TCON(IT,JT),DEN(IT,JT),DISS(IT,JT)
      COMMON
     1   /UVEL/RESORU,NSWPU,URFU,SD
     1   /VVEL/RESORV,NSWPV,URFV
     1   /PCOR/RESORM,NSWPP,URFP,IPREF,JPREF
     1   /TMP/RESORT,NSWPT,URFT
      COMMON/INPUT/NI,NJ,NIM1,NJM1,GREAT,INDCOS,INDSM
     1            ,DATAR,DATAW,IFORM,ILASER,CLASIN,NRAYS
     2            ,FOCUS,IFOCUS,BDIAM,ITRACE,ISUPER
     3            ,ANGI,ANGE,RCI,RCT,RT,RI,XEXIT,XI,RTIOY1
      COMMON/IINPUT/
     4            RTIOX1,RTIOX2,XDENSE,JS1,JS2,IS1,IS2
     5            ,URSUP,URVIS,IDENSE,JDENSE,YENRAT,RTIOY2
     6            ,NCONST,XCONST
     6            ,INITP,INITER,SCALE
      COMMON/COND/CCN(IT,JT),CCE(IT,JT),DDN(IT,JT),DDE(IT,JT)
     1    ,DDN1(IT,JT),DDE1(IT,JT)
      COMMON/LASER/QINP(IT,JT),GRA(IT,JT),TRANS(IT,JT),CAB(IT,JT)
     1    ,TNG(LMAX),ING(LMAX,IT)
     2    ,POWER(LMAX),QRA(IT,JT),TH(IT,JT)
      COMMON/LASER2/HT(3000,4),HMU(400,4),HDEN(400,4)
     1    ,HCCP(400,4),HCAB(400,4),HRA(400,4)
        COMMON /ADD8/ANU(IT,JT),ASU(IT,JT),AEU(IT,JT),AWU(IT,JT)
        COMMON /ADD9/ANV(IT,JT),ASV(IT,JT),AEV(IT,JT),AWV(IT,JT)
        COMMON /ADD10/AAN(IT,JT),AAE(IT,JT),COEF(IT),UTEMP(IT,JT),
     1              VTEMP(IT,JT),DYDX(IT),XP(IT)
        COMMON/EXTRA/HINLET
     1       /EXTRA1/UINLET,TBOUND
     1/MMAIN/MAXIT,JMON,IMON,INDPRI,SOLPAT
     1/ADD5/NITER
     1/ADD6/SORMAX,TRSMT,RDL
        COMMON/PROP/PTL,TTL,GAMMA,RG,WGHT,WGHT1,RATIO
        COMMON/EXTRA/PDUMMY(IT,JT)
        COMMON/PLUS/LROAT,NVS,NVS1,NVE,NVE1
CHAPTER  0  0  0  0  0  0  0  PRELIMINARIES  0  0
CHAPTER  2  2  2  2  2  2  2  2  U MOMENTUM  2  2
      ENTRY MODU
C-----TOP WALL
        DO 1 I=2,NIM1
C       SP(I,NJM1)=SP(I,NJM1)-AN(I,NJM1)
C       AN(I,NJM1)=0.
1       CONTINUE
C-------CENTERLINE
        DO 2 I=2,NIM1
C       AS(I,2)=0.
2       CONTINUE
C-------INLET
        DO 3 J=2,NJM1
C       SU(2,J)=SU(2,J)+AW(2,J)*U(1,J)
C       SP(2,J)=SP(2,J)-AW(2,J)
C       AW(2,J)=0.
3       CONTINUE
```

```
C------OUTLET
       DO 4 J=2,NJM1
C      SU(NIM1,J)=SU(NIM1,J)+AE(NIM1,J)*U(NI,J)
C      SP(NIM1,J)=SP(NIM1,J)-AE(NIM1,J)
C      AE(NIM1,J)=0.
4      CONTINUE
      RETURN
C
CHAPTER  3  3  3  3  3  3  3  3  V MOMENTUM  3  3
C
      ENTRY MODV
C-----TOP WALL
       DO 11 I=2,NIM1
C      SP(I,NJM1)=SP(I,NJM1)-AN(I,NJM1)
C      AN(I,NJM1)=0.
11     CONTINUE
C-------CENTERLINE
       DO 12 I=2,NIM1
C      SP(I,2)=SP(I,2)-AS(I,2)
C      AS(I,2)=0.
12     CONTINUE
C-------INLET
       DO 13 J=2,NJM1
C      SU(2,J)=SU(2,J)+AW(2,J)*V(1,J)
C      SP(2,J)=SP(2,J)-AW(2,J)
C      AW(2,J)=0.
13     CONTINUE
C------OUTLET
       DO 14 J=2,NJM1
C      SU(NIM1,J)=SU(NIM1,J)+AE(NIM1,J)*V(NI,J)
C      SP(NIM1,J)=SP(NIM1,J)-AE(NIM1,J)
C      AE(NIM1,J)=0.
14     CONTINUE
      RETURN
C
CHAPTER  4  4  4  4  4  PRESSURE CORRECTION  4  4  4
      ENTRY MODP
C-----TOP WALL
       DO 191 I=2,NIM1
C      AN(I,NJM1)=0.
191    CONTINUE
C-------CENTERLINE
       DO 192 I=2,NIM1
C      AS(I,2)=0.
192    CONTINUE
C-------INLET
       DO 193 J=2,NJM1
C      AW(2,J)=0.
193    CONTINUE
C------OUTLET
       DO 194 J=2,NJM1
C      AE(NIM1,J)=0.
194    CONTINUE
      RETURN
C
       ENTRY MODT
```



```
C-----TOP WALL
       DO 91 I=2,NIM1
C      AN(I,NJM1)=0.
91     CONTINUE
C-------CENTERLINE
       DO 92 I=2,NIM1
       AS(I,2)=0.
92     CONTINUE
C-------INLET
       DO 93 J=2,NJM1
       SU(2,J)=SU(2,J)+AW(2,J)*TH(1,J)
       SP(2,J)=SP(2,J)-AW(2,J)
       AW(2,J)=0.
93     CONTINUE
C------OUTLET
       DO 94 J=2,NJM1
       SU(NIM1,J)=SU(NIM1,J)+AE(NIM1,J)*TH(NI,J)
       SP(NIM1,J)=SP(NIM1,J)-AE(NIM1,J)
       AE(NIM1,J)=0.
94     CONTINUE
      RETURN
      END
      SUBROUTINE PROPS(NIS,NJS,NIE,NJE)
C       INCLUDE 'DIMENSION1'
C       INCLUDE 'DIMENSION'
C       IMPLICIT REAL*8 (A-H,O-Z)
        PARAMETER (IT=100,JT=60,LMAX=500)
        CHARACTER*8 PFOR1,PUFOR1,FILIN,FILOUT
        CHARACTER*8 PFOR2,PUFOR2
        CHARACTER*8 PFOR3,PUFOR3
        CHARACTER*8 PFOR4,PUFOR4
      COMMON /FNAME1/PFOR1,PUFOR1,FILIN,FILOUT
      COMMON /FNAME2/PFOR2,PUFOR2,PFOR3,PUFOR3
      COMMON /FNAME3/PP1,PP2,PP3,PP4,MPL,MPL1
      COMMON /FNAME4/PFOR4,PUFOR4
      COMMON /COEFF/Q1P(IT,JT),Q2P(IT,JT),Q3P(IT,JT),COB(IT,JT)
     1    ,SEW(IT,JT),YSEW(IT,JT),SNS(IT,JT),XSNS(IT,JT)
     2    ,DU(IT,JT),DU1(IT,JT),DV(IT,JT),DV1(IT,JT)
     3    ,AP(IT,JT),AN(IT,JT),AS(IT,JT),AE(IT,JT),AW(IT,JT),SU(IT,JT)
     1    ,SP(IT,JT)
      COMMON /POS/ YPOS(IT,JT),XPOS(IT,JT),R(IT,JT)
      COMMON /VAR/ U(IT,JT),V(IT,JT),P(IT,JT),TM(IT,JT),PP(IT,JT)
     1    ,UDUMMY(IT,JT),VDUMMY(IT,JT)
     2    ,TVIS(IT,JT),TCON(IT,JT),DEN(IT,JT),DISS(IT,JT)
      COMMON
     1    /UVEL/RESORU,NSWPU,URFU,SD
     1    /VVEL/RESORV,NSWPV,URFV
     1    /PCOR/RESORM,NSWPP,URFP,IPREF,JPREF
     1    /TMP/RESORT,NSWPT,URFT
      COMMON/INPUT/NI,NJ,NIM1,NJM1,GREAT,INDCOS,INDSM
     1             ,DATAR,DATAW,IFORM,ILASER,CLASIN,NRAYS
     2             ,FOCUS,IFOCUS,BDIAM,ITRACE ISUPER
     3             ,ANGI,ANGE,RCI,RCT,RT,RI,XEXIT,XI,RTIOY1
      COMMON/IINPUT/
     4             RTIOX1,RTIOX2,XDENSE,JS1,JS2,IS1,IS2
     5             ,URSUP,URVIS,IDENSE,JDENSE,YENRAT,RTIOY2
```

```
     6            ,NCONST,XCONST
     6            ,INITP,INITER,SCALE
      COMMON/COND/CCN(IT,JT),CCE(IT,JT),DDN(IT,JT),DDE(IT,JT)
     1    ,DDN1(IT,JT),DDE1(IT,JT)
      COMMON/LASER/QINP(IT,JT),GRA(IT,JT),TRANS(IT,JT),CAB(IT,JT)
     1    ,TNG(LMAX),ING(LMAX,IT)
     2    ,POWER(LMAX),QRA(IT,JT),TH(IT,JT)
      COMMON/LASER2/HT(3000,4),HMU(400,4),HDEN(400,4)
     1    ,HCCP(400,4),HCAB(400,4),HRA(400,4)
        COMMON /ADD8/ANU(IT,JT),ASU(IT,JT),AEU(IT,JT),AWU(IT,JT)
        COMMON /ADD9/ANV(IT,JT),ASV(IT,JT),AEV(IT,JT),AWV(IT,JT)
        COMMON /ADD10/AAN(IT,JT),AAE(IT,JT),COEF(IT),UTEMP(IT,JT),
     1              VTEMP(IT,JT),DYDX(IT),XP(IT)
        COMMON/EXTRA/HINLET
     1       /EXTRA1/UINLET,TBOUND
     1/MMAIN/MAXIT,JMON,IMON,INDPRI,SOLPAT
     1/ADD5/NITER
     1/ADD6/SORMAX,TRSMT,RDL
        COMMON/PROP/PTL,TTL,GAMMA,RG,WGHT,WGHT1,RATIO
        COMMON/EXTRA/PDUMMY(IT,JT)
        COMMON/PLUS/LROAT,NVS,NVS1,NVE,NVE1
        DO 305 J=1,NJ
        AAA=TH(NIM1,J)*1.5
        IF(TH(NI,J).GT.AAA) TH(NI,J)=AAA
305     CONTINUE
C       PP1=1.E5
C       PP2=2.E5
C       PP3=3.E5
C       PP4=4.E5
      DO 100 I=NIS,NIE
      DO 101 J=NJS,NJE
        PTEMP=PTL+P(I,J)
        K=0
        IF(PTEMP.GE.PP3) K=3
        IF(PTEMP.GE.PP2.AND.PTEMP.LT.PP3)K=2
        IF(PTEMP.GE.PP1.AND.PTEMP.LT.PP2)K=1
        IF(K.EQ.1) ARATIO=(PP2-PTEMP)/(PP2-PP1)
        IF(K.EQ.2) ARATIO=(PP3-PTEMP)/(PP3-PP2)
        IF(K.EQ.3) ARATIO=(PP4-PTEMP)/(PP4-PP3)
        IF(K.EQ.0) GO TO 234
        AAA=TH(I,J)-MPL
        IF(AAA.GE.0.) TH(I,J)=MPL-400.
        II=TH(I,J)
        AT=TH(I,J)-II
        IF(II.GE.MPL1) II=MPL
        IF(II.GE.MPL1) AT=1.
        IF(II.GE.1)
     1  T1=HT(II,K)*(1.-AT)+AT*HT(II+1,K)
        IF(II.LT.1)
     1  T1=TH(I,J)/1.*HT(1,K)
234     CONTINUE
        AAA=TH(I,J)-MPL
        IF(AAA.GE.0.) TH(I,J)=MPL-400.
        II=TH(I,J)
        AT=TH(I,J)-II
        IF(II.GE.MPL1) II=MPL
```



```
        IF(II.GE.MPL1) AT=1.
        IF(II.GE.1)
     1  T2=HT(II,K+1)*(1.-AT)+AT*HT(II+1,K+1)
        IF(II.LT.1)
     1  T2=TH(I,J)/1.*HT(1,K+1)
        IF(K.EQ.0) ARATIO=0.
        TM(I,J)=T1*ARATIO+T2*(1.-ARATIO)
        IF(K.EQ.0) GO TO 235
        II=T1
        AT=T1-II
        IF(II.GE.348) II=348
        IF(II.GE.348) AT=1.
        AT1=1.-AT
        IJ=II+1
        IF(II.EQ.0) GO TO 199
        TVIS(I,J)=HMU(II,K)*AT1+HMU(IJ,K)*AT
        DEN(I,J)=HDEN(II,K)*AT1+HDEN(IJ,K)*AT
        T18=18.
        IF(TM(I,J).LE.T18)
     1  DEN(I,J)=II/T1*HDEN(II,K)
        TRANS(I,J)=HCCP(II,K)*AT1+HCCP(IJ,K)*AT
        CAB(I,J)=HCAB(II,K)*AT1+HCAB(IJ,K)*AT
        QRA(I,J)=HRA(II,K)*AT1+HRA(IJ,K)*AT
        GO TO 102
199     TVIS(I,J)=HMU(1,K)
        TRANS(I,J)=HCCP(1,K)
        CAB(I,J)=0.
        QRA(I,J)=0.
        DEN(I,J)=1./T1*HDEN(1,K)
102     CONTINUE
235     CONTINUE
        II=T2
        AT=T2-II
        IF(II.GE.348) II=348
        IF(II.GE.348) AT=1.
        AT1=1.-AT
        IJ=II+1
        IF(II.EQ.0) GO TO 299
        TVIS(I,J)=(HMU(II,K+1)*AT1+HMU(IJ,K+1)*AT)
     1*(1.-ARATIO)+ARATIO*TVIS(I,J)
        DEN(I,J)=(HDEN(II,K+1)*AT1+HDEN(IJ,K+1)*AT)
     1*(1.-ARATIO)+ARATIO*DEN(I,J)
        IF(K.EQ.0) DEN(I,J)=DEN(I,J)*(PTL+P(I,J))/PP1
        IF(TM(I,J).LE.18.D0)
     1  DEN(I,J)=((II/T2)*HDEN(II,K+1))*(1.-ARATIO)
     1  +DEN(I,J)*ARATIO
        IF(TM(I,J).LE.18.D0.AND.K.EQ.0)
     1  DEN(I,J)=((II/T2)*HDEN(II,K+1))*(1.-ARATIO)
     1  *(PTL+P(I,J))/PP1
        TRANS(I,J)=(HCCP(II,K+1)*AT1+HCCP(IJ,K+1)*AT)
     1*(1.-ARATIO)+ARATIO*TRANS(I,J)
        CAB(I,J)=(HCAB(II,K+1)*AT1+HCAB(IJ,K+1)*AT)
     1*(1.-ARATIO)+ARATIO*CAB(I,J)
        QRA(I,J)=(HRA(II,K+1)*AT1+HRA(IJ,K+1)*AT)
     1*(1.-ARATIO)+ARATIO*QRA(I,J)
        GO TO 101
```

```
299     IF(K.EQ.0) GO TO 399
        TVIS(I,J)=HMU(1,K+1)*(1.-ARATIO)+ARATIO*HMU(1,K)
        TRANS(I,J)=HCCP(1,K+1)*(1.-ARATIO)+ARATIO*HCCP(1,K)
        CAB(I,J)=0.
        QRA(I,J)=0.
        DEN(I,J)=1./T2*HDEN(1,K+1)*(1.-ARATIO)
    1  +ARATIO*HDEN(1,K)
        GO TO 101
399     CONTINUE
        TVIS(I,J)=HMU(1,K+1)
        TRANS(I,J)=HCCP(1,K+1)
        CAB(I,J)=0.
        QRA(I,J)=0.
        DEN(I,J)=1./T2*HDEN(1,K+1)*(PTL+P(I,J))/PP1
  101 CONTINUE
  100 CONTINUE
      RETURN
      END
      SUBROUTINE COORD
C       INCLUDE 'DIMENSION1'
C       INCLUDE 'DIMENSION'
C       IMPLICIT REAL*8 (A-H,O-Z)
        PARAMETER (IT=100,JT=60,LMAX=500)
        CHARACTER*8 PFOR1,PUFOR1,FILIN,FILOUT
        CHARACTER*8 PFOR2,PUFOR2
        CHARACTER*8 PFOR3,PUFOR3
        CHARACTER*8 PFOR4,PUFOR4
      COMMON /FNAME1/PFOR1,PUFOR1,FILIN,FILOUT
      COMMON /FNAME2/PFOR2,PUFOR2,PFOR3,PUFOR3
      COMMON /FNAME3/PP1,PP2,PP3,PP4,MPL,MPL1
      COMMON /FNAME4/PFOR4,PUFOR4
      COMMON /COEFF/Q1P(IT,JT),Q2P(IT,JT),Q3P(IT,JT),COB(IT,JT)
     1    ,SEW(IT,JT),YSEW(IT,JT),SNS(IT,JT),XSNS(IT,JT)
     2    ,DU(IT,JT),DU1(IT,JT),DV(IT,JT),DV1(IT,JT)
     3    ,AP(IT,JT),AN(IT,JT),AS(IT,JT),AE(IT,JT),AW(IT,JT),SU(IT,JT)
     1    ,SP(IT,JT)
      COMMON /POS/ YPOS(IT,JT),XPOS(IT,JT),R(IT,JT)
      COMMON /VAR/ U(IT,JT),V(IT,JT),P(IT,JT),TM(IT,JT),PP(IT,JT)
     1    ,UDUMMY(IT,JT),VDUMMY(IT,JT)
     2    ,TVIS(IT,JT),TCON(IT,JT),DEN(IT,JT),DISS(IT,JT)
      COMMON
     1    /UVEL/RESORU,NSWPU,URFU,SD
     1    /VVEL/RESORV,NSWPV,URFV
     1    /PCOR/RESORM,NSWPP,URFP,IPREF,JPREF
     1    /TM?/RESORT,NSWPT,URFT
      COMMON 'INPUT/NI,NJ,NIM1,NJM1,GREAT,INDCOS,INDSM
     1              ,DATAR,DATAW,IFORM,ILASER,CLASIN,NRAYS
     2              ,FOCUS,IFOCUS,BDIAM,ITRACE,ISUPER
     3              ,ANGI,ANGE,RCI,RCT,RT,RI,XEXIT,XI,RTIOY1
      COMMON/IINPUT/
     4              RTIOX1,RTIOX2,XDENSE,JS1,JS2,IS1,IS2
     5              ,URSUP,URVIS,IDENSE,JDENSE,YENRAT,RTIOY2
     6              ,NCONST,XCONST
     6              ,INITP,INITER,SCALE
      COMMON/COND/CCN(IT,JT),CCE(IT,JT),DDN(IT,JT),DDE(IT,JT)
     1    ,DDN1(IT,JT),DDE1(IT,JT)
```



```
      COMMON/LASER/QINP(IT,JT),GRA(IT,JT),TRANS(IT,JT),CAB(IT,JT)
     1    ,TNG(LMAX),ING(LMAX,IT)
     2    ,POWER(LMAX),QRA(IT,JT),TH(IT,JT)
      COMMON/LASER2/HT(3000,4),HMU(400,4),HDEN(400,4)
     1    ,HCCP(400,4),HCAB(400,4),HRA(400,4)
        COMMON /ADD8/ANU(IT,JT),ASU(IT,JT),AEU(IT,JT),AWU(IT,JT)
        COMMON /ADD9/ANV(IT,JT),ASV(IT,JT),AEV(IT,JT),AWV(IT,JT)
        COMMON /ADD10/AAN(IT,JT),AAE(IT,JT),COEF(IT),UTEMP(IT,JT),
     1              VTEMP(IT,JT),DYDX(IT),XP(IT)
        COMMON/EXTRA/HINLET
     1       /EXTRA1/UINLET,TBOUND
     1/MMAIN/MAXIT,JMON,IMON,INDPRI,SOLPAT
     1/ADD5/NITER
     1/ADD6/SORMAX,TRSMT,RDL
        COMMON/PROP/PTL,TTL,GAMMA,RG,WGHT,WGHT1,RATIO
        COMMON/EXTRA/PDUMMY(IT,JT)
        COMMON/PLUS/LROAT,NVS,NVS1,NVE,NVE1
C
C ****************** COORDINATE TRANSFORM ********************
C
      DO 100 I=1,NI
      DO 100 J=1,NJ
100   R(I,J)=YPOS(I,J)
        NIM2=NIM1-1
        NJM2=NJM1-1
      DO 101 J=1,NJ
        SEW(1,J)=(XPOS(2,J)-XPOS(1,J))*2.
        SEW(NI,J)=(XPOS(NI,J)-XPOS(NIM1,J))*2.
        YSEW(1,J)=(YPOS(2,J)-YPOS(1,J))*2.
        YSEW(NI,J)=(YPOS(NI,J)-YPOS(NIM1,J))*2.
        SEW(2,J)=(.5*XPOS(3,J)+.5*XPOS(2,J)-XPOS(1,J))*1.
        SEW(NIM1,J)=(2.*XPOS(NI,J)-XPOS(NIM1,J)-XPOS(NIM2,J))/2.
        YSEW(2,J)=(.5*YPOS(3,J)+.5*YPOS(2,J)-YPOS(1,J))*1.
        YSEW(NIM1,J)=(2.*YPOS(NI,J)-YPOS(NIM1,J)-YPOS(NIM2,J))/2.
      DO 101 I=3,NIM2
        YSEW(I,J)=0.5*(YPOS(I+1,J)-YPOS(I-1,J))
        SEW(I,J)=0.5*(XPOS(I+1,J)-XPOS(I-1,J))
  101 CONTINUE
      DO 102 I=1,NI
        SNS(I,1)=(YPOS(I,2)-YPOS(I,1))*2.
        SNS(I,NJ)=(YPOS(I,NJ)-YPOS(I,NJM1))*2.
        XSNS(I,1)=(XPOS(I,2)-XPOS(I,1))*2.
        XSNS(I,NJ)=(XPOS(I,NJ)-XPOS(I,NJM1))*2.
        SNS(I,2)=(YPOS(I,3)+YPOS(I,2)-2.*YPOS(I,1))/2.
        SNS(I,NJM1)=(2.*YPOS(I,NJ)-YPOS(I,NJM1)-YPOS(I,NJM2))/2.
        XSNS(I,2)=(XPOS(I,3)+XPOS(I,2)-2.*XPOS(I,1))/2.
        XSNS(I,NJM1)=(2.*XPOS(I,NJ)-XPOS(I,NJM1)-XPOS(I,NJM2))/2.
      DO 102 J=3,NJM2
        XSNS(I,J)=0.5*(XPOS(I,J+1)-XPOS(I,J-1))
        SNS(I,J)=0.5*(YPOS(I,J+1)-YPOS(I,J-1))
  102 CONTINUE
        BTEMP=0.
      DO 103 J=1,NJ
      DO 103 I=1,NI
        Q1P(I,J)=XSNS(I,J)*XSNS(I,J)+SNS(I,J)*SNS(I,J)
        Q2P(I,J)=YSEW(I,J)*SNS(I,J)+SEW(I,J)*XSNS(I,J)
```

```
        Q3P(I,J)=SEW(I,J)*SEW(I,J)+YSEW(I,J)*YSEW(I,J)
        COB(I,J)=SNS(I,J)*SEW(I,J)-XSNS(I,J)*YSEW(I,J)
        IF(COB(I,J).EQ.BTEMP) PRINT *,I,J,'COB,ERROR'
        IF(SEW(I,J).LE.BTEMP) PRINT *,I,J,'SEW,ERROR'
        IF(SNS(I,J).LE.BTEMP) PRINT *,I,J,'SNS,ERROR'
  103 CONTINUE
      DO 104 I=1,NI
      DO 104 J=1,NJ
        UDUMMY(I,J)=U(I,J)*SNS(I,J)-V(I,J)*XSNS(I,J)
        VDUMMY(I,J)=V(I,J)*SEW(I,J)-U(I,J)*YSEW(I,J)
104     CONTINUE
      DO 105 I=1,NI
C       UDUMMY(I,NJ)=0.
C       VDUMMY(I,NJ)=0.
        VDUMMY(I,1)=0.
105   CONTINUE
      DO 106 J=1,NJ
        UDUMMY(1,J)=U(1,J)*SNS(1,J)-V(1,J)*XSNS(1,J)
106   CONTINUE
      DO 109 I=1,NI
      DO 109 J=1,NJ
  109  IF(INDCOS.EQ.1) R(I,J)=1.0
      RETURN
      END
C***********CALCULATE DISSIPATION OF ENERGY EQUATION ***********
        SUBROUTINE DISSIP
C       INCLUDE 'DIMENSION1'
C       INCLUDE 'DIMENSION'
C       IMPLICIT REAL*8 (A-H,O-Z)
        PARAMETER (IT=100,JT=60,LMAX=500)
        CHARACTER*8 PFOR1,PUFOR1,FILIN,FILOUT
        CHARACTER*8 PFOR2,PUFOR2
        CHARACTER*8 PFOR3,PUFOR3
        CHARACTER*8 PFOR4,PUFOR4
      COMMON /FNAME1/PFOR1,PUFOR1,FILIN,FILOUT
      COMMON /FNAME2/PFOR2,PUFOR2,PFOR3,PUFOR3
      COMMON /FNAME3/PP1,PP2,PP3,PP4,MPL,MPL1
      COMMON /FNAME4/PFOR4,PUFOR4
      COMMON /COEFF/Q1P(IT,JT),Q2P(IT,JT),Q3P(IT,JT),COB(IT,JT)
     1   ,SEW(IT,JT),YSEW(IT,JT),SNS(IT,JT),XSNS(IT,JT)
     2   ,DU(IT,JT),DU1(IT,JT),DV(IT,JT),DV1(IT,JT)
     3   ,AP(IT,JT),AN(IT,JT),AS(IT,JT),AE(IT,JT),AW(IT,JT),SU(IT,JT)
     1   ,SP(IT,JT)
      COMMON /POS/ YPOS(IT,JT),XPOS(IT,JT),R(IT,JT)
      COMMON /VAR/ U(IT,JT),V(IT,JT),P(IT,JT),TM(IT,JT),PP(IT,JT)
     1   ,UDUMMY(IT,JT),VDUMMY(IT,JT)
     2   ,TVIS(IT,JT),TCON(IT,JT),DEN(IT,JT),DISS(IT,JT)
      COMMON
     1   /UVEL/RESORU,NSWPU,URFU,SD
     1   /VVEL/RESORV,NSWPV,URFV
     1   /PCOR/RESORM,NSWPP,URFP,IPREF,JPREF
     1   /TMP/RESORT,NSWPT,URFT
      COMMON/INPUT/NI,NJ,NIM1,NJM1,GREAT,INDCOS,INDSM
     1            ,DATAR,DATAW,IFORM,ILASER,CLASIN,NRAYS
     2            ,FOCUS,IFOCUS,BDIAM,ITRACE,ISUPER
     3            ,ANGI,ANGE,RCI,RCT,RT,RI,XEXIT,XI,RTIOY1
```



```
      COMMON/IINPUT/
     4            RTIOX1,RTIOX2,XDENSE,JS1,JS2,IS1,IS2
     5            ,URSUP,URVIS,IDENSE,JDENSE,YENRAT,RTIOY2
     6            ,NCONST,XCONST
     6            ,INITP,INITER,SCALE
      COMMON/COND/CCN(IT,JT),CCE(IT,JT),DDN(IT,JT),DDE(IT,JT)
     1   ,DDN1(IT,JT),DDE1(IT,JT)
      COMMON/LASER/QINP(IT,JT),GRA(IT,JT),TRANS(IT,JT),CAB(IT,JT)
     1   ,TNG(LMAX),ING(LMAX,IT)
     2   ,POWER(LMAX),QRA(IT,JT),TH(IT,JT)
      COMMON/LASER2/HT(3000,4),HMU(400,4),HDEN(400,4)
     1   ,HCCP(400,4),HCAB(400,4),HRA(400,4)
      COMMON /ADD8/ANU(IT,JT),ASU(IT,JT),AEU(IT,JT),AWU(IT,JT)
      COMMON /ADD9/ANV(IT,JT),ASV(IT,JT),AEV(IT,JT),AWV(IT,JT)
      COMMON /ADD10/AAN(IT,JT),AAE(IT,JT),COEF(IT),UTEMP(IT,JT),
     1            VTEMP(IT,JT),DYDX(IT),XP(IT)
      COMMON/EXTRA/HINLET
     1      /EXTRA1/UINLET,TBOUND
     1/MMAIN/MAXIT,JMON,IMON,INDPRI,SOLPAT
     1/ADD5/NITER
     1/ADD6/SORMAX,TRSMT,RDL
      COMMON/PROP/PTL,TTL,GAMMA,RG,WGHT,WGHT1,RATIO
      COMMON/EXTRA/PDUMMY(IT,JT)
      COMMON/PLUS/LROAT,NVS,NVS1,NVE,NVE1
      DO 100 I=2,NIM1
      DO 100 J=2,NJM1
      XU=(U(I+1,J)-U(I-1,J))/2.
      YU=(U(I,J+1)-U(I,J-1))/2.
      XV=(V(I+1,J)-V(I-1,J))/2.
      YV=(V(I,J+1)-V(I,J-1))/2.
      IF(I.EQ.2) THEN
      XU=.5*U(I+1,J)+.5*U(I,J)-U(I-1,J)
      XV=.5*V(I+1,J)+.5*V(I,J)-V(I-1,J)
      ELSE
      ENDIF
      IF(I.EQ.NIM1) THEN
      XU=U(I+1,J)-.5*U(I,J)-.5*U(I-1,J)
      XV=V(I+1,J)-.5*V(I,J)-.5*V(I-1,J)
      ELSE
      ENDIF
      IF(J.EQ.2) THEN
      YU=.5*U(I,J+1)+.5*U(I,J)-U(I,J-1)
      YV=.5*V(I,J+1)+.5*V(I,J)-V(I,J-1)
      ELSE
      ENDIF
      IF(J.EQ.NJM1) THEN
      YU=U(I,J+1)-.5*U(I,J)-.5*U(I,J-1)
      YV=V(I,J+1)-.5*V(I,J)-.5*V(I,J-1)
      END IF
      UX=(SNS(I,J)*XU-YSEW(I,J)*YU)/COB(I,J)
      VX=(SNS(I,J)*XV-YSEW(I,J)*YV)/COB(I,J)
      UY=(SEW(I,J)*YU-XSNS(I,J)*XU)/COB(I,J)
      VY=(SEW(I,J)*YV-XSNS(I,J)*XV)/COB(I,J)
      DISS(I,J)=5./3.*UX**2+5./3.*VY**2+VX**2+UY**2-2./3.
     1  *UX*VY+2.*UY*VX
      DISS(I,J)=DISS(I,J)*TVIS(I,J)
```

```
      DISS(I,J)=DISS(I,J)+(5./3.*(V(I,J)/YPOS(I,J))**2
     1-2./3.*V(I,J)/YPOS(I,J)*(VY+UX))*TVIS(I,J)
      DISS(I,J)=DISS(I,J)*COB(I,J)*R(I,J)/SCALE
100   CONTINUE
      RETURN
      END
      SUBROUTINE ENERGE
C     INCLUDE 'DIMENSION1'
C     INCLUDE 'DIMENSION'
C     IMPLICIT REAL*8 (A-H,O-Z)
      PARAMETER (IT=100,JT=60,LMAX=500)
      CHARACTER*8 PFOR1,PUFOR1,FILIN,FILOUT
      CHARACTER*8 PFOR2,PUFOR2
      CHARACTER*8 PFOR3,PUFOR3
      CHARACTER*8 PFOR4,PUFOR4
      COMMON /FNAME1/PFOR1,PUFOR1,FILIN,FILOUT
      COMMON /FNAME2/PFOR2,PUFOR2,PFOR3,PUFOR3
      COMMON /FNAME3/PP1,PP2,PP3,PP4,MPL,MPL1
      COMMON /FNAME4/PFOR4,PUFOR4
      COMMON /COEFF/Q1P(IT,JT),Q2P(IT,JT),Q3P(IT,JT),COB(IT,JT)
     1   ,SEW(IT,JT),YSEW(IT,JT),SNS(IT,JT),XSNS(IT,JT)
     2   ,DU(IT,JT),DU1(IT,JT),DV(IT,JT),DV1(IT,JT)
     3   ,AP(IT,JT),AN(IT,JT),AS(IT,JT),AE(IT,JT),AW(IT,JT),SU(IT,JT)
     1   ,SP(IT,JT)
      COMMON /POS/ YPOS(IT,JT),XPOS(IT,JT),R(IT,JT)
      COMMON /VAR/ U(IT,JT),V(IT,JT),P(IT,JT),TM(IT,JT),PP(IT,JT)
     1   ,UDUMMY(IT,JT),VDUMMY(IT,JT)
     2   ,TVIS(IT,JT),TCON(IT,JT),DEN(IT,JT),DISS(IT,JT)
      COMMON
     1   /UVEL/RESORU,NSWPU,URFU,SD
     1   /VVEL/RESORV,NSWPV,URFV
     1   /PCOR/RESORM,NSWPP,URFP,IPREF,JPREF
     1   /TMP/RESORT,NSWPT,URFT
      COMMON/INPUT/NI,NJ,NIM1,NJM1,GREAT,INDCOS,INDSM
     1            ,DATAR,DATAW,IFORM,ILASER,CLASIN,NRAYS
     2            ,FOCUS,IFOCUS,BDIAM,ITRACE,ISUPER
     3            ,ANGI,ANGE,RCI,RCT,RT,RI,XEXIT,XI,RTIOY1
      COMMON/IINPUT/
     4            RTIOX1,RTIOX2,XDENSE,JS1,JS2,IS1,IS2
     5            ,URSUP,URVIS,IDENSE,JDENSE,YENRAT,RTIOY2
     6            ,NCONST,XCONST
     6            ,INITP,INITER,SCALE
      COMMON/COND/CCN(IT,JT),CCE(IT,JT),DDN(IT,JT),DDE(IT,JT)
     1   ,DDN1(IT,JT),DDE1(IT,JT)
      COMMON/LASER/QINP(IT,JT),GRA(IT,JT),TRANS(IT,JT),CAB(IT,JT)
     1   ,TNG(LMAX),ING(LMAX,IT)
     2   ,POWER(LMAX),QRA(IT,JT),TH(IT,JT)
      COMMON/LASER2/HT(3000,4),HMU(400,4),HDEN(400,4)
     1   ,HCCP(400,4),HCAB(400,4),HRA(400,4)
      COMMON /ADD8/ANU(IT,JT),ASU(IT,JT),AEU(IT,JT),AWU(IT,JT)
      COMMON /ADD9/ANV(IT,JT),ASV(IT,JT),AEV(IT,JT),AWV(IT,JT)
      COMMON /ADD10/AAN(IT,JT),AAE(IT,JT),COEF(IT),UTEMP(IT,JT),
     1            VTEMP(IT,JT),DYDX(IT),XP(IT)
      COMMON/EXTRA/HINLET
     1      /EXTRA1/UINLET,TBOUND
     1/MMAIN/MAXIT,JMON,IMON,INDPRI,SOLPAT
```



```
     1/ADD5/NITER
     1/ADD6/SORMAX,TRSMT,RDL
      COMMON/PROP/PTL,TTL,GAMMA,RG,WGHT,WGHT1,RATIO
      COMMON/EXTRA/PDUMMY(IT,JT)
      COMMON/PLUS/LROAT,NVS,NVS1,NVE,NVE1
      PABOR=0.
C
C
C ***************** CALCULATE LASER POWER INPUT ***************************
C ******** ASSUME ZERO FOR GRID I FROM 1 TO 5 AND GRID FROM NI-5 TO NI ***
C ******** THIS CAN BE CHANGED EITHER TO SAVE CPU TIME OR MAKE PROBLEM ***
C ******** MORE PEFECT ***********************************************
C
C
      DO 1 I=1,NI
      DO 1 J=1,NJ
      QINP(I,J)=0.
1     CONTINUE
      TRSMT=0.
      NIM5=NI-5
      DO 20 N=1,NRAYS
      P1=POWER(N)
      DO 10 I=6,67
      JJ=ING(N,I)
      IF(JJ.EQ.NJ) GO TO 101
      XYZ=CAB(I,JJ)*TNG(N)*SEW(I,JJ)
      XYZ=-1.*XYZ
      XYZ=EXP(XYZ)
      XYZ=1.-XYZ
      QINP(I,JJ)=QINP(I,JJ)+P1*XYZ
      P1=P1*(1.-XYZ)
101   CONTINUE
10    CONTINUE
      TRSMT=TRSMT+P1
20    CONTINUE
      TRSMT=TRSMT*6.28
      RETURN
      END
     SUBROUTINE LISOLH(ISTART,JSTART,NI,NJ,PHI)
C     INCLUDE 'DIMENSION1'
C     IMPLICIT REAL*8 (A-H,O-Z)
      PARAMETER (IT=100,JT=60,LMAX=500)
C
C *************** HORIZONTAL SWEEP USED ***********************
C
     DIMENSION PHI(IT,JT),A(IT),B(IT),C(IT),D(IT)
     COMMON /COEFF/Q1P(IT,JT),Q2P(IT,JT),Q3P(IT,JT),COB(IT,JT)
    1,SEW(IT,JT),YSEW(IT,JT),SNS(IT,JT),XSNS(IT,JT)
    2,DU(IT,JT),DU1(IT,JT),DV(IT,JT),DV1(IT,JT)
    3,AP(IT,JT),AN(IT,JT),AS(IT,JT),AE(IT,JT),AW(IT,JT),SU(IT,JT)
    1,SP(IT,JT)
     NIM1=NI-1
     NJM1=NJ-1
     ISTM1=ISTART-1
     A(ISTM1)=0.0
C ************************ COMMENCE N-S SWEEP **************
```

```
      DO 100 J=JSTART,NJM1
      C(ISTM1)=PHI(ISTM1,J)
C ******************  COMMENCE W-E TRAVERSE ***************
      DO 101 I=ISTART,NIM1
      A(I)=AE(I,J)
      B(I)=AW(I,J)
      C(I)=AN(I,J)*PHI(I,J+1)+AS(I,J)*PHI(I,J-1)+SU(I,J)
      D(I)=AP(I,J)
      TERM=1./(D(I)-B(I)*A(I-1))
      A(I)=A(I)*TERM
  101 C(I)=(C(I)+B(I)*C(I-1))*TERM
C ********************** OBTAIN NEW PHI'S ********************
      DO 102  II=ISTART,NIM1
      I=NI+ISTM1-II
  102 PHI(I,J)=A(I)*PHI(I+1,J)+C(I)
  100 CONTINUE
      RETURN
      END
      SUBROUTINE LISOLV(ISTART,JSTART,NI,NJ,PHI)
C       INCLUDE 'DIMENSION1'
C       IMPLICIT REAL*8 (A-H,O-Z)
        PARAMETER (IT=100,JT=60,LMAX=500)
      DIMENSION PHI(IT,JT),A(JT),B(JT),C(JT),D(JT)
        COMMON /COEFF/Q1P(IT,JT),Q2P(IT,JT),Q3P(IT,JT),COB(IT,JT)
     1,SEW(IT,JT),YSEW(IT,JT),SNS(IT,JT),XSNS(IT,JT)
     2,DU(IT,JT),DU1(IT,JT),DV(IT,JT),DV1(IT,JT)
     3,AP(IT,JT),AN(IT,JT),AS(IT,JT),AE(IT,JT),AW(IT,JT),SU(IT,JT)
     1,SP(IT,JT)
      NIM1=NI-1
      NJM1=NJ-1
      JSTM1=JSTART-1
      A(JSTM1)=0.0
C ************** COMMENCE W-E SWEEP *********************************
      DO 100 I=ISTART,NIM1
      C(JSTM1)=PHI(I,JSTM1)
C************** COMMENCE S-N TRAVERSE  *********************************
      DO 101 J=JSTART,NJM1
C************** ASSEMBLE TDMA COEFFICIENTS  ***************************
      A(J)=AN(I,J)
      B(J)=AS(I,J)
      C(J)=AE(I,J)*PHI(I+1,J)+AW(I,J)*PHI(I-1,J)+SU(I,J)
      D(J)=AP(I,J)
C******* CALCULATE COEFFICIENTS OF RECURRENCE FORMULA ****************
      TERM=1./(D(J)-B(J)*A(J-1))
      A(J)=A(J)*TERM
  101 C(J)=(C(J)+B(J)*C(J-1))*TERM
C************ OBTAIN NEW PHI'S     *********************************
      DO 102 JJ=JSTART,NJM1
      J=NJ+JSTM1-JJ
  102 PHI(I,J)=A(J)*PHI(I,J+1)+C(J)
  100 CONTINUE
      RETURN
      END
      SUBROUTINE MACHEX(NIS,NJS,NIE,NJE)
C       INCLUDE 'DIMENSION1'
C       INCLUDE 'DIMENSION'
```



```
C       IMPLICIT REAL*8 (A-H,O-Z)
        PARAMETER (IT=100,JT=60,LMAX=500)
        CHARACTER*8 PFOR1,PUFOR1,FILIN,FILOUT
        CHARACTER*8 PFOR2,PUFOR2
        CHARACTER*8 PFOR3,PUFOR3
        CHARACTER*8 PFOR4,PUFOR4
      COMMON /FNAME1/PFOR1,PUFOR1,FILIN,FILOUT
      COMMON /FNAME2/PFOR2,PUFOR2,PFOR3,PUFOR3
      COMMON /FNAME3/PP1,PP2,PP3,PP4,MPL,MPL1
      COMMON /FNAME4/PFOR4,PUFOR4
      COMMON /COEFF/Q1P(IT,JT),Q2P(IT,JT),Q3P(IT,JT),COB(IT,JT)
     1   ,SEW(IT,JT),YSEW(IT,JT),SNS(IT,JT),XSNS(IT,JT)
     2   ,DU(IT,JT),DU1(IT,JT),DV(IT,JT),DV1(IT,JT)
     3   ,AP(IT,JT),AN(IT,JT),AS(IT,JT),AE(IT,JT),AW(IT,JT),SU(IT,JT)
     1   ,SP(IT,JT)
      COMMON /POS/ YPOS(IT,JT),XPOS(IT,JT),R(IT,JT)
      COMMON /VAR/ U(IT,JT),V(IT,JT),P(IT,JT),TM(IT,JT),PP(IT,JT)
     1   ,UDUMMY(IT,JT),VDUMMY(IT,JT)
     2   ,TVIS(IT,JT),TCON(IT,JT),DEN(IT,JT),DISS(IT,JT)
      COMMON
     1   /UVEL/RESORU,NSWPU,URFU,SD
     1   /VVEL/RESORV,NSWPV,URFV
     1   /PCOR/RESORM,NSWPP,URFP,IPREF,JPREF
     1   /TMP/RESORT,NSWPT,URFT
      COMMON/INPUT/NI,NJ,NIM1,NJM1,GREAT,INDCOS,INDSM
     1            ,DATAR,DATAW,IFORM,ILASER,CLASIN,NRAYS
     2            ,FOCUS,IFOCUS,BDIAM,ITRACE,ISUPER
     3            ,ANGI,ANGE,RCI,RCT,RT,RI,XEXIT,XI,RTIOY1
      COMMON/IINPUT/
     4            RTIOX1,RTIOX2,XDENSE,JS1,JS2,IS1,IS2
     5            ,URSUP,URVIS,IDENSE,JDENSE,YENRAT,RTIOY2
     6            ,NCONST,XCONST
     6            ,INITP,INITER,SCALE
      COMMON/COND/CCN(IT,JT),CCE(IT,JT),DDN(IT,JT),DDE(IT,JT)
     1    ,DDN1(IT,JT),DDE1(IT,JT)
      COMMON/LASER/QINP(IT,JT),GRA(IT,JT),TRANS(IT,JT),CAB(IT,JT)
     1    ,TNG(LMAX),ING(LMAX,IT)
     2    ,POWER(LMAX),QRA(IT,JT),TH(IT,JT)
      COMMON/LASER2/HT(3000,4),HMU(400,4),HDEN(400,4)
     1    ,HCCP(400,4),HCAB(400,4),HRA(400,4)
        COMMON /ADD8/ANU(IT,JT),ASU(IT,JT),AEU(IT,JT),AWU(IT,JT)
        COMMON /ADD9/ANV(IT,JT),ASV(IT,JT),AEV(IT,JT),AWV(IT,JT)
        COMMON /ADD10/AAN(IT,JT),AAE(IT,JT),COEF(IT),UTEMP(IT,JT),
     1              VTEMP(IT,JT),DYDX(IT),XP(IT)
        COMMON/EXTRA/HINLET
     1       /EXTRA1/UINLET,TBOUND
     1/MMAIN/MAXIT,JMON,IMON,INDPRI,SOLPAT
     1/ADD5/NITER
     1/ADD6/SORMAX,TRSMT,RDL
        COMMON/PROP/PTL,TTL,GAMMA,RG,WGHT,WGHT1,RATIO
        COMMON/EXTRA/PDUMMY(IT,JT)
        COMMON/PLUS/LROAT,NVS,NVS1,NVE,NVE1
        COMMON/MACH0/MAEX(JT),PEX(JT)
C       PP4=4.E5
C       PP3=3.E5
C       PP2=2.E5
```

```
C       PP1=1.E5
        GAMT2=1.
        GAMT1=1.
        DO 100 I=NIS,NIE
        DO 100 J=NJS,NJE
        PTEMP=PTL+P(I,J)
        PPPL=0.005*PTL
        IF(PTEMP.LE.PPPL) PTEMP=PPPL
        TPPL=0.005*TH(2,1)
        IF(TH(NI,J).LE.TPPL) TH(NI,J)=TPPL
        K=0
        IF(PTEMP.GE.PP3) K=3
        IF(PTEMP.GE.PP2.AND.PTEMP.LT.PP3)K=2
        IF(PTEMP.GE.PP1.AND.PTEMP.LT.PP2)K=1
        IF(K.EQ.1) ARATIO=(PP2-PTEMP)/(PP2-PP1)
        IF(K.EQ.2) ARATIO=(PP3-PTEMP)/(PP3-PP2)
        IF(K.EQ.3) ARATIO=(PP4-PTEMP)/(PP4-PP3)
        IF(K.EQ.0) GO TO 234
        II=TH(I,J)
        AT=TH(I,J)-II
        IF(II.GE.MPL1) II=MPL
        IF(II.GE.MPL1) AT=1.
C       II=II+1
        IF(II.GE.1)
     1  T1=HT(II,K)*(1.-AT)+AT*HT(II+1,K)
        IF(II.GE.1)
     1  GAMT1=(HT(II+1,K)-HT(II,K))*100./SCALE
        IF(II.LT.1)
     1  T1=TH(I,J)/1.*HT(1,K)
        IF(II.LT.1)
     1  GAMT1=HT(1,K)*100./SCALE
234     CONTINUE
        II=TH(I,J)
        AT=TH(I,J)-II
        IF(II.GE.MPL1) II=MPL
        IF(II.GE.MPL1) AT=1.
C       II=II+1
        IF(II.GE.1)
     1  T2=HT(II,K+1)*(1.-AT)+AT*HT(II+1,K+1)
        IF(II.GE.1)
     1  GAMT2=(HT(II+1,K+1)-HT(II,K+1))*100./SCALE
        IF(II.LT.1)
     1  T2=TH(I,J)/1.*HT(1,K+1)
        IF(II.LT.1)
     1  GAMT2=HT(1,K+1)*100./SCALE
        IF(K.EQ.0) ARATIO=0.
        TM(I,J)=T1*ARATIO+T2*(1.-ARATIO)
        IF(K.EQ.0) GO TO 235
        II=T1
        AT=T1-II
        IF(II.GE.348) II=348
        IF(II.GE.348) AT=1.
        AT1=1.-AT
        IJ=II+1
        IF(II.EQ.0) GO TO 199
        DEN(I,J)=HDEN(II,K)*AT1+HDEN(IJ,K)*AT
```



```
C       DEN(I,J)=DEN(I,J)*(PTL+P(I,J))/3.E5
        T18=18.
        IF(TM(I,J).LE.T18)
     1  DEN(I,J)=II/T1*HDEN(II,K)
        GO TO 102
199     DEN(I,J)=1./T1*HDEN(1,K)
102     CONTINUE
235     CONTINUE
        II=T2
        AT=T2-II
        IF(II.GE.348) II=348
        IF(II.GE.348) AT=1.
        AT1=1.-AT
        IJ=II+1
        IF(II.EQ.0) GO TO 299
        CPPP=1./GAMT2*(1.-ARATIO)+1./GAMT1*ARATIO
        DEN(I,J)=(HDEN(II,K+1)*AT1+HDEN(IJ,K+1)*AT)
     1*(1.-ARATIO)+ARATIO*DEN(I,J)
        IF(K.EQ.0) DEN(I,J)=DEN(I,J)*(PTL+P(I,J))/PP1
        IF(TM(I,J).LE.T18)
     1  DEN(I,J)=((II/T2)*HDEN(II,K+1))*(1.-ARATIO)
     1  +DEN(I,J)*ARATIO
        IF(TM(I,J).LE.T18.AND.K.EQ.0)
     1  DEN(I,J)=((II/T2)*HDEN(II,K+1))*(1.-ARATIO)
     1  *(PTL+P(I,J))/PP1
        GO TO 101
299     IF(K.EQ.0) GO TO 399
        DEN(I,J)=1./T2*HDEN(1,K+1)*(1.-ARATIO)
     1  +ARATIO*HDEN(1,K)
        CPPP=1./GAMT2*(1.-ARATIO)+1./GAMT1*ARATIO
        GO TO 101
399     CONTINUE
        CPPP=1./GAMT2*(1.-ARATIO)+1./GAMT1*ARATIO
        DEN(I,J)=1./T2*HDEN(1,K+1)*(PTL+P(I,J))/PP1
  101 CONTINUE
        RG=(P(I,J)+PTL)/DEN(I,J)/TM(I,J)/100.
        SONIC=(RG*TM(I,J)*100.*CPPP/(CPPP-RG))**.5
        PDUMMY(I,J)=(U(I,J)**2+V(I,J)**2)**.5/SONIC
  100 CONTINUE
        IF(NIE.LT.NI) GO TO 103
        DO 104 J=1,NJ
        BTEMP=1.
        MAEX(J)=0
        IF(PDUMMY(NI,J).GE.BTEMP) MAEX(J)=1
104     CONTINUE
103     CONTINUE
      RETURN
      END
      SUBROUTINE TTRUST
C       INCLUDE 'DIMENSION1'
C       INCLUDE 'DIMENSION'
C       IMPLICIT REAL*8 (A-H,O-Z)
        PARAMETER (IT=100,JT=60,LMAX=500)
        CHARACTER*8 PFOR1,PUFOR1,FILIN,FILOUT
        CHARACTER*8 PFOR2,PUFOR2
        CHARACTER*8 PFOR3,PUFOR3
```

```
      CHARACTER*8 PFOR4,PUFOR4
     COMMON /FNAME1/PFOR1,PUFOR1,FILIN,FILOUT
     COMMON /FNAME2/PFOR2,PUFOR2,PFOR3,PUFOR3
     COMMON /FNAME3/PP1,PP2,PP3,PP4,MPL,MPL1
     COMMON /FNAME4/PFOR4,PUFOR4
     COMMON /COEFF/Q1P(IT,JT),Q2P(IT,JT),Q3P(IT,JT),COB(IT,JT)
    1   ,SEW(IT,JT),YSEW(IT,JT),SNS(IT,JT),XSNS(IT,JT)
    2   ,DU(IT,JT),DU1(IT,JT),DV(IT,JT),DV1(IT,JT)
    3   ,AP(IT,JT),AN(IT,JT),AS(IT,JT),AE(IT,JT),AW(IT,JT),SU(IT,JT)
    1   ,SP(IT,JT)
     COMMON /POS/ YPOS(IT,JT),XPOS(IT,JT),R(IT,JT)
     COMMON /VAR/ U(IT,JT),V(IT,JT),P(IT,JT),TM(IT,JT),PP(IT,JT)
    1   ,UDUMMY(IT,JT),VDUMMY(IT,JT)
    2   ,TVIS(IT,JT),TCON(IT,JT),DEN(IT,JT),DISS(IT,JT)
     COMMON
    1   /UVEL/RESORU,NSWPU,URFU,SD
    1   /VVEL/RESORV,NSWPV,URFV
    1   /PCOR/RESORM,NSWPP,URFP,IPREF,JPREF
    1   /TMP/RESORT,NSWPT,URFT
     COMMON/INPUT/NI,NJ,NIM1,NJM1,GREAT,INDCOS,INDSM
    1             ,DATAR,DATAW,IFORM,ILASER,CLASIN,NRAYS
    2             ,FOCUS,IFOCUS,BDIAM,ITRACE,ISUPER
    3             ,ANGI,ANGE,RCI,RCT,RT,RI,XEXIT,XI,RTIOY1
     COMMON/IINPUT/
    4             RTIOX1,RTIOX2,XDENSE,JS1,JS2,IS1,IS2
    5             ,URSUP,URVIS,IDENSE,JDENSE,YENRAT,RTIOY2
    6             ,NCONST,XCONST
    6             ,INITP,INITER,SCALE
     COMMON/COND/CCN(IT,JT),CCE(IT,JT),DDN(IT,JT),DDE(IT,JT)
    1    ,DDN1(IT,JT),DDE1(IT,JT)
     COMMON/LASER/QINP(IT,JT),GRA(IT,JT),TRANS(IT,JT),CAB(IT,JT)
    1    ,TNG(LMAX),ING(LMAX,IT)
    2    ,POWER(LMAX),QRA(IT,JT),TH(IT,JT)
     COMMON/LASER2/HT(3000,4),HMU(400,4),HDEN(400,4)
    1    ,HCCP(400,4),HCAB(400,4),HRA(400,4)
      COMMON /ADD8/ANU(IT,JT),ASU(IT,JT),AEU(IT,JT),AWU(IT,JT)
      COMMON /ADD9/ANV(IT,JT),ASV(IT,JT),AEV(IT,JT),AWV(IT,JT)
      COMMON /ADD10/AAN(IT,JT),AAE(IT,JT),COEF(IT),UTEMP(IT,JT),
    1              VTEMP(IT,JT),DYDX(IT),XP(IT)
      COMMON/EXTRA/HINLET
    1       /EXTRA1/UINLET,TBOUND
    1/MMAIN/MAXIT,JMON,IMON,INDPRI,SOLPAT
    1/ADD5/NITER
    1/ADD6/SORMAX,TRSMT,RDL
      COMMON/PROP/PTL,TTL,GAMMA,RG,WGHT,WGHT1,RATIO
      COMMON/EXTRA/PDUMMY(IT,JT)
      COMMON/PLUS/LROAT,NVS,NVS1,NVE,NVE1
      COMMON/THRUS1/AMASS(IT),ADD1(IT),AFLUX(IT),BFLUX(IT)
      DIMENSION DDFLUX(IT)
C
C ***************** EXIT BOUNDARY CONDITIONS ********************
      DO 356 I=1,NI
      AMASS(I)=0.
      ADD1(I)=0.
      AFLUX(I)=0.
      BFLUX(I)=0.
```



```
      DDFLUX(I)=0.
      DO 949 J=2,NJM1
      AREA=DEN(I,J)*R(I,J)*SNS(I,J)*6.28
      AMASS(I)=AMASS(I)+AREA*U(I,J)
      AMASS1=AMASS(I)
      IF(AMASS1.LE.1.E-10) AMASS1=1.E-10
      ADD1(I)=ADD1(I)+AREA*U(I,J)**2
      AFLUX(I)=AFLUX(I)+AREA*U(I,J)**2+(PTL+P(I,J))
    1 *R(I,J)*SNS(I,J)*6.28
      DDFLUX(I)=DDFLUX(I)+CCE(I,J)*6.28
949   CONTINUE
      BFLUX(I)=ADD1(I)/AMASS1/9.8
      ADD1(I)=AFLUX(I)/AMASS1/9.8
      AFLUX(I)=AFLUX(I)/AMASS1*AMASS1
356   CONTINUE
C AMASS--------MASS FLUX
C AFLUX---------THRUST
C BFLUX---------ISP
C ADD1----------ISP+PRESSURE
      PRINT *, 'I=','MASS FLUX (KG/S)','   THRUST (NT) '
    1 ,'  ISP (S)','  ISP+P'
      DO 187 I=1,NI
       WRITE(6,388) I,AMASS(I),AFLUX(I),BFLUX(I),ADD1(I),DDFLUX(I)
187   CONTINUE
388   FORMAT(1X,I3,8E15.6)
      RETURN
      END
       PROGRAM FU
      PARAMETER (IT=100,JT=60,LMAX=500)
      CHARACTER*8 PFOR1,PUFOR1,FILIN,FILOUT
      CHARACTER*8 PFOR2,PUFOR2
      CHARACTER*8 PFOR3,PUFOR3
      CHARACTER*8 PFOR4,PUFOR4
     COMMON /FNAME1/PFOR1,PUFOR1,FILIN,FILOUT
     COMMON /FNAME2/PFOR2,PUFOR2,PFOR3,PUFOR3
     COMMON /FNAME3/PP1,PP2,PP3,PP4,MPL,MPL1
     COMMON /FNAME4/PFOR4,PUFOR4
     COMMON /COEFF/Q1P(IT,JT),Q2P(IT,JT),Q3P(IT,JT),COB(IT,JT)
    1   ,SEW(IT,JT),YSEW(IT,JT),SNS(IT,JT),XSNS(IT,JT)
    2   ,DU(IT,JT),DU1(IT,JT),DV(IT,JT),DV1(IT,JT)
    3   ,AP(IT,JT),AN(IT,JT),AS(IT,JT),AE(IT,JT),AW(IT,JT),SU(IT,JT)
    1   ,SP(IT,JT)
     COMMON /POS/ YPOS(IT,JT),XPOS(IT,JT),R(IT,JT)
     COMMON /VAR/ U(IT,JT),V(IT,JT),P(IT,JT),TM(IT,JT),PP(IT,JT)
    1   ,UDUMMY(IT,JT),VDUMMY(IT,JT)
    2   ,TVIS(IT,JT),TCON(IT,JT),DEN(IT,JT),DISS(IT,JT)
     COMMON
    1   /UVEL/RESORU,NSWPU,URFU,SD
    1   /VVEL/RESORV,NSWPV,URFV
    1   /PCOR/RESORM,NSWPP,URFP,IPREF,JPREF
    1   /TMP/RESORT,NSWPT,URFT
     COMMON/INPUT/NI,NJ,NIM1,NJM1,GREAT,INDCOS,INDSM
    1             ,DATAR,DATAW,IFORM,ILASER,CLASIN,NRAYS
    2             ,FOCUS,IFOCUS,BDIAM,ITRACE,ISUPER
    3             ,ANGI,ANGE,RCI,RCT,RT,RI,XEXIT,XI,RTIOY1
     COMMON/IINPUT/
```

```
     4            RTIOX1,RTIOX2,XDENSE,JS1,JS2,IS1,IS2
     5            ,URSUP,URVIS,IDENSE,JDENSE,YENRAT,RTIOY2
     6            ,NCONST,XCONST
     6            ,INITP,INITER,SCALE
      COMMON/COND/CCN(IT,JT),CCE(IT,JT),DDN(IT,JT),DDE(IT,JT)
     1    ,DDN1(IT,JT),DDE1(IT,JT)
      COMMON/LASER/QINP(IT,JT),GRA(IT,JT),TRANS(IT,JT),CAB(IT,JT)
     1    ,TNG(LMAX),ING(LMAX,IT)
     2    ,POWER(LMAX),QRA(IT,JT),TH(IT,JT)
      COMMON/LASER2/HT(3000,4),HMU(400,4),HDEN(400,4)
     1    ,HCCP(400,4),HCAB(400,4),HRA(400,4)
      COMMON /ADD8/ANU(IT,JT),ASU(IT,JT),AEU(IT,JT),AWU(IT,JT)
      COMMON /ADD9/ANV(IT,JT),ASV(IT,JT),AEV(IT,JT),AWV(IT,JT)
      COMMON /ADD10/AAN(IT,JT),AAE(IT,JT),COEF(IT),UTEMP(IT,JT),
     1             VTEMP(IT,JT),DYDX(IT),XP(IT)
      COMMON/EXTRA/HINLET
     1       /EXTRA1/UINLET,TBOUND
     1/MMAIN/MAXIT,JMON,IMON,INDPRI,SOLPAT
     1/ADD5/NITER
     1/ADD6/SORMAX,TRSMT,RDL
      COMMON/PROP/PTL,TTL,GAMMA,RG,WGHT,WGHT1,RATIO
      COMMON/EXTRA/PDUMMY(IT,JT)
      COMMON/PLUS/LROAT,NVS,NVS1,NVE,NVE1
C     INCLUDE 'DIMENSION1'
C     INCLUDE 'DIMENSION'
      COMMON/THRUS1/AMASS(IT),ADD1(IT),AFLUX(IT),BFLUX(IT)
      COMMON/MACHO/MAEX(JT),PEX(JT)
      CHARACTER*20 HEDU,HEDV,HEDP,HEDTEM,HEDUT,HEDVT
     1            ,HEDRAD,HEDABS,HEDENT,HEDS
      LOGICAL INCALU,INCALV,INCALP,INCALT,IPRRAD,IPRABS
     1       ,IPRENT,IPRUB,IPRVB
      CHARACTER*40 IIIPUT
C
C
C
C
C     NAMELIST /JENG1/ FILIN,FILOUT
C     NAMELIST /JENG2/ PFOR1,PUFOR1,PFOR2,PUFOR2
C     NAMELIST /JENG21/ PFOR3,PUFOR3,PFOR4,PUFOR4
      NAMELIST /JENGZ1/ DATAR,DATAW,SCALE
      NAMELIST /JENGZ2/ IFORM
      NAMELIST /JENGP/ PP1,PP2,PP3,PP4,MPL,MPL1
      NAMELIST /JENG3/ ILASER,CLASIN,BDIAM,FOCUS,IFOCUS,NRAYS,ITRACE,
     1                 INITER
      NAMELIST /JENG4/ ISUPER,INDCOS,HINLET,UINLET,GAMMA,PTL,TTL
      NAMELIST /JENG5/ NJ,NI
      NAMELIST /JENG6/ANGI,ANGE,RCI,RCT,RT,RI,XI,XEXIT
      NAMELIST /JENG7/RTIOY1,RTIOY2,JDENSE,YENRAT
      NAMELIST /JENG8/IDENSE,XDENSE,NCONST,XCONST,RTIOX1,RTIOX2
      NAMELIST /JENG9/IMON,JMON,JS1,IS1,JS2,IS2,INDSM,MAXIT,INDPRI,
     1               INITP
      NAMELIST /JENGA/ SOLPAT,URFP,URFU,URFV,URFT,URSUP,URVIS
      NAMELIST /JENGB/ NSWPU,NSWPV,NSWPP,NSWPT,SORMAX
      NAMELIST /JENGC/ IPRRAD,IPRABS,
     1                 IPRENT,IPRUB,IPRVB
      NAMELIST /JENGD/ NVS,NVE
```



```
C
C
C
C
               JPREF=5
               IPREF=2
                  INCALU=.TRUE.
                  INCALV=.TRUE.
                  INCALP=.TRUE.
                  INCALT=.TRUE.
                  IPRRAD=.FALSE.
                  IPRABS=.FALSE.
                  IPRENT=.FALSE.
                  IPRUB=.FALSE.
                  IPRVB=.FALSE.
      READ(5,*) IIIPUT
      OPEN (UNIT=9,FILE=IIIPUT,FORM='FORMATTED',
     1 ACCESS='SEQUENTIAL')
      REWIND(UNIT=9)
      READ(9,*) FILIN
      READ(9,*) FILOUT
C     READ(9,JENG1)
C     READ(9,JENG2)
      READ(9,JENGZ1)
      READ(9,JENGZ2)
C     READ(9,JENG21)
      READ(9,JENGP)
      READ(9,JENG3)
      READ(9,JENG4)
      READ(9,JENG5)
      READ(9,JENG6)
      READ(9,JENG7)
      READ(9,JENG8)
      READ(9,JENG9)
      READ(9,JENGA)
      READ(9,JENGB)
      READ(9,JENGC)
      READ(9,JENGD)
      CLOSE(9)
      NVS1=NVS-1
      NVE1=NVE+1
      OPEN (UNIT=7,FILE='OUTPUT1',FORM='FORMATTED',
     1 ACCESS='SEQUENTIAL')
      REWIND(UNIT=7)
C     WRITE(7,JENG1)
C     WRITE(7,JENG2)
      WRITE(7,JENGZ1)
      WRITE(7,JENGZ2)
C     WRITE(7,JENG21)
      WRITE(7,JENGP)
      WRITE(7,JENG3)
      WRITE(7,JENG4)
      WRITE(7,JENG5)
      WRITE(7,JENG6)
      WRITE(7,JENG7)
      WRITE(7,JENG8)
```

```
      WRITE(7,JENG9)
      WRITE(7,JENGA)
      WRITE(7,JENGB)
      WRITE(7,JENGC)
C     CLOSE(7)
      CLASIN=CLASIN/SCALE
                GREAT=1.E30
                NITER=0
                HEDU='U VEL.(PHY)'
                HEDS='MACH NO.'
                HEDUT='U VEL.(CAL)'
                HEDV='V VEL.(PHY)'
                HEDVT='V VEL.(CAL)'
                HEDP='PRESSURE'
                HEDTEM='TEMPERATURE'
                HEDENT='ENTHALPY'
                HEDABS='ENERGY ABORBED'
                HEDRAD='RADIATION LOSS'
                NIM1=NI-1
                NJM1=NJ-1
C
C************** READIN PROPERTY FILE *******************************
C************** IFORMAT=1, FORMATTED FILE **************************
C************** IFORMAT=0, UNFORMATTED FILE ************************
      IF(IFORM.NE.1) GO TO 854
      OPEN (UNIT=4,FILE='HP0.1',FORM='FORMATTED',ACCESS='SEQUENTIAL')
      REWIND(UNIT=4)
      DO 855 I=1,350
      READ(4,856)HRA(I,1),HCAB(I,1),HMU(I,1),HDEN(I,1),HCCP(I,1)
855   CONTINUE
856   FORMAT(5X,5D13.6)
      READ(4,*) (HT(I,1),I=1,MPL)
      CLOSE(UNIT=1)
      OPEN (UNIT=1,FILE='HP0.3',FORM='FORMATTED',ACCESS='SEQUENTIAL')
      REWIND(UNIT=1)
      DO 355 I=1,350
      READ(1,856)HRA(I,2),HCAB(I,2),HMU(I,2),HDEN(I,2),HCCP(I,2)
355   CONTINUE
      READ(1,*) (HT(I,2),I=1,MPL)
      CLOSE(UNIT=1)
      OPEN (UNIT=2,FILE='HP01.',FORM='FORMATTED',ACCESS='SEQUENTIAL')
      REWIND(UNIT=2)
      DO 356 I=1,350
      READ(2,856)HRA(I,3),HCAB(I,3),HMU(I,3),HDEN(I,3),HCCP(I,3)
356   CONTINUE
      READ(2,*) (HT(I,3),I=1,MPL)
      CLOSE(UNIT=3)
      OPEN (UNIT=3,FILE='HP03.',FORM='FORMATTED',ACCESS='SEQUENTIAL')
      REWIND(UNIT=3)
      DO 357 I=1,350
      READ(3,856)HRA(I,4),HCAB(I,4),HMU(I,4),HDEN(I,4),HCCP(I,4)
357   CONTINUE
      READ(3,*) (HT(I,4),I=1,MPL)
      CLOSE(UNIT=3)
      OPEN (UNIT=24,FILE='uprop1.0',FORM='UNFORMATTED',
     1  ACCESS='SEQUENTIAL')
```



```
      REWIND(UNIT=24)
      WRITE(24) (HRA(I,1),I=1,350),
     1 (HCAB(I,1),I=1,350),
     1 (HMU(I,1),I=1,350),
     1 (HDEN(I,1),I=1,350),
     1 (HCCP(I,1),I=1,350),
     1 (HT(I,1),I=1,MPL)
      CLOSE(UNIT=24)
      OPEN (UNIT=21,FILE='uprop2.0',FORM='UNFORMATTED',
     1 ACCESS='SEQUENTIAL')
      REWIND(UNIT=21)
      WRITE(21) (HRA(I,2),I=1,350),
     1 (HCAB(I,2),I=1,350),
     1 (HMU(I,2),I=1,350),
     1 (HDEN(I,2),I=1,350),
     1 (HCCP(I,2),I=1,350),
     1 (HT(I,2),I=1,MPL)
      CLOSE(UNIT=21)
      OPEN (UNIT=22,FILE='uprop3.0',FORM='UNFORMATTED',
     1 ACCESS='SEQUENTIAL')
      REWIND(UNIT=22)
      WRITE(22) (HRA(I,3),I=1,350),
     1 (HCAB(I,3),I=1,350),
     1 (HMU(I,3),I=1,350),
     1 (HDEN(I,3),I=1,350),
     1 (HCCP(I,3),I=1,350),
     1 (HT(I,3),I=1,MPL)
      CLOSE(UNIT=22)
      OPEN (UNIT=23,FILE='uprop4.0',FORM='UNFORMATTED',
     1 ACCESS='SEQUENTIAL')
      REWIND(UNIT=23)
      WRITE(23) (HRA(I,4),I=1,350),
     1 (HCAB(I,4),I=1,350),
     1 (HMU(I,4),I=1,350),
     1 (HDEN(I,4),I=1,350),
     1 (HCCP(I,4),I=1,350),
     1 (HT(I,4),I=1,MPL)
      CLOSE(UNIT=23)
      GO TO  853
854   CONTINUE
      OPEN (UNIT=34,FILE='uprop1.0',FORM='UNFORMATTED',
     1 ACCESS='SEQUENTIAL')
      REWIND(UNIT=34)
      READ(34) (HRA(I,1),I=1,350),
     1 (HCAB(I,1),I=1,350),
     1 (HMU(I,1),I=1,350),
     1 (HDEN(I,1),I=1,350),
     1 (HCCP(I,1),I=1,350),
     1 (HT(I,1),I=1,MPL)
      CLOSE(UNIT=34)
      OPEN (UNIT=31,FILE='uprop2.0',FORM='UNFORMATTED',
     1 ACCESS='SEQUENTIAL')
      REWIND(UNIT=31)
      READ(31) (HRA(I,2),I=1,350),
     1 (HCAB(I,2),I=1,350),
     1 (HMU(I,2),I=1,350),
```

```
     1  (HDEN(I,2),I=1,350),
     1  (HCCP(I,2),I=1,350),
     1  (HT(I,2),I=1,MPL)
        CLOSE(UNIT=31)
        OPEN (UNIT=32,FILE='uprop3.0',FORM='UNFORMATTED',
     1  ACCESS='SEQUENTIAL')
        REWIND(UNIT=32)
        READ(32) (HRA(I,3),I=1,350),
     1  (HCAB(I,3),I=1,350),
     1  (HMU(I,3),I=1,350),
     1  (HDEN(I,3),I=1,350),
     1  (HCCP(I,3),I=1,350),
     1  (HT(I,3),I=1,MPL)
        CLOSE(UNIT=32)
        OPEN (UNIT=33,FILE='uprop4.0',FORM='UNFORMATTED',
     1  ACCESS='SEQUENTIAL')
        REWIND(UNIT=33)
        READ(33) (HRA(I,4),I=1,350),
     1  (HCAB(I,4),I=1,350),
     1  (HMU(I,4),I=1,350),
     1  (HDEN(I,4),I=1,350),
     1  (HCCP(I,4),I=1,350),
     1  (HT(I,4),I=1,MPL)
        CLOSE(UNIT=33)
853   CONTINUE
C
C
C ****************** END OF READIN ****************************************
C
C ****************** SET UP INITIAL CONDITIONS ****************************
C
        CALL GEOM
        BTEMP=0.
        IF(DATAR.EQ.BTEMP)      CALL ONEDIM
        CALL COORD
        IF(ILASER.EQ.1) CALL LENSE
C
C ****************** READ IN PREVIOUS RESULTS *****************************
C
      IF(DATAR.EQ.BTEMP) GO TO 968
        OPEN (UNIT=43,FILE=FILIN,FORM='UNFORMATTED',
     1  ACCESS='SEQUENTIAL')
        REWIND(UNIT=43)
        READ(43)
     2 ((UTEMP(I,J),  I=1,NI),J=1,NJ),((VTEMP(I,J), I=1,NI),J=1,NJ),
     1 ((TM(I,J), I=1,NI),J=1,NJ),
     1 ((TH(I,J), I=1,NI),J=1,NJ),
     1 ((P(I,J), I=1,NI),J=1,NJ),
     3 ((U(I,J), I=1,NI),J=1,NJ),
     1 ((V(I,J), I=1,NI),J=1,NJ)
     1 ,((UTEMP(I,J), I=1,NI),J=1,NJ)
       READ(43)
     1(AMASS(I),I=1,NI),(AFLUX(I),I=1,NI),(ADD1(I),I=1,NI),
     1(BFLUX(I),I=1,NI),((DU(I,J),I=1,NI),J=1,NJ),
     1((DU1(I,J),I=1,NI),J=1,NJ),((DV(I,J),I=1,NI),J=1,NJ),
     1((DV1(I,J),I=1,NI),J=1,NJ)
```



```
        CLOSE(UNIT=43)
        DO 399 I=1,NI
        DO 399 J=1,NJ
C       TM(I,J)=TM(NVE,NJ)
C       TH(I,J)=TH(NVE,NJ)
C       P(I,J)=P(I,J)*1.5
399     CONTINUE
C        DO 399 I=1,20
C        V(I,NJ)=0.
C        DO 399 J=2,NJM1
c        V(I,NJ-J+1)=0.
C       IF(P(I,J).GE.PTL) P(I,J)=PTL
C       IF(U(I,J).GE.10.) U(I,J)=10.
C       IF(U(I,J).LE.0.) U(I,J)=0.
C       IF(V(I,J).LE.-5.) V(I,J)=-5.
C       IF(V(I,J).GE.5.) V(I,J)=5.
C399     CONTINUE
        DO 499 I=1,NI
C       U(I,1)=0.
        DO 499 J=1,NJ
C       U(I,J)=0.
C        U(I,J)=0.
C       IF(P(I,J).GE.PTL) P(I,J)=PTL
499     CONTINUE
968     CONTINUE
C
C ****************END OF READ IN ***********************************
C ****************** END OF SET UP ***********************************
C
C
C******************* PRINT INITIAL CONDITIONS ****************************
C
        IF(INITP.NE.1) GO TO 958
             IF(INCALU) CALL PRINT(1,1,NI,NJ,U,HEDU,IS1,JS1)
             IF(IPRUB) CALL PRINT(1,1,NI,NJ,UDUMMY,HEDUT,IS1,JS1)
             IF(INCALV) CALL PRINT(1,1,NI,NJ,V,HEDV,IS1,JS1)
             IF(IPRVB) CALL PRINT(1,1,NI,NJ,VDUMMY,HEDVT,IS1,JS1)
             IF(INCALP) CALL PRINT(1,1,NI,NJ,P,HEDP,IS1,JS1)
             IF(INCALT) CALL PRINT(1,1,NI,NJ,TM,HEDTEM,IS1,JS1)
             IF(IPRENT) CALL PRINT(1,1,NI,NJ,TH,HEDENT,IS1,JS1)
             IF(IPRRAD) CALL PRINT(1,1,NI,NJ,QRA,HEDRAD,IS1,JS1)
             IF(IPRABS) CALL PRINT(1,1,NI,NJ,QINP,HEDABS,IS1,JS1)
958     CONTINUE
C
C ***************************END OF PRINTING INITIAL CONDITIONS ***********
C
C
C*************** SET UP FOR X-Y SWEEP ***************************************
C ******SOLPAT-  -1. HOR SWEEP,0. VERTICAL SWEEP,1. ALTERNATING SWEEPS ******
C
C
      IF(SOLPAT)5,6,7
  5   SD=-1.
      GO TO 8
  6   SD=0.
      GO TO 8
```

```
  7   SD=-1.
  8   CONTINUE
      WRITE(6,310) IMON,JMON
  300 NITER=NITER+1
C
C************* BEGIN OF ITERATION LOOP ************************************
C
       CALL PROPS(1,1,NI,NJ)
970    IF(NITER.GE.INITER) GO TO 969
       CALL PROPS(1,1,NI,NJ)
       ISTART=IFOCUS-NI/5.
       IEND=IFOCUS+NI/70.
       JEND=NJ/5.
       DO 956 II=28,45
       DO 956 JJ=1,30
       ATEMP=1200.*(1.-NITER/1.5/INITER)+400.
        TH(II,JJ)=MAX(ATEMP,TH(II,JJ))
956    CONTINUE
       DO 832 I=1,NI
       DO 832 J=1,NJ
       V(I,J)=V(I,J)*DEN(I,J)**.5
832    U(I,J)=U(I,J)*DEN(I,J)**.5
       CALL PROPS(1,1,NI,NJ)
       DO 834 I=1,NI
       DO 834 J=1,NJ
       V(I,J)=V(I,J)/DEN(I,J)**.5
834    U(I,J)=U(I,J)/DEN(I,J)**.5
       CALL ENERGE
     IF(INCALT) CALL CALTM
       GO TO 833
969    CONTINUE
C
C ************* END OF INITIAL ITERATIONS WITHOUT READING IN **********
C ************* THE PREVIOUS RESULTS **************************************
C
C ************* BEGIN OF REGULAR ITERATION ********************************
C
       CALL BUNDXL
       CALL BUNDYT
      IF(INCALU) CALL CALCU
      IF(INCALV) CALL CALCV
       CALL MACHEX(NI,NJ,NI,NJ)
       CALL BUNDXL
       CALL BUNDXR
C       CALL BUNDYT
       CALL BUNDYB
      IF(INCALP) CALL CALCP
      IF(ILASER.EQ.1) CALL ENERGE
      IF(INCALT) CALL CALTM
       CALL PROPS(1,1,NI,NJ)
       CALL BUNDXL
       CALL BUNDXR
C       CALL BUNDYT
       CALL BUNDYB
C
C       CALL HEAT
```



```
C ************* INTERMEDIATE OUTPUT ***************************************
C
833    DUMMY=0.0
       IF(MOD(NITER,INDSM).NE.0) GO TO 303
       WRITE(6,311) NITER,RESORU,RESORV,RESORM,RESORT,TRSMT,RDL
     1             ,U(IMON,JMON),V(IMON,JMON),P(IMON,JMON),TM(IMON,JMON)
303    CONTINUE
       IF(MOD(NITER,INDPRI).NE.0) GO TO 301
            IF(INCALU) CALL PRINT(1,1,NI,NJ,U,HEDU,IS1,JS1)
            IF(IPRUB) CALL PRINT(1,1,NI,NJ,UDUMMY,HEDUT,IS1,JS1)
            IF(INCALV) CALL PRINT(1,1,NI,NJ,V,HEDV,IS1,JS1)
            IF(IPRVB) CALL PRINT(1,1,NI,NJ,VDUMMY,HEDVT,IS1,JS1)
       DO 738 I=1,NI
       DO 738 J=1,NJ
       PDUMMY(I,J)=PTL+P(I,J)
738    CONTINUE
            IF(INCALP) CALL PRINT(1,1,NI,NJ,PDUMMY,HEDP,IS1,JS1)
            IF(INCALT) CALL PRINT(1,1,NI,NJ,TM,HEDTEM,IS1,JS1)
            IF(IPRENT) CALL PRINT(1,1,NI,NJ,TH,HEDENT,IS1,JS1)
            IF(IPRRAD) CALL PRINT(1,1,NI,NJ,QRA,HEDRAD,IS1,JS1)
            IF(IPRABS) CALL PRINT(1,1,NI,NJ,QINP,HEDABS,IS1,JS1)
     WRITE(6,310) IMON,JMON
  301 CONTINUE
C
C ********************* SET X-Y SWEEP AGAIN ***************************
C
      IF(SOLPAT)352,352,380
  380 IF(SD) 351,350,350
  350 SD=-1.
      GO TO 352
  351 SD=0.
  352 CONTINUE
C
C ***************** TERMINATION TESTS *****************************
C
      SORCE=MAX(RESORU,RESORV,RESORM,RESORT)
      IF(NITER.EQ.MAXIT) GO TO 302
      IF(SORCE.GT.SORMAX) GO TO 300
302   CONTINUE
C
C***************** FINAL OPERATIONS AND OUTPUT  **********************
C
            IF(INCALU) CALL PRINT(1,1,NI,NJ,U,HEDU,IS2,JS2)
            IF(IPRUB) CALL PRINT(1,1,NI,NJ,UDUMMY,HEDUT,IS2,JS2)
            IF(INCALV) CALL PRINT(1,1,NI,NJ,V,HEDV,IS2,JS2)
            IF(IPRVB) CALL PRINT(1,1,NI,NJ,VDUMMY,HEDVT,IS2,JS2)
            IF(INCALP) CALL PRINT(1,1,NI,NJ,P,HEDP,IS2,JS2)
            IF(INCALT) CALL PRINT(1,1,NI,NJ,TM,HEDTEM,IS2,JS2)
            IF(IPRENT) CALL PRINT(1,1,NI,NJ,TH,HEDENT,IS2,JS2)
            IF(IPRRAD) CALL PRINT(1,1,NI,NJ,QRA,HEDRAD,IS2,JS2)
            IF(IPRABS) CALL PRINT(1,1,NI,NJ,QINP,HEDABS,IS2,JS2)
C
C ************** WRITE RESULTS ON TAPE ****************************
C
       CALL MACHEX(1,1,NI,NJ)
       CALL HEAT
```

```
        CALL TTRUST
              IF(INCALU) CALL PRINT(1,1,NI,NJ,PDUMMY,HEDS,IS2,JS2)
       IF(DATAW.EQ.BTEMP) GO TO 56
         OPEN (UNIT=53,FILE=FILOUT,FORM='UNFORMATTED',
      1  ACCESS='SEQUENTIAL'
      1)
         REWIND(UNIT=53)
         WRITE(53)
      2 ((XPOS(I,J),  I=1,NI),J=1,NJ),((YPOS(I,J), I=1,NI),J=1,NJ),
      1 ((TM(I,J), I=1,NI),J=1,NJ),
      1 ((TH(I,J), I=1,NI),J=1,NJ),((P(I,J),I=1,NI),J=1,NJ),
      3 ((U(I,J), I=1,NI),J=1,NJ),((V(I,J),I=1,NI),J=1,NJ),
      1 ((PDUMMY(I,J), I=1,NI),J=1,NJ)
        WRITE(53)
      1(AMASS(I),I=1,NI),(AFLUX(I),I=1,NI),(ADD1(I),I=1,NI),
      1(BFLUX(I),I=1,NI),((DU(I,J),I=1,NI),J=1,NJ),
      1((DU1(I,J),I=1,NI),J=1,NJ),((DV(I,J),I=1,NI),J=1,NJ),
      1((DV1(I,J),I=1,NI),J=1,NJ)
         CLOSE (UNIT=53)
56       CONTINUE
         CALL STREAM
       STOP
C
C************ FORMAT STATEMENTS **********************************
C
  489   FORMAT(1X,'UINLET  =  ',E13.6/1X,'LASER INPUT =  ',E13.6,
     1  /1X,'LASER TRANSMIT.  =  ',E13.6/1X,'RADIATION =  ',E13.6)
C 188   FORMAT(1P8E10.3)
  288   FORMAT(1X,7E13.6)
  210   FORMAT(1H0,47X,'   LASER-SUSTAINED ARGON PLASMA'
     1  ,////)
  240   FORMAT(1H0,15X,15HASPECT RATIO   ,T60,1H=,3X,1PE11.3)
  310 FORMAT(1H0,4HITER,4X,106HI------------ABSOLUTE RESIDUAL SOURCE SUM
     1S-----------I       I-------FIELD VALUES AT MONITORING LOCATION,
     2     1H(,I2,1H,,I2,1H),9H--------I/2X,2HNO,6X,4HUMOM,6X,4HVMOM,6X,
     34HMASS,6X,4HENER,6X,4HLAS.,6X,4HRAD.,10X,1HU,9X,1HV,9X,1HP,9X,1HT,
     49X,1HK,9X,1HD/)
  311  FORMAT(1H0,I4,3X,6E10.3,3X,6E10.3)
  404  FORMAT(1H0,'  RELAXATION FACTORS   ')
  405 FORMAT(1H0,60H     U-VEL          V-VEL        PRESSURE       TEMPE
     1RATURE      ,5X)
  406  FORMAT(1H0,F10.3,6F15.3)
       END
```